AN INVESTIGATION OF INTERGRANULAR OXIDATION IN STAINLESS STEEL

Clarence A. Siebert
Maurice J. Sinnott
Robert E. Keith

University of Michigan

January 1954

United States Air Force
Air Materiel Command
Wright-Patterson Air Force Base, Dayton, Ohio

WADC TR 54-120

FOREWORD

This report was prepared by the University of Michigan, under USAF Contract No. AF 33(616)-353. The contract was initiated under Research and Development Order No. 615-13, "High Temperature Alloys", and was administered under the direction of the Materials Laboratory, Directorate of Research, Wright Air Development Center, with Capt. M. J. Whitman and Lt. J. H. DeVan acting as project engineers.

NOTICES

When Government drawings, specifications, or other data are used for any purpose other than in connection with a definitely related Government procurement operation, the United States Government thereby incurs no responsibility nor any obligation whatsoever; and the fact that the Government may have formulated, furnished, or in any way supplied the said drawings, specifications, or other data, is not to be regarded by implication or otherwise as in any manner licensing the holder or any other person or corporation, or conveying any rights or permission to manufacture, use or sell any patented invention that may in any way be related thereto.

The information furnished herewith is made available for study upon the understanding that the Government's proprietary interests in and relating thereto shall not be impaired. It is desired that the Judge Advocate (WCJ), Wright Air Development Center, Wright-Patterson Air Force Base, Ohio, be promptly notified of any apparent conflict between the Government's proprietary interests and those of others.

ABSTRACT

Specimens from one heat of type 309 - Nb and eight heats of type 310 stainless steel were oxidized in dry, moving air for times up to 100 hr in the temperature range 1600°-2000°F. Intergranular oxidation severity measurements were made microscopically. X-ray powder patterns were made of representative scales. Visual and magnetic examinations were made of both the specimens and the oxide scales. No appreciable difference in the severity of intergranular oxidation was observed that could be attributed to differences in alloy content among the heats. In general, intergranular penetration increased with time and temperature. X-ray analysis showed Cr_2O_3, Cr_2O_3-Fe_2O_3 solid solutions, Fe_2O_3, and a high-parameter spinel phase in the scales. All of the scales examined were protective in nature, and no improvement in penetration characteristics is foreseen by making minor changes in alloy contents.

PUBLICATION REVIEW

This report has been reviewed and is approved.

FOR THE COMMANDER:

M. E. Sorte
Colonel, USAF
Chief, Materials Laboratory
Directorate of Research

TABLE OF CONTENTS

LIST OF TABLES

LIST OF ILLUSTRATIONS

LIST OF ILLUSTRATIONS (cont.)

LIST OF ILLUSTRATIONS (cont.)

LIST OF ILLUSTRATIONS (cont.)

LIST OF ILLUSTRATIONS (cont.)

FINAL REPORT

AN INVESTIGATION OF INTERGRANULAR OXIDATION IN STAINLESS STEEL

INTRODUCTION

When a metal oxidizes the usual result is the formation of a more or less continuous and adherent layer of oxide on the exposed surface. In general, with increasing time and/or temperature of exposure to the oxidizing medium this oxide scale, which may be quite complex in its physical and chemical makeup, tends to increase in amount, becoming thicker at the expense of the underlying metal. This results in a progressive movement of the interface between the metal and the oxide layer toward the center of the metallic body. With some alloys, however, in addition to this progressive type of oxidation there is also oxidation occurring in the metal ahead of the metal-oxide interface. This latter type of oxidation has been variously known as internal oxidation or subscale formation. Internal oxidation may be further subdivided into cases in which the oxide occurs in a fine dispersion throughout the metal layer just beneath the metal-oxide interface, and cases in which the oxidation takes place principally in grain boundaries. In this latter type, the surface metal grains retain something like their original appearance even though they may become completely surrounded by a network of grain-boundary oxide. It is this last type of oxidation with which this report is concerned.

Compared with the total volume of literature concerned with the problem of metallic oxidation, the portion devoted to the study of intergranular oxidation is small. Intergranular oxidation becomes important in applications where thin sections are exposed to air at high temperatures. Under these conditions, premature failures may result. The conditions favoring intergranular oxidation have never been clearly defined; consequently, very little is known about the mechanism or mechanisms by which this type of oxidation occurs.

The present program arose from the need of the U.S. Air Force for information concerning intergranular oxidation in high-alloy stainless steels at very high temperatures. The alloy of principal interest is the type 310 analysis (25% Cr-20% Ni), although there is also interest in other compositions. There were four objectives of this research program:

(1) to determine the effect of temperatures between 1600° and 2000°F on intergranular oxidation;

(2) to examine the effects of alloy composition on intergranular oxidation;

(3) to determine the nature of the penetrating material in areas of intergranular attack; and

(4) to devise methods of reducing or eliminating intergranular oxidation.

The oxidizing medium used in the experimental work was dry air under controlled flow conditions. During the past year, research has been concentrated on objectives (1) and (2).

MATERIALS

The stainless steels used in this investigation consisted of specimens from one heat of type 309 + Nb steel and from eight heats of type 310 steel. The specimens of type 309 and two of type 310 steel were from special heats (64177 and 64270) and were supplied by the General Electric Company. The specimens from the remaining six heats of type 310, selected to provide as wide a compositional variation as possible within the specification limits, were from commercial production heats and were supplied by the United States Steel Company. The chemical analyses of these heats are presented in Table I.

All the material was in the form of cold-rolled and annealed sheet stock, the thickness of which varied from heat to heat but was in the range from 0.04 to 0.07 in.

Metallographic Examination

Photomicrographs of each of the nine heats in the as-received condition are presented in Fig. 1-9. These photomicrographs are intended to provide a standard of reference for photomicrographs taken following testing. In the as-received photomicrographs, the plane of polish was the plane of the sheet. Differences between the structures in the plane of rolling and in cross section will be enumerated and discussed in the Results and Discussion section of this report.

The grain size of the type 309 + Nb heat (Fig. 1) was extremely fine. Examination at 1000X showed that there was no grain-boundary carbide network, but that there was a considerable quantity of randomly distributed carbide.

Heat 64177 (Fig. 2) had a duplex grain structure, and examination at 1000X after etching revealed an almost continuous grain-boundary carbide network (Fig. 10). This duplex structure persisted throughout the thickness of the sheet. To determine whether this structure was the result of an unstable condition, a

specimen of this heat was re-solution-treated at 1900°F for 20 minutes and water-quenched. It was then polished and etched in a concentrated Murakami's reagent. The only appreciable change resulting from the re-solution treatment was found to be slight coalescence of the carbides. Furthermore, this heat showed grain-boundary penetration in the as-received condition, an example of which appears in Fig. 12. Although the other heats showed what may have been extremely slight amounts of initial penetration, the amount occurring in heat 64177 was appreciable. A typical edge from one of the other heats (heat X11338) is shown in Fig. 13 for comparison.

A duplex structure also occurred in heat 64270 (Fig. 3), although it was less pronounced than in heat 64177. The grain boundaries etched easily, and at 1000X a boundary network similar in appearance to that in heat 64177 was apparent.

In etching the as-received steels, it was found that certain of the heats were very difficult to etch, notably the type 309 + Nb, X11306, X27258, X45558, and, to a lesser extent, X46063. The procedure finally adopted with these heats was to etch them electrolytically with 10% chromic acid or chemically with a 1:1:1 mixture of nitric acid, hydrochloric acid, and water. When viewed under oblique light, the resulting surfaces showed the grains fairly well. Examination of all these difficult-to-etch heats at 1000X showed complete absence of any grain-boundary carbide networks, and the typical grain-boundary appearance is shown in Fig. 11.

Heat X11306 (Fig. 4) showed a rather fine, uniform grain structure.

Heat X11338 etched easily and looked very similar to heat 64270, but had a more uniform grain size (Fig. 5). Again examination at 1000X showed an almost complete grain-boundary carbide network.

Heat 27258 (Fig. 6) had a relatively large grain size, no carbide network, and in addition exhibited a fairly large amount of a randomly dispersed phase, presumably carbide.

Heat X45558 (Fig. 7) was similar to heat X27258, but had a smaller grain size and less of the dispersed phase.

Heat X46063 (Fig. 8) showed a large grain size, similar in structure to heats X27258 and X45558, although it etched somewhat differently. There was little dispersed phase, and again no trace of a boundary network.

Heat X46572 (Fig. 9) was more like heats 64270 and X11338 in appearance, except that the grain-boundary network was incomplete.

Magnetic Tests

Magnetic tests of the type to be described in detail in the Procedure section of this report indicated the presence of a very slight amount of magnetism (much less than the amount regularly classified as "weak" in the routine test) in all the as-received materials. Etching with Murakami's reagent showed nothing except the networks and/or dispersed phases revealed by the other etchants. Actually, these particles were too small for definite identification using Murakami's reagent,

and thus, on the basis of that etch alone, could possibly have been at least partly composed of delta ferrite. Since the particles showed up with the other etches, however, it is fairly certain that the particles were principally carbides. Therefore, any delta-ferrite (or sigma phase, which should also be revealed by Murakami's reagent) could have been present in the as-received material only in very small amounts, although the slight magnetism would seem to indicate the presence of some delta-ferrite.

EQUIPMENT

The oxidation equipment used in the investigation consisted of four tube-type laboratory furnaces. A schematic drawing of such a furnace with its associated air and power supply is shown in Fig. 14. Air at approximately 90 psig is first passed through a porous Al_2O_3 filter to remove any entrained oil, sediment, or other foreign matter. The air then passes through a pressure-reducing valve and then through two drying towers, the first filled with activated alumina and the second filled with phosphorus pentoxide. A valve is provided to bleed off a sample of the dried air for a dewpoint determination at suitable time intervals. The air is delivered to a manifold from which four side streams are withdrawn, one to each of the four horizontal tube furnaces. Flow to each furnace is controlled by a needle valve, and is metered by a flowmeter of the rotameter type in conjunction with a manometer. The air is then delivered to one end of a 2-in. sillimanite tube in the furnace. This tube is concentric with a similar, but shorter, 3-in. tube. The chromel heating wire is wound about the latter tube and imbedded in alundum cement. There is a 5-in. layer of vermiculite insulation contained in an aluminum shell around the heating coils. The furnace draws approximately 12 amperes at 220 volts. The 2-in. tube is packed for approximately one-third its length with broken pieces of ceramic, the purpose of which is to provide a large surface area to preheat the incoming air. A thermocouple well extends into the furnace as close as possible to the location of the specimens, which are in the center portion of the 2-in. tube and are supported on ceramic fixtures consisting of combustion carbon-analysis boats with their covers cemented in an inverted position (Fig. 15). The uniform-temperature zone of the furnace, in which as many as three of these boats are placed, is approximately 8 in. long. The temperature is controlled by means of a Foxboro controller with the control thermocouple imbedded in the furnace windings.

Considerable difficulty was encountered in the early part of the program from an inablility to maintain a sufficiently low dewpoint throughout a 100-hr run using only the alumina dryer. Although the form of alumina used contained a cobalt salt intended to indicate when the alumina became useless, it was found that the alumina ceased to adsorb an appreciable amount of moisture long before the color change took place. Furthermore, the alumina dryer alone was seldom capable of producing air with a dewpoint lower than -20°F, whereas it was felt that a dewpoint of -40°F would have been more desirable. Accordingly, a stainless-steel vessel was constructed to hold alternate layers of phosphoric anhydride and glass wool. This dryer was connected in series following the alumina dryer between runs 13 and 14. The alumina was replaced with regenerated material every 100 hr; the phosphoric anhydride dryer, once filled, has lasted over 1500 hr without attention. With this combination of dryers, it was possible to maintain a dewpoint of -35° to -60°F consistently.

PROCEDURE

Specimen Preparation

Rectangles 1/2 x 1 in. were first scribed on the sheet stock. Single small punch marks were then placed on one side of the sheet in one corner of each rectangle, thus permanently identifying the sides of the specimens relative to the original sheet. The specimens were then cut from the sheet using a shear. Shearing was found to be superior to bandsawing because it resulted in a neater edge and also gave fewer scratches on the faces of the specimens, which were tested without further surface treatment other than cleaning. Specimens were given code numbers which identified their original positions in the sheets. These numbers were recorded on the individual envelopes in which the specimens were stored, no markers being placed on the specimens themselves.

Equipment Operation

Before starting an oxidation run, the furnaces were brought to temperature and the air was allowed to flow through them for a period of 2-4 hours to establish thermal equilibrium. An air flow rate of 30 ft/min at the furnace temperature was selected as standard. Usually, one furnace was operated at each of the temperatures 1600°, 1700°, 1800°, and 1900°F, and one specimen of each of three heats was assigned to each furnace at random. In the later runs, in which all the furnaces were operated at 2000°F, specimens from all nine heats, including some duplicates, could be run simultaneously. Prior to charging, the specimens were cleaned with acetone and placed in the ceramic fixtures described in the Equipment section of this report and illustrated in Fig. 15.

During the runs, readings of furnace temperatures, air flow rates, air pressure, and room temperature were taken twice a day. Barometer readings and dewpoint readings of the furnace air were taken once a day, and the furnace temperature controllers were balanced once a day. Runs during this year's program were of 10, 30, and 100-hour duration, except for one 50-hr run and one 77-hr run.

At the conclusion of the runs, the specimens were quenched into distilled water in stainless-steel beakers, in order to avoid the loss of any scale, to arrest any phase transformations which might have taken place in the oxides on slower cooling, and to preserve the carbide distributions existing at the test temperatures. The contents of the beakers were then filtered through coarse filter paper and washed with acetone and then with ether to accelerate the drying the loose scales. After the filter papers had dried, their contents were bottled. The total elapsed time between the quenching and the completion of the bottling operation was about 1 hr. Any loosely adhering scale was gently scraped off the surfaces of the specimens with a surgical scapel and combined with the bottled scale.

Evaluation of Specimens

The visual appearances of the specimens were recorded, after which a lengthwise strip approximately 1/8 in. wide was cut from each specimen and discarded, in order to assure freedom from edge effects in the subsequent measurements. A 90° bend was then accurately put into each of the specimens perpendicular to the sawed edge using the specially designed die illustrated in Fig. 16.

At this point, qualitative magnetic tests were made on the specimens. To make these tests, a specimen was placed on a glass plate resting on the bent portion, both "legs" extending upward. The specimen was then set in motion by a gentle tap, and, while it oscillated, an Alnico magnet was brought near but not touching, the specimen and parallel to one of the flat faces. If there was no noticeable attractive effect or change in periodicity of the motion, the specimen was classified as "not detectably" magnetic. If the reverse was true, the specimen was allowed to come to rest and the magnet was again brought up parallel to a flat face. If the specimen moved violently so that the face touched the magnet, it was classified as "strongly" magnetic. If the specimen could be made to move slightly, although not sufficiently to touch the magnet, it was classified as having "medium" magnetism. If a specimen proved to belong to neither of these latter two classifications, it was recorded as being "weakly" magnetic in view of the magnetism shown in the first test, when the specimen was already in motion. Obviously, this test is qualitative, and too much emphasis must not be placed on the classifications themselves. Their only importance is the fact that almost all the specimens showed increases in magnetism after oxidation, as will be discussed subsequently.

Following the magnetic tests, the specimens from each heat were mounted, several to the mount, in bakelite with the sawed sides exposed. An untested specimen from the same heat was included in each mount. Considerable experimentation was carried out before a satisfactory polishing technique was developed. The technique finally adopted consisted of grinding the sawed edge of each specimen smooth and beveling it very slightly before mounting. Rough polishing was done under water using 240-grit silicon carbide paper. Finer polishing was done using 400- and 600-grit silicon carbide papers, also wet, which were mounted on metallographic wheels. Final polishing was done on a low-nap metallographic wheel impregnated with 2-micron diamond dust. The resulting polish was not scratch-free, but it was adequate. It was not possible to use such relatively soft abrasives as Gamal, Linde "B", and C-RO to obtain a smoother surface, since with these abrasives the oxides and inclusions present tended to tear out. A finer, 1/2-micron, diamond polishing compound was also tried, but it proved excessively difficult to keep the wheel free from contamination, and its use was stopped.

All the early specimens, and many of the later ones, were examined at 1000X in the unetched condition using bright field, dark field, and polarized illumination. The latter two contributed little to the investigation. Unusual areas were noted for future reference and/or photographed.

After polishing and metallographic examination, measurements were made of the extent of intergranular penetration, which was clearly visible in properly

polished unetched specimens. To make these measurements, a desk microscope with a 4-mm objective lens, a travelling stage, and a Bausch and Lomb grain-size eyepiece was used. Magnification was approximately 500X. The edge of a specimen cross section was aligned with one edge of the square A.S.T.M. No. 6 grid of the eyepiece, and the entire straight portion of the specimen edge was traversed. The bent portion of the specimen was not read (except in Run 9). For convenience, scratches had been previously made on the polished surface to mark the beginnings of the bent portion of the specimen, and readings were made up to a scratch. Initial and final stage positions were recorded for each straight portion. As a traverse was made, the number of intergranular fissures ending in each of the six rows of the grid parallel to the specimen edge was counted using a desk counter, and was recorded. This procedure was repeated for the other three straight portions of each specimen (both sides of both straight "legs" — a total of four).

During the course of the project, penetration measurements were made by five different technicians. Considerable pains were taken to see that satisfactory agreement was attained among the technicians reading the same specimens before they were allowed to proceed to specimens which had not yet been measured. Checks were made from time to time by having different technicians repeat a specimen counted by one of the other technicians. It was found that readings of the number of penetrations in a given surface made by different technicians usually agreed within about 5% on all but the shallowest group of fissures, those between 0 and 0.00063 in. in depth. On these shallow penetrations, operator variability ran as high as 30%. This lack of agreement in the shallow group is understandable when it is considered that many of the fissures in this group were of the order of 0.0002 in. or less in depth, the order of magnitude of the surface roughness. In addition, even slight polishing scratches and tears can produce effects likely to be mistaken for shallow penetration, especially in specimens in which there is little true penetration. For these reasons, too much confidence must not be placed in the actual magnitudes obtained for penetrations less than 0.00063 in. deep.

The figures for penetration in the four portions of a single specimen were added and divided by the total length traversed (from 1.1 to 1.4 in.) to put data from different specimens on a comparative basis. The sizes of the squares of the eyepiece grid had been previously determined, by calibration with a stage micrometer, to be 0.00063 in. on a side. Using this calibration, a frequancy-vs.-depth curve could be constructed for each specimen by plotting a bar chart and then drawing a smooth curve to fit the data. Curves constructed by this process appear in Figs. 17 through 67. Theoretically, any curve obtained by this method would tend to be biased toward the shallow side, even if the counting were completely accurate, because the probability of any fissure's ending precisely at the plane of polish, and thus the probability of its being observed in its true depth, is quite small.

To condense the data further, it was decided to examine the behavior of two parameters of the frequency-vs.-depth curves. The parameters, N and X, are defined as follows:

$$N = \int_0^s n(s)ds \cong \sum_{i=1}^{7} n_i \qquad (1)$$

and

$$X = \frac{\int_0^s sn(s)ds}{N} \cong \frac{\sum_{i=1}^{7} a_i n_i}{N} , \qquad (2)$$

where n_i is the number of fissures per inch of specimen surface in the ith group, a_i is the midpoint of the ith group measured from the surface, and s is the depth coordinate. The data were taken in seven groups: the six levels of the grid and a seventh class, rarely occuring, consisting of fissures which extended past the sixth grid level and which were arbitrarily assigned a group midpoint one grid level (0.00063 in.) beyond the sixth level. It can be seen that the parameter N is simply the total number of fissures per inch of all depths. The parameter X is a mean penetration depth; more precisely, X is the first moment of the penetration-vs.-depth curve with respect to the y-axis (or specimen surface) divided by the total number of fissures. Alternatively, X may be considered as being the depth coordinate of the centroid of the penetration-vs.-depth curve. Having obtained these two parameters for each specimen, the penetration data could be concisely summarized.

One word of caution is necessary, however, in the interpretation of the meaning of the X parameter. Referring to the summation form of Equation (2), it will be noted that it is impossible to have a value of X less than the midpoint of the first data group. Suppose, for example, that a specimen contains penetration fissures of the first group only. The quantity n_i then becomes equal to N, and can be taken outside the summation sign, where it cancels with the N in the denominator, leaving only a_1, the first group midpoint. In the present case, the midpoint of the first group was 0.00032 in. Therefore, a number of the specimens are recorded as having X - 0.00032 in. in which the penetration was actually much less than this average depth. The 0.00032 in. is not a lower limit in the size of fissure detectable, but is, rather, a consequence of the group size selected. The question may legitimately be asked, why was not a smaller group size chosen? There are two answers to this question: first, that when these standards were set up, only a small fraction of the specimens had been examined, and there was no way of knowing what sizes of penetration would be encountered later in the program; and, second, that any number of groups more than about six becomes excessively clumsy for an operator to use in obtaining data. In retrospect, it seems that the group size chosen was about ideal.

After penetration measurements had been completed, specimens were etched and again examined metallographically, photomicrographs being taken of significant areas.

Evaluation of Oxide Scales

The physical appearances of the oxides were recorded after thay had been bottled. Magnetic tests were then run, which were somewhat similar to those on the specimens themselves. The magnet was placed in contact with the outside of a bottle containing an oxide sample at a point nearest the sample itself. The bottle and magnet were then rotated, without moving the magnet relative to the bottle, until the weight of the oxide overcame the attractive force of the magnet and the oxide

dropped to the bottom of the bottle. Oxides which could not be attracted by the magnet at all were classified as "not detectably" magnetic. Oxides which dropped back when the bottle wall was approximately 90° to the horizontal were classified as "weakly" magnetic. Oxides which were attracted by the magnet sufficiently to allow 180° rotation of the bottle, suspending them under the magnet, were classified as "medium" or "strongly" magnetic, the latter classification being used when oscillatory movement of the magnet outside the bottle produced pronounced movement of the oxide particles within the bottle. This test is even more qualitative than the tests of the metallic specimen, since it is influenced by the amount and density of the oxide, the oxide particle size, and the smoothness and cleanliness of the inside of the bottle. It is valuable, nevertheless, as an indication of the presence of significant quantities of magnetic components in the scales.

Following the visual and magnetic examinations, oxides were pulverized in an agate mortar and pestle, mixed with Duco cement, and rolled out into thin cylinders between two glass microscope slides. The diameters of these cylindrical specimens were approximately 0.2 mm, and the cross sections were quite uniform. Specimens were mounted and centered in a 57.3-mm-diameter Norelco x-ray powder camera, utilizing a Straumanis-mounted film. X-ray exposures were made on a Norelco water-cooled diffraction unit using V-filtered Cr K_α radiation. A standard exposure time of 2 hr was selected, and all exposures were of this length except two, which required somewhat longer times. One series of four samples was run using a Norelco 114.6-mm camera, which required an exposure time of 10 hr. After the films had been processed, traces were made of them on a Leeds and Northrup Knorr-Albers type of microphotometer. These traces were then measured using a ruler of adequate length. This method of measurement was used in preference to an optical comparator, first because it is believed to be more accurate, and second because it gives quantitative values for diffraction line intensities. Interplanar spacings were computed from the distances measured on the microphotometer traces in the same manner as they would have been from distances measured on the film, a shrinkage correction being included. This technique is well-known, and will not be elaborated here. Comparison was then made with interplanar spacings of the compounds expected to be present, as made available by Yearian and Radavich (1).

For precise identification of the compounds present, which were solid solutions, it developed that additional corrections for such factors as the finite specimen size and small errors in specimen placement had to be applied to the computed interplanar spacings. This was done for the cubic spinel phase by plotting the value of the lattice parameter calculated from each back-reflection spinel line against the function $1/2\ (\cos^2\theta/\sin\theta + \cos^2\theta/\theta)$, as proposed by Taylor and Sinclair (2) and recommended by Henry, Lipson, and Wooster (3). This particular function linearizes the error θ-dependence somewhat better than other similar functions that have been proposed, according to the above authors. The straight line obtained in this plot was extrapolated to obtain the y-intercept, which represents the error-free value of the lattice parameter. For the rhombohedral Cr_2O_3-Fe_2O_3 solid-solution phase, the same method was attempted, as described by Henry, Lipson, and Wooster (3), but there was too much uncertainty in the line positions to obtain more than $\pm$10 atomic percent accuracy in the composition. Since this was hardly better than estimating compositions from the interplanar spacing data, extrapolations were not used in reporting the compositions of the rhombohedral phase.

The use of longer exposure times would have been beneficial in increasing the accuracy of the x-ray data, since longer exposure would have resulted in denser lines in the back-reflection region. In a number of cases, there was insufficient oxide to prepare an x-ray specimen by the usual means. In such cases, the specimen was omitted, but if it should later develop that any of these specimens are of critical importance, patterns can be obtained using methods of specimen preparation suited to smaller amounts of material.

Interface Movement

In reporting the penetration data, it would be desirable to refer the penetration depth always to the original metal surface. Early in the experimental work, attempts were made to measure the specimen thickness losses directly by mounting an untested specimen from the same heat and nearly the same location in the sheet stock along with the specimens from a given heat. After polishing, several thickness measurements were made of each specimen with a travelling microscope, the object being to subtract these values from the thickness of the untested specimen. It was found, however, that the interface movement was of the order of magnitude of the experimental error and normal thickness variation in the sheet, so that it was not possible to obtain consistent results by this method.

Attempts were then made to carry out weight-loss measurements on specimens given the same oxidation cycle as the specimens used in the regular procedure. Specimens were weighed and their dimensions were measured before and after oxidation and after descaling treatment and brushing. The descaling treatment consisted of making the specimen the cathode in a 10% H_2SO_4 electrolyte as described by Upthegrove and Murphy (4) and Siebert (5). A current of 10 amp was passed through each specimen for 1 min. The treatment was not successful in removing any but interference-film types of scale, although it is known to be very effective for the scales found on lower-alloy steels. In an effort to remove the scale further, the specimens were brushed with a rotary wire brush attached to a hand power tool. This treatment succeeded in removing all but the pit-type oxide withour removing any appreciable amount of metal. Density measurements were made on specimens from each heat by measuring the loss of weight in water. Knowing the density and the weight loss, the movement of one metal-oxide interface could be calculated by the formula:

$$\Delta s = \frac{\Delta w}{(4ab - c)\, d} \qquad (3)$$

where Δs is the interface movement, Δw is the weight loss, a and b are the dimensions of the sheet faces of the specimen, c is a correction for the rounded corners of the specimen, and d is the density of the metal. The results of these interface measurements are presented in Table 12, and are discussed more fully in the Results and Discussion section of this report. It should be noted here, however, that the interface movements were, as the early thickness measurements indicated, quite small. In view of the uncertainty in the interface movements arising from the small amounts of oxide remaining on the surfaces and from the roughness of the surfaces, it was decided to report the penetration data relative to the existing metal-oxide interfaces.

RESULTS AND DISCUSSION

Theory

The general mechanism of oxidation of metals has been broken down into several steps for purposes of fundamental study. Expressed briefly, these steps are as follows:

(1) Diffusion of oxygen to the surface,
(2) Adsorption of the oxygen on the surface,
(3) Dissociation and ionization of the oxygen,
(4) Inward diffusion of the oxygen, through any scale that is present,
(5) Outward diffusion of metal ions and electrons,
(6) Reaction between oxygen and metal ions to form oxide.

In any given case, this mechanism may be complicated by the existence of multiple valence states for the metal ions, presence of minor elements, existence of multi-layered oxide scales, volatility, cracking, or spalling of the scales, and the like. Any one of the basic steps may prove to be the slowest, or rate-controlling, step of the process. For an excellent review of the present state of knowledge in the entire field of oxidation the reader is referred to the recent book by Kubaschewski and Hopkins (6).

In the case of an alloy which is subject to intergranular oxidation, it seems reasonable that the grain boundaries must be attacked by oxygen ions reaching the metal-oxide interface, either by means of cracks in the scale layer or by true diffusion through the scale. Since the stainless steels as a group have dense, adherent scales, it would seem that oxygen must reach the metal-oxide interface by true diffusion in these steels. Davies, Simnad, and Birchenall (7) in their study of the scaling of pure iron have shown that of the three oxides of iron, FeO grows almost entirely by outward diffusion of Fe ions, Fe_3O_4 grows principally (80%) by outward diffusion of Fe ions, and Fe_2O_3 grows almost entirely by inward diffusion of O ions. Thus it would appear that if the scales formed on the steel contained appreciable amounts of either Fe_3O_4 or Fe_2O_3, there would be a possibility of the existence of mobile O ions at the metal-oxide interface. Hickman and Gulbransen (8), Boren (9), Warr (10) and Radavich (11), in work on the oxidation of stainless steels of composition similar to the ones used in this investigation, in no case report presence of FeO in the scale, but do report the presence of Fe_3O_4, Fe_2O_3, Cr_2O_3, and a Cr-rich spinel phase. FeO might be present, but it would have to be in the form of an extremely thin layer. Radavich also reports the presence of a solid solution of Fe_2O_3 and Cr_2O_3 in some cases and notes that such a phase could easily be mistaken for either pure component, especially by reflection electron diffraction, since the two compounds have complete solid solubility, the same crystal structure, and only slightly different lattice parameters. In the present investigation all these compounds except for the Fe_3O_4 were found in the scales. As for the role of Cr_2O_3 in O diffusion Cr_2O_3 is an oxide in which the ionic transport rates are very slow (12). The low ionic transport is associated with good refractory characteristics, which

have come to be recognized as necessary for formation of a protective oxide such as Cr_2O_3 (13). Randall and Robb (14) have shown that Cr_2O_3 and a high-parameter (about 8.43 kX) spinel are associated in high Cr and Cr-Ni steels with a protective type of scale, while a second type of scale containing a low-parameter (about 8.37 kX) spinel and no excess Cr_2O_3, though more tenacious than the first type, was not nearly as protective. It would thus appear that the key oxide scale component for oxidation resistance is Cr_2O_3.

Turning now to the question of intergranular oxidation, the differences that may exist between the volume diffusion coefficient and the grain boundary diffusion coefficient of a metal were pointed out by Turnbull (15), who carried out a mathematical analysis of an idealized model, and on the basis of the results of this analysis showed that grain boundary diffusion coefficients may be 105 times the corresponding volume diffusion coefficients or more. This difference is basically the result of the nature of the grain boundary itself. Although there is not complete agreement at the present time as to the detailed structures and properties of grain boundaries, it is generally agreed that at least those grain boundaries for which there is a large angular difference between the lattices on either side of the boundary are regions of relatively large disorder on an atomic scale. This means that the mean interatomic distance in a large-angle grain boundary must be greater than the mean interatomic distance in the lattice itself (since the lattice represents a close-packed array). One would therefore expect a larger diffusion coefficient in the grain boundary than in the lattice. Looking at the diffusion process from the thermodynamic point of view, the grain boundary is a region of high strain energy relative to the lattice as a result of its more or less random packing. Therefore, the activation energy for diffusion of foreign atoms can more easily be supplied in the vicinity of the grain boundary. Research soon to be published (16) indicates that the grain boundaries have a very important part in the solid-state diffusion of Bi in Cu, Ni in Fe, and Ni in Cu, the latter two systems having previously been considered to be classical examples of volume diffusion. In short, the major role played by grain boundaries in diffusion processes is only beginning to be fully realized, and comes about as a result of the nature of the boundaries themselves.

Thus far, we have seen how, in the case of oxidation of stainless steel, a certain amount of O in the ionic form can reach the metal-oxide interface by transport through the scale, the amount depending on the scale composition and, of course, on the scale thickness. Once the O ions are at the metal-oxide interface, a plausible argument has been presented to show that the ions which do not immediately react to form oxides will tend to diffuse preferentially into the grain boundaries of the metal. Once in a grain boundary, an O ion can do one of two things. It may at some point leave the boundary and diffuse out into a grain, where it ultimately becomes contiguous with that fraction of the O ions that diffuses from the metal-oxide interface to form the O-rich layer that ultimately becomes part of the scale. The other alternative for the O ion diffusing down a grain boundary is that it may react with a cation and other O ions if necessary in the boundary to form an oxide.

The role of the cations, especially the minor alloying elements, is a particularly complex one. The general rules of behavior of alloying elements have been summarized by Lustman (13), and are as follows:

(1) Alloy elements tend to become concentrated in the layer of scale adjacent to the metal, either as oxides in the case of elements more easily oxidizable than the base metal, or as metal islands in the case of elements less easily oxidizable than the base metal.

(2) Marked improvement in oxidation resistance requires that the oxide of a more easily oxidizable alloying element be refractory (which implies that it is a poor ionic conductor, such as Cr_2O_3) and that it be practically the only component of the innermost scale layer.

(3) Little, if any, improvement in oxidation resistance is to be expected from the addition of alloying elements less easily oxidizable than the base metal.

Considering the relative thermodynamic stability of the various oxides formed from the elements in stainless steel, one finds that SiO_2 is the most stable, followed in order of decreasing stability by MnO, Cr_2O_3, FeO, and NiO. On the basis of thermodynamics, then, one would expect to find Si oxidizing first, then Mn, and so on. Indeed, Baeyertz (17) demonstrated metallographically the prior oxidation of Si and Cr in 1936. Unfortunately, however, the role of alloying elements is more complex than is indicated by thermodynamics. Investigators using the most advanced techniques available, including electron diffraction and electron microscopy (18), believe at present that the order in which alloying elements will oxidize cannot be predicted in general from the thermodynamic data. Recent work by Gulbransen and McMillan (19) on 80% ni-20%Cr alloys and by Radavich and Yearian (20) on ferritic stainless steels of the 400 AISI series points to the possible importance to the alloy oxidation resistance of a thin layer of SiO_2 at the metal-oxide interface. Baeyertz showed that Si also precipitates as SiO_2 and as glassy silicates within the oxide-rich metal layer near the interface. Mn occurs as a major component of the high-parameter spinel phase in the scale, which has been identified as being $MnCr_2O_4$ and has been studied in detail by Longo (21). In addition, Mn probably occurs below the metal surface as particles of a silicate. Cr, as has been mentioned previously, occurs in the scale as free Cr_2O_3, as the Cr-rich spinel, and in solid solution with Fe_2O_3. Some Cr is present in the intergranular oxides also, as Baeyertz has shown. Neither Ni nor Ni oxide has been reported as a separate phase in the scale from 18%Cr-8%Ni, 25%Cr-12%Ni, 25%Cr-20%Ni, or 35%Ni-15%Cr steels in the investigations of Hickman and Gulbransen (8), Boren (9), Warr (10), Radavich (11), and McCullough, Fontana, and Beck (22). The last named investigators did report the presence of small amounts of Ni in their scales, as determined by chemical analysis, however. In the present investigation, a limited program was carried out to determine whether any substantial amount of Ni was present in the scales by means of a qualitative dimethylglyoxime test following Na_2CO_3 fusion of the scales. The results of these tests were negative, confirming that if Ni is present, at least in the scales tested, it is present only in very small amounts. The dimethylglyoxime tests could be carried out on only a few of the largest specimens of scale. C appears to be depleted in the metal near the surface, as will be discussed later, but it is difficult to see how C can influence the oxidation resistance of low C alloys such as those used in this investigation, since its oxides are gaseous and presumably escape in some manner through the scale. In summary, the process of oxidation in stainless steels, as well as in other alloyed materials, is accompanied by diffusion from the metal towards the metal-oxide interface of those alloying elements less noble than the base metal, and by an increase in concentration

of alloying elements more noble than the base metal in the metal layer beneath the interface and probably some subsequent diffusion of these elements away from the interface.

Summarizing the probable mechanism of intergranular oxidation, mobile O ions, reaching the metal-oxide interface by diffusion through the external scale, diffuse preferentially into the grain boundaries which intersect the surface, though appreciable O volume diffusion also occurs and some O diffusion may take place from the grain boundaries into the grains. Simultaneously, alloying elements present in the metal diffuse both toward the metal-oxide interface and at least at the lower temperatures toward the grain boundaries, where chemical reaction takes place between them and the O ions, producing an intergranular oxide which may be different in overall composition from the external scale. As time proceeds, the intergranular oxidation product at any given point may be consumed by the advancing external scale layer. Another effect of time which would be accelerated at high temperatures would be changes that might result in the O transport in the external scale due to its changing composition with time. Such changes could conceivably produce an oxide layer at the interface that grows principally by cation transport, thus reducing the free O ion concentration at the interface and preventing further grain boundary oxidation. On the other hand, however, an oxide layer that grows by principally cation transport, in steels at least, would imply a nonprotective type of scale, and under such conditions the scaling rate of the steel would become excessive.

Penetration Measurements

The technique by which the curves of number of intergranular cracks vs. depth below the oxide-metal interface were arrived at was explained in detail in the Procedure section of this report. The curves obtained by this method appear in Figs. 17 through 67. The basic type of penetration curve was found to be a curve which we have called a "decay" type, monotonically decreasing to zero fissures per in. with increasing depth. With increasing time and/or temperature, the mean depth of this curve tended to increase and a maximum in the curve tended to develop and move toward greater depths. The explanation for this behavior is twofold. First, the number of grain boundary sites for oxygen penetration is finite, and as the process continues, a state is reached where the existing penetration fissures have grown deep while relatively few new fissures are being formed. The second factor that tends to deplete the number of small fissures is the progressive surface oxidation.

The behavior of the 1900°F penetration curve for type 310 alloy, heat X11338, Run 16 (100hr) as shown in Fig. 51 should be mentioned. This specimen showed some very deep penetration, photomicrographs of which appear in Figs. 99, 107, and 108. A number of the fissures were of greater depth than the six-row grid used in making the count of the fissures, and were recorded only as being beyond the grid. When the data were assembled, an arbitrary group interval equal to that of the six regular groups was assigned to these fissures. Since there was an appreciable number of the fissures, the resulting curve has an abnormal shape. If the deep fissures were subdivided into groups, the curve would no doubt be of normal shape. Since this particular specimen was the only instance in which the shape of the curve was affected by the excessively deep penetration, it was not considered worth while to alter the routine of measurement.

In each metallographic mount, one untested specimen was included as a control. Originally, it was planned to use this control specimen to obtain a value of the original thickness, from which thicknesses of the tested specimens were to have been subtracted to obtain thickness losses. This proved to be impractical because of the small magnitude of the thickness losses, but it was found in the meantime that the control specimens gave an indication of the effect of surface roughness and of polishing on an otherwise undamaged surface. Surface irregularities gave rise to a background count of small artifacts on the control specimen which varied somewhat in different mounts from the same heat and were presumably indicative of the amount of error included in the fissure counts of the tested specimens. The fact that the penetration curves of some of the control specimens are the same order of magnitude as the curves for some tested specimens reflects the uncertainty in the count of the very small penetrations, as explained in the Procedure section. It is to be observed that the control penetration curves almost always decay at a rate much faster than tested specimens, which results from the fact that only rarely was anything seen on a control specimen that would be interpreted as being a fissure extending as deep as the second grid level.

The maximum fissure depths, except for the one specimen from heat X11338 previously referred to, were never found to be over 0.005 in. in depth, and usually were much less.

As is apparent from referring to Fig. 17 through 67, an analysis of the intergranular penetration characteristics of the alloys which was based on the detailed shapes of the penetration curves themselves would be a sprawling one which would be very difficult for the reader to assimilate. Therefore, the two parameters N, the penetration frequency, and X, the mean penetration depth, as referred to in the Procedure section, were adopted which summarize the essential features of the penetration curves. The behavior of these parameters with temperature are presented in Figs. 68 through 94.

In several early runs (Nos. 5, 6, 8, 9 and 13), the air velocity through the furnaces was varied and the duration of the runs was held constant at 100 hr. These runs are summarized in Figs. 68 and 69, 73 and 74, and 78 and 79 for the 309 + Nb alloy and heats 64177 and 64270 of type 310 alloy, respectively. Since the humidity was also a variable in these runs, the results are inconclusive, and the penetration data are included only for the sake of completeness. Run 7, and also Run 25, were discarded because of temperature control difficulties during the oxidation period.

One run, No. 9, was carried out to determine the effect of cold work prior to exposure. The penetration results appear in Figs. 70, 75, and 80. Cold work was introduced into the specimens by making a sharp angle bend in each specimen. After the specimens had been oxidized, quenched, mounted, and polished, penetration readings were made on the bent sections as well as the straight sections, the lengths of the bent sections being estimated by difference between the overall specimen length and the measured lengths of the straight sections. These results showed that there were fewer penetration fissures in the cold-worked areas, but that the penetration present was somewhat more severe than that in the straight sections. There was no catastrophic effect of the cold work, most of the residual stress having relaxed out

before appreciable oxidation occurred. The case of a continuously applied stress during the oxidation period would be a different matter, however, and would likely lead to substantial increases in the penetration depth.

The effect of time on penetration for the 309 + Nb, 64177, and 64270 alloys is presented in Figs. 71 and 72, 76 and 77, and 81 and 82. In general, the penetration became deeper and the fissures more numerous with time, although there was considerable overlapping. There does not appear to be any marked difference in the number of fissures occurring in the three alloys, and, if there is any difference in the penetration depth, it would be that the depth in the type 309 + Nb alloy is slightly less than in the two type 310 alloys.

Figs. 83 through 94 show the effect of time on the penetration in the remaining six heats of type 310 steel. Heat X11306 (Figs 83 and 84) showed severe penetration, both from the standpoint of number and depth of fissures. Of the other five heats, all showed penetration frequencies of the order of those of the 309 + Nb, 64177, and 64270 heats. Except for the previously-mentioned 1900°F specimen of heat X11338 from Run 16 (Fig. 85), penetration depths were all somewhat lower that those found in the 309 + Nb, 64177, and 64270 heats. Of the five heats, the penetration depth of heat X45558 was least by a narrow margin, with heat X46063 next best. This ranking is probably not significant, since the differences among these heats are of the order of the experimental error. It is also noteworthy that in the six alloys, the magnitudes of the penetration frequencies at a given temperature did not usually increase in the order of increasing times. In the case of the penetration depths, however, magnitudes at a given temperature did in general increase in the order of increasing times. The values obtained for penetration depths appear to be more significant than the values for penetration frequency, since the depths are not as strongly influenced by the uncertainty in the count of the smallest fissures.

Interface Movement Measurements

The results of the measurements of the metal interface movements with temperature after 100-hr oxidation treatments are reported in Table 12. The method by which these measurements were made was outlined in the Procedure section of this report. As the results in Table 12 show, measurements made on specimens which had a powdery gray black surface appeared to be low relative to the values that would have been expected on the basis of the specimens of light gray appearance, on which it was possible to remove all of the scale. Warr (10) gives oxidation attack rates for type 309 and type 310 steels, gathered from the literature. At 1600°, 1800°, 2000°, and 2200°F, these figures are 0.004, 0.02, 0.05, and 0.06 in./yr for type 309 steel and 0.007, 0.02, 0.03, and 0.05 in./yr. for type 310 steel. When these figures are recomputed for 100 hr oxidation time, the results are somewhat higher than the experimentally-measured figures presented in Table 12, but are of the same order of magnitude. The highest measured value was about 0.0003 in., and the highest calculated value (type 309 alloy at 2000°F) was about 0.0006 in. No measurements were made on 10- or 30-hr specimens, but they would be expected to show correspondingly smaller interface movements. The size of the interface movements after 100-hr oxidation explains the reason that it was not possible to obtain consistent data by subtraction of measured thicknesses from the thickness of a control specimen--the interface movements were too small. In view of the variability of the apparent

interface movements calculated from the loss in weight measurements, it was decided to present the penetration data relative to the existing metal-oxide interfaces, rather than to make any attempt to correct for the interface movement.

Visual and Magnetic Examination

The results of the visual examintaion of both the specimens and the oxide scales are presented in Tables 3 through 11. A key to the abbreviations used is supplied in Table 2. Where more than one appearance is recorded for a specimen, the abbreviations are ranked in descending order of the proportion of the surface having that appearance. Great variations in the visual appearance of specimens and scales were observed, and a fuller description of the more or less arbitrary classifications adopted for their systematization is in order.

Powdery gray black - This type of specimen surface appearance, when it constituted the majority of the specimen surface, was accompanied by small quantities of free scale loosened in quenching. Although it was possible to scrape some of the powdery oxide off the specimen, a tough, continuous, adherent film always remained which could not be removed without damage to the underlying metal.

Powdery gray black with orange substrate - If a specimen like that described above showed a red-orange color after scraping, it was given this classification. This color may have been partly due to Fe_2O_3, but in some cases, at least, was due to an interference film beneath the powdery gray black scale. The x-ray results are inconclusive on the former possibility.

Shiny gray black - This appearance was not found as often as the powdery gray black and appeared to be associated with oxidation times of 30 hr or less. The adherent scale causing this appearance was very thin and often discontinuous, showing smooth light gray areas beneath, and had almost a metallic sheen.

Black and scoriated - Occurrence of this appearance was unpredictable. Specimens having this appearance looked almost as though the oxide had once been liquid. The surfaces were checked, and individual segments of scale were plain and shiny. The scale was extremely dense, hard, and adherent.

Light gray - This type of appearance was associated with a loose, flaky scale which often came off entirely on quenching. The appearance of the specimen was a very smooth light gray.

Light gray with interference colors - Specimens of the preceding basic appearance often showed orange, blue, or magenta interference films in swirling patterns.

Light gray with black pits - In some cases, the light gray surface was pitted, the pits containing an adherent gray-black material. Often the light gray areas around the pits showed interference colors.

Black pits with light gray - This classification differs from the previous one in degree, the pits being the predominant feature.

Oxide appearances varied in color from metallic gray to dull black, and from fine powders to flakes sometimes almost as large as the specimen faces.

The magnetism of the specimens and the oxides varied from those with no detectable magnetism to one or two specimens in which the magnetism was sufficiently strong so that the specimens could be suspended from the magnet and a few oxide specimens which could be made to follow a magnet beneath the sheet of paper on which they rested in the same manner as iron filings. It was found that specimen magnetism was usually concomitant with scale magnetism. There was no definite segregation of magnetic components in the one to the exclusion of the other. It should be remembered that the presence of ferromagnetism does not necessarily imply the presence of body-centered iron, since all of the transition metals have appreciable values of saturation magnetization and a number of their oxides (ferrites) are also magnetic. The scale magnetism may in some cases be due to islands of Ni, but no such islands were observed metallographically, and in some cases, the finely-divided oxide appears to be magnetic in its own right. Scale magnetism is not in general due to the presence of the magnetic oxide of Fe, Fe_3O_4, since in no case was this oxide found by x-ray analysis (although not all of the oxide specimens were x-rayed). Strong specimen magnetism is associated to a degree with the occurrence of a light gray specimen surface.

In Table 12 are recorded the specimen and oxide appearances of three duplicate runs the purpose of which was to obtain weight loss data. These runs duplicate Runs 15, 16, and 17, and comparison with descriptions from these runs shows that there is considerable variability in the specimen and oxide appearances even in specimens which are as nearly duplicates as we could possibly make them. Furthermore, there seems to be little correlation of specimen and oxide appearance and magnetism with time or temperature of oxidation, or with scale composition as revealed by x-ray analysis. The only explanation of the visual and magnetic examination data presently at hand would be that they depend upon the rapidity with which the specimens are quenched from the high temperatures. Although in no case was the time between extraction of the specimen from the furnace and its submersion in the distilled water greater than 7 sec, it is true that some specimens stuck to the holding fixtures and had to be pried loose, which took more time than if the specimen did not stick.

X-Ray Diffraction

The scaling of high alloy steels has been extensively studied by a research group at Purdue University and their findings (1, 9, 10, 11) have proved most valuable in the interpretation of the x-ray powder patterns of scales which were obtained. For types 309 and 310 stainless steels, the Purdue group reports scales after 100 hr oxidation at temperatures from 1600° to 2200°F consisting of Cr_2O_3, rhombohedral solid solutions of Cr_2O_3 and Fe_2O_3 having complete solid solubility, and a spinel the lattice parameter of which varied from 8.310 to 8.330 kX in type 309 steel and from 8.323 to 8.429 kX in type 310 steel. The low-parameter spinel was identified as an Fe-Cr oxide, and the high-parameter spinel as an Mn-Cr oxide. Individual scales always contained the spinel except the type 309 alloy at 2200°F. All but a few of the scales contained one solid solution, and a few contained two solid solutions of differing compositions. Most of the scales contained either Cr_2O_3 or a solid solution high in Cr_2O_3. Type 310 scales were found to contain two layers.

The x-ray results obtained in the present program are presented as part of Tables 3 through 11, with a key to the symbols used being given in Table 2. Agreement with the above-noted findings is good in the sense that the compounds found were the same, the only exception being occurrence of Fe_2O_3 in this investigation. Since the accuracy in specifying the percentage composition of the Cr_2O_3-Fe_2O_3 solid solution was estimated to be about $\pm$ 10 atomic percent, compounds reported as being Fe_2O_3 may well have been the same as Fe_2O_3-rich solid solutions reported by the Purdue group. There were no clear trends of scale composition with time or temperature. It was found that the heats differed among themselves in the compositions of the scales formed under the same time and temperature conditions. Warr (10) reported similar behavior in duplicate specimens. Either Cr_2O_3 or a Cr_2O_3-rich solid solution was present in every scale analyzed. The spinel phase was widely distributed, and the lattice parameters of the spinel were 8.37 to 8.48 kX, with most of the values being from 8.41 to 8.43 kX. All of the scales analyzed were of the protective type, by Randall and Robb's criteria of the presence of Cr_2O_3 and high-parameter spinel. This includes the scales found on heat X11306, which showed much more severe penetration than the rest of the heats. It was observed that the two type 310 heats in which penetration was slightly less deep than the rest, heats X45558 and X46063, seemed to show less tendency towards Fe_2O_3 or solid solutions in their scales than the other heats. It seems likely that, since all of the scales were protective, not much improvement in penetration resistance can be hoped for by making small changes in the alloy compositions in order to obtain an exceptionally protective scale.

Metallographic Examination

The results of the metallographic examination of the specimens following testing are presented in Table 13, and include, in addition to penetration appearance, changes in micro-structure which took place in the alloys during the oxidation cycles. For convenience in presenting the data, the metallographic appearances of the intergranular penetration encountered were classified in seven arbitrary groups. Examples of six of these groups appear in Figs. 95 through 100. Type 0, which consisted of penetration fissures so small that they could not be definitely typed as belonging to any of the other six groups, was omitted. Referring to Table 13, the very shallow Type 0 penetration was found at low temperatures of oxidation, 1600°F and sometimes 1700°F after 100-hr exposure. At the other extreme, Type VI penetration (Fig. 100) occurred at the highest temperature, 2000°F, especially at the longer times. Type VI, which we have called "coalesced web" penetration, is characterized by a coalescence of the intergranular oxide into discrete particles spaced along the grain boundaries. This effect is doubtless the result of relatively high atomic mobility at the high temperature. At intermediate temperatures, there is considerable variation in the precise appearance of the penetration. Some heats, notably heats 64177 and X46063, show Type III penetration consistently, a rough-edged web. The other heat show no specific trends, and there were no penetration characteristics that could be associated with composition. Figs. 101 and 102 show the typical appearance of the subsurface metal associated with penetration. In all of the heats except heat 64177, which showed penetration in the as-received condition (see Figs. 12 and 13), the specimen surfaces were initially smooth, and etching (Fig. 101) revealed the grain boundaries extending all the way to the surface. After oxidation, the etched structures resembled Fig. 102. As far as could be seen, penetration took place along grain boundaries, but not along twin boundaries. A prominent characteristic was the

occurrence of a layer in which no structure was revealed between the surface and a point beyond the ends of the visible penetration fissures. This layer gives the appearance of having an altered composition from that of the original alloy. The region is likely high in oxygen content, though not high enough for oxide formation. Consequently, there is a possibility that the layer is decarburized. Furthermore, since no Ni was observed in the scales, the region may be Ni-rich. Below the subsurface layer, the typical grain structure and carbide precipitation were observed.

Figs 103 through 106 show the appearance of heat X11306 in the etched condition after oxidation. Heat X11306 behaved in a unique manner in two respects: its penetration was far greater, both in depth and number of fissures, than any of the other alloys; and its metallographic appearance differed from that of the other heats. Large quantities of precipitate appeared throughout the matrix following testing which could be observed without etching. It was also interesting to note that recognizable penetration fissures disappeared after 100 hr at 2000°F, as shown in Fig. 105, but were still present after 10 hr at the same temperature and at all times at lower temperatures.

Another example of penetration which looked unusual was the penetration occurring in the 100-hr specimen from heat X11338 tested at 1900°F, which was abnormally deep and of the developed web type. Photomicrographs of this specimen appear in Figs. 99, 107, and 108. Characteristics of the penetration included the presence of islands of intergranular material. Small particles also appeared in the metal adjacent to the intergranular islands, and seemed to be associated with them. More general matrix precipitation was revealed by etching. No explanation can be offered at this time for the occurrence of this unique type of penetration in this particular specimen and, to a lesser extent, in the specimen of the same heat tested for the same time at 2000°F.

In the heat X45558 specimen tested for 100 hr at 2000°F, several examples of a deep pit type of penetration were noted, as shown in Fig. 109. This type of attack may only represent points where grains had fallen out as a result of being encircled by oxide, and in any event, does not appear to be of great significance, since these pits were not abnormally deep.

Several other structural features were observed which it would be appropriate to note here, although it is not known whether they have any appreciable effect on the penetration. The first two of these are the occurrence of delta ferrite and sigma phase. The temperatures at which these constituents were observed are tabulated in Table 13. Identification was made by means of Murakami's reagent. This reagent, when used concentrated, as described by Burgess and Forgeng (21), colors sigma light blue and ferrite yellow. Representative photomicrographs are presented in Figs. 110 and 111. It appears that all of the heats tested were subject to one or the other of these constituents, but that there was only one instance (heat 64177) where even a tentative identification of both constituents could be made in the same heat. Neither of these constituents was found in the region near the metal surface in any case, but tended to occur throughout the remainder of the cross section. No features of the observed penetration could be related to the presence of either delta ferrite of sigma phase.

A check was made to determine the effects of the 30-hr oxidation treatments on the grain sizes and carbide distributions in the alloys. An electrolytic chromic acid etching treatment was used, and the results appear in Table 13. On series of

specimens oxidized for 100 hr, heat X11338, was etched to reveal grain size, and representative photomicrographs at 1600° and 1900°F appear in Figs. 112 and 113 at 250X. Reference is also made to the as-received structure as shown in Fig. 5 at 100X. The appearance of the specimens at 1700° and 1800°F was the same as at 1600°F, but at 1900°F, agglomeration and probably some solution of the carbides was noted, along with a slight increase in grain size. At 2000°F, grain boundaries could not be revealed by the electrolytic chromic acid etching treatment. This is taken as meaning that all of the carbides in the grain boundaries had gone into solution. Precipitation, agglomeration, and re-solution of carbide with increasing temperature was the typical behavior of all the materials. The temperature at which the grain boundaries could no longer be distinguished varied somewhat, and was lowest in heat X11306 by some 200°F. As the photomicrographs show, however, (Figs. 103-106) a second phase in the matrix remained. It was true in all of the heats that all of the second phase or phases did not go into solution within the 100-hr period.

Fig. 114, taken using oblique light, shows in a striking manner the distinct surface metal layer mentioned previously. In fact, a second intermediate layer etching darker than the matrix is also apparently present. The increased thickness of the surface layer in the vicinity of a grain boundary is also clearly visible, though the grain boundary itself is not visible for some distance further back into the metal. This photomicrograph illustrates the greater activity of the grain boundary relative to the bulk of the material even prior to the formation of a penetration fissure in the boundary.

When certain of the specimens were originally etched in chromic acid, a structure was developed consisting of many long parallel stringers which appeared black under the microscope. Examination under oblique light at high magnification revealed that these stringers were troughs gouged in the metal surface by severe overetching. When the specimens were repolished and etched using a very low current density, a structure consisting of bands of carbide particles was revealed. Careful etching of the as-received heat X45558 and examination under oblique light showed the existence of depressions (Fig. 115), accompanied by several pits along the depressions where particles had etched out. These depressions are interpreted as being concentration gradients in the matrix. Following exposure for 10 hr at 1600°F, carbide particles had precipitated as shown in Fig. 116, and the depressions no longer appeared on etching. Figs. 117 and 118, taken at lower magnification, show that the bands of carbides were sometimes associated with a refinement in grain size, and sometimes not. It was observed that the bands tended to disappear, presumably by diffusion, with increasing time and/or temperature. Cross section specimens from all nine of the heats were examined to determine whether banding could be observed. A second series of cross section specimens at right angles to the first series were prepared and examined, since it was believed that the stringers would lie in the rolling direction and would hence be revealed in one series of specimens or the other if they were present at all. Results of this examination appear in Table 13. The particles are identified as being carbides because the bands were not found near the surfaces on the oxidized specimens. It was reasoned that, if the particles were either oxides or nitrides, they would tend to be concentrated at the surface, rather than away from it. No penetration effects were observed that could by attributed to the presence of the carbide bands.

SUMMARY AND CONCLUSIONS

1. Specimens from eight heats of type 310 stainless steel and one heat of type 309 stainless steel were oxidized in moving air at temperatures of 1600°, 1700°, 1800°, 1900°, and 2000°F for times of 10, 30, and 100 hr. Following the oxidation periods, specimens were quenched into distilled water.

2. Visual and magnetic examinations were made on the oxidized specimens and the oxide scales. It was found that the visual and magnetic characteristics of the specimens and scales had no relation to the resistance of the alloys to intergranular penetration or to the composition of the scales.

3. Specimens were mounted and metallographically polished, and counts of the number and depth of the intergranular fissures were made on each specimen. Curves were constructed plotting number of fissures vs. depth. For the purpose of analysis of the data, these curves were described in terms of two parameters, N and X, the total number of fissures and the mean depth of fissures. It was found that N was not a particularly useful parameter, due largely to uncertainty in the numbers of very shallow fissures. The parameter X was less affected by this uncertainty, however, and it was determined that the depth of the penetration fissures increased with time and with temperature. In addition, there was no appreciable difference in penetration characteristics among the heats tested, except in heat X11306. Since the heats were selected to show a wide spread in the percentages of alloying elements within the specification limits, it can be concluded that minor modifications in alloy content have no effect on intergranular penetration. There was no appreciable difference between the depth of penetration in the type 309 + Nb alloy and the type 310 alloys.

4. Measurements were made of the rate of external scaling, or volume oxidation. These measurements showed the rates of scaling to be small and of the order of those reported by other investigators for the 25%Cr-20%Ni analysis, and can be expressed as a recession of the metal surface amounting to 0.0005 in. or less per 100 hr.

5. X-ray powder patterns were taken for many of the oxide scales. Phases composing the scales always included Cr_2O_3 or a solid solution of Cr_2O_3 and Fe_2O_3. Most of the scales also contained a high-parameter spinel (8.43 kX) believed to be essentially $MnCr_2O_4$. No separate phases identifiable as containing Ni were observed in the scales by x-ray diffraction, nor was Ni found to be present by qualitative chemical analysis of a limited number of specimens of scale. All of the scales analyzed can be classified as being protective, since they contained Cr_2O_3, and there is little chance therefore, that minor compositional changes would result in scales which would give better resistance to intergranular penetration. This is in agreement with the conclusions reached on the basis of the measurements of penetration depths.

6. The effect of prior cold working was to increase slightly the depth of the intergranular fissures. The conclusion is drawn that severe stressing of the metal is not particularly harmful provided that this stressing is done at temperatures below those at which oxidation of the steel takes place and that the stressing is discontinued before elevating the temperature.

BIBLIOGRAPHY

1. Yearian, H. J. and Radavich, J. F., Dept of Physics, Purdue University, Unpublished data.

2. Taylor, A. and Sinclair, H. B., Proc. Phys. Soc. 57 (1945), 126.

3. Henry, N. F. M., Lipson, H., and Wooster, W. A. The Interpretation of X-Ray Diffraction Photographs , Macmillan, 1951 (London).

4. Upthegrove, C. and Murphy, D. W., Trans. Amer. Soc. Steel Treat., 21 (1933), 93.

5. Siebert, C. A. and Upthegrove, C., Trans. Amer. Soc. Metals, 23 (1935), 187.

6. Kubaschewski, O. and Hopkins, B. E., Oxidation of Metals and Alloys , Academic Press, 1953 (New York).

7. Davies, M. H., Simnad, M. T., and Birchenall, C. E., Trans. Amer. Inst. Metall. Engrs., 191 (1951), 889 and J. Met. 5 (1953), 1250.

8. Hickman, J. W. and Gulbransen, E. A., Trans. Electrochem. Soc. 91 (1947), 605.

9. Boren, H. E., Jr., M. S. Thesis, Dept. of Physics, Purdue University, August,1950.

10. Warr, R. E., M. S. Thesis, Dept. of Physics, Purdue University, August, 1951.

11. Radavich, J. F., Ph. D. Thesis, Dept. of Physics, Purdue University, May, 1953.

12. Hauffe, K. and Block, J., Z. Phys. Chem., 198 (1951), 232.

13. Lustman, B., in Amer. Soc. Metals, Metals Handbook, 1948 ed., 223.

14. Randall, E. C., M. S. Thesis, Dept of Physics, Purdue University, 1950. Robb, P. F., Dept. of Physics, Purdue University, Unpublished research.

15. Turnbull, D., in Amer. Soc. Metals, Atom Movements , 1951, 129.

16. Yukawa, S. and Sinnott, M. J., Dept. of Chem. and Metall. Engrs., University of Michigan, Unpublished research.

17. Baeyertz, M., Trans. Amer. Soc. Metals, 24 (1936), 420.

18. Gulbransen, E. A., Phelps, R. T., and Hickman, J. W., Ind. Eng. Chem. (Anal. Ed.), 18 (1946), 391.

19. Gulbransen, E. A. and McMillan, W. R., Ind. Eng. Chem. 45 (1953), 1734.

20. Radavich, J. F. and Yearian, H. J., Dept. of Physics, Purdue University, Undated report.

21. Longo, T. A., M. S. Thesis, Dept. of Physics, Purdue University, August, 1953.

22. McCullough, H. M., Fontana, M. G., and Beck, F. H., Trans. Amer. Soc. Metals 43 (1951), 404.

23. Burgess, C. O. and Forgeng, W. D., Trans. Amer. Inst. Metall. Engrs. 131 (1938), 277.

TABLE 1

COMPOSITION OF STAINLESS STEEL STOCK, WEIGHT PERCENT

Heat No.	C	Ni	Cr	Si	Mn	P	S	Mo	Cu	Co	W	Nb
309 + Nb	0.08	15.39	22.64	0.46	2.31	0.012	0.008	-	-	-	-	0.82
64177	0.13	16.96	24.03	0.55	0.42	0.018	0.008	0.033	0.13	0.01	<0.01	-
64270	0.12	19.14	22.30	0.43	0.50	0.025	0.008	0.042	0.10	0.01	<0.01	-
X11306	0.07	20.33	25.48	0.78	1.41	0.023	0.013	-	-	-	-	-
X11338	0.085	20.08	24.28	0.83	1.53	0.029	0.029	0.14	0.25	-	-	-
X27258	0.073	20.81	24.64	0.75	1.58	0.025	0.008	0.15	0.30	-	-	-
X45558	0.069	21.56	24.71	0.58	1.54	0.025	0.011	0.12	0.27	-	-	-
X46063	0.059	20.67	24.28	0.31	1.57	0.024	0.014	0.12	0.25	-	-	-
X46572	0.089	19.48	24.35	0.67	1.60	0.021	0.022	0.14	0.34	-	-	-

TABLE 2

EXPLANATION OF SYMBOLS USED IN OXIDATION DATA TABULATIONS

SPECIMEN APPEARANCE:

PGB	- Powdery gray black
PGB w/ OS	- Powdery gray black with orange substrate
SGB	- Shiny gray black
B and S	- Black and scoriated
BP w/ LG	- Black pits with light gray surface (mostly pits)
LG	- Light gray surface
LG w/ BP	- Light gray with black pits (mostly light gray)
LG w/ IC	- Light gray with interference colors

MAGNETISM:

ND	- Not detectable
W	- Weak
M	- Medium
S	- Strong

OXIDE APPEARANCE:

Quantity:

N	- None
S	- Small amount
M	- Medium amount
L	- Large amount

Flake Size:

P	- Powder
SF	- Small flake (<1/32 in.)
MF	- Medium flake (1/32 - 1/8 in.)
LF	- Large flake (>1/8 in.)

Color:

G	- Gray
B	- Black
GB	- Gray-black

OXIDE COMPOSITION:

S.S. xQ	- Cr_2O_3- Fe_2O_3 solid solution with Q $\pm$ 10 atomic percent Cr_2O_3
HPS	- High-parameter spinel
a = p	- Lattice parameter of spinel in kX units
*	- Lattice parameter determined from two-point extrapolation
Insuf.	- Insufficient oxide for x-ray pattern
W	- Weak pattern
M	- Medium pattern
S	- Strong pattern

TABLE 3

RESULTS OF OXIDATION TESTS, TYPE 309 + Nb ALLOY

0.08% C, 15.39% Ni, 22.64% Cr, 0.82% Nb, 0.46% Si, 2.31% Mn, 0.012% P, 0.008% S

Run No.	Duration, hr	Air Velocity, ft/min	Dew-point, °F	Penetration Curve, Fig. No.	Temp., °F	Specimen				Oxide Scale				
						Appearance	Magnetism	No. of Fissures/in.	Mean Fissure Depth, in.x10^3	Amount	Color	Flake Size	Magnetism	Composition (x-ray)
5	100	40	< -20	17	1600	LG w/ BP LG w/ IC	-	222.1	0.433	M	GB	SF	ND	-
					1700	PGB LG w/ IC	-	1011.1	0.692	L	G	LF	ND	-
					1800	PGB LG w/ IC	-	699.8	1.523	M	GB	LF	ND	-
					1900	LG w/ IC	-	719.0	1.700	L	B	MF	M	-
6	100	20	-	20	1600	LG w/ IC	-	96.0	0.332	M	GB	MF	ND	-
					1700	LG w/ IC	-	480.9	0.368	M	GB	LF	ND	-
					1800	LG w/ BP	-	723.3	0.403	S	GB	MF	M	-
					1900	PGB LG	-	869.1	1.307	S	GB	P	M	-
8	100	30	from +15 to +20	23	1600	LG w/ BP LG	-	435.9	0.371	M	B	P	ND	-
					1700	B and S	-	423.3	0.344	L	GB	MF	M	-
					1800	B and S PGB	-	321.6	0.486	L	GB	MF	M	-
					1900	LG w/ IC	-	386.8	1.117	L	GB	MF	M	-
								Straight Section						
9	100	30	from <-60 to -30	26	1600	PGB	-	611.4	0.544	S	GB	P	M	-
					1700	PGB LG	-	547.5	0.513	S	GB	P	M	-
					1800	LG LG w/ IC	-	837.8	0.936	S	GB	MF	M	-
					1900	LG	-	852.6	1.499	L	GB	MF	S	-
								Curved Section						
				29	1600	-	-	376.9	0.683	-	-	-	-	-
					1700	-	-	553.3	0.727	-	-	-	-	-
					1800	-	-	438.6	1.605	-	-	-	-	-
					1900	-	-	623.0	1.319	-	-	-	-	-
10	50	30	from -45 to +10	32	Control	-	-	280.6	0.343	-	-	-	-	-
					1600	BP w/ LG PGB	M	938.0	0.459	M	GB	P-SF	M	-
					1700	PGB LG w/ IC	M	772.2	0.774	L	GB	MF	ND	-
					1800	LG w/ IC	S	1016.0	0.369	L	GB	LF	M	-
					1900	LG w/ IC	S	859.6	0.572	L	G	LF	M	-
11	30	30	from -45 to -22	35	Control	-	-	1066.1	0.361	-	-	-	-	-
					1600	PGB LG w/ BP	-	862.4	0.408	S	B	P	ND	Insuf.
					1700	LG w/ BP PGB	-	1288.0	0.487	S	B	P-SF	M	Insuf.
					1800	LG w/ IC LG w/ BP	-	1023.4	0.455	L	GB	MF	S	Cr_2O_3(S) Fe_2O_3(M) HPS(W)
					1900	LG w/ IC LG w/ BP	-	1071.6	0.567	L	GB	MF	S	Cr_2O_3(S) Fe_2O_3(W) HPS(W) a=8.43*
12	10	30	from -22 to -16	38	Control	-	-	274.1	0.320	-	-	-	-	-
					1600	PGB LG w/IC	W	318.8	0.320	S	B	SF	W	Insuf.
					1700	PGB PGB	W	818.4	0.323	S	B	P	ND	Insuf.
					1800	BP w/ LG LG	M	900.6	0.330	M	GB	P-SF	S	Cr_2O_3(S) Fe_2O_3(M) HPS(M)
					1900	LG w/ BP PGB	M	719.6	0.365	M	B	P-SF	M	S.S.x50
13	100	40	from -30 to +20	41	Control	-	-	113.0	0.320	-	-	-	-	-
					1600	LG w/ IC BP w/ LG LG w/ BP PGB w/ OS	ND	785.4	0.336	L	B	SF	ND	-
					1700	SGB BP w/ LG LG w/ BP	M	831.4	0.336	L	G	MF	S	-
					1800	LG w/ IC LG w/ BP	M	778.3	0.580	L	G	LF	S	-
					1900	LG w/ IC	M	775.7	0.449	L	G	LF	S	-
14	77	30	from -45 to -35	44	Control	-	-	340.3	0.329	-	-	-	-	-
					1600	LG w/ BP B and S PGB	W	409.4	0.334	S	B	P	M	-
					1700	LG w/ BP PGB B and S	W	949.0	0.328	S	B	P	M	-
					1800	PGB B and S LG w/ IC BP w/ LG	W	1125.7	0.510	M	GB	P-SF	W	-
					1900	B and S PGB BP w/ LG	M	851.2	0.843	L	GB	P-SF	S	-
15	100	30	from -55 to -40	47	Control	-	-	146.6	0.339	-	-	-	-	-
					1600	LG w/ IC LG w/ BP	S	1218.6	0.372	L	B	LF	ND	Cr_2O_3(S) HPS(S)
					1700	BP w/ LG	M	1242.6	0.363	S	B	P	M	Cr_2O_3(S) Fe_2O_3(S) HPS(W)
					1800	LG w/ IC	S	475.2	0.529	L	G	LF	S	Cr_2O_3(S) Fe_2O_3(M) HPS(M) a=8.43*
					1900	LG w/ IC	M	504.5	0.496	L	G	LF	S	Cr_2O_3(S) Fe_2O_3(M) HPS(M) a=8.45*
26	10	30	-38	38	2000	PGB LG LG w/ IC	S	1456.2	0.562	M	GB	MF	S	-
27	30	30	from -46 to -38	35	2000	PGB w/ OS BP w/ LG PGB	M	1100.6	0.686	S	B	P	M	-

TABLE 4

RESULTS OF OXIDATION TESTS, TYPE 310 ALLOY, HEAT 64177

0.13% C, 16.96% Ni, 24.03% Cr, 0.55% Si, 0.42% Mn, 0.018% P, 0.008% S, 0.033% Mo, 0.13% Cu, 0.01% Co, <0.01% W

Run No.	Duration, hr	Air Velocity, ft/min	Dew-point, °F	Penetration Curve, Fig. No.	Temp., °F	Specimen				Oxide Scale				
						Appearance	Magnetism	No. of Fissures/in.	Mean Fissure Depth, in.x10^3	Amount	Color	Flake Size	Magnetism	Composition (x-ray)
5	100	40	<-20	18	1600	PGB	-	530.7	0.836	M	GB	P-SF	W	-
					1700	PGB	-	222.6	0.817	S	GB	P	S	-
					1800	PGB	-	130.9	0.630	M	GB	P-SF	ND	-
					1900	BP w/ LG	-	536.6	0.856	S	GB	P	ND	-
6	100	20	-	21	1600	PGB w/ OS	-	341.6	0.743	S	GB	P	ND	-
					1700	PGB w/ OS	-	451.5	0.730	S	GB	P	ND	-
					1800	PGB w/ OS	-	495.6	0.705	S	GB	P	W	-
					1900	PGB LG	-	440.0	0.703	S	GB	P	ND	-
8	100	30	from +15 to +20	24	1600	PGB LG w/ BP	-	438.4	0.749	S	GB	P	M	-
					1700	PGB	-	470.5	0.752	S	B	P	M	-
					1800	LG w/ BP	-	435.2	0.983	M	GB	MF	M	-
					1900	LG w/ BP LG w/ IC	-	280.4	0.730	S	B	P	M	-
						Straight Section								
9	100	30	from <-60 to -30	27	1600	PGB	-	421.2	0.773	M	B	P	M	-
					1700	PGB	-	356.2	0.883	S	B	P	M	-
					1800	PGB	-	443.2	0.771	S	B	P	W	-
					1900	PGB	-	461.7	0.709	S	GB	P	M	-
						Curved Section								
				30	1600	-	-	194.5	1.032	-	-	-	-	-
					1700	-	-	205.5	0.723	-	-	-	-	-
					1800	-	-	227.6	0.931	-	-	-	-	-
					1900	-	-	180.2	0.823	-	-	-	-	-
10	50	30	from -45 to +10	33	Control	-	-	525.7	0.455	-	-	-	-	-
					1600	PGB BP w/ LG	ND	589.0	0.770	S	B	P	ND	-
					1700	PGB BP w/ LG	ND	675.6	0.697	S	B	P-SF	M	-
					1800	PGB LG w/ IC	ND	662.9	0.740	M	GB	P-SF	S	-
					1900	BP w/ LG PGB	ND	883.9	0.812	S	B	P	M	-
11	30	30	from -45 to -22	36	Control	-	-	460.2	0.547	-	-	-	-	-
					1600	BP w/ LG PGB	-	757.0	0.548	S	B	P	ND	Insuf.
					1700	PGB BP w/ LG	-	1004.2	0.556	S	B	P	M	Insuf.
					1800	BP w/ LG	-	666.4	0.341	S	B	P	ND	Insuf.
					1900	BP w/ LG	-	882.1	0.505	S	B	P	ND	Insuf.
12	10	30	from -22 to -16	39	Control	-	-	447.6	0.428	-	-	-	-	-
					1600	PGB w/ OS LG	ND	490.9	0.563	S	B	SF	W	Insuf.
					1700	PGB LG w/ BP BP w/ LG	ND	548.5	0.531	S	B	P	M	Insuf.
					1800	LG w/ BP LG w/ IC	ND	572.7	0.538	M	B	P-SF	S	S.S.x50(S) S.S.x25(W)
					1900	PGB PGB LG w/BP LG w/ IC	ND	655.2	0.586	M	B	P-SF	S	Cr_2O_3 (S) Fe_2O_3 (M) HPS (M) a = 8.42*
13	100	40	from -30 to +20	42	Control	-	-	608.3	0.468	-	-	-	-	-
					1600	PGB w/ OS BP w/ LG	ND	1099.1	0.528	S	B	P	M	-
					1700	PGB w/ OS	ND	1076.6	0.547	S	B	P	M	-
					1800	PGB w/ OS BP w/ LG LG w/ IC	ND	991.5	0.787	M	GB	P-SF	M	-
					1900	PGB w/ OS LG w/ BP	ND	1222.3	0.698	L	B	SF	M	-
14	77	30	from -45 to -35	45	Control	-	-	217.8	0.408	-	-	-	-	-
					1600	PGB BP w/ LG	M	544.0	0.683	S	B	P	W	-
					1700	PGB	W	822.1	0.564	S	B	P	M	-
					1800	BP w/ LG PGB	W	625.2	0.648	S	B	P	M	-
					1900	BP w/ LG PGB	W	671.6	0.652	S	B	P	M	-
15	100	30	from -55 to -40	48	Control	-	-	634.6	0.537	-	-	-	-	-
					1600	PGB	M	895.6	0.710	S	B	P	M	Cr_2O_3
					1700	PGB	M	1147.5	0.802	S	B	P	M	Insuf.
					1800	PGB BP w/ LG	W	1275.0	0.842	S	B	P	M	S.S.x50
					1900	BP w/ LG	M	1283.9	0.766	M	B	P	M	S.S.x50
26	10	30	-38	39	2000	PGB	M	980.2	0.606	S	B	P	M	-
27	30	30	from -46 to -38	36	2000	LG w/ IC B and S	S	1281.3	0.774	L	G	M	S	-

TABLE 5

RESULTS OF OXIDATION TESTS, TYPE 310 ALLOY, HEAT 64270

0.12% C, 19.14% Ni, 22.30% Cr, 0.43% Si, 0.50% Mn, 0.025% P, 0.008% S, 0.042% Mo, 0.10% Cu, 0.01% Co, < 0.01% W

Run No.	Duration, hr	Air Velocity, ft/min	Dew-point, °F	Penetration Curve, Fig. No.	Temp., °F	Specimen				Oxide Scale				
						Appearance	Magnetism	No. of Fissures/in.	Mean Fissure Depth, in.x10³	Amount	Color	Flake Size	Magnetism	Composition (x-ray)
5	100	40	<-20	19	Control	-	-	56.2	0.508	-	-	-	-	-
					1600	PGB	-	269.4	0.605	S	B	P	ND	-
					1700	PGB LG	-	295.3	0.573	L	GB	P-SF	M	-
					1800	LG w/IC PGB LG w/IC	-	147.3	0.593	S	GB	P-SF	ND	-
					1900	LG w/BP	-	131.4	0.666	S	B	P	ND	-
6	100	20	-	22	1600	PGB w/OS	-	225.9	0.386	S	GB	P	W	-
					1700	PGB w/OS	-	370.4	0.439	S	GB	P-SF	S	-
					1800	PGB w/OS	-	323.8	1.127	S	GB	P	ND	-
					1900	PGB w/OS	-	223.3	1.063	S	GB	P	W	-
8	100	30	from +15 to + 20	25	1600	PGB	-	328.0	0.387	S	GB	P-SF	M	-
					1700	PGB	-	373.2	0.345	S	B	P	M	-
					1800	PGB	-	460.6	0.411	S	B	P	M	-
					1900	PGB LG w/BP PGB w/OS	-	232.0	0.416	S	B	P	M	-
9	100	30	from <-60 to -30	28				Straight Section						
					1600	PGB	-	216.0	0.370	S	GB	P	M	-
					1700	PGB	-	350.3	0.431	S	B	P	M	-
					1800	PGB	-	284.1	0.469	M	B	P	M	-
					1900	PGB	-	305.6	0.503	M	B	P	M	-
								Curved Section						
				31	1600	-	-	68.8	0.389	-	-	-	-	-
					1700	-	-	109.5	0.808	-	-	-	-	-
					1800	-	-	93.1	0.511	-	-	-	-	-
					1900	-	-	108.9	0.511	-	-	-	-	-
10	50	30	from -45 to +10	34	Control	-	-	442.3	0.336	-	-	-	-	-
					1600	PGB PGB	ND	500.4	0.390	S	B	P	S	-
					1700	BP w/LG LG w/IC B and S	ND	445.4	0.482	M	B	P-SF	S	-
					1800	BP w/LG LG w/IC	ND	604.7	0.808	L	B	P-SF	S	-
					1900	PGB	ND	784.3	0.615	L	B	P-SF	S	-
11	30	30	from -45 to -22	37	Control	-	-	106.0	0.351	-	-	-	-	-
					1600	PGB BP w/LG LG w/IC	-	533.4	0.332	S	B	P	M	Cr_2O_3
					1700	PGB LG w/IC	-	579.2	0.359	S	B	P-SF	M	Insuf.
					1800	PGB BP w/LG	-	597.0	0.485	S	B	P-SF	S	Insuf.
					1900	LG w/IC BP w/LG	-	791.3	0.777	M	B	P-SF	S	Insuf.
12	10	30	from -22 to -16	40	Control	-	-	242.4	0.324	-	-	-	-	-
					1600	PGB w/OS BP w/LG	W	457.9	0.345	S	B	P-SF	M	Insuf.
					1700	PGB BP w/LG	ND	453.3	0.373	S	B	P	W	Insuf.
					1800	PGB LG	ND	945.0	0.359	S	GB	SF	W	Insuf.
					1900	PGB LG	W	845.0	0.376	M	B	P-SF	M	S.S.x50
13	100	40	from -30 to +20	43	Control	-	-	380.0	0.328	-	-	-	-	-
					1600	PGB w/OS	ND	660.1	0.355	S	B	SF	M	-
					1700	PGB w/OS LG	ND	739.4	0.430	M	B	P	M	-
					1800	PGB w/OS B and S LG w/BP	ND	769.1	0.509	M	B	P	M	-
					1900	LG w/IC B and S PGB w/OS	W	967.5	0.603	L	B	P-SF	M	-
14	77	30	from -45 to -35	46	Control	-	-	361.9	0.323	-	-	-	-	-
					1600	PGB	W	940.2	0.369	S	B	P	M	-
					1700	PGB	M	986.4	0.362	S	B	P	M	-
					1800	PGB LG w/IC	W	870.2	0.499	S	B	P	M	-
					1900	PGB BP w/LG	ND	1104.1	0.426	S	B	P	M	-
15	100	30	from -55 to -40	49	Control	-	-	354.1	0.325	-	-	-	-	-
					1600	PGB	M	621.0	0.374	S	B	P	M	S.S.x50
					1700	LG LG B and S	S	752.0	0.784	L	B	M	S	S.S.x50(S) Cr_2O_3(M)
					1800	PGB	M	927.9	0.508	S	B	P	M	Cr_2O_3(S) HPS (W)
					1900	BP w/LG PGB	W	1154.7	0.512	M	B	P	W	S.S.x50(S) Fe_2O_3?(W)
26	10	30	-38	40	2000	PGB B and S	W	438.2	0.467	S	B	P	M	-
27	30	30	from -46 to -38	37	2000	BP w/LG PGB w/OS B and S	M	1411.8	0.794	S	B	P	S	-

TABLE 6

RESULTS OF OXIDATION TESTS, TYPE 310 ALLOY, HEAT X11306

0.07% C, 20.33% Ni, 25.48% Cr, 0.78% Si, 1.41% Mn, 0.023% P, 0.013% S

Run No.	Duration, hr	Air Velocity, ft/min	Dew-point, °F	Penetration Curve, Fig. No.	Temp., °F	Specimen				Oxide Scale				
						Appearance	Magnetism	No. of Fissures/in.	Mean Fissure Depth, in.x10^3	Amount	Color	Flake Size	Magnetism	Composition (x-ray)
16	100	30	from -52 to -42	50	Control	-	-	318.0	0.326	-	-	-	-	-
					1600	LG w/ BP	S	1106.1	0.421	M	B	P-SF	ND	Cr_2O_3(S) Fe_2O_3(M) HPS (M)
					1700	LG w/ BP	S	620.0	1.360	L	G	MF	ND	Cr_2O_3(S) S.S.x25(M) HPS (M) a=8.48*
					1800	LG w/ IC	W	631.6	1.631	L	G	LF	ND	Cr_2O_3(S) HPS (S) a=8.42
					1900	PGB w/ OS BP w/ LG B and S	W	1791.0	2.099	M	B	P	ND	HPS (S) a=8.42 Cr_2O_3(M)
21	30	30	from -50 to -42	56	Control	-	-	219.6	0.322	-	-	-	-	-
					1600	SGB	M	1393.3	0.407	S	B	P	M	Insuf.
					1700	LG w/ IC LG w/ BP	M	600.0	0.456	M	GB	SF	W	S.S.x75(S) HPS (M)
					1800	PGB w/ OS	M	1340.0	0.921	S	B	P	M	Cr_2O_3(S) HPS (M)
					1900	LG w/ BP LG w/ IC	M	1305.8	1.585	M	B	P-SF	ND	Cr_2O_3(S) HPS (M) a=8.44*
24	10	30	from -52 to -44	65	Control	-	-	178.8	0.323	-	-	-	-	-
					1600	LG LG w/ BP PGB LG w/ IC	M	548.0	0.343	M	B	P-SF	M	-
					1700	LG w/ IC LG w/ BP	W	667.5	0.641	M	GB	P-MF	M	-
					1800	LG w/ IC LG w/ BP	M	1031.2	0.839	M	B	P-SF	M	-
					1900	LG w/ IC LG w/ BP	M	1148.8	1.247	M	B	P-SF	W	-
26	10	30	-38	65	2000	PGB	M	2590.5	0.716	S	B	P	W	-
27	30	30	from -46 to -38	56	2000	BP w/ LG B and S	M	2589.7	0.998	M	B	P-SF	S	-
28	100	30	from -50 to -40	50	2000	BP w/ LG	M	2134.5	0.962	S	B	P	M	-

TABLE 7

RESULTS OF OXIDATION TESTS, TYPE 310 ALLOY, HEAT X11338

0.085% C, 20.08% Ni, 24.28% Cr, 0.83% Si, 1.53% Mn, 0.029% P, 0.029% S, 0.25% Cu, 0.14% Mo

Run No.	Duration, hr	Air Velocity, ft/min	Dew-point, °F	Penetration Curve, Fig. No.	Temp., °F	Specimen				Oxide Scale				
						Appearance	Magnetism	No. of Fissures/in.	Mean Fissure Depth, in.x10^3	Amount	Color	Flake Size	Magnetism	Composition (x-ray)
16	100	30	from -52 to -42	51	Control	-	-	363.6	0.404	-	-	-	-	-
					1600	BP w/ LG PGB LG	M	592.1	0.381	M	GB	M	ND	S.S.x75(S) HPS(M) a=8.37*
					1700	LG w/ IC	M	363.3	0.392	L	G	MF	ND	S.S.x25(W) S.S.x85(S) HPS(M) a=8.43
					1800	LG w/ IC	M	202.9	0.323	L	G	MF	ND	S.S.x95(S) HPS(M) a=8.43*
					1900	B and S LG w/ BP LG w/ IC	M	1364.7	1.765	L	B	P-SF	ND M	S.S.x90(S) HPS(M) a=8.43
21	30	30	from -50 to -42	57	Control	-	-	378.3	0.325	-	-	-	-	-
					1600	SGB LG	W	845.1	0.324	S	B	P	M	Cr_2O_3(S) HPS(M) a=8.41*
					1700	SGB LG	M	1030.1	0.335	S	B	P	S	Cr_2O_3(S) HPS(M)
					1800	LG w/ IC LG w/ BP	M	1005.7	0.354	M	GB	MF	ND	Cr_2O_3(S) HPS(S) a=8.42*
					1900	LG w/ IC	M	728.2	0.857	M	GB	M	ND	Cr_2O_3(S) HPS(S) a=8.44*
24	10	30	from -52 to -44	66	Control	-	-	762.7	0.344	-	-	-	-	-
					1600	SGB LG LG w/ IC	M	1163.1	0.365	S	B	P	M	-
					1700	SGB LG w/ IC LG w/ BP	M	1266.1	0.417	S	B	P-SF	M	-
					1800	SGB LG w/ IC	M	1417.5	0.420	S	B	P-SF	M	-
					1900	BP w/ LG LG w/ IC	M	1186.4	0.593	L	B	MF	W	-
26	10	30	-38	66	2000	LG w/ IC	S	699.2	0.734	L	GB	MF	S	-
27	30	30	from -46 to -38	57	2000	PGB w/ OS BP w/ LG	ND	1327.4	0.869	S	B	P	S	-
28	100	30	from -50 to -40	51	2000	BP w/ LG	M	1425.4	0.707	S	B	P	S	-

TABLE 8

RESULTS OF OXIDATION TESTS, TYPE 310 ALLOY, HEAT X27258

0.073% C, 20.81% Ni, 24.64% Cr, 0.75% Si, 1.58% Mn, 0.025% P, 0.008% S, 0.30% Cu, 0.15% Mo

Run No.	Duration, hr	Air Velocity, ft/min	Dew-point, °F	Penetration Curve, Fig. No.	Temp., °F	Specimen				Oxide Scale				
						Appearance	Magnetism	No. of Fissures/in.	Mean Fissure Depth, in.x10^3	Amount	Color	Flake Size	Magnetism	Composition (x-ray)
16	100	30	from -52 to -42	52	Control	-	-	501.7	0.442	-	-	-	-	-
					1600	PGB BP w/ LG LG	M	1370.4	0.405	S	B	P	M	Cr_2O_3(S) S.S.x25(W)
					1700	LG w/ BP PGB w/ OS PGB	W	779.3	0.566	L	B	MF	ND	Cr_2O_3(S) HPS(M) a=8.43*
					1800	PGB w/ OS BP w/ LG LG w/ BP LG w/ IC	W	1010.5	0.661	S	B	P-SF	ND M	Cr_2O_3(S) HPS(S) a= 8.43
					1900	LG w/ BP LG w/ IC BP w/ LG B and S LG	W	1235.4	0.665	M	G	P-SF	ND	Cr_2O_3(S) HPS(M)
21	30	30	from -50 to -42	58	Control	-	-	463.8	0.321	-	-	-	-	-
					1600	SGB PGB LG	W	801.8	0.321	S	B	P	M	Cr_2O_3(S) Fe_2O_3(M) HPS(W)
					1700	SGB LG	W	1203.5	0.320	S	B	P	M	Insuf.
					1800	BP w/ LG PGB w/ OS LG w/ IC	W	900.9	0.384	S	B	P	M	Cr_2O_3(S) Fe_2O_3(M) HPS(W)
					1900	LG PGB w/ OS B and S	M	894.1	0.527	S	B	P	M	S.S.x75(S) Fe_2O_3(M)
24	10	30	from -52 to -44	67	Control	-	-	985.8	0.329	-	-	-	-	-
					1600	SGB LG w/ IC	M	1214.6	0.347	S	B	P-SF	S	-
					1700	PGB w/ OS LG w/ BP LG w/ IC	ND	1300.0	0.384	S	B	P-SF	S	-
					1800	BP w/ LG LG w/ IC	W	1147.8	0.410	M	B	P-SF	W	-
					1900	LG w/ IC BP w/ LG	S	911.1	0.343	M	B	MF	W	-
26	10	30	-38	67	2000	PGB w/ OS PGB B and S	S	1269.7	0.526	M	GB	MF	S	-
27	30	30	from -46 to -38	58	2000	BP w/ LG PGB w/ OS B and S	M	1214.8	0.800	S	B	P	S	-
28	100	30	from -50 to -40	52	2000	BP w/ LG B and S PGB w/ OS	W	956.2	0.645	S	B	P	S	-

TABLE 9

RESULTS OF OXIDATION TESTS, TYPE 310 ALLOY, HEAT X45558

0.069% C, 21.56% Ni, 24.71% Cr, 0.58% Si, 1.54% Mn, 0.025% P, 0.011% S, 0.27% Cu, 0.12% Mo

Run No.	Duration, hr	Air Velocity, ft/min	Dew-point, °F	Penetration Curve, Fig. No.	Temp., °F	Specimen				Oxide Scale				
						Appearance	Magnetism	No. of Fissures/in.	Mean Fissure Depth, in.x10^3	Amount	Color	Flake Size	Magnetism	Composition (x-ray)
17	100	30	from -55 to -38	53	Control	-	-	955.0	0.352	-	-	-	-	-
					1600	PGB LG LG w/ IC	M	748.1	0.338	S	B	P	ND	Insuf.
					1700	PGB BP w/ LG LG w/ IC	M	1145.6	0.337	S	B	P	W	Insuf.
					1800	BP w/ LG PGB w/ OS	M	1303.3	0.486	S	B	P	S	Insuf.
					1900	PGB BP w/ LG LG w/ IC	M	1124.6	0.514	M	B	P	ND	HPS (S) a = 8.41 Cr_2O_3 (M)
22	10	30	from -46 to -42	59	Control	-	-	252.7	0.322	-	-	-	-	-
					1600	SGB LG w/ IC	W	450.0	0.320	S	B	P	M	Cr_2O_3 (S) Fe_2O_3 (M)
					1700	SGB PGB w/ OS LG w/ IC	M	1164.1	0.323	S	B	P	M	Insuf.
					1800	SGB PGB w/ OS	W	1137.6	0.334	S	B	P	M	Insuf.
					1900	PGB w/ OS LG w/ IC	M	943.8	0.367	S	B	P	M	Cr_2O_3 (S) HPS (M)
23	30	30	from -52 to -41	62	Control	-	-	88.9	0.320	-	-	-	-	-
					1600	SGB LG w/ IC PGB w/ OS	-	748.5	0.320	S	B	P	M	-
					1700	SGB LG w/ IC PGB w/ OS	-	878.4	0.334	S	B	P	M	-
					1800	SGB BP w/ LG	-	662.3	0.370	S	B	P	M	-
					1900	BP w/ LG PGB w/ OS	-	679.6	0.372	S	B	P	M	-
26	10	30	-38	59	2000	SGB	M	841.3	0.398	S	B	P	S	-
27	30	30	from -46 to -38	62	2000	BP w/ LG PGB	ND	872.9	0.490	S	B	P	M	-
28	100	30	from -50 to -40	53	2000	B and S BP w/ LG	M	1075.6	0.590	M	B	P-SF	S	-

TABLE 10

RESULTS OF OXIDATION TESTS, TYPE 310 ALLOY, HEAT X46063

0.059% C, 20.67% Ni, 24.28% Cr, 0.31% Si, 1.57% Mn, 0.024% P, 0.014% S, 0.25% Cu, 0.12% Mo

Run No.	Duration, hr	Air Velocity, ft/min	Dew-point, °F	Penetration Curve, Fig. No.	Temp., °F	Specimen				Oxide Scale				
						Appearance	Magnetism	No. of Fissures/in.	Mean Fissure Depth, in.x10^3	Amount	Color	Flake Size	Magnetism	Composition (x-ray)
17	100	30	from -55 to -38	54	Control	-	-	728.9	0.354	-	-	-	-	-
					1600	PGB LG w/BP LG	W	1010.0	0.360	S	B	P-SF	ND	Cr_2O_3(S) HPS(M)
					1700	BP w/ LG LG	W	1024.9	0.487	M	B	P-SF	ND	Cr_2O_3(S) HPS(M) a=8.42*
					1800	LG w/ IC LG w/ BP	W	1116.6	0.622	L	B	MF	ND	Cr_2O_3(S) HPS(M) a=8.46
					1900	LG w/ BP LG	W	806.7	0.582	L	B	MF	ND	Cr_2O_3(S) HPS(M) a=8.42*
22	10	30	from -46 to -42	60	Control	-	-	269.7	0.330	-	-	-	-	-
					1600	SGB PGB w/ OS LG w/ IC	M	553.2	0.332	S	B	P	M	Insuf.
					1700	SGB LG w/ IC	M	565.1	0.321	S	B	P-SF	M	Cr_2O_3(S) Fe_2O_3(M)
					1800	LG w/ BP SGB LG w/ IC	M	560.2	0.386	S	B	P	W	Cr_2O_3(S) HPS(M)
					1900	SGB LG w/ IC LG w/ BP PGB w/ OS	M	635.3	0.402	M	B	P-SF	W	Cr_2O_3(S) HPS(M) a=8.42*
23	30	30	from -52 to -41	63	Control	-	-	65.5	0.320	-	-	-	-	-
					1600	SGB LG w/ IC	W	194.9	0.334	S	B	P-SF	M	-
					1700	SGB LG w/ IC LG w/ BP	ND	287.3	0.354	M	B	P-SF	M	-
					1800	BP w/ LG PGB w/ OS LG w/ IC	W	425.0	0.393	M	B	P-SF	M	-
					1900	LG w/ IC SGB LG w/ BP	S	366.1	0.443	M	B	P-SF	S	-
26	10	30	-38	60	2000	LG w/ BP LG w/ IC	S	523.5	0.436	M	B	P-SF	M	-
27	30	30	from -46 to -38	63	2000	LG w/ IC PGB	W	1130.0	0.588	S	B	P	W	-
28	100	30	from -50 to -40	54	2000	BP w/ LG B and S	M	343.4	0.437	M	B	P-SF	S	-

TABLE 11

RESULTS OF OXIDATION TESTS, TYPE 310 ALLOY, HEAT X46572

0.089% C, 19.48% Ni, 24.35% Cr, 0.67% Si, 1.60% Mn, 0.021% P, 0.022% S, 0.34% Cu, 0.14% Mo

Run No.	Duration, hr	Air Velocity, ft/min	Dew-point, °F	Penetration Curve, Fig. No.	Temp., °F	Specimen				Oxide Scale				
						Appearance	Magnetism	No. of Fissures/in.	Mean Fissure Depth, in.x10^3	Amount	Color	Flake Size	Magnetism	Composition (x-ray)
17	100	30	from -55 to -38	55	Control	-	-	422.1	0.339	-	-	-	-	
					1600	PGB LG w/ IC LG	W	520.1	0.358	M	B	P-SF	M	Cr_2O_3(S) HPS(M) a=8.43*
					1700	BP w/ LG PGB	M	781.3	0.361	M	B	P-SF	M	Cr_2O_3(S) HPS(M) a=8.43*
					1800	BP w/ LG LG w/ BP	W	686.4	0.631	M	B	P-SF	M	Cr_2O_3(S) HPS(M) a=8.42
					1900	B and S LG LG w/ IC LG w/ BP	M	1220.2	0.634	M	B	P-MF	S	HPS(S) a=8.46* S.S. x75(M) S.S. x25(M)
22	10	30	from -46 to -42	61	Control	-	-	145.0	0.330	-	-	-	-	-
					1600	SGB PGB w/ OS LG w/ BP	M	496.6	0.322	S	B	P	W	Insuf.
					1700	PGB w/ OS SGB LG w/ BP LG w/ IC	M	495.0	0.359	S	B	P	M	Cr_2O_3(S) HPS(M)
					1800	SGB LG w/ IC LG w/ BP PGB w/ OS	M	366.4	0.327	M	B	P-SF	M	Cr_2O_3(S) HPS(M) a=8.42*
					1900	LG w/ IC SGB LG w/ BP	M	488.3	0.405	M	B	M	W	Cr_2O_3(S) HPS(M) a=8.42*
23	30	30	from -52 to -41	64	Control	-	-	299.1	0.322	-	-	-	-	-
					1600	SGB PGB w/ OS LG w/ IC	-	630.7	0.323	S	B	P	M	-
					1700	SGB LG w/ IC PGB w/ OS BP w/ LG	-	611.1	0.346	S	B	P-SF	M	-
					1800	LG w/ IC BP w/ LG	-	571.7	0.442	M	B	P-SF	W	-
					1900	LG w/ IC BP w/ LG	-	432.2	0.608	M	B	P-SF	W	-
26	10	30	-38	61	2000	LG w/ IC PGB	S	1211.4	0.800	L	GB	MF	S	-
27	30	30	from -46 to -38	64	2000	PGB	M	1434.0	0.733	S	B	P	S	-
28	100	30	from -50 to -40	55	2000	B and S	M	1084.5	0.749	M	B	P-SF	S	-

TABLE 12

OXIDE-METAL INTERFACE MOVEMENT IN 100 HOURS CALCULATED FROM WEIGHT LOSS MEASUREMENTS

Run No.	Alloy	Measured Density, gm/cc	Temp., °F	Total Weight Loss, percent	Interface Movement, in.x10^5	Specimen Appearance	Oxide Scale			
							Amount	Color	Flake Size	Magnetism
20	309+Nb	7.94	Control	0.01	0.2	-	-	-	-	-
			1600	0.10	1.1	LG w/ BP BP w/ LG	S	B	P	M
			1700	0.79	9.2	BP w/ LG LG LG	M	GB	P-SF	M
			1800	1.32	14.8	LG w/ BP BP w/ LG LG w/ IC	M	G	MF	S
			1900	1.90	21.7	LG w/ IC LG w/ BP	L	G-GB	MF	S
20	64177	7.90	Control	0.01	0.1	-	-	-	-	-
			1600	-0.05	-0.8	PGB w/ OS	N	-	-	-
			1700	0.01	0.1	PGB w/ OS	S	B	P	M
			1800	0.08	1.2	BP w/ LG PGB w/ OS	S	B	P	M
			1900	0.02	0.3	PGB BP w/ LG	S	B	P	W
20	64270	7.93	Control	0.01	0.2	-	-	-	-	-
			1600	-0.04	-0.6	PGB w/ OS	N	-	-	-
			1700	-0.03	-0.4	PGB w/ OS	S	B	P	M
			1800	0.24	3.8	PGB w/ OS	S	B	P	M
			1900	0.08	1.3	PGB	S	B	P	M
18	X11306	7.83	Control	0.04	0.4	-	-	-	-	-
			1600	0.54	5.7	LG	M	GB	SF	M
			1700	0.99	10.3	LG w/ IC	L	G	MF	ND
			1800	0.74	7.4	LG w/ BP LG w/ IC	M	B	P	ND
			1900	1.94	20.5	LG LG w/ BP	M	B	P-SF	ND
28			2000	1.81	19.0	LG w/ IC LG w/ BP	M	GB	MF	M
18	X11338	7.90	Control	0.02	0.2	-	-	-	-	-
			1600	0.31	3.6	LG w/ IC LG w/ BP	M	B	MF	M
			1700	0.69	8.0	LG w/ IC	L	B	LF	W
			1800	1.12	12.8	LG w/ IC PGB w/ OS	L	GB	MF	ND
			1900	2.09	2.4	BP w/ LG LG	S	B	P-SF	M
28			2000	0.52	6.0	B and S BP w/ LG	S	B	P	S
18	X27258	7.89	Control	0.01	0.2	-	-	-	-	-
			1600	0.21	2.8	BP w/ LG LG w/ IC LG PGB w/ OS	M	B	P-SF	W
			1700	0.29	3.8	LG w/ BP BP w/ LG	S	B	P-SF	M
			1800	0.95	12.6	LG w/ IC BP w/ LG	L	B	MF	ND
			1900	0.33	4.4	PGB w/ OS LG BP w/ LG	S	B	P-SF	M
28			2000	0.12	1.6	PGB w/ OS B and S LG w/ BP	S	B	P	S
19	X45558	7.90	Control	0.00	0.0	-	-	-	-	-
			1600	-0.02	-0.2	PGB LG LG w/ IC	S	B	P	M
			1700	0.45	4.9	LG w/ IC BP w/ LG	M	B	P-SF	W
			1800	0.79	8.7	LG w/ IC PGB w/ OS	M	B	MF	ND
			1900	0.46	5.0	BP w/ LG LG PGB w/ OS	M	B	P	M
28			2000	0.14	1.6	BP w/ LG B and S	S	B	P	ND
19	X46063	7.93	Control	0.00	0.0	-	-	-	-	-
			1600	0.27	3.3	SGB LG w/ BP LG w/ IC	S	B	P-SF	M
			1700	0.51	6.2	LG w/ BP LG w/ IC	M	B	P-SF	W
			1800	1.23	15.2	LG w/ BP LG w/ IC	M	B	P-MF	W
			1900	2.23	26.6	LG w/ IC	M	GB	MF	ND
19	X46572	7.89	Control	0.01	0.2	-	-	-	-	-
			1600	0.14	1.8	SGB PGB LG	S	B	P-SF	W
			1700	0.48	6.2	LG w/ BP LG w/ IC	M	B	P-SF	W
			1800	1.10	14.6	LG w/ IC	L	GB	MF	ND
			1900	0.86	11.2	PGB PGB w/ OS	M	B	P-SF	M

TABLE 13

RESULTS OF METALLOGRAPHIC ANALYSIS

Alloy Type	100 hr Runs			30-hr Runs Chromic Acid Etch Results	100-hr Runs (Unless Otherwise Specified) Penetration Types (see Figs. 95-100)						hr
	Banding	σ Phase	δ Ferrite		Control	1600°F	1700°F	1800°F	1900°F	2000°F	
309 + Nb	Not Detectable		1600°F 1700°F	No Detectable G.S. Change. Carbides Agglomerate.	S O	S IV	M IV	L IV	M II	M II M III	10 3
64177	Small Amt.	1600°F 1700°F 1800°F	1900°F S	G.S. Increase with Temp. Carbides Agglomerate. No Grains Visible at 2000°F.	F O	M III	M III	M III	M III	M III M III	10 80
64270	Not Detectable	2000°F		G.S. Increase with Temp. Carbides Agglomerate. No Grains Visible at 2000°F.	S O	O	M I	S II	S III	S III M VI	10 30
X11306	Small Amt.		1600°F 1700°F 1800°F 1900°F	No Detectable G.S. Change. No Grains Visible at 1800, 1900, 2000°F. Carbides Agglomerate.	S O	S IV	M III	M IV	See Figs. 103-106 for 1600°F and 1900°F and 2000°F.		
X11338	Small Amt.	1600°F 1700°F 1800°F 1900°F		G.S. Increase with Temp. Carbides Agglomerate. No Grains Visible at 2000°F.	S O	S IV	S IV	L I	L	M III M II S V	10 30 100

TABLE 13 (cont.)

Alloy Type	100 hr Runs: Banding	100 hr Runs: σ Phase	100 hr Runs: δ Ferrite	30-hr Runs: Chromic Acid Etch Results	100-hr Runs (Unless Otherwise Specified): Penetration Types (see Figs. 95-100): Control	1600°F	1700°F	1800°F	1900°F	2000°F	hr
X27258	Yes	1600°F 1700°F 1800°F 1900°F		Band of Small Grains. Increase G.S. with Temp. Carbides Agglomerate. No General G.S. Change. No Grains Visible at 2000°F.	M 0	S III	M III	M I	L I	S II M II L VI	10 30 100
X45558	Yes		1600°F 1700°F 1800°F 1900°F	Band of Small Grains Increase G.S. with Temp. General G.S. Increase	S 0	0	S III	M II	S II	S VI M VI M VI	10 30 100
X46063	Not Detectable		1800°F 1900°F	No Detectable G.S. Change. Carbides Agglomerate. No Grains Visible at 2000°F.	M 0	0	S III	S III	M III	S VI S VI M VI	10 30 100
X46572	Yes	1800°F 1900°F		No Detectable G.S. Change. Carbides Agglomerate.	S 0	S II	S I	S III	S III	M I S III M VI	10 30 100

S = small penetrations
M = medium penetrations
L = large penetrations
F = fine penetrations

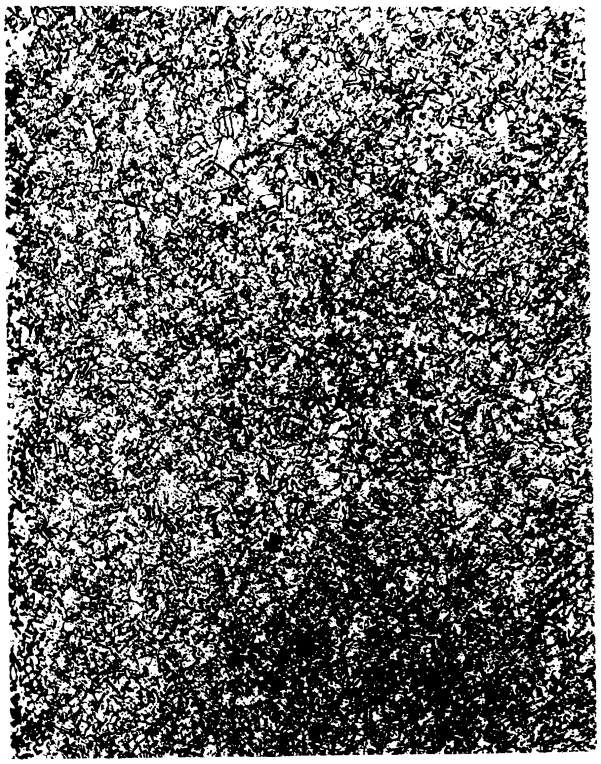

Fig. 1. Type 309+ Nb Alloy. As Received. 100x. Plane of Rolling. Etch: Electr. Chromic Acid.

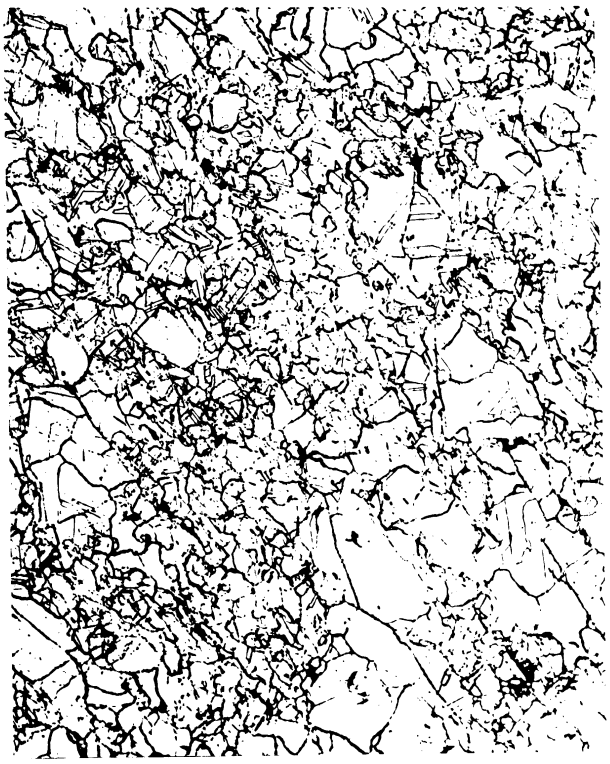

Fig. 2. Type 310 Alloy, Heat 64177. As Received. 100x. Plane of Rolling. Etch: Electr. Chromic Acid.

Fig. 3. Type 310 Alloy, Heat 64270. As Received. 100x. Plane of Rolling. Etch: Electr. Chromic Acid.

Fig. 4. Type 310 Alloy, Heat X 11306. As Received. 100x. Obl. Light. Plane of Rolling. Etch: Electr. 1:1:1 HCl, HNO_3, H_2O.

Fig. 5. Type 310 Alloy, Heat X 11338. As Received. 100x. Plane of Rolling. Etch: Electr. Chromic Acid.

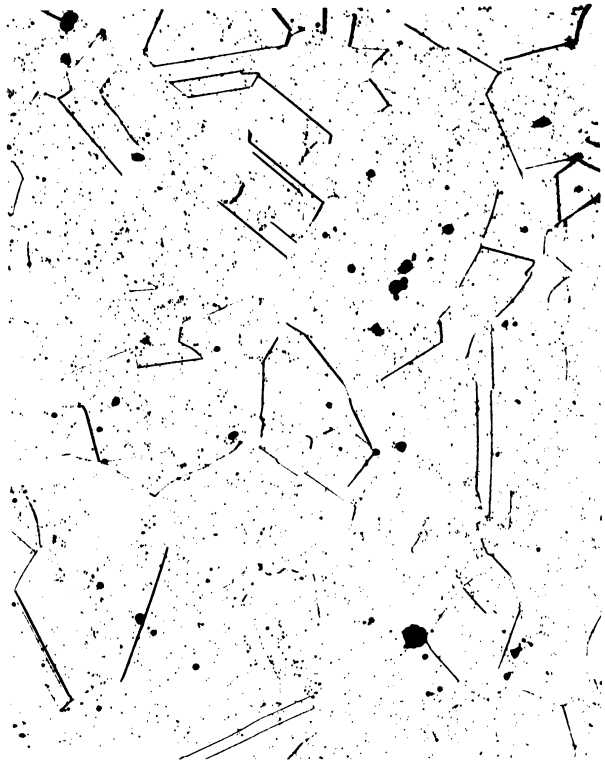

Fig. 6. Type 310 Alloy, Heat X 27258. As Received. 100x. Obl. Light. Plane of Rolling. Etch: Electr. 1:1:1 HCl, HNO_3, H_2O.

Fig. 7. Type 310 Alloy, Heat X 45558. As Received. 100x. Obl. Light. Plane of Rolling. Etch: Electr. 1:1:1 HCl, HNO_3, H_2O.

Fig. 8. Type 310 Alloy, Heat X 46063. As Received. 100x. Plane of Rolling. Etch: Electr. Chromic Acid.

Fig. 9. Type 310 Alloy, Heat X 46572. As Received. 100x. Obl. Light. Plane of Rolling. Etch: Electr. Chromic Acid.

Fig. 10. Grain Boundary Network. Type 310 Alloy, Heat 64177. As Received. 1000x. Plane of Rolling. Etch: Electr. Chromic Acid.

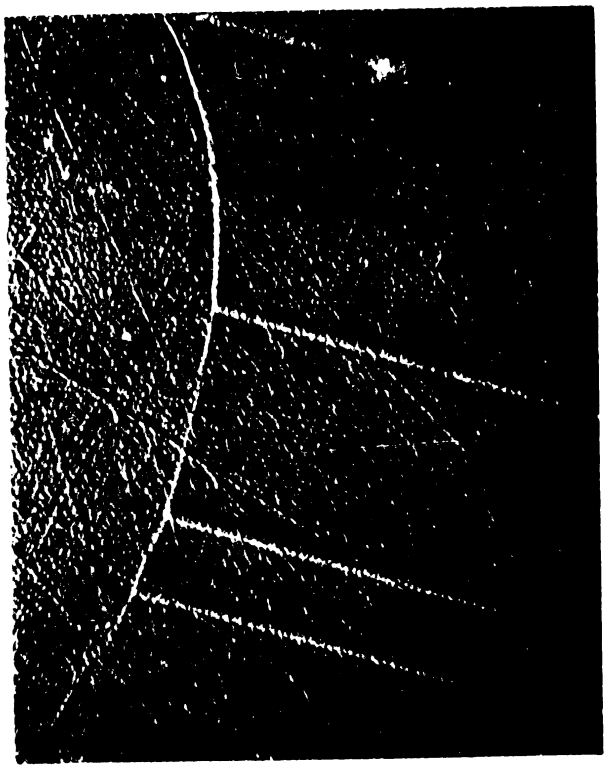

Fig. 11. Grain Boundary. Type 310 Alloy, Heat X 45558. As Received. 1000x. Obl. Light. Plane of Rolling. Etch: Electr. 1:1:1 HCl, HNO_3, H_2O.

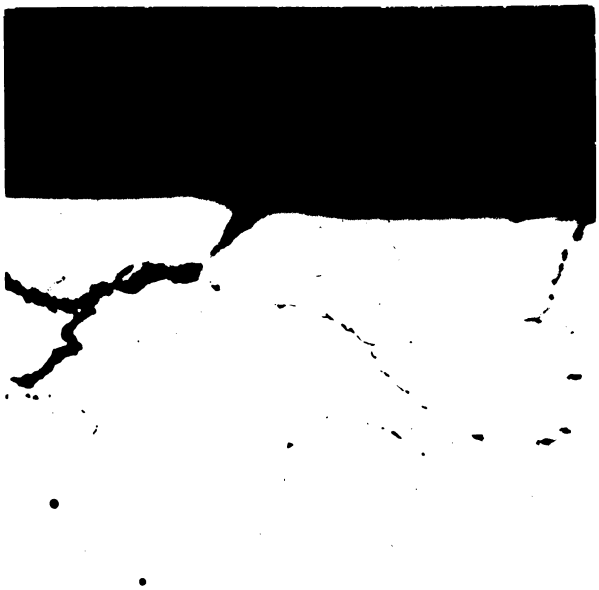

Fig. 12. Type 310 Alloy, Heat 64177. As Received. 1000x. Cross Section. Unetched.

Fig. 13. Type 310 Alloy, Heat X 11338. As Received. 1000x. Cross Section. Unetched.

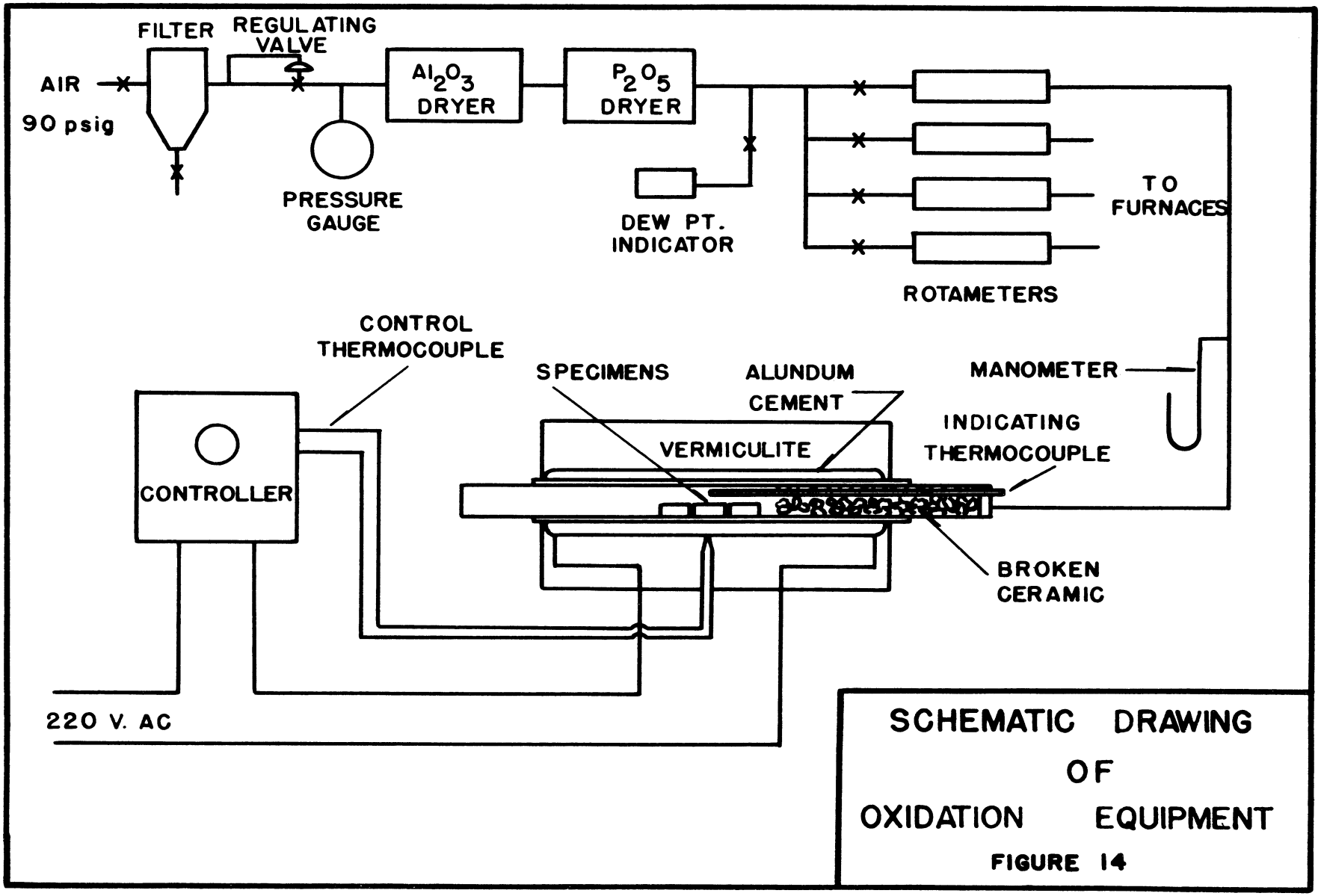

SCHEMATIC DRAWING OF OXIDATION EQUIPMENT

FIGURE 14

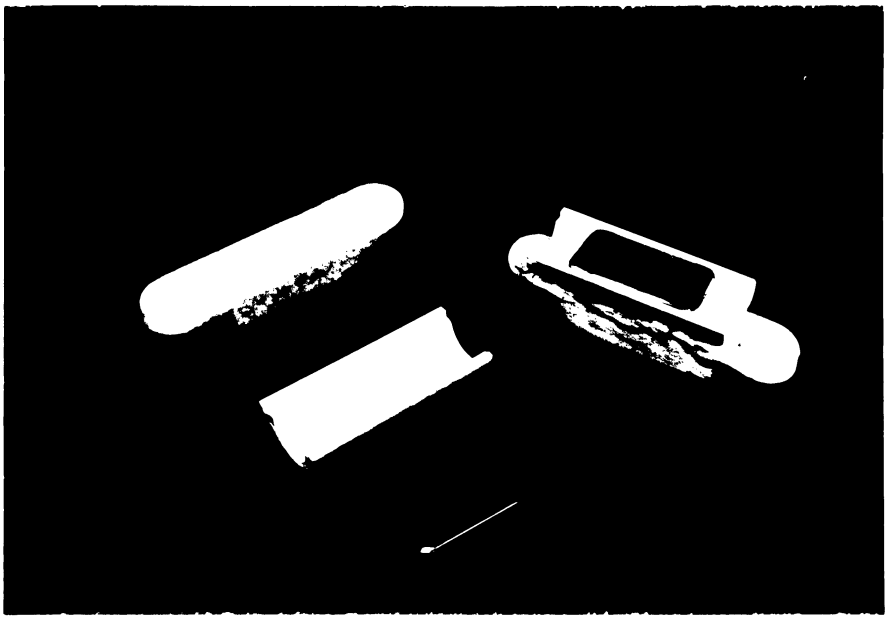

Fig. 15. Specimens and Ceramic Holders.

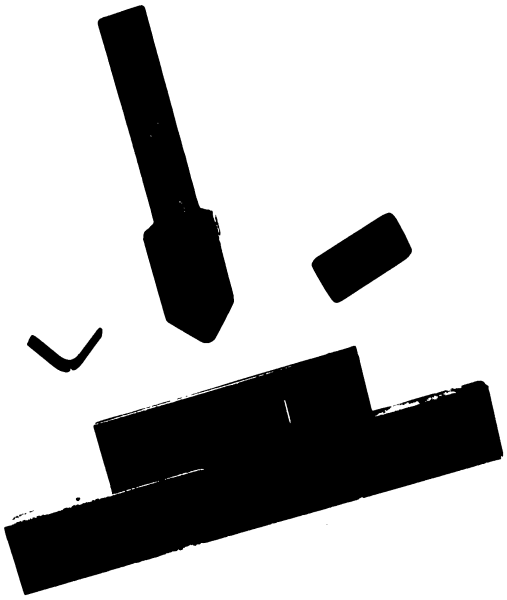

Fig. 16. Bending Die and Specimens.

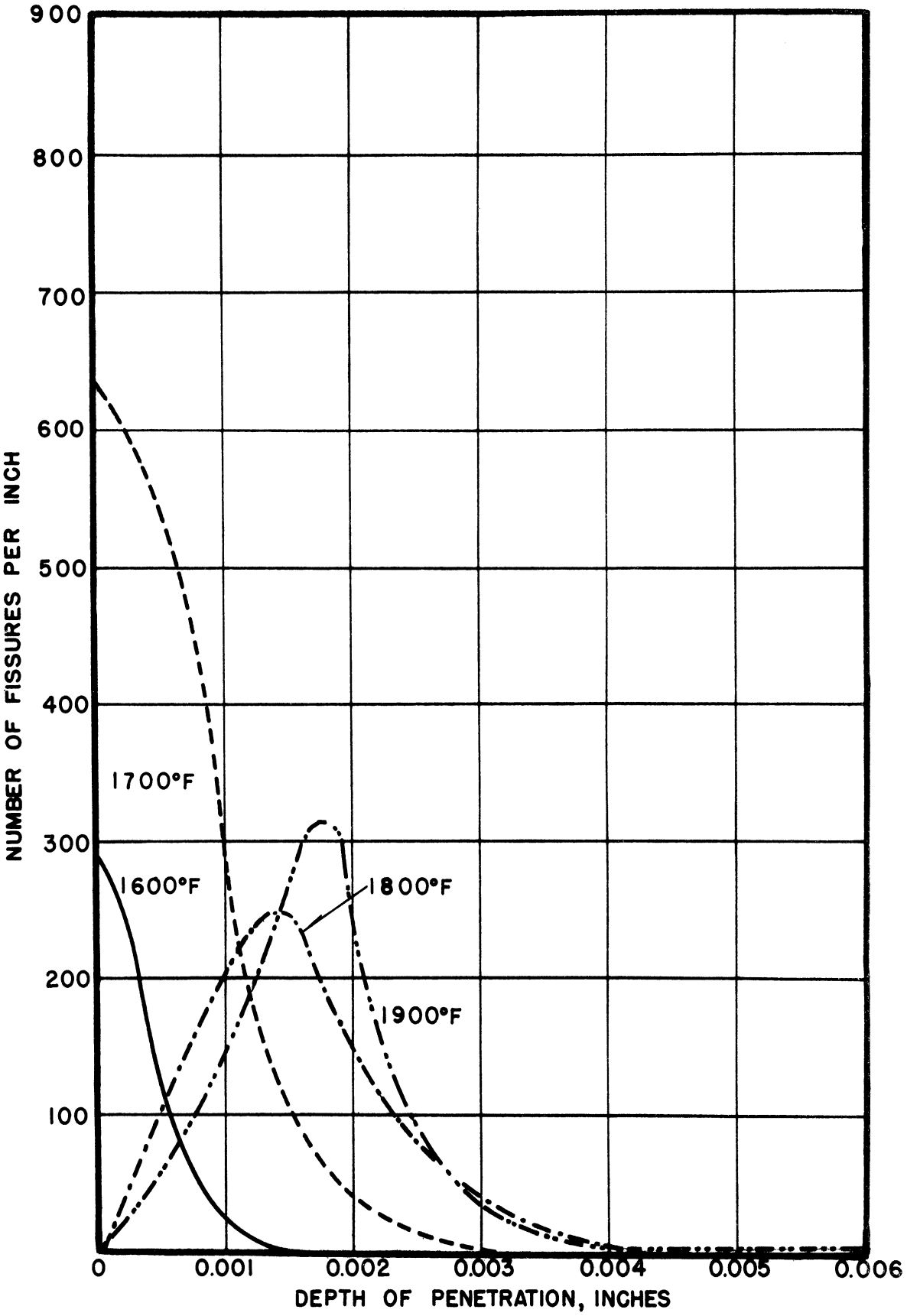

FIG. 17 – PENETRATION VS. DEPTH BELOW SURFACE. TYPE 309+Nb ALLOY. RUN 5.

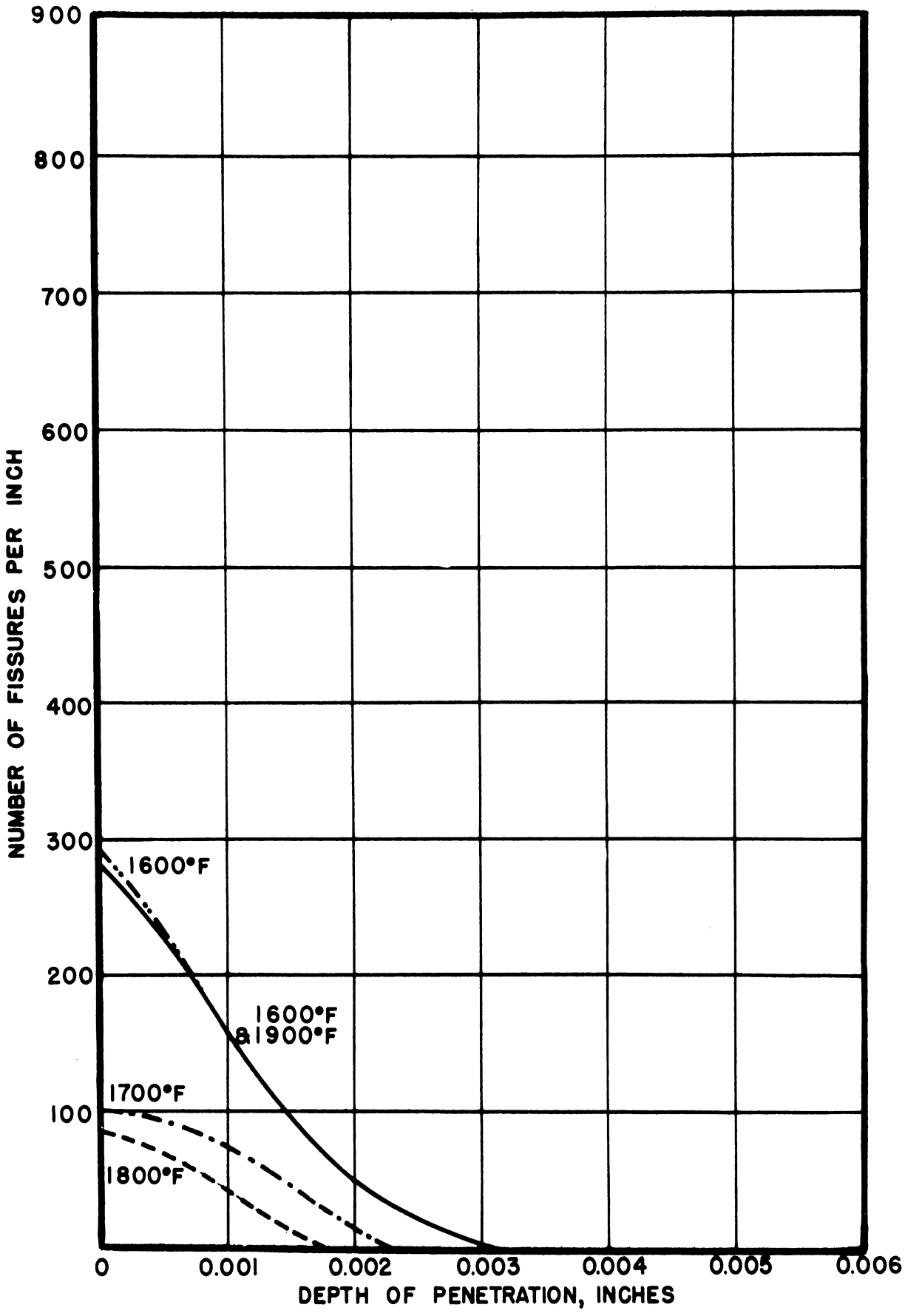

FIG. 18 - PENETRATION VS. DEPTH BELOW SURFACE.
TYPE 310 ALLOY, HEAT 64177. RUN 5.

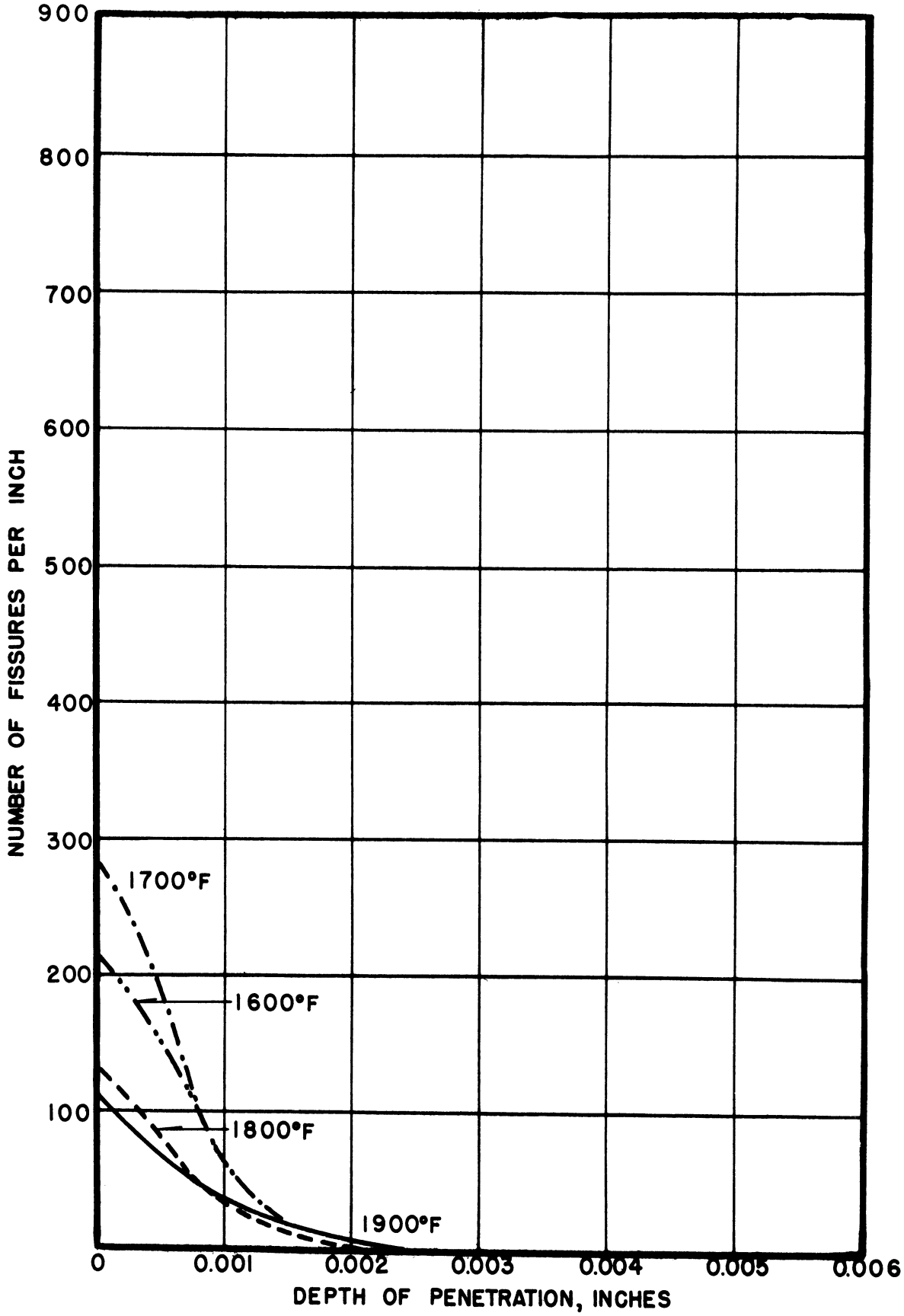

FIG. 19 - PENETRATION VS. DEPTH BELOW SURFACE.
TYPE 310 ALLOY, HEAT 64270. RUN 5.

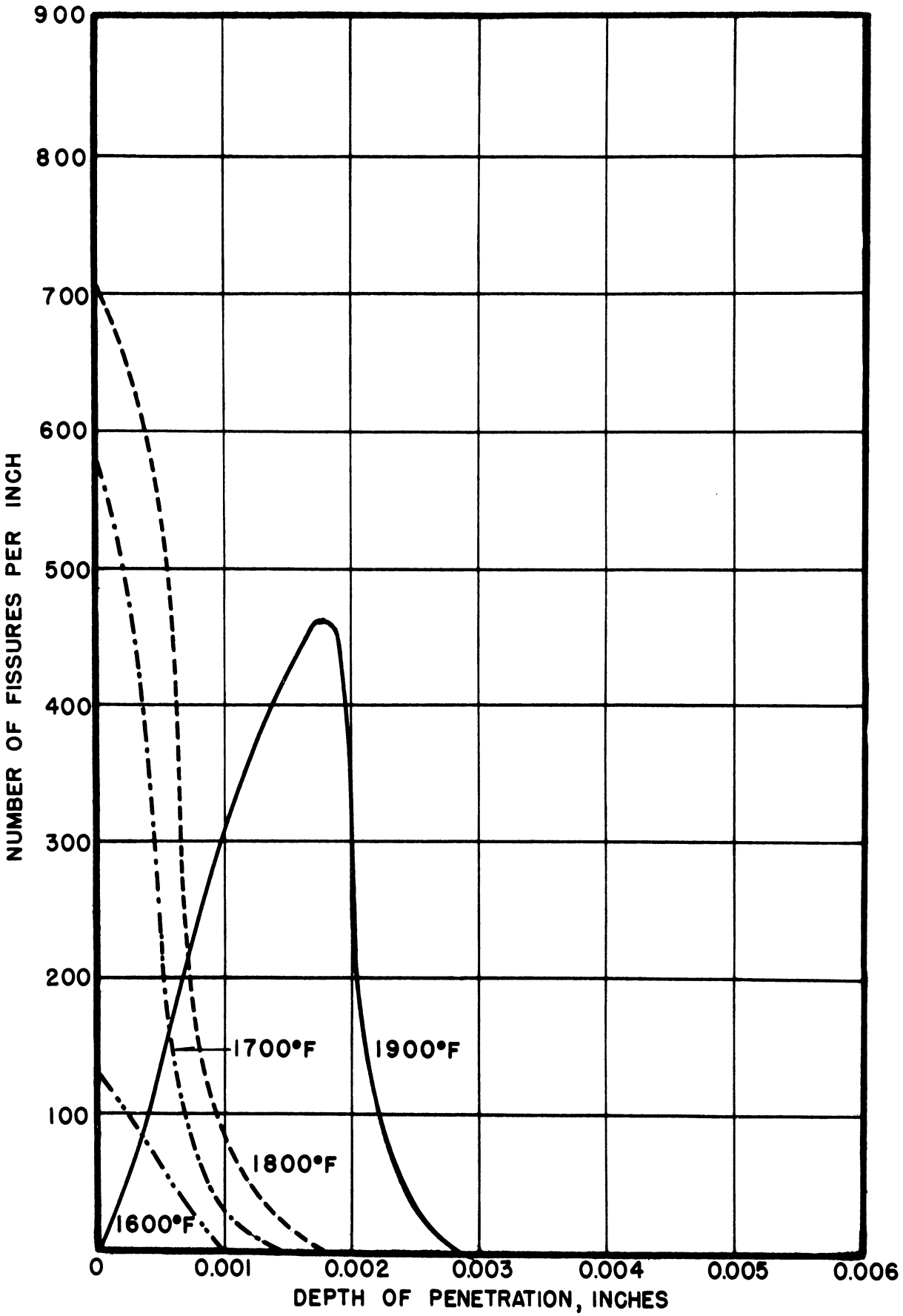

FIG. 20 - PENETRATION VS. DEPTH BELOW SURFACE. TYPE 309+Nb ALLOY. RUN 6.

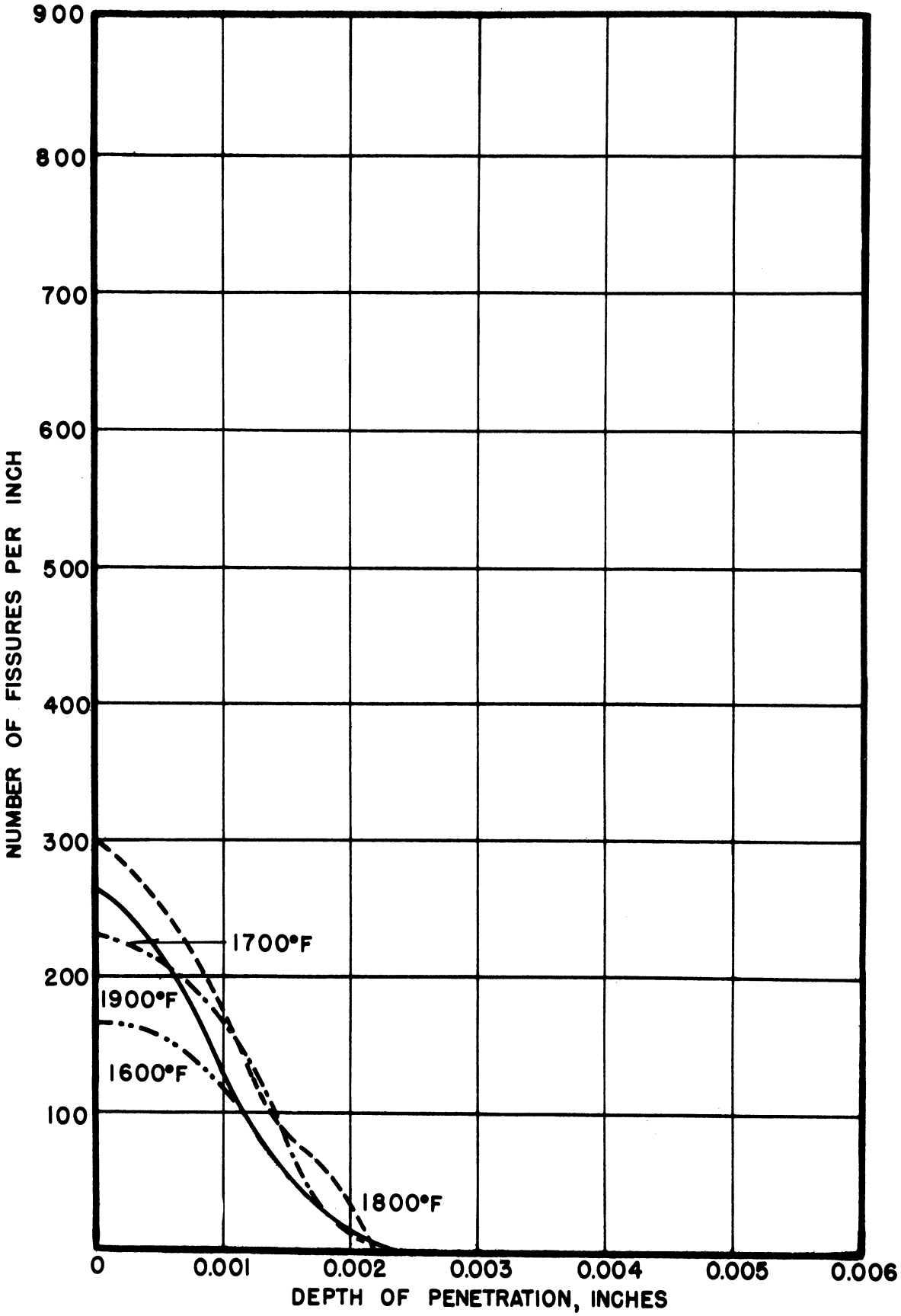

FIG. 21 - PENETRATION VS. DEPTH BELOW SURFACE.
TYPE 310 ALLOY, HEAT 64177. RUN 6.

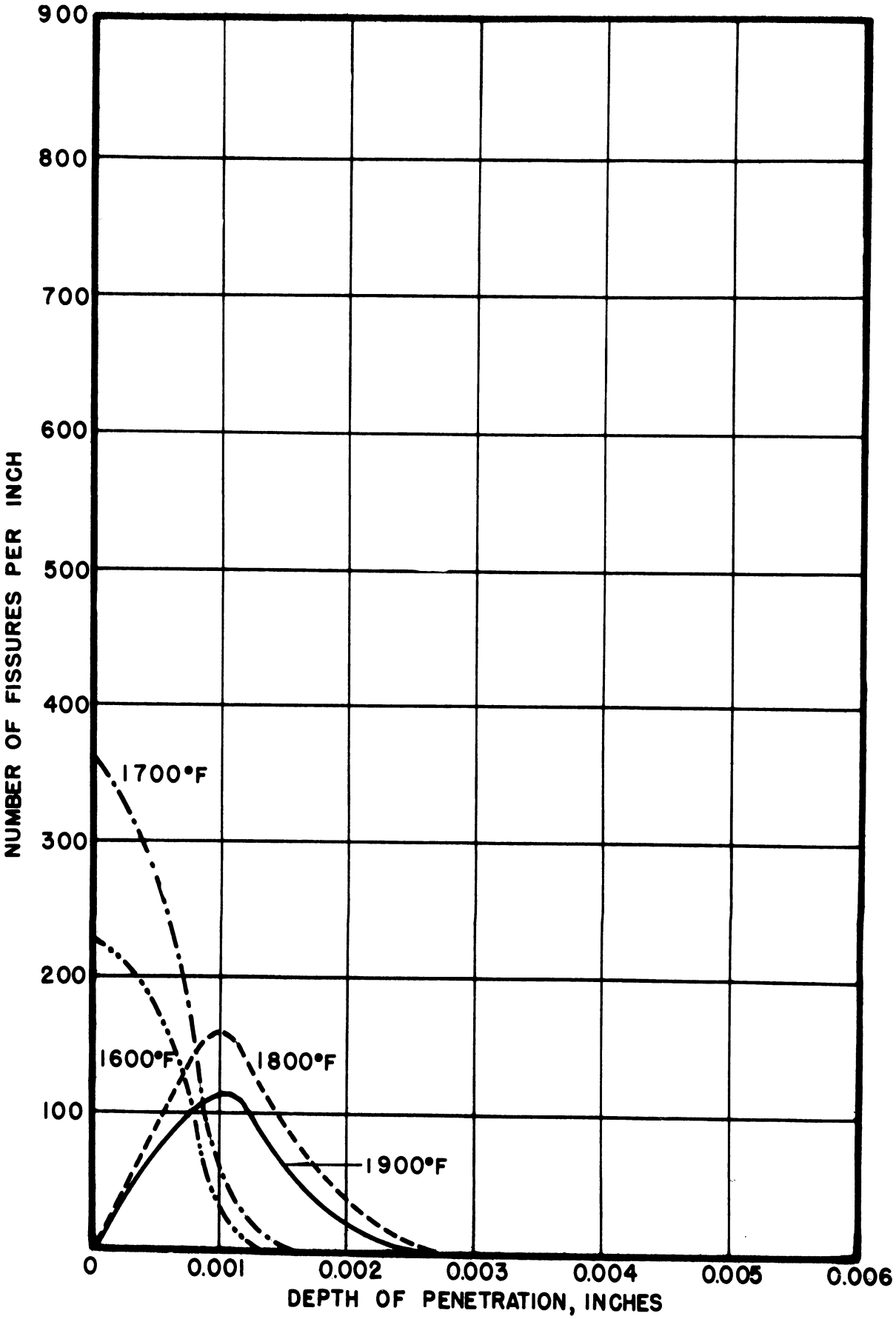

FIG. 22 - PENETRATION VS. DEPTH BELOW SURFACE.
TYPE 310 ALLOY, HEAT 64270. RUN 6.

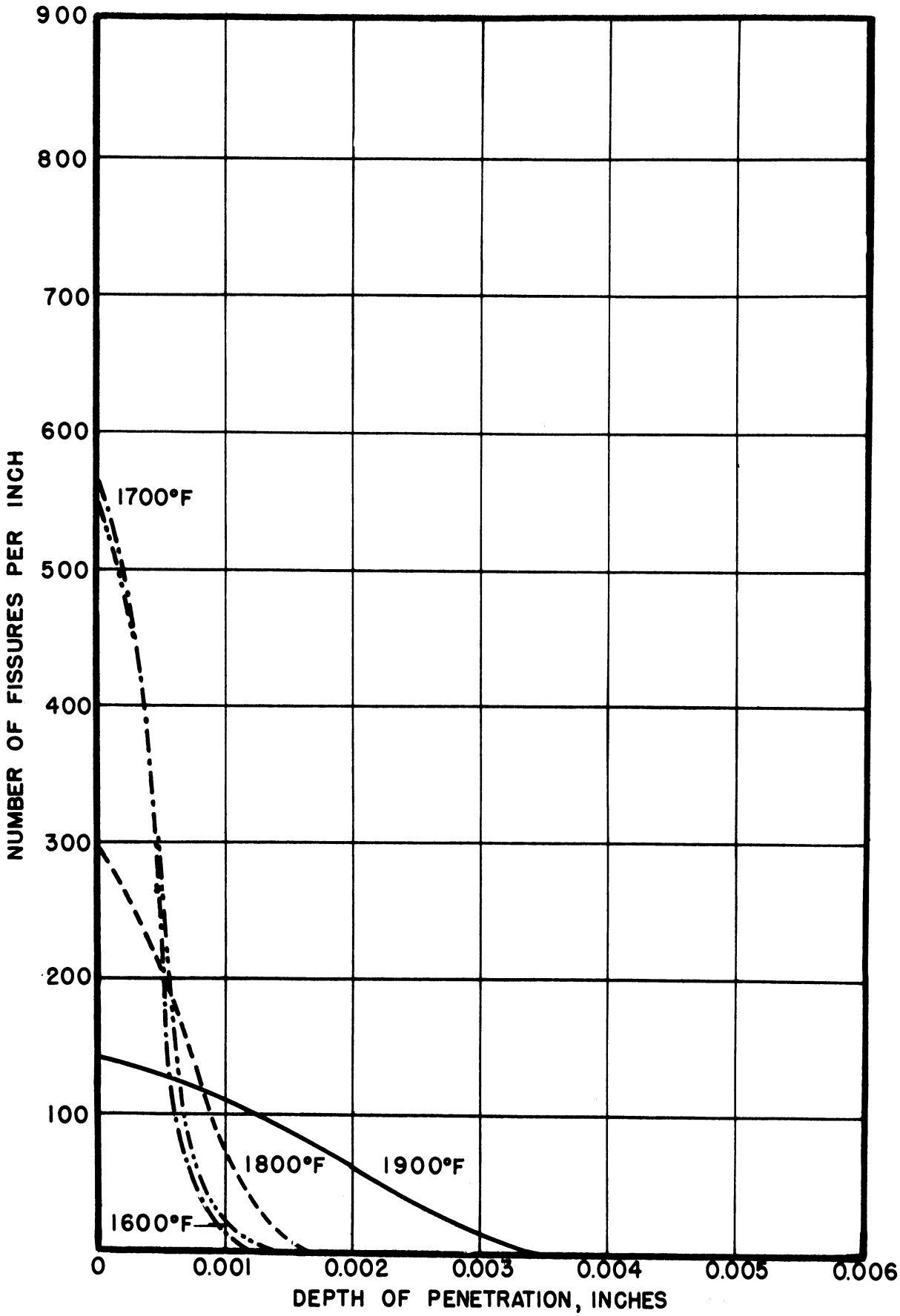

FIG. 23- PENETRATION VS. DEPTH BELOW SURFACE. TYPE 309+Nb ALLOY. RUN 8.

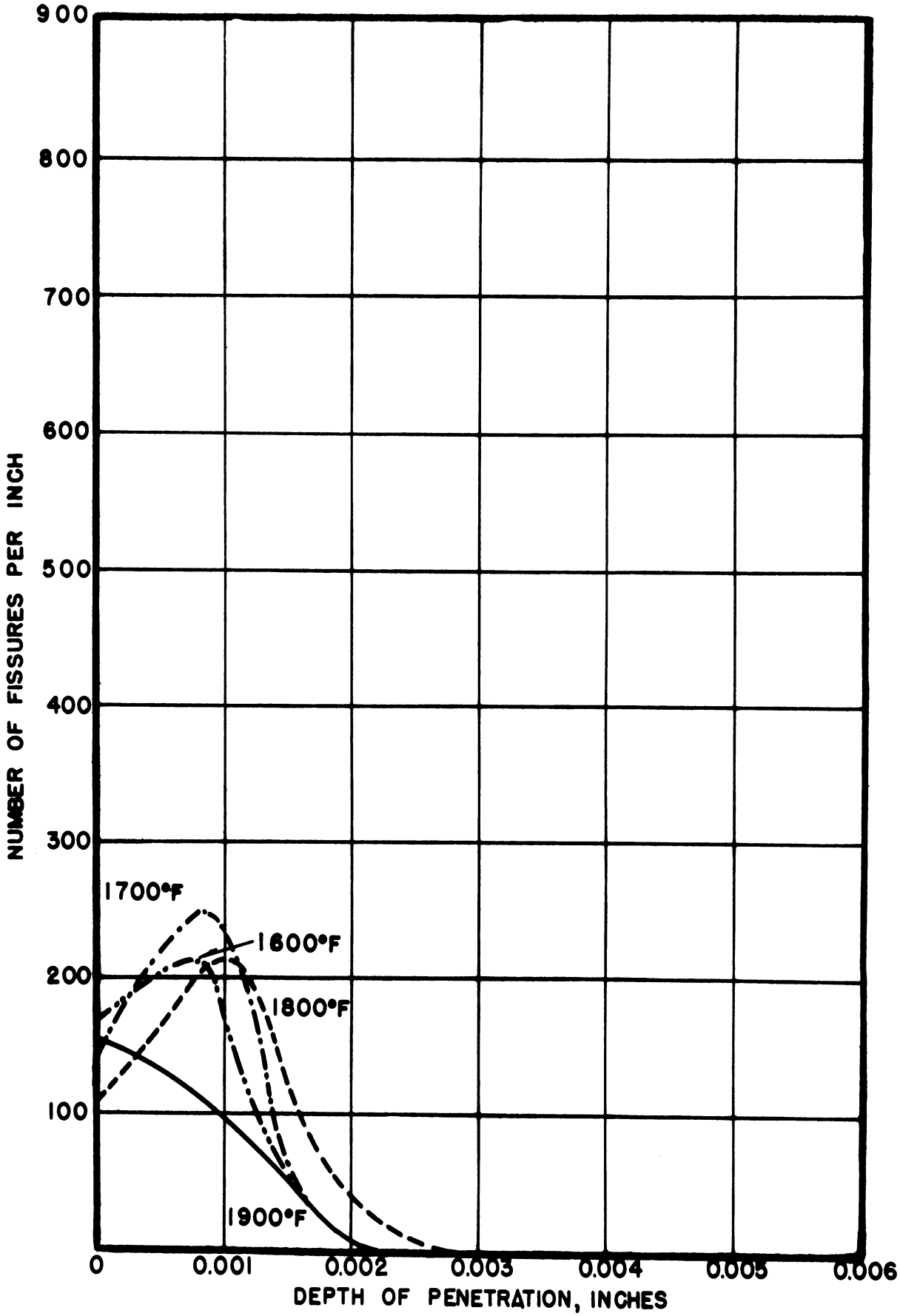

FIG. 24- PENETRATION VS. DEPTH BELOW SURFACE.
TYPE 310 ALLOY, HEAT 64177. RUN 8.

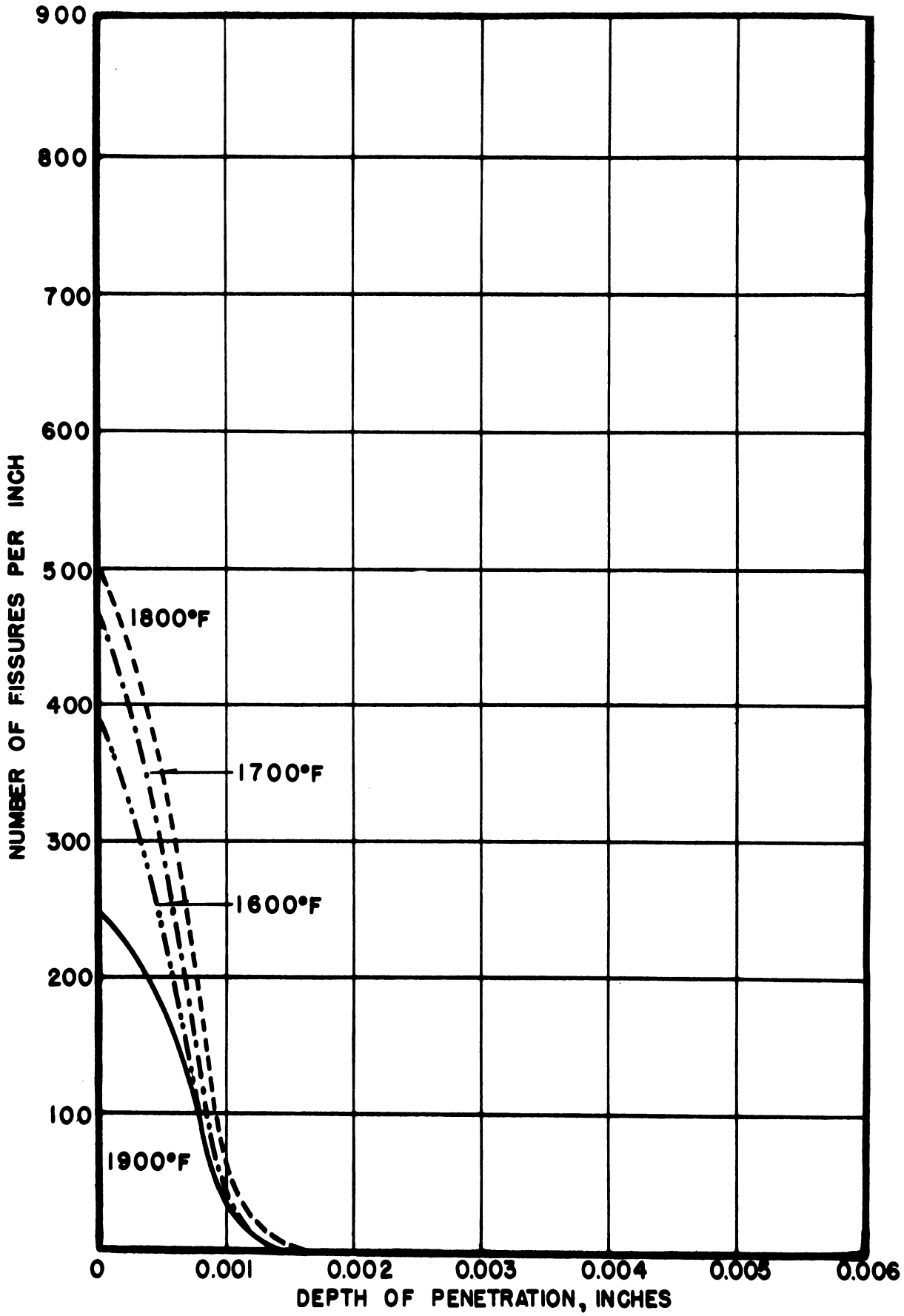

FIG. 25 - PENETRATION VS. DEPTH BELOW SURFACE.
TYPE 310 ALLOY, HEAT 64270. RUN 8.

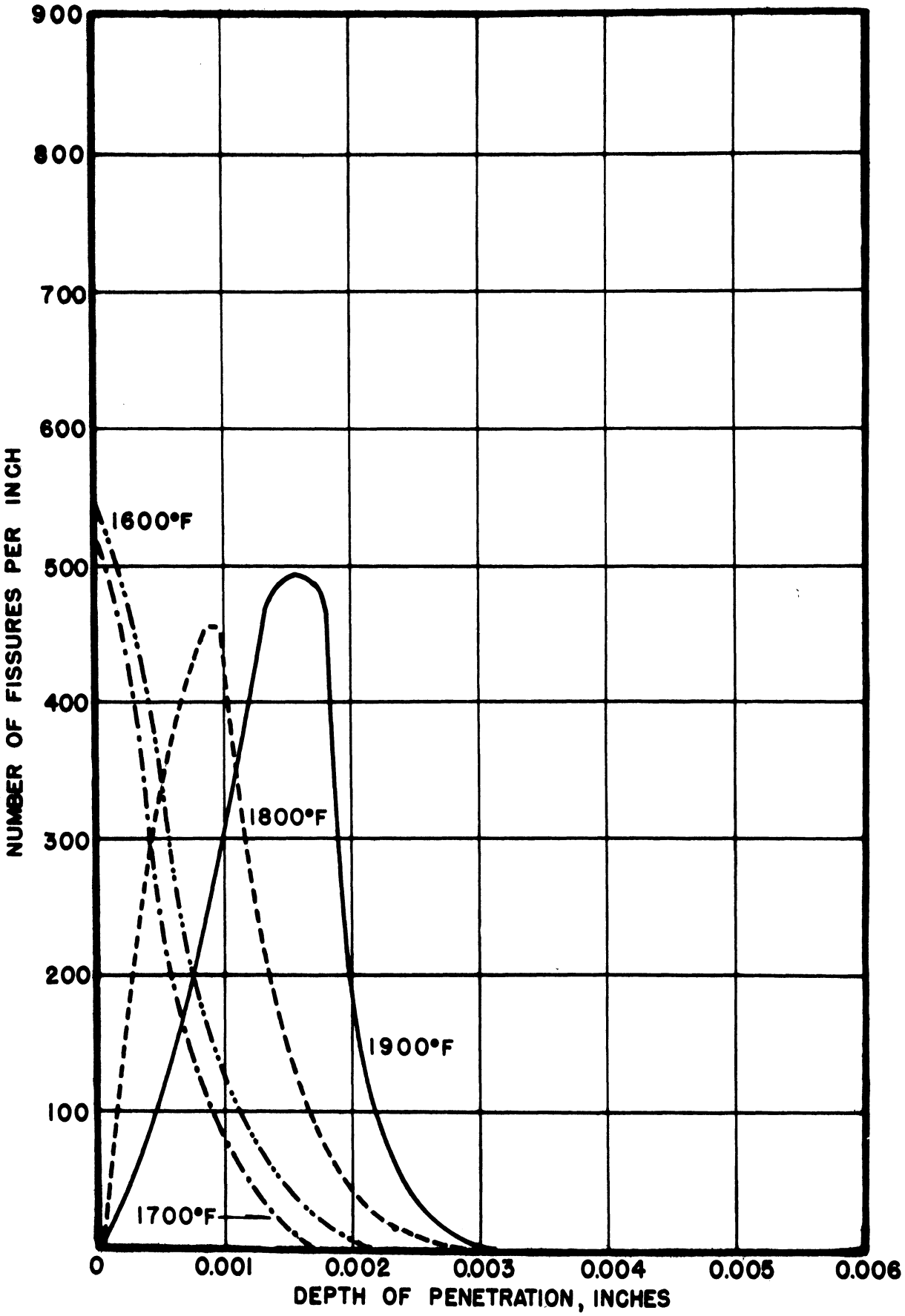

FIG.26-PENETRATION VS. DEPTH BELOW SURFACE.
TYPE 309+Nb ALLOY. RUN 9.
STRAIGHT SECTION.

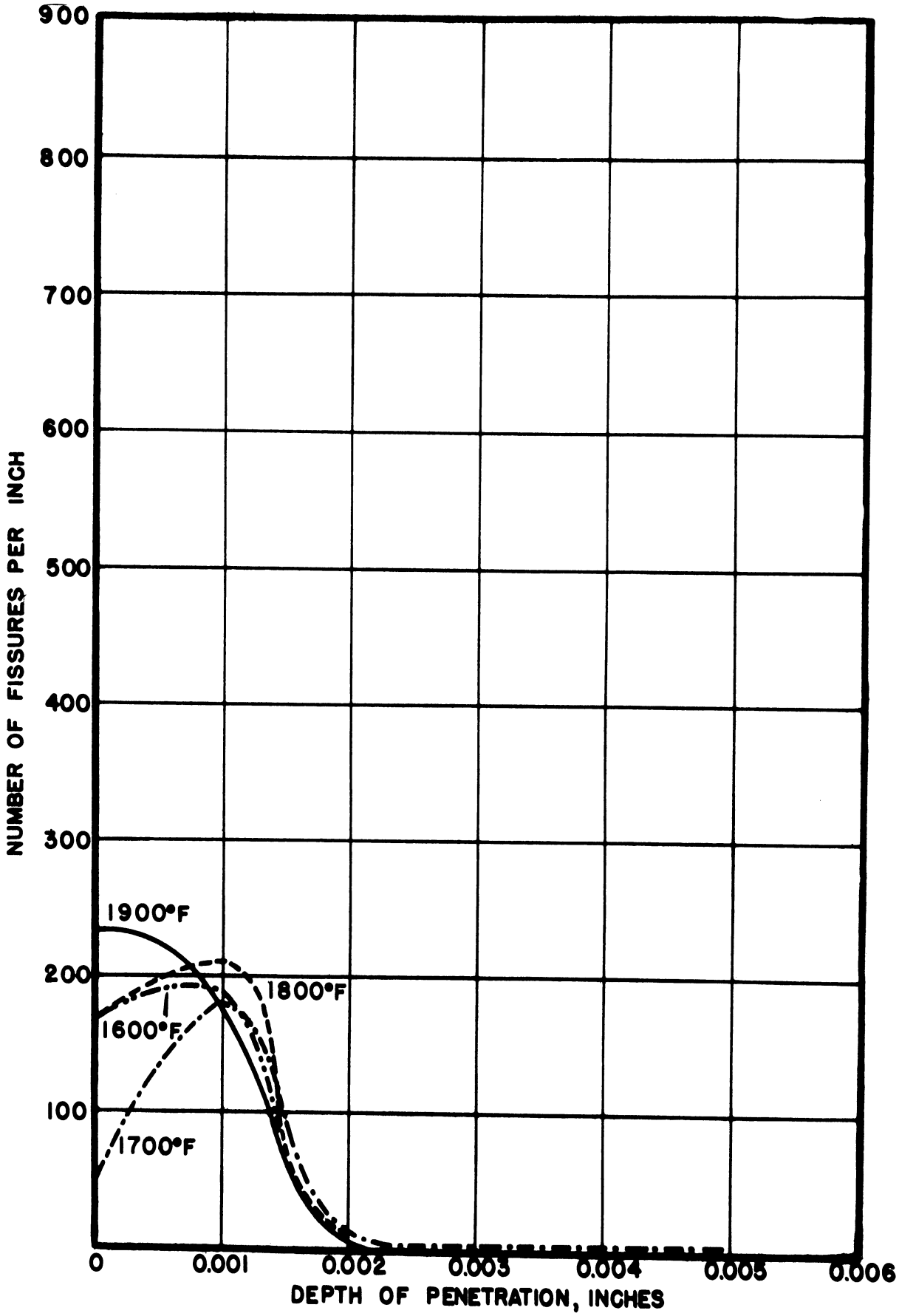

FIG. 27 - PENETRATION VS. DEPTH BELOW SURFACE.
TYPE 310 ALLOY, HEAT 64177. RUN 9.
STRAIGHT SECTION.

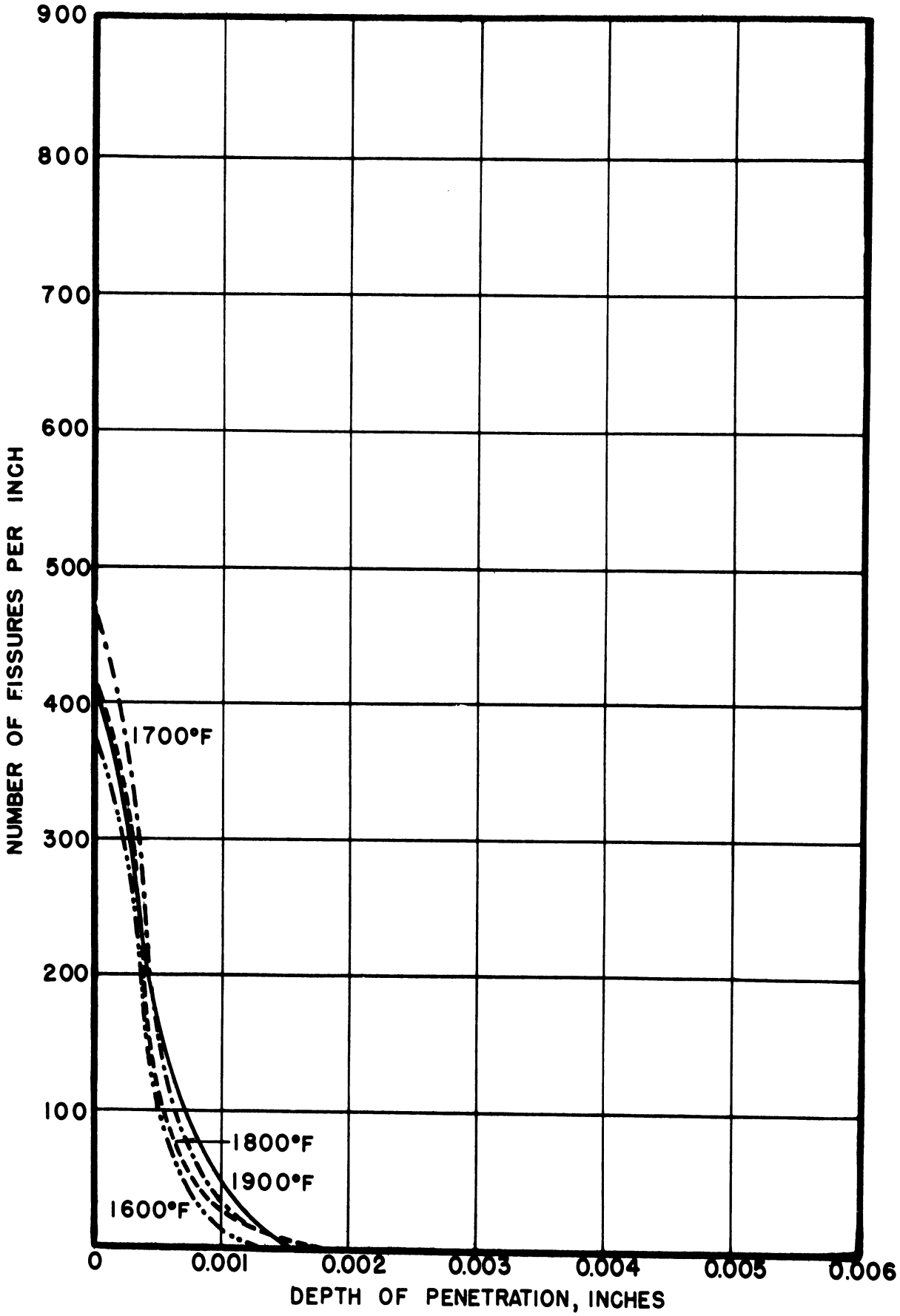

FIG. 28- PENETRATION VS. DEPTH BELOW SURFACE.
TYPE 310 ALLOY, HEAT 64270. RUN 9.
STRAIGHT SECTION.

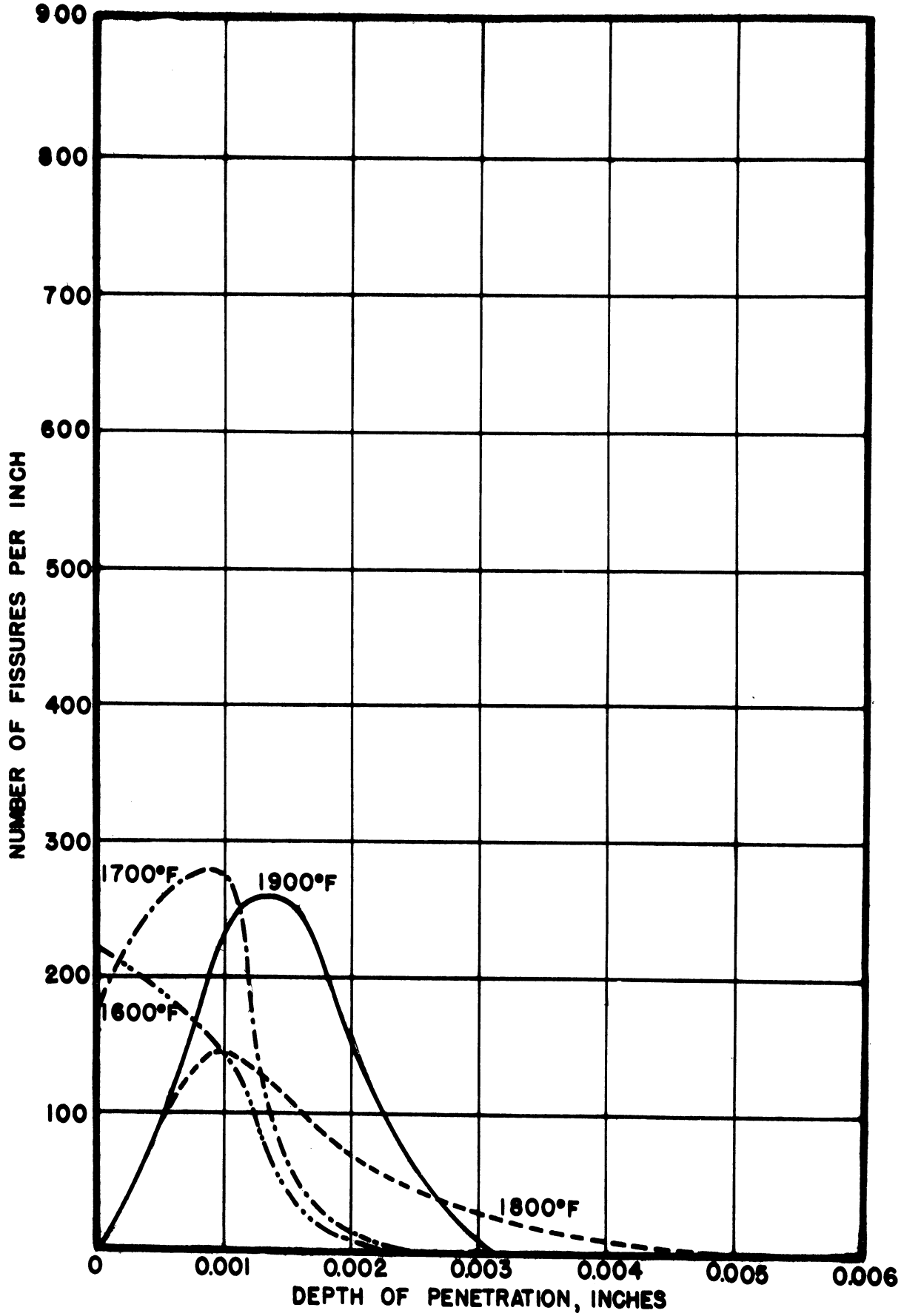

FIG. 29 - PENETRATION VS. DEPTH BELOW SURFACE.
TYPE 309 + Nb ALLOY. RUN 9.
CURVED SECTION.

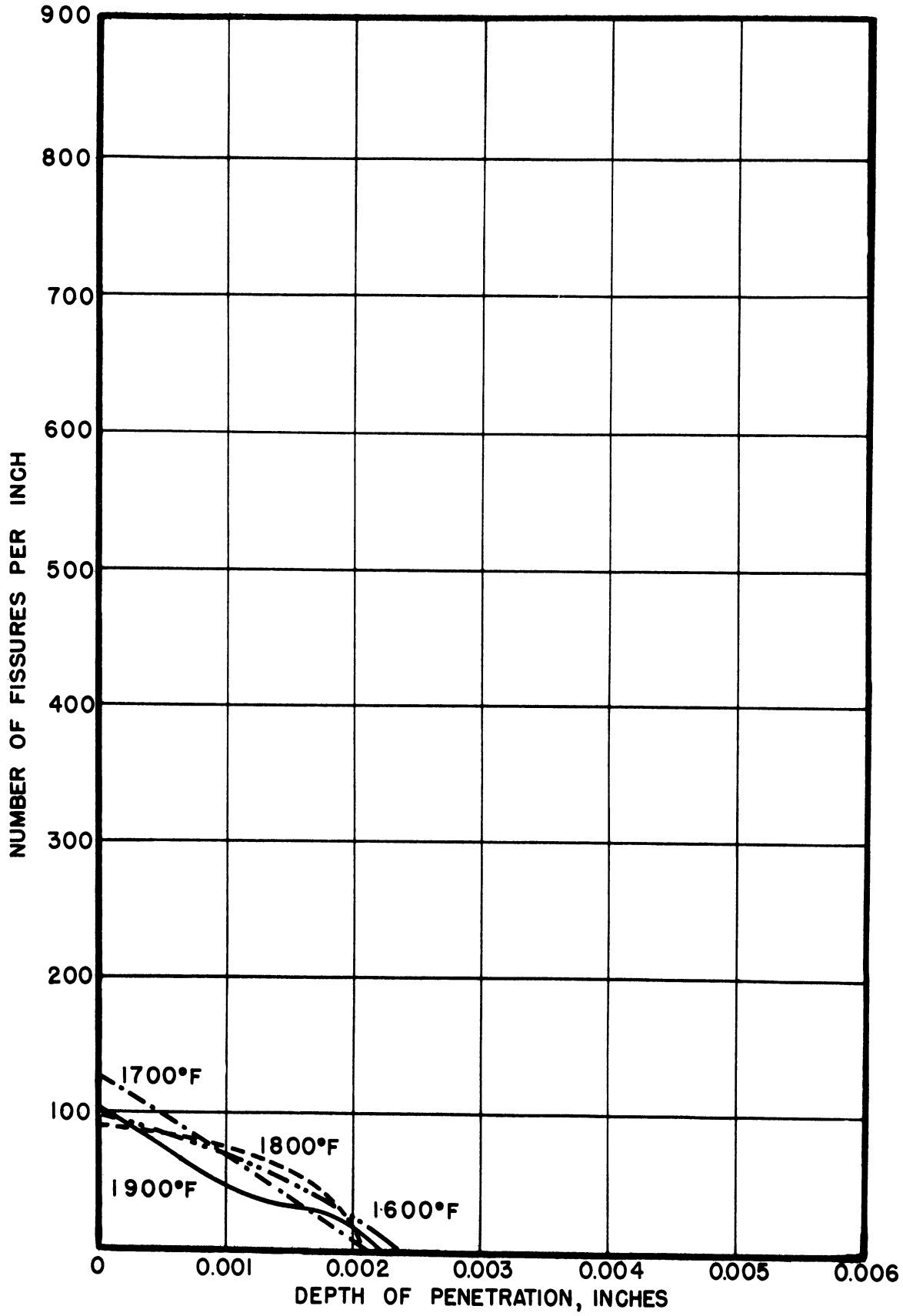

FIG. 30-PENETRATION VS. DEPTH BELOW SURFACE. TYPE 310 ALLOY, HEAT 64177. RUN 9. CURVED SECTION.

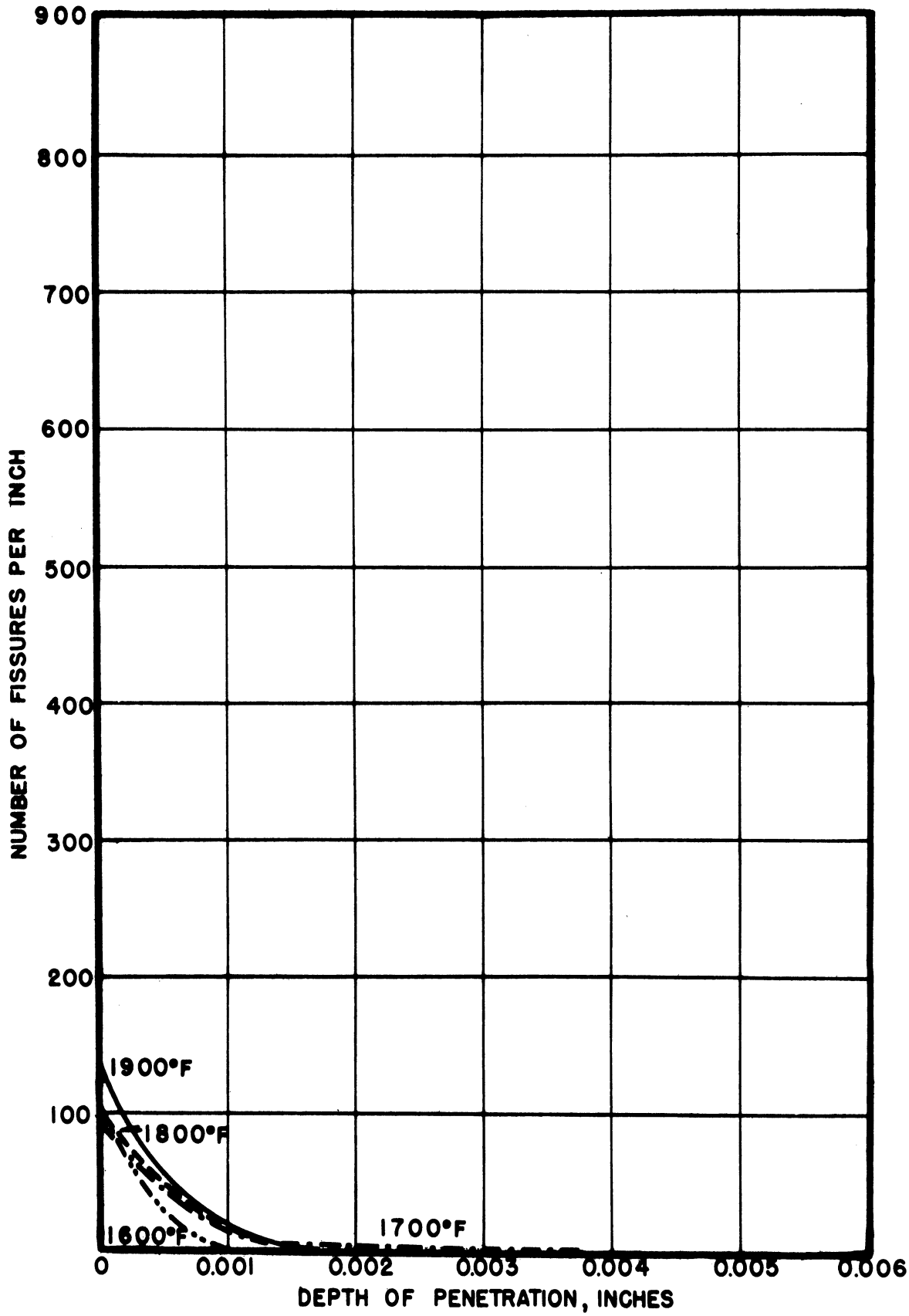

FIG. 31 - PENETRATION VS. DEPTH BELOW SURFACE. TYPE 310 ALLOY, HEAT 64270. RUN 9. CURVED SECTION.

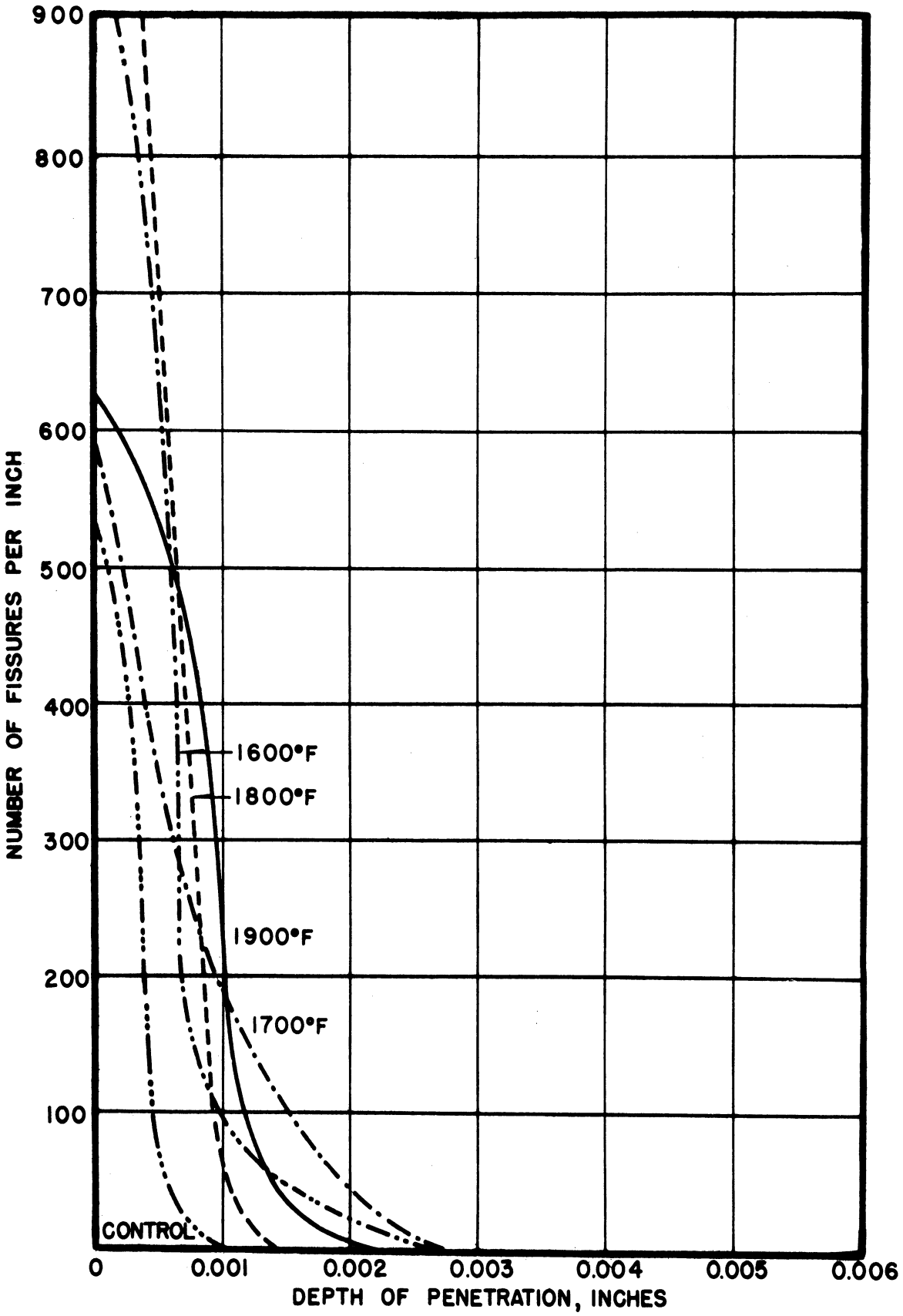

FIG.32 - PENETRATION VS. DEPTH BELOW SURFACE. TYPE 309+Nb ALLOY. RUN 10.

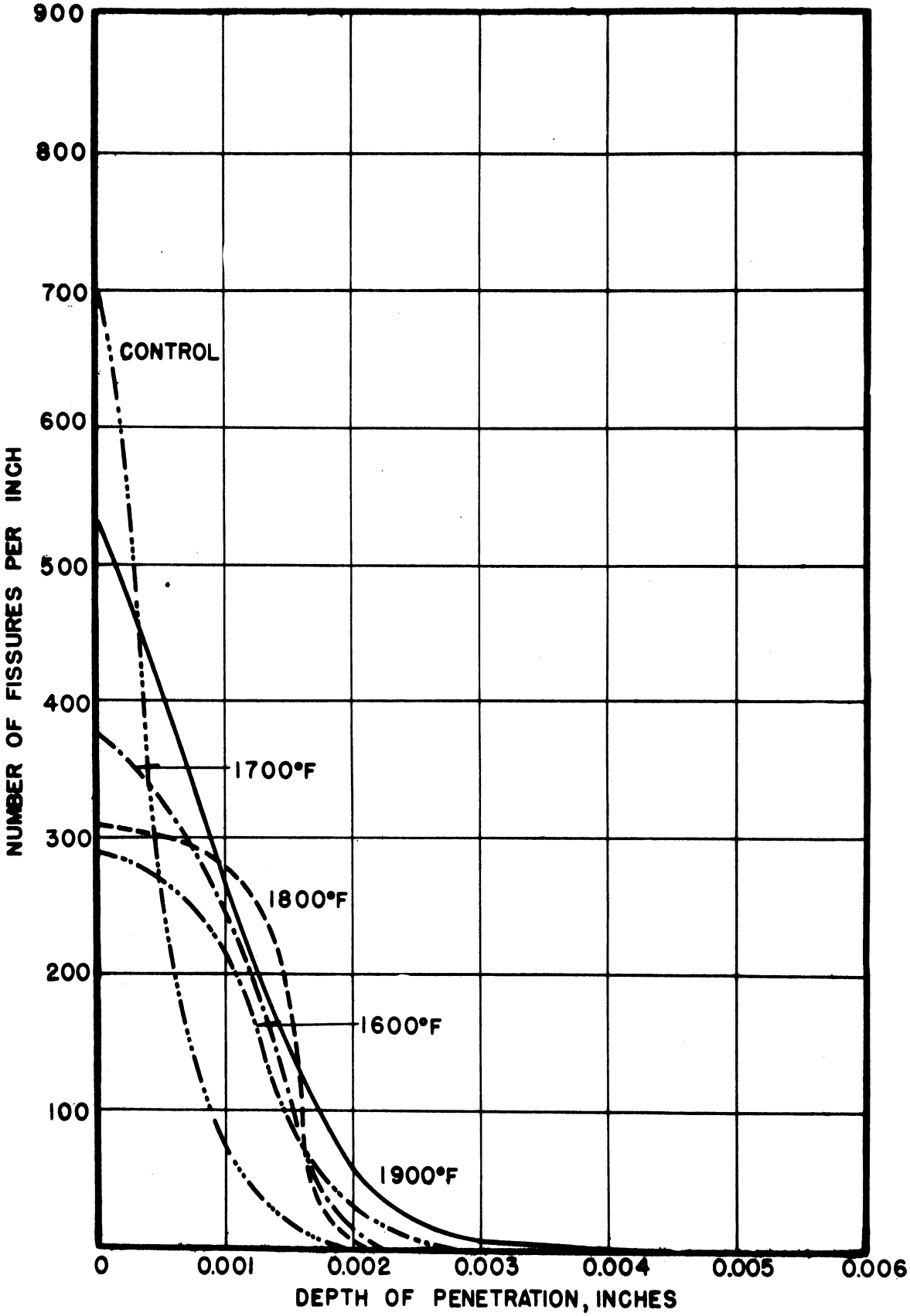

FIG. 33- PENETRATION VS. DEPTH BELOW SURFACE. TYPE 310 ALLOY, HEAT 64177. RUN 10.

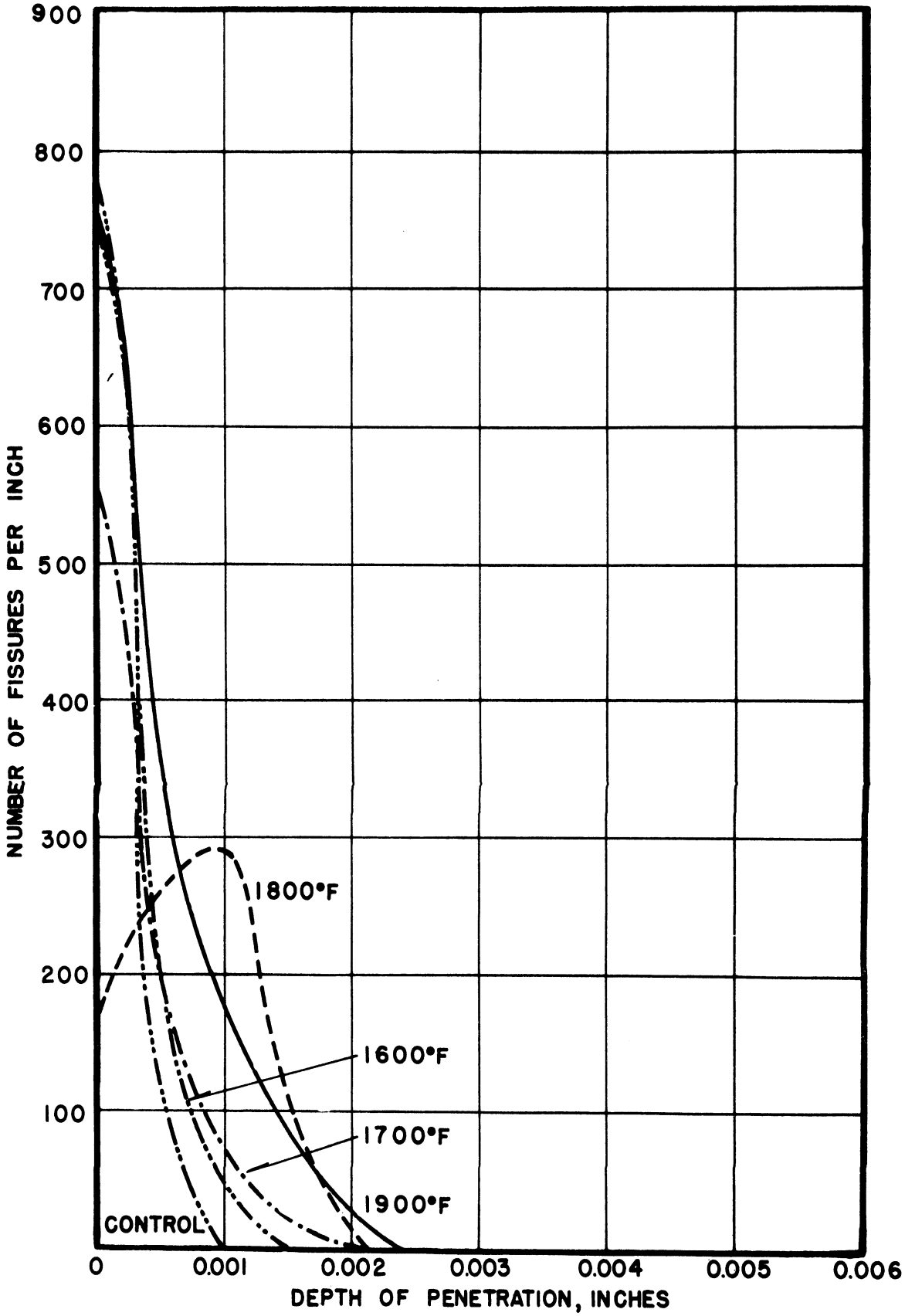

FIG. 34-PENETRATION VS. DEPTH BELOW SURFACE.
TYPE 310 ALLOY, HEAT 64270. RUN 10.

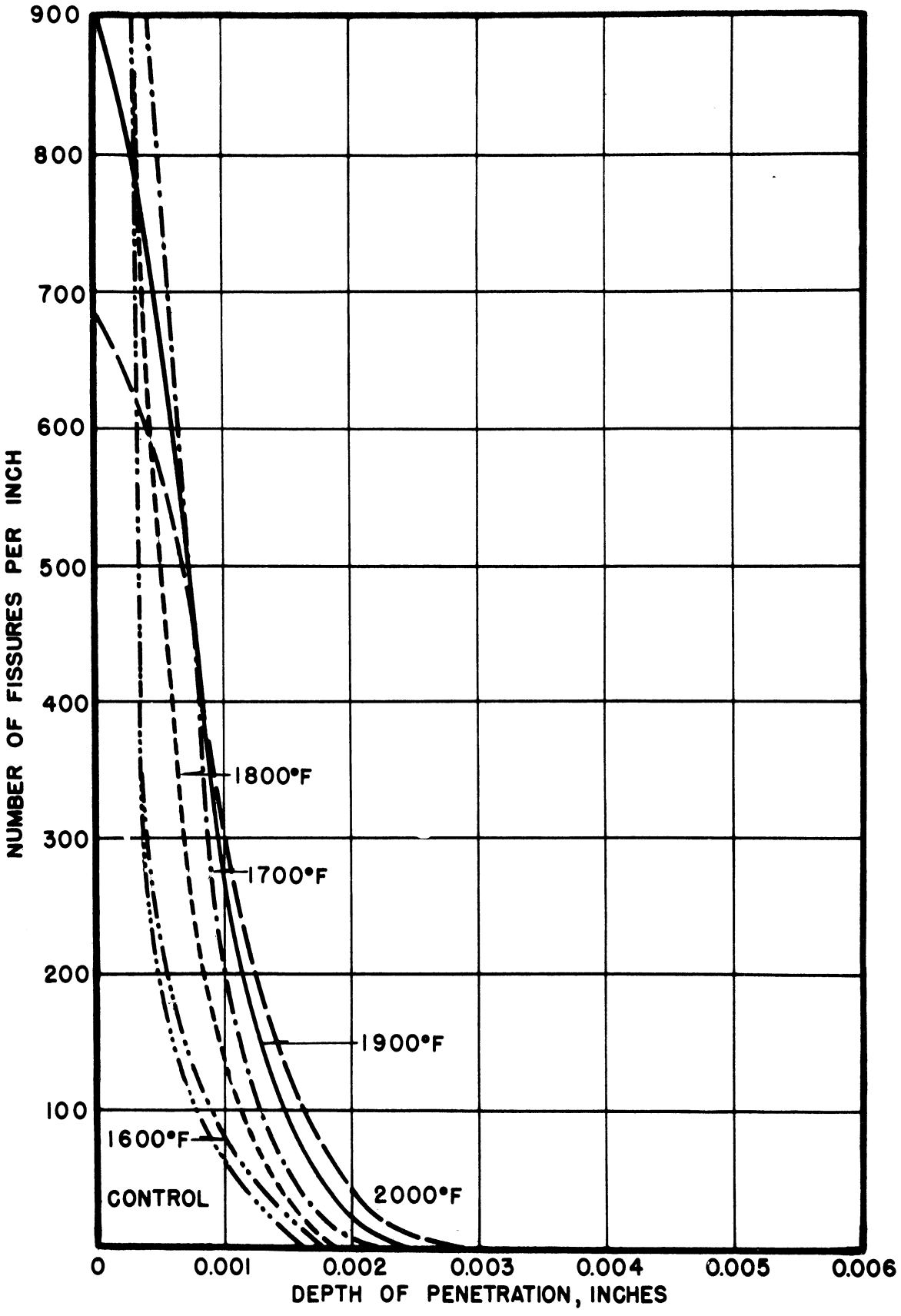

FIG. 35 - PENETRATION VS. DEPTH BELOW SURFACE.
TYPE 309 + Nb ALLOY. RUNS 11 & 27.

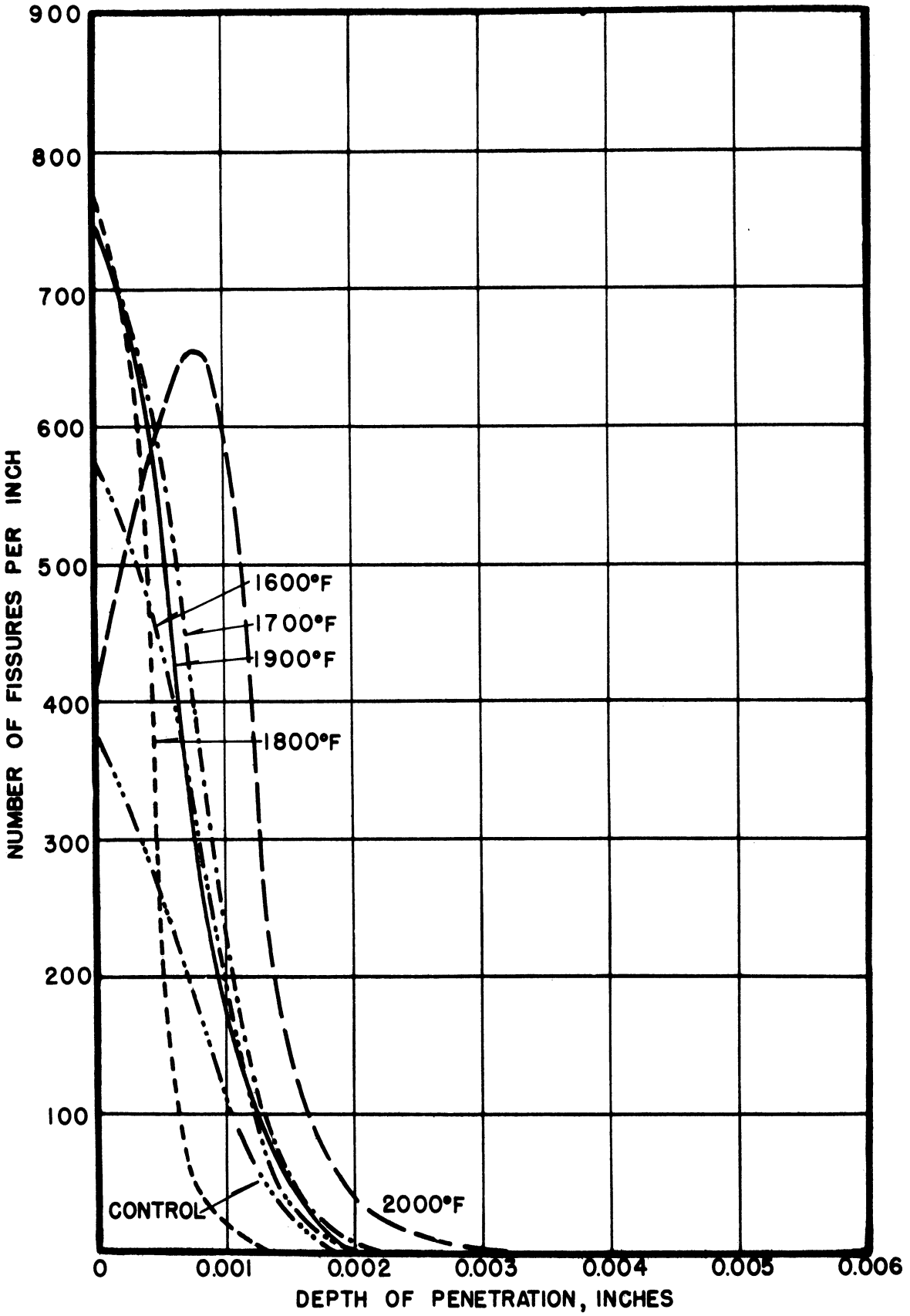

FIG. 36 - PENETRATION VS. DEPTH BELOW SURFACE.
TYPE 310 ALLOY, HEAT 64177. RUNS 11 & 27.

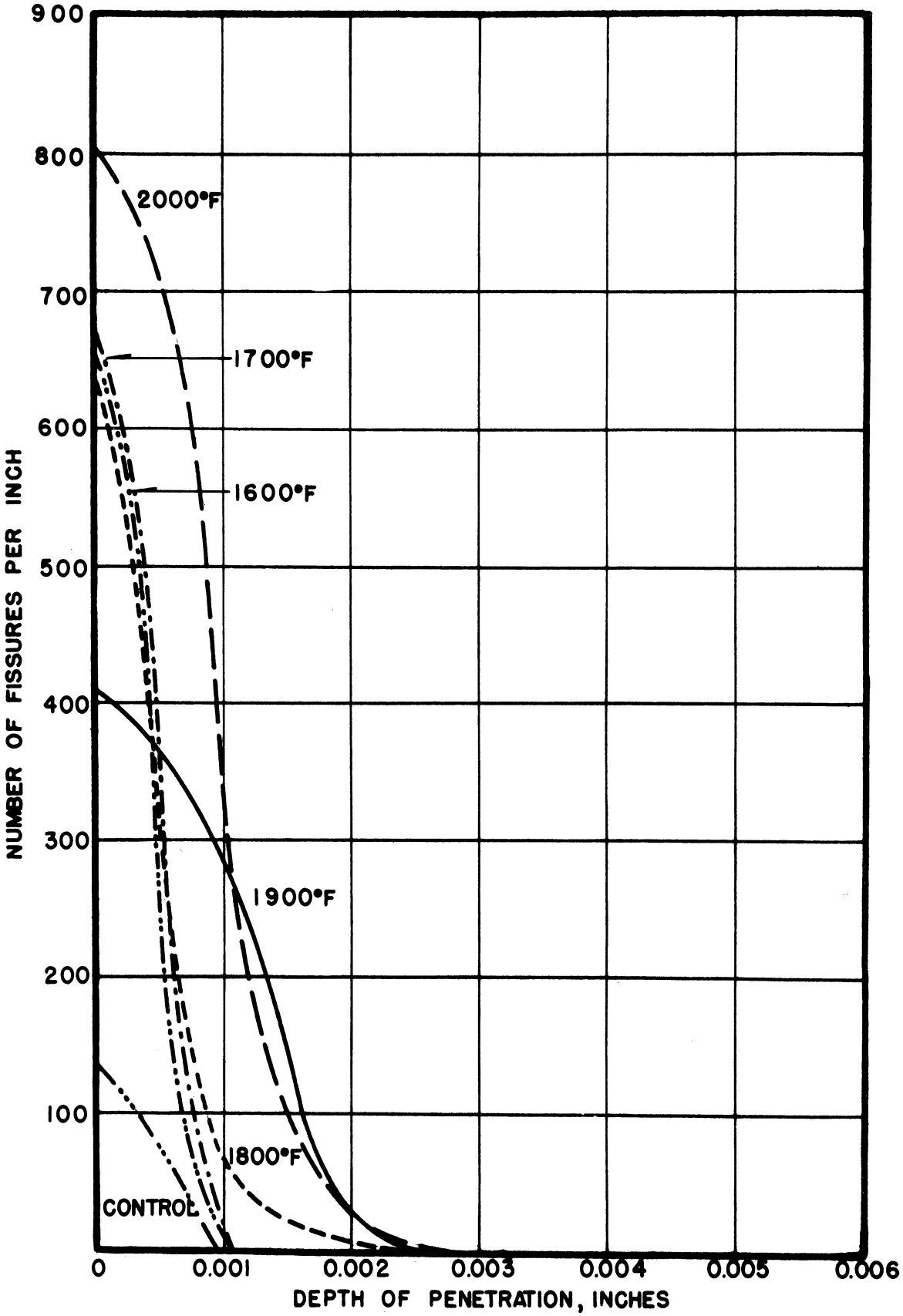

FIG. 37- PENETRATION VS. DEPTH BELOW SURFACE. TYPE 310 ALLOY, HEAT 64270. RUNS 11 & 27.

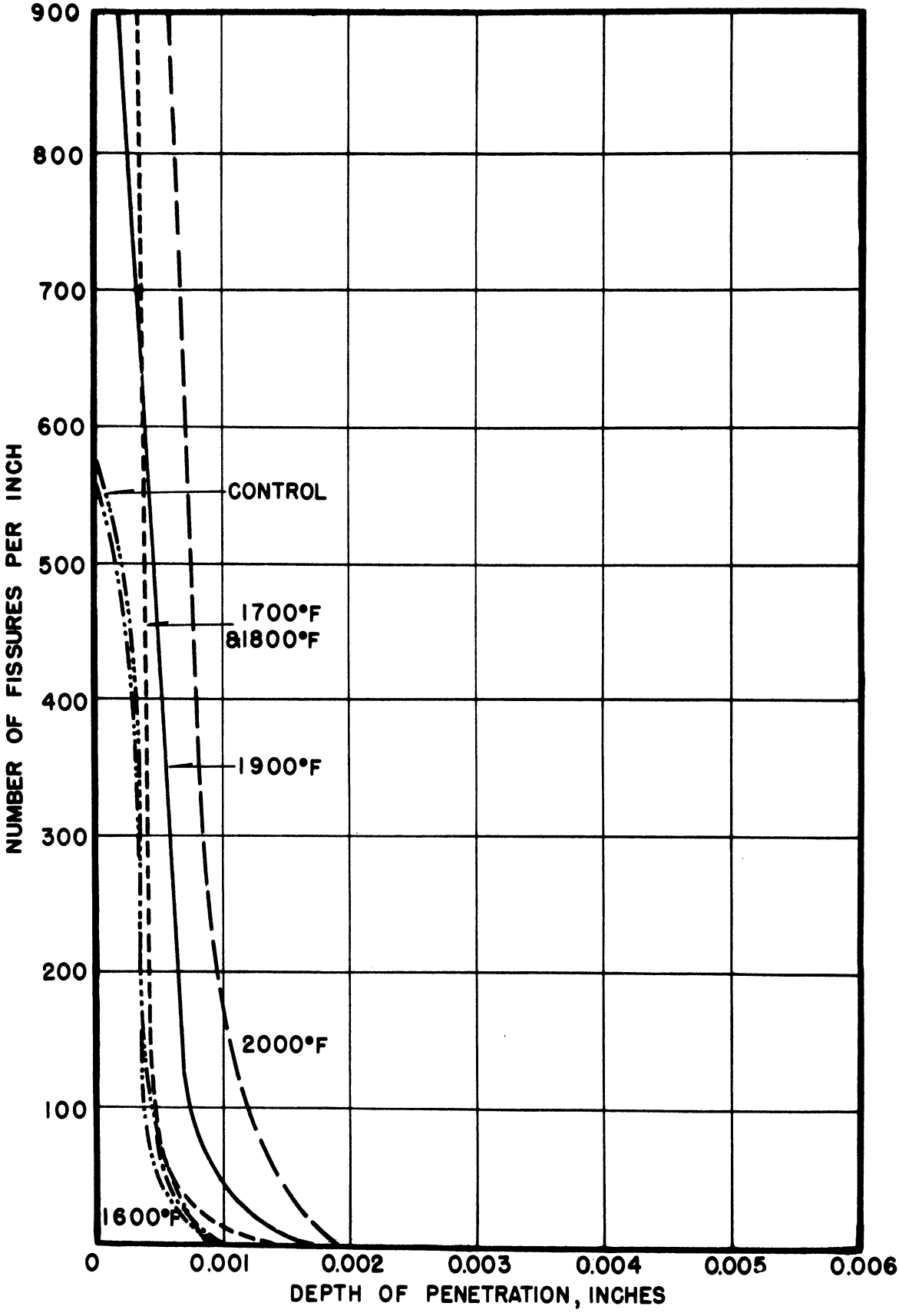

FIG. 38- PENETRATION VS. DEPTH BELOW SURFACE. TYPE 309+Nb ALLOY. RUNS 12 & 26.

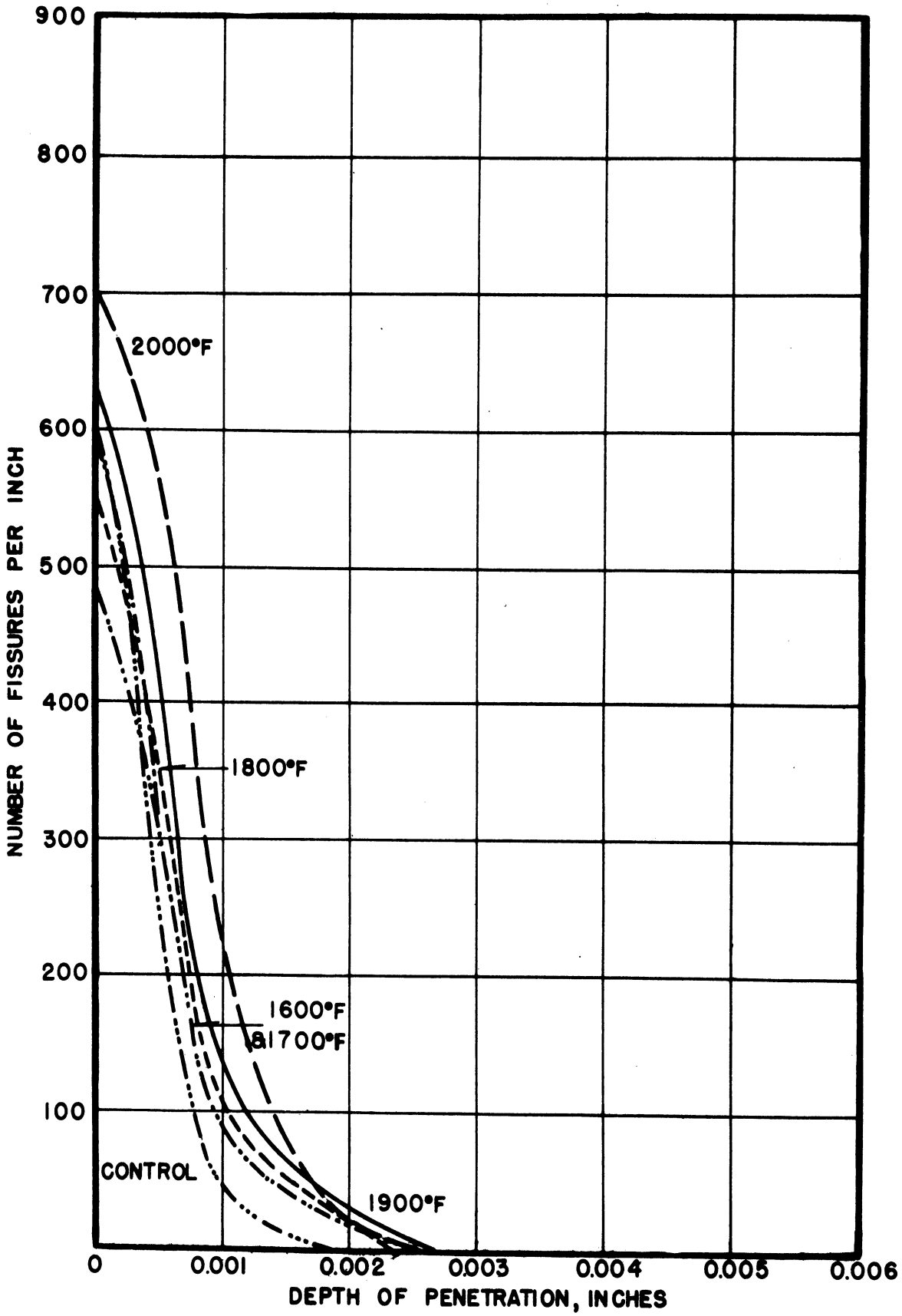

FIG. 39 - PENETRATION VS. DEPTH BELOW SURFACE.
TYPE 310 ALLOY, HEAT 64177. RUNS 12 & 26.

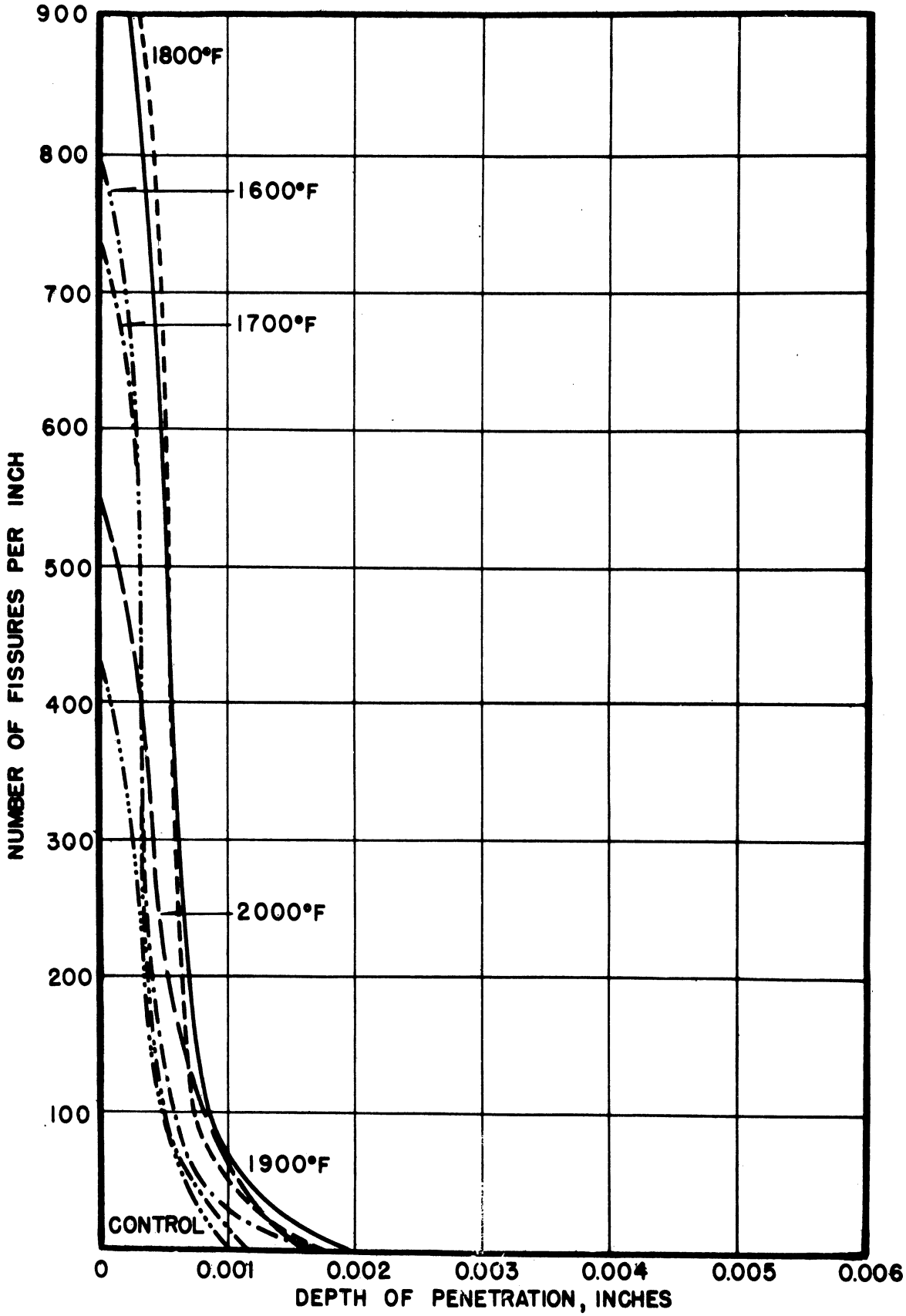

FIG. 40 - PENETRATION VS. DEPTH BELOW SURFACE.
TYPE 310 ALLOY. HEAT 64270. RUNS 12 & 26.

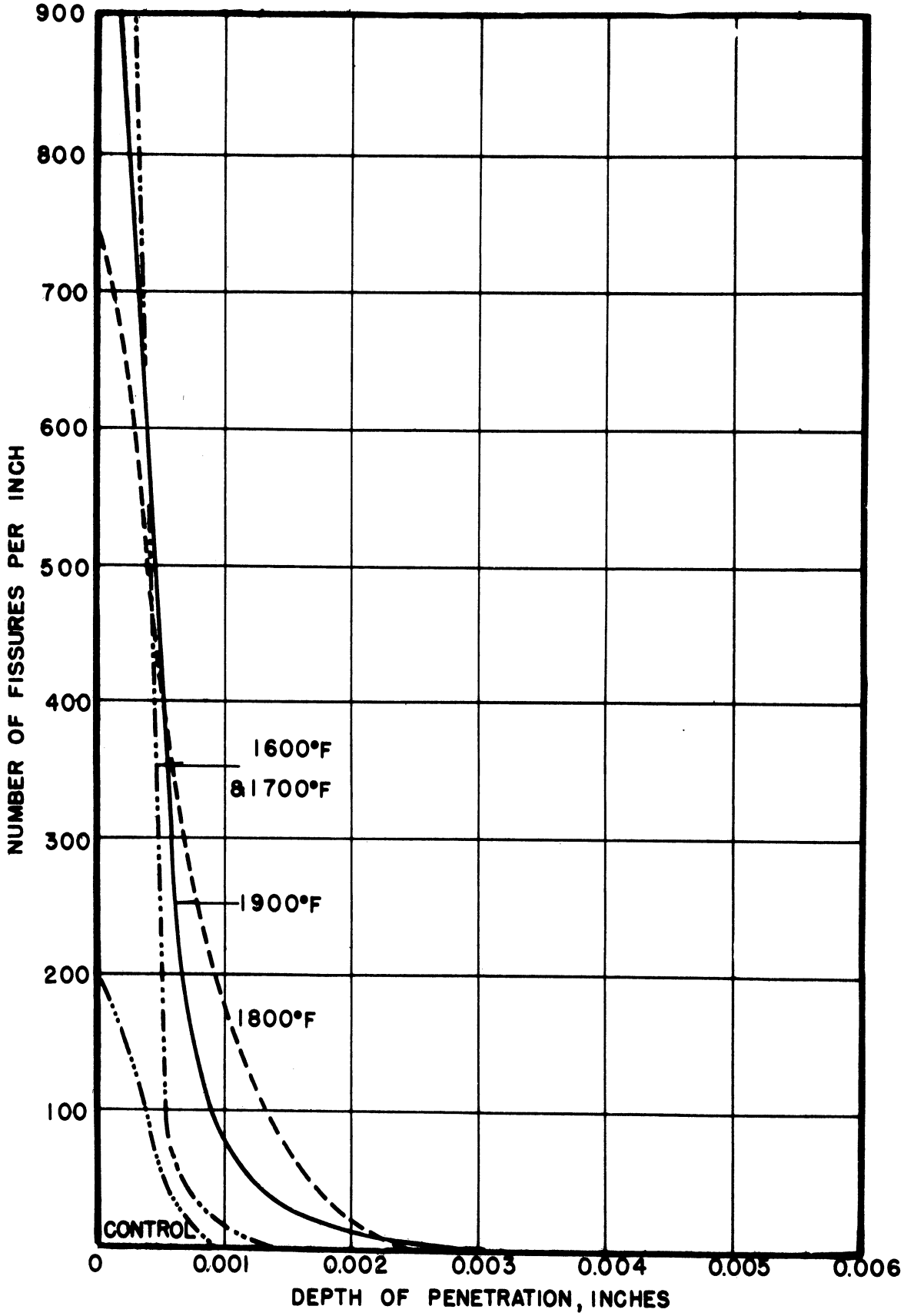

FIG. 41- PENETRATION VS. DEPTH BELOW SURFACE.
TYPE 309 + Nb ALLOY. RUN 13.

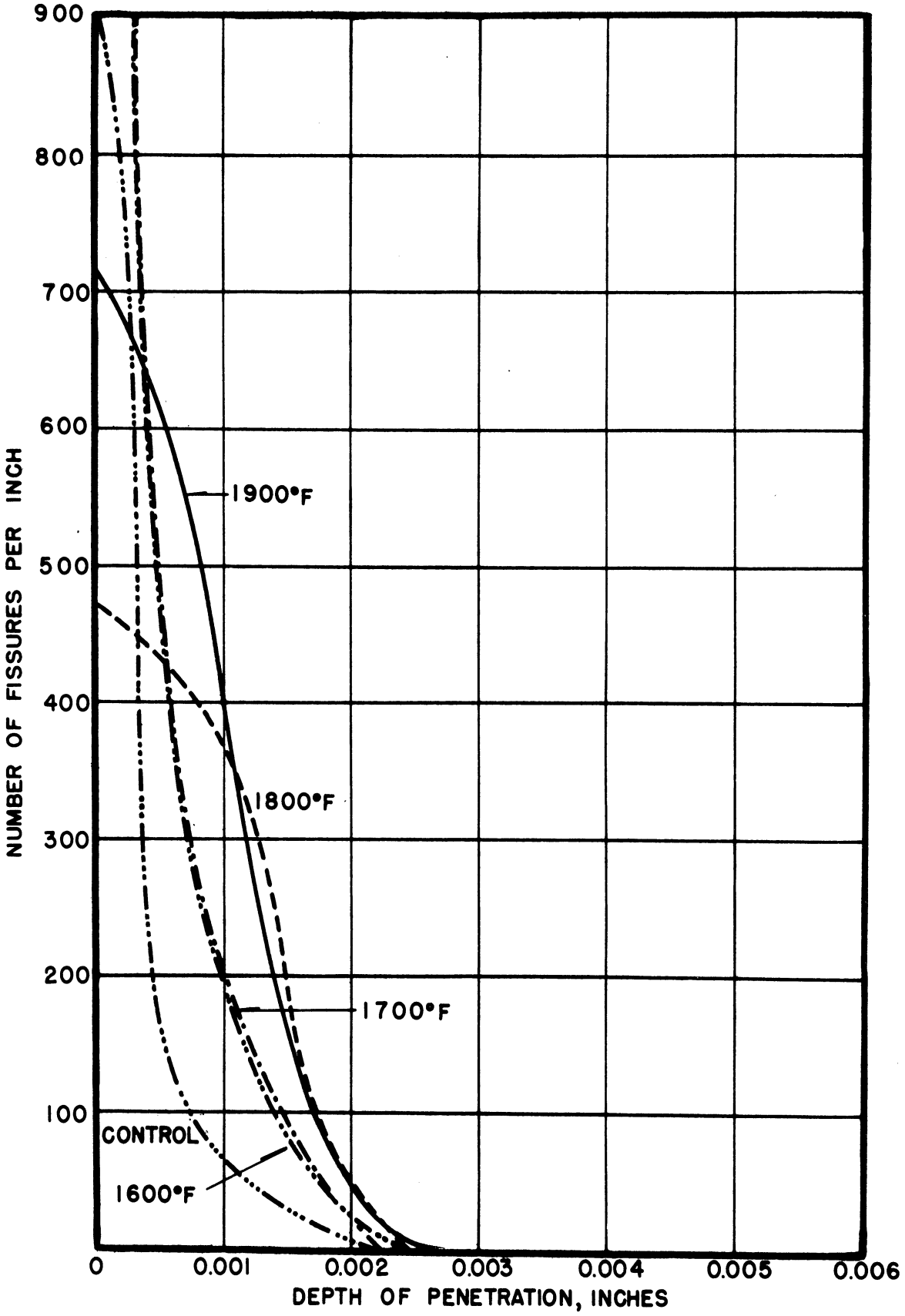

FIG. 42 - PENETRATION VS. DEPTH BELOW SURFACE. TYPE 310 ALLOY, HEAT 64177. RUN 13.

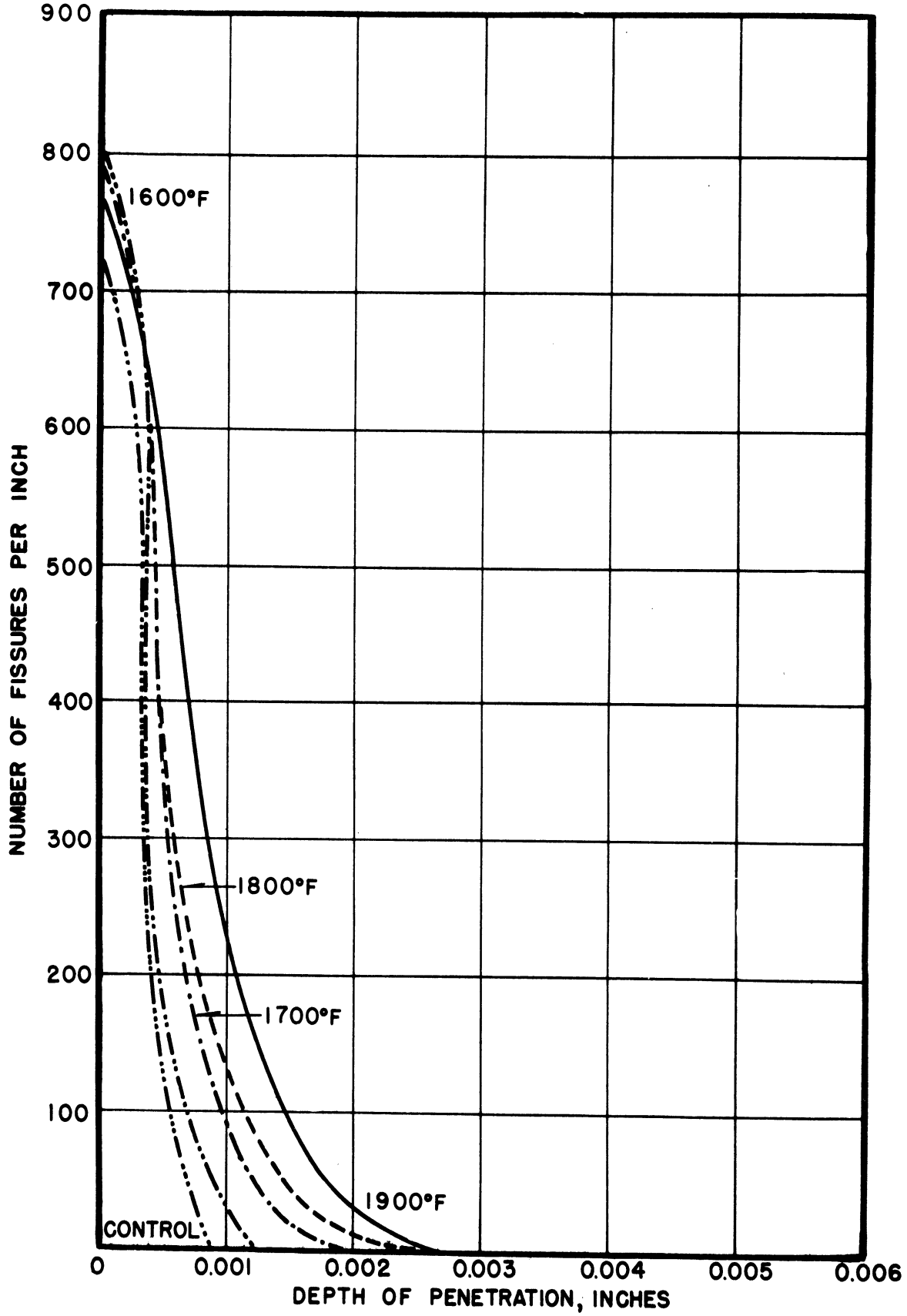

FIG. 43- PENETRATION VS. DEPTH BELOW SURFACE.
TYPE 310 ALLOY, HEAT 64270. RUN 13.

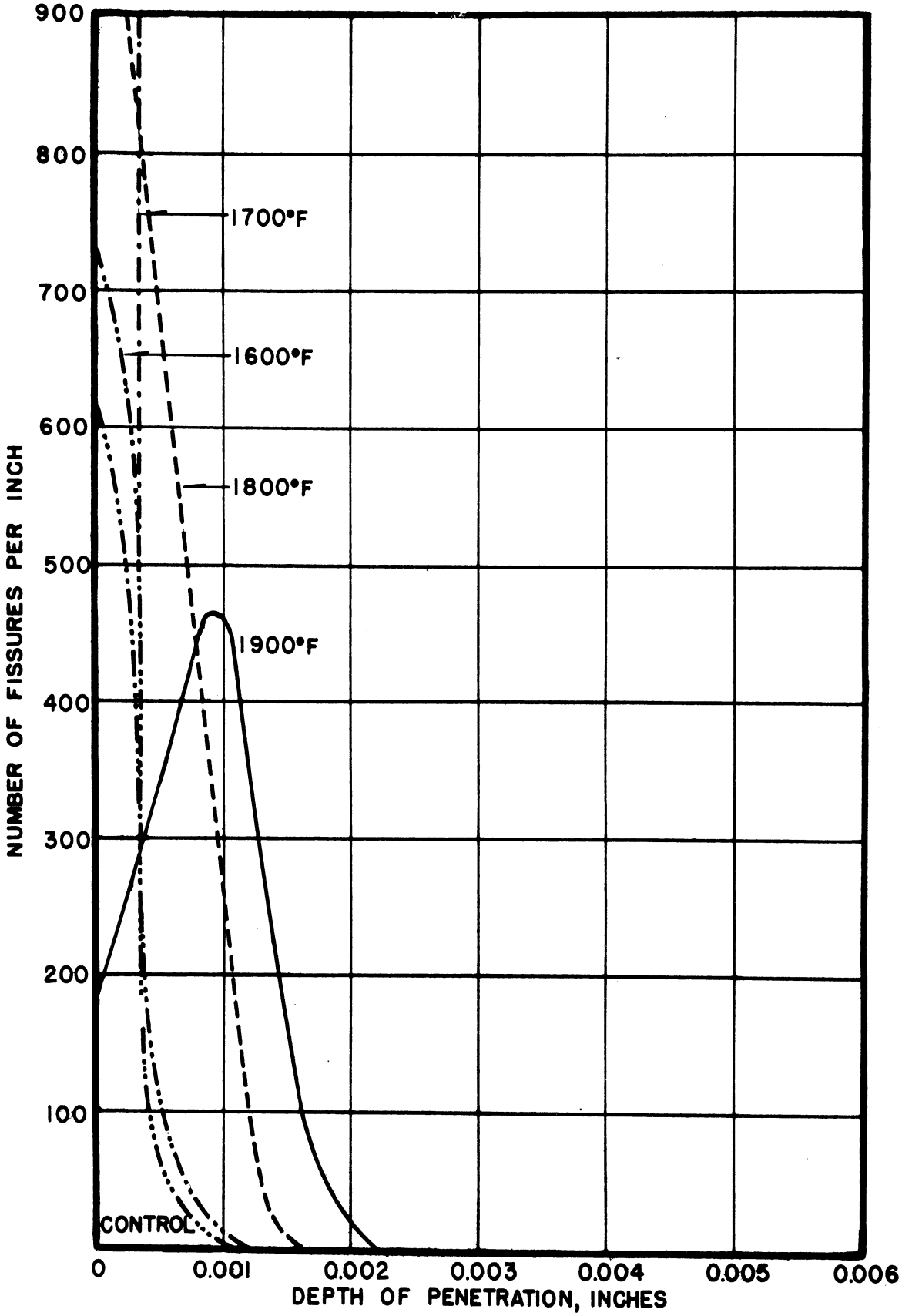

FIG. 44- PENETRATION VS. DEPTH BELOW SURFACE. TYPE 309 + Nb ALLOY. RUN 14.

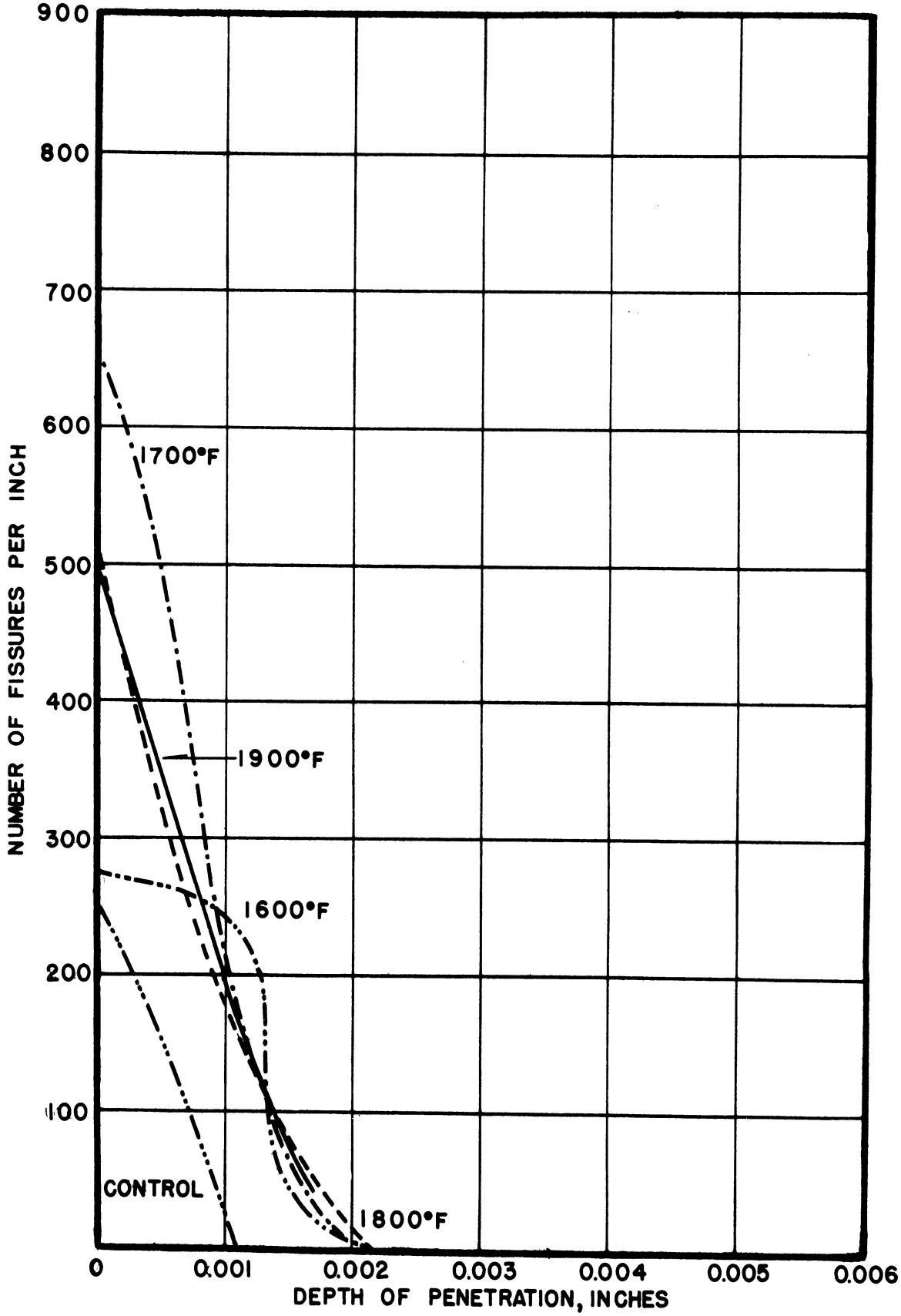

FIG. 45-PENETRATION VS. DEPTH BELOW SURFACE. TYPE 310 ALLOY, HEAT 64177. RUN 14.

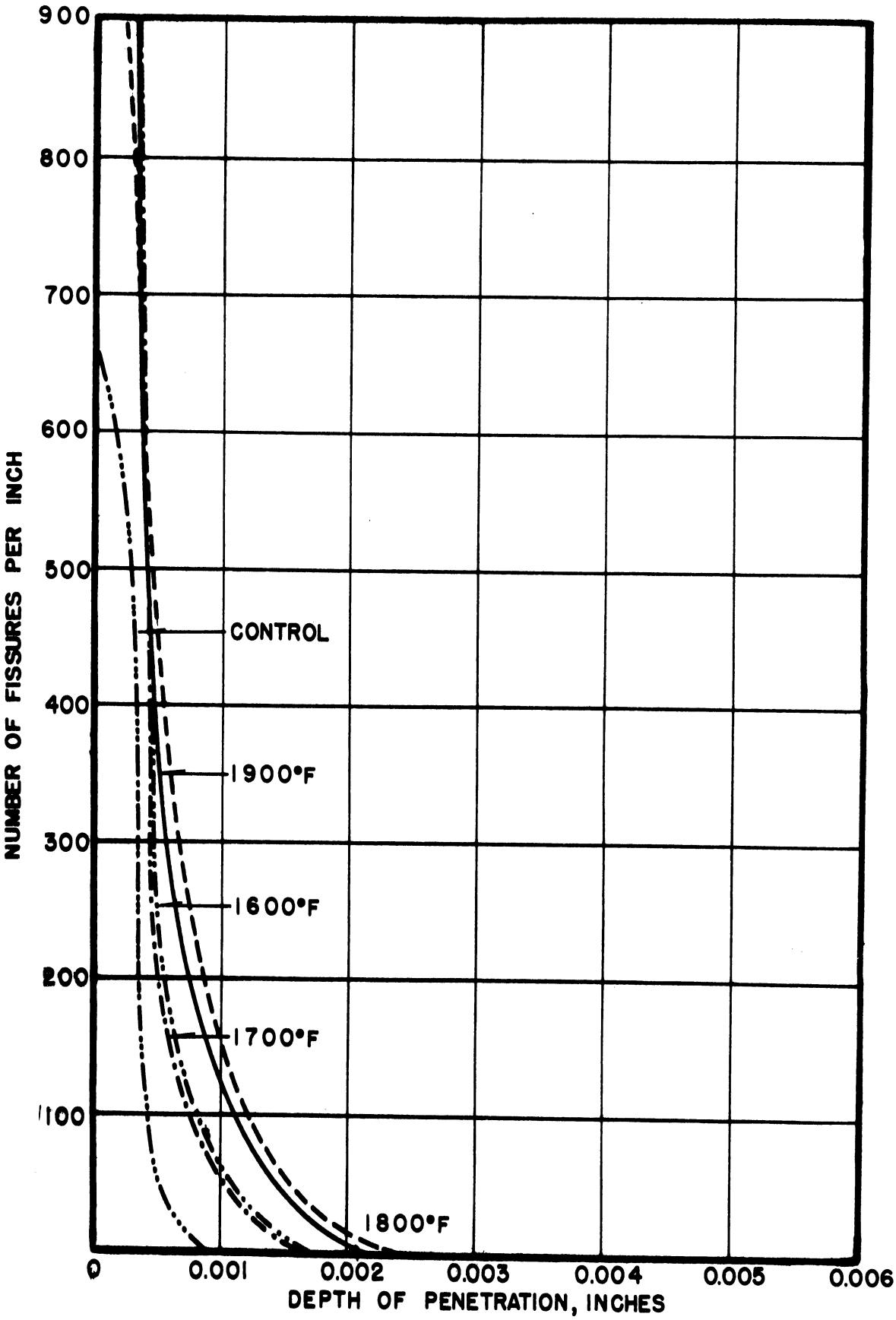

FIG. 46-PENETRATION VS. DEPTH BELOW SURFACE.
TYPE 310 ALLOY, HEAT 64270. RUN 14.

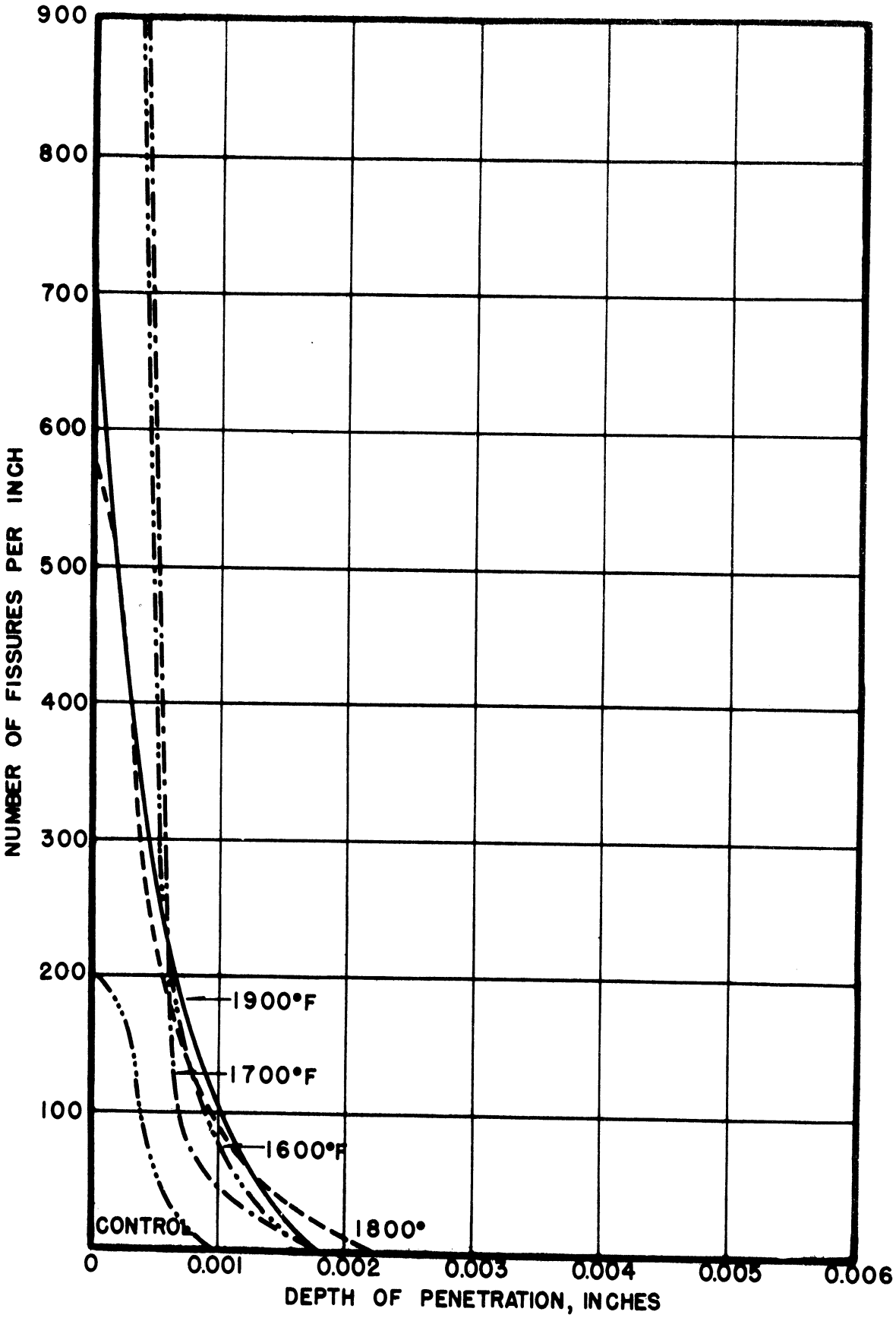

FIG. 47-PENETRATION VS. DEPTH BELOW SURFACE. TYPE 309+Nb ALLOY. RUN 15.

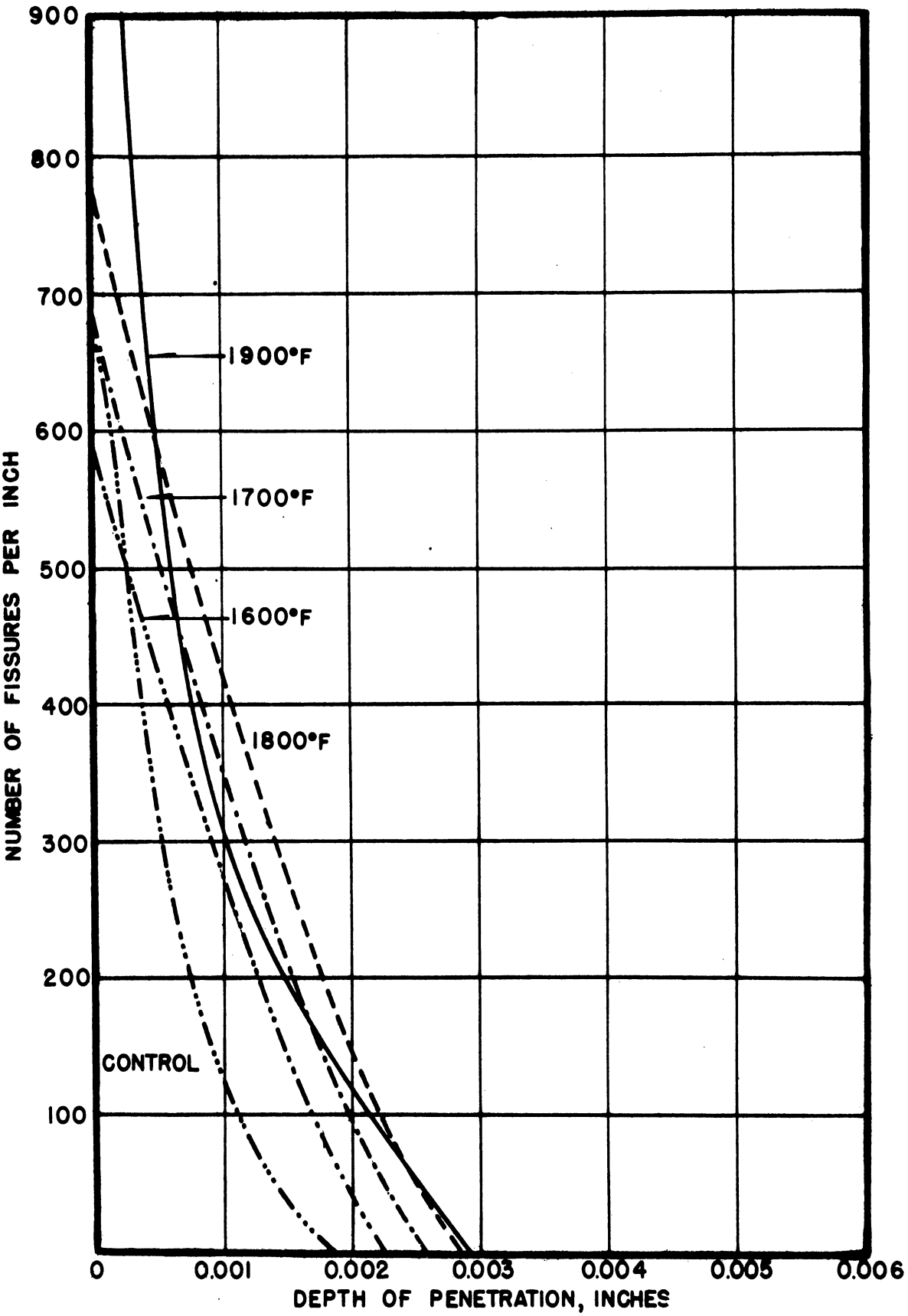

FIG. 48 - PENETRATION VS. DEPTH BELOW SURFACE. TYPE 310 ALLOY, HEAT 64177. RUN 15.

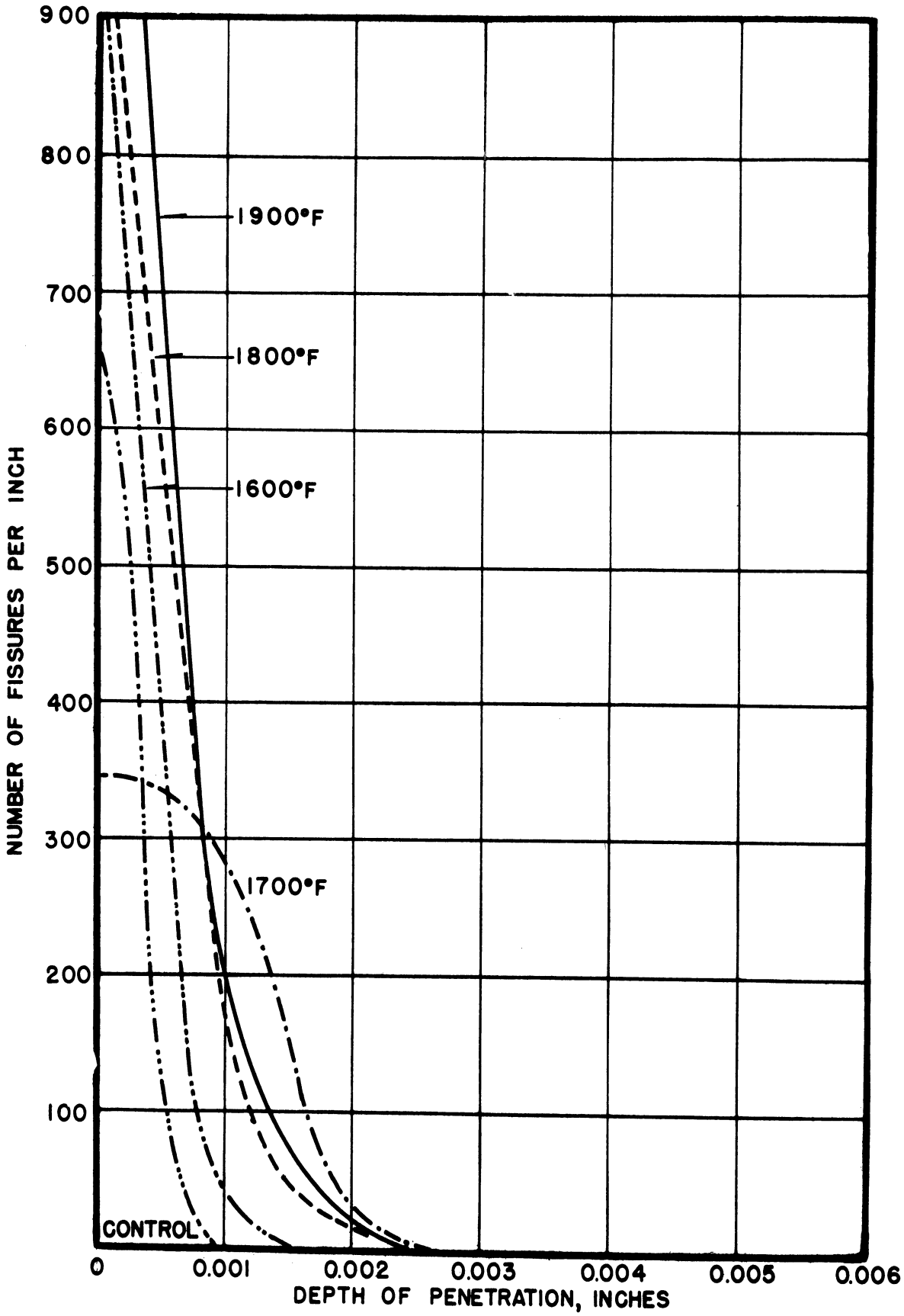

FIG. 49 - PENETRATION VS. DEPTH BELOW SURFACE. TYPE 310 ALLOY, HEAT 64270. RUN 15.

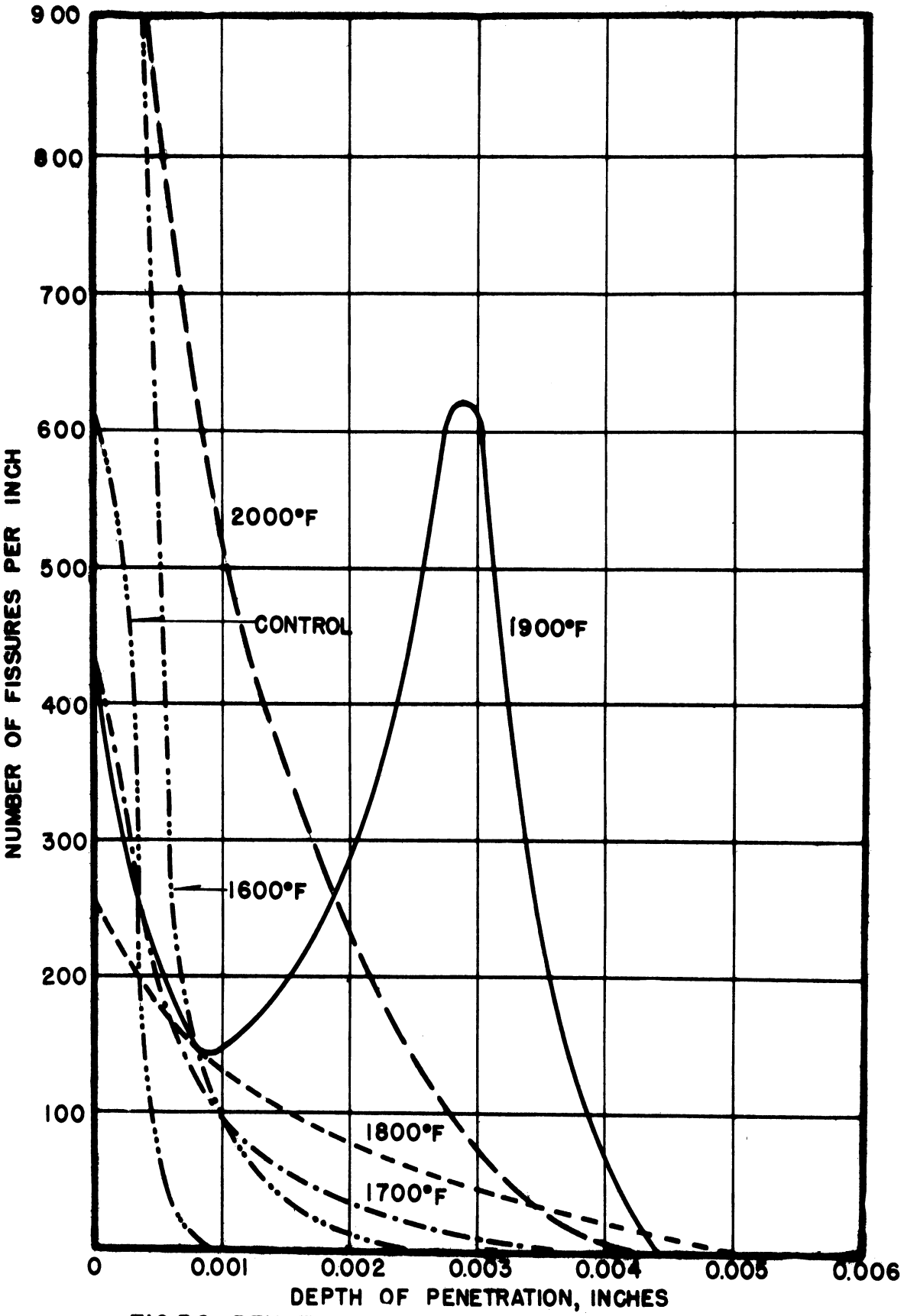

FIG.50- PENETRATION VS. DEPTH BELOW SURFACE. TYPE 310 ALLOY, HEAT X11306. RUNS 16 & 28.

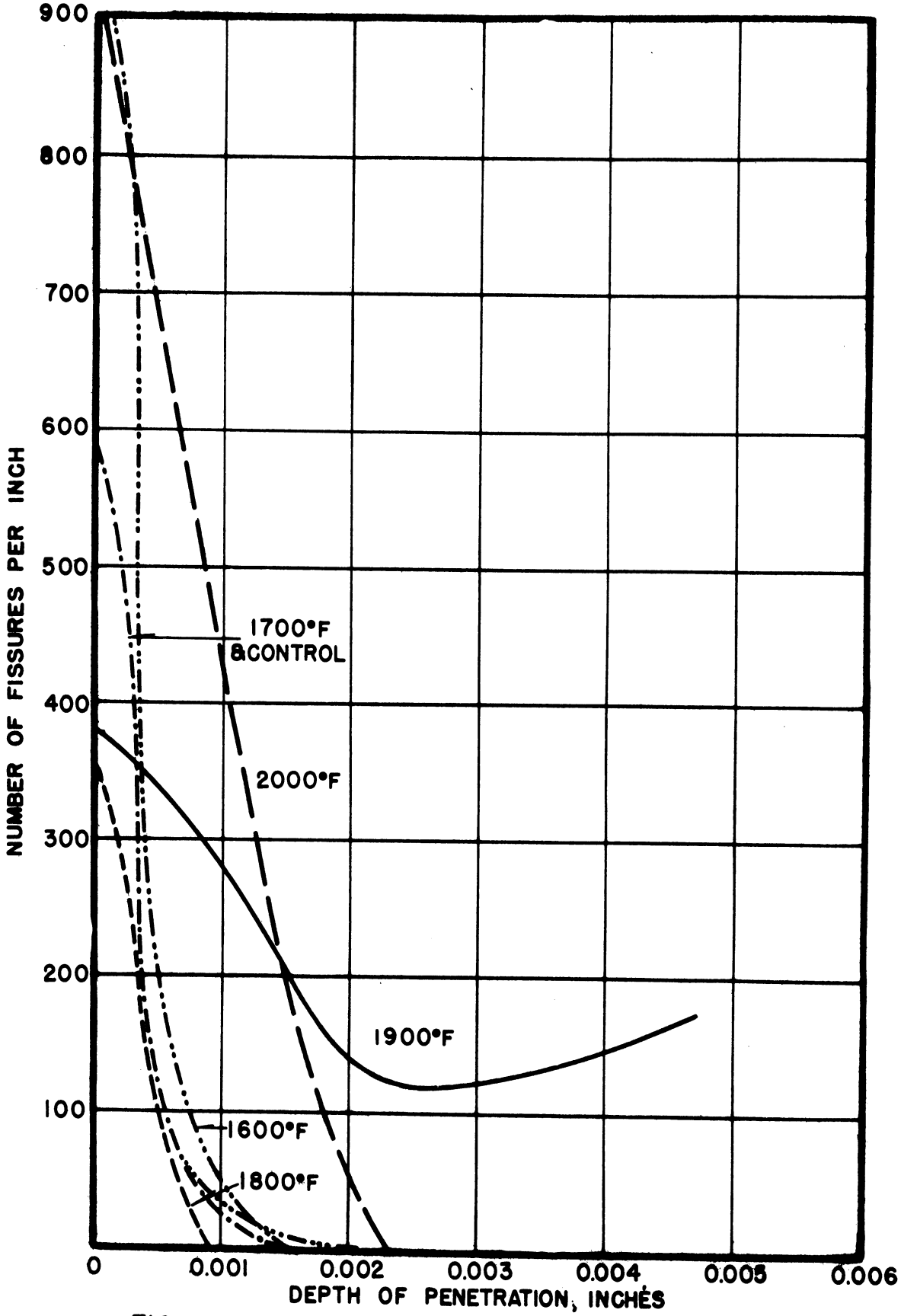

FIG. 51 - PENETRATION VS. DEPTH BELOW SURFACE.
TYPE 310 ALLOY, HEAT X11338. RUNS 16 & 28.

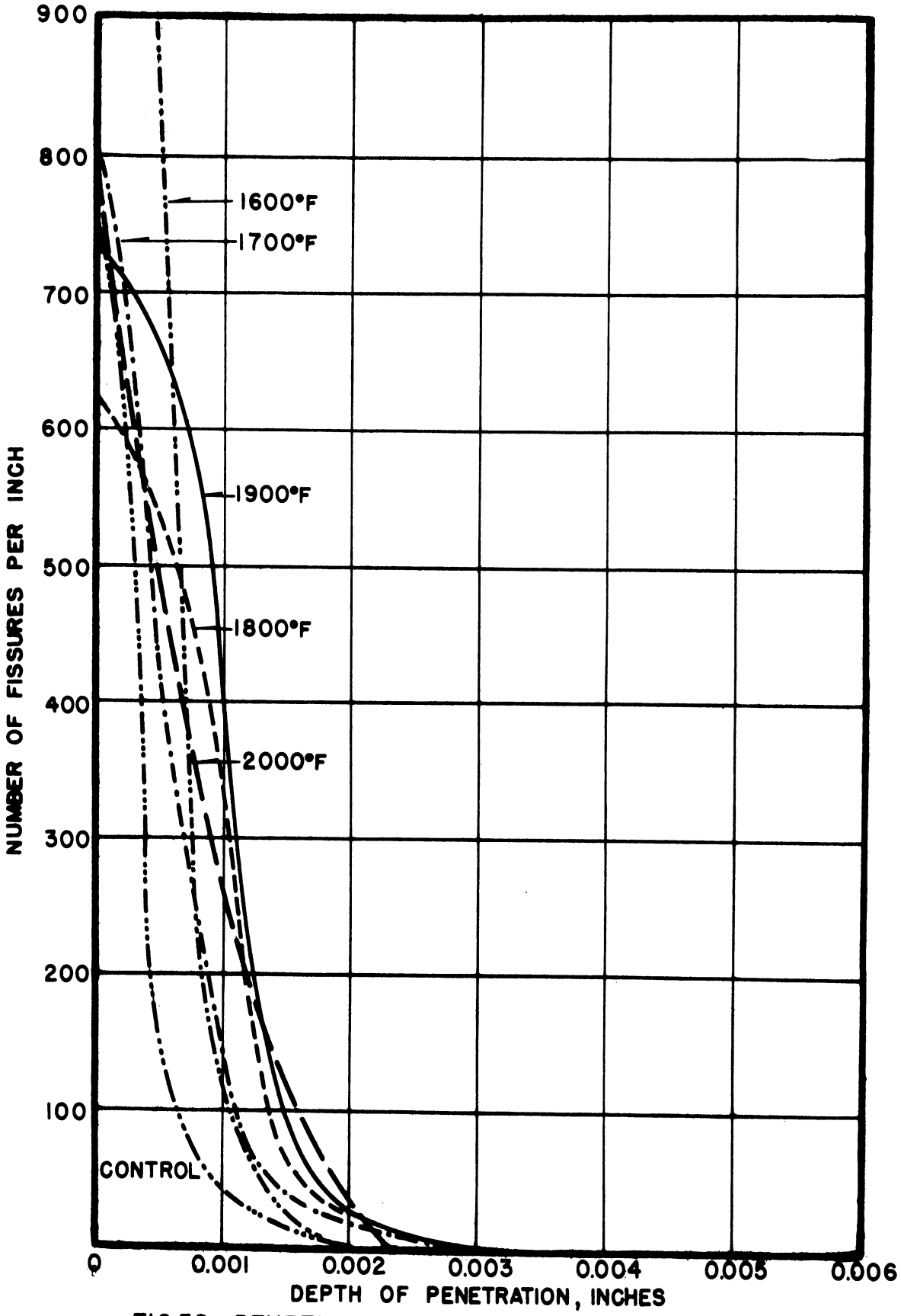

FIG.52 - PENETRATION VS. DEPTH BELOW SURFACE.
TYPE 310 ALLOY, HEAT X27258. RUNS 16 & 28.

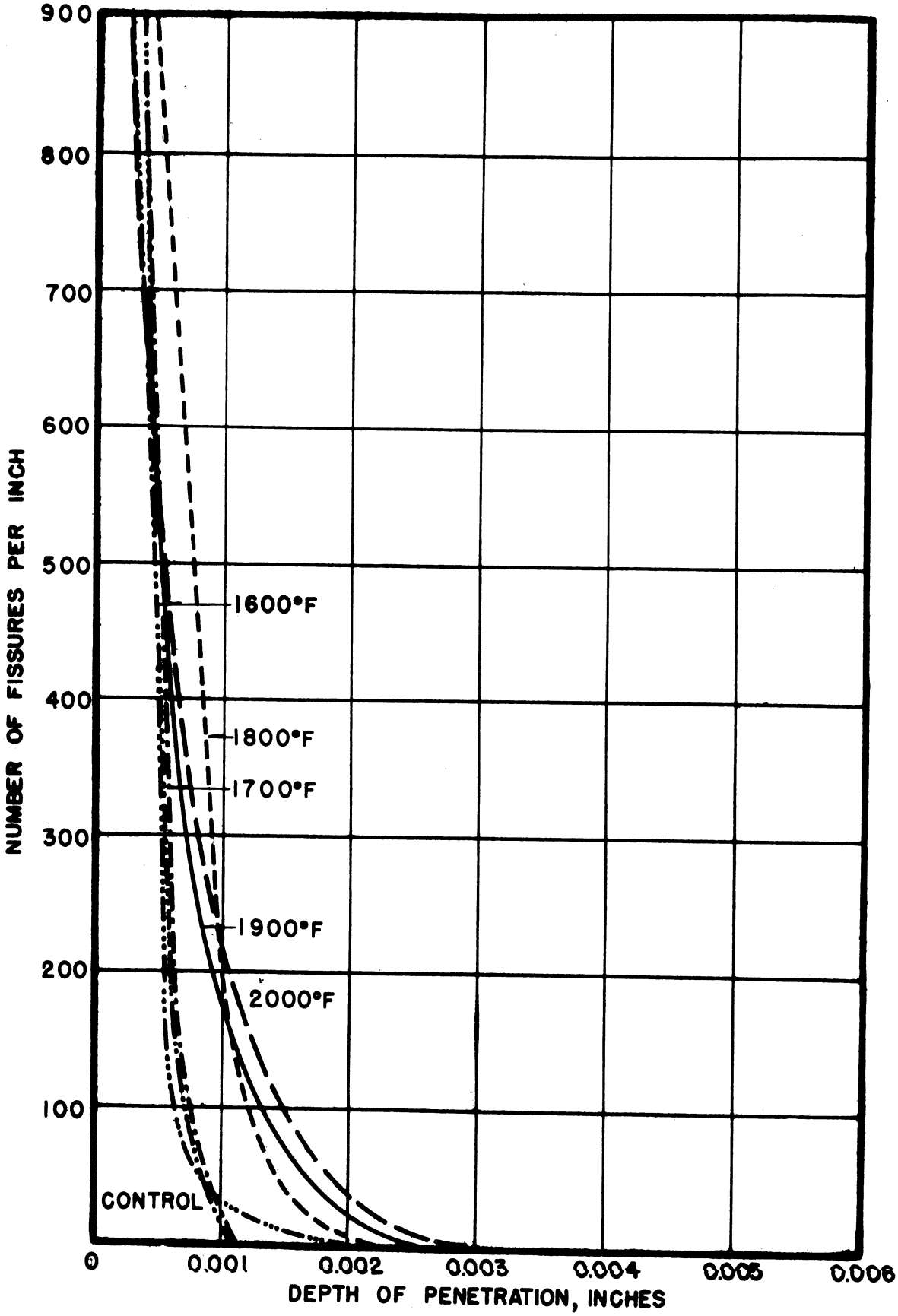

FIG.53 - PENETRATION VS. DEPTH BELOW SURFACE.
TYPE 310 ALLOY, HEAT X45558. RUNS 17 & 28.

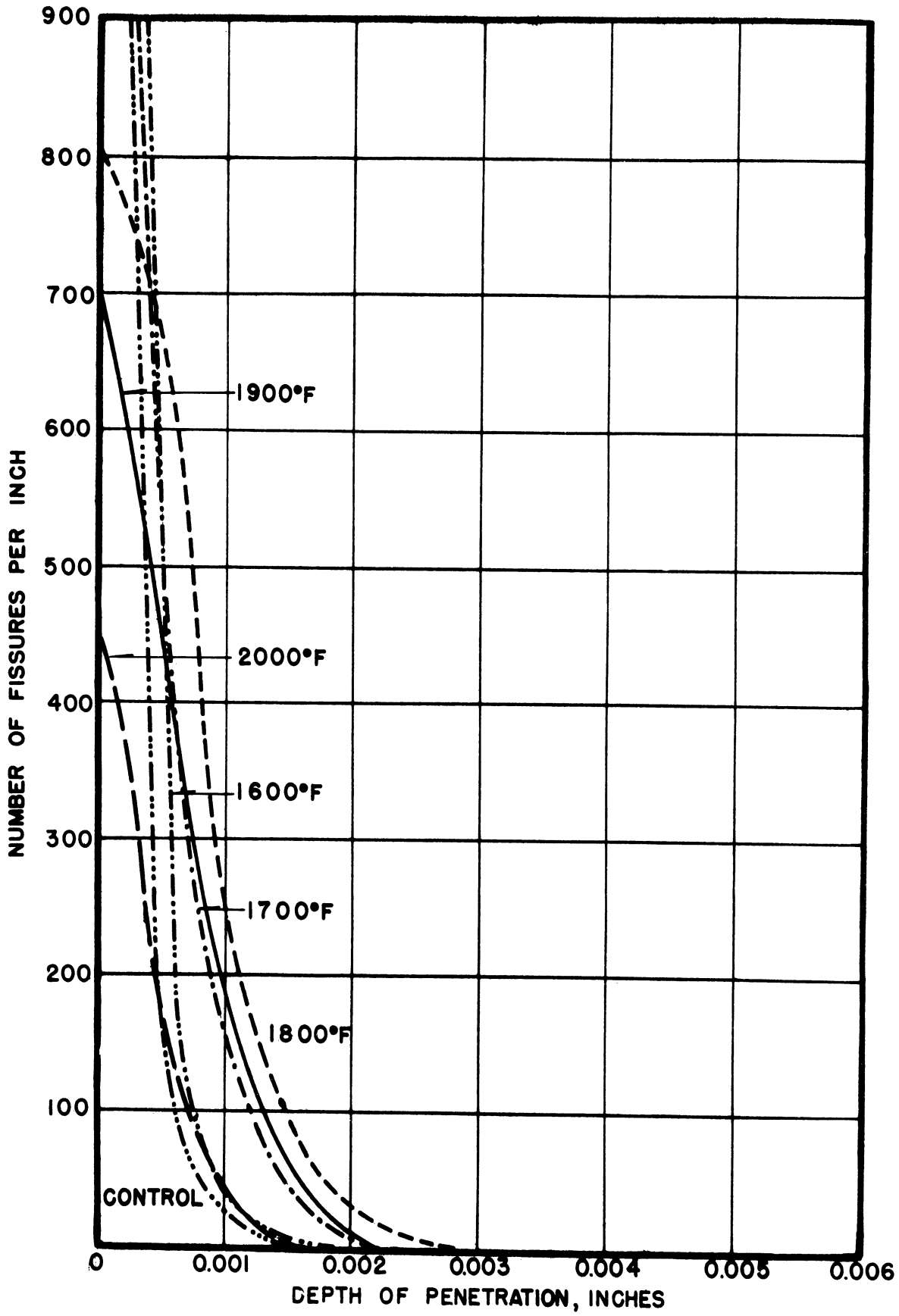

FIG. 54 - PENETRATION VS. DEPTH BELOW SURFACE.
TYPE 310 ALLOY, HEAT X46063. RUNS 17 & 28.

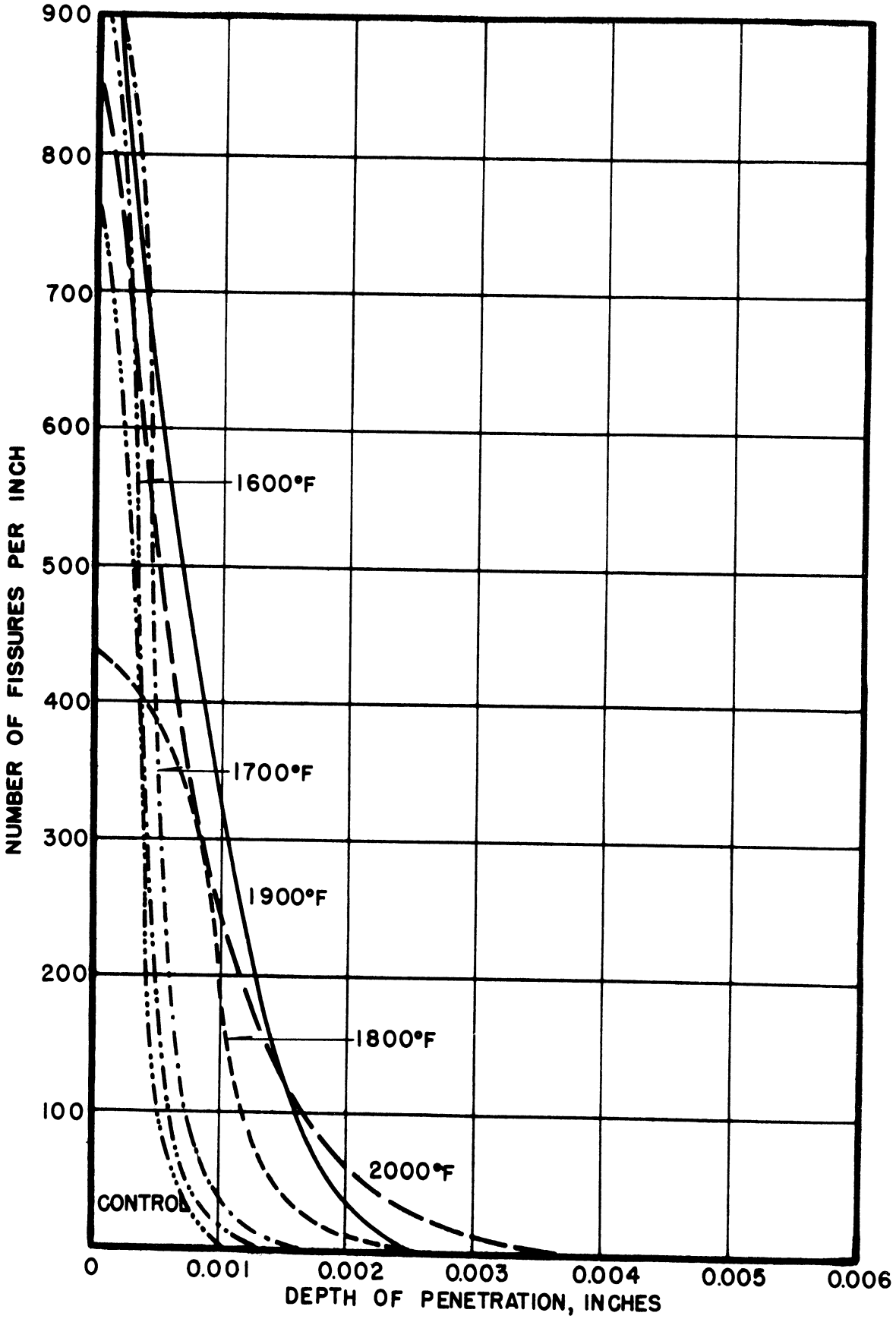

FIG.55- PENETRATION VS. DEPTH BELOW SURFACE.
TYPE 310 ALLOY, HEAT X46572. RUNS 17 & 28.

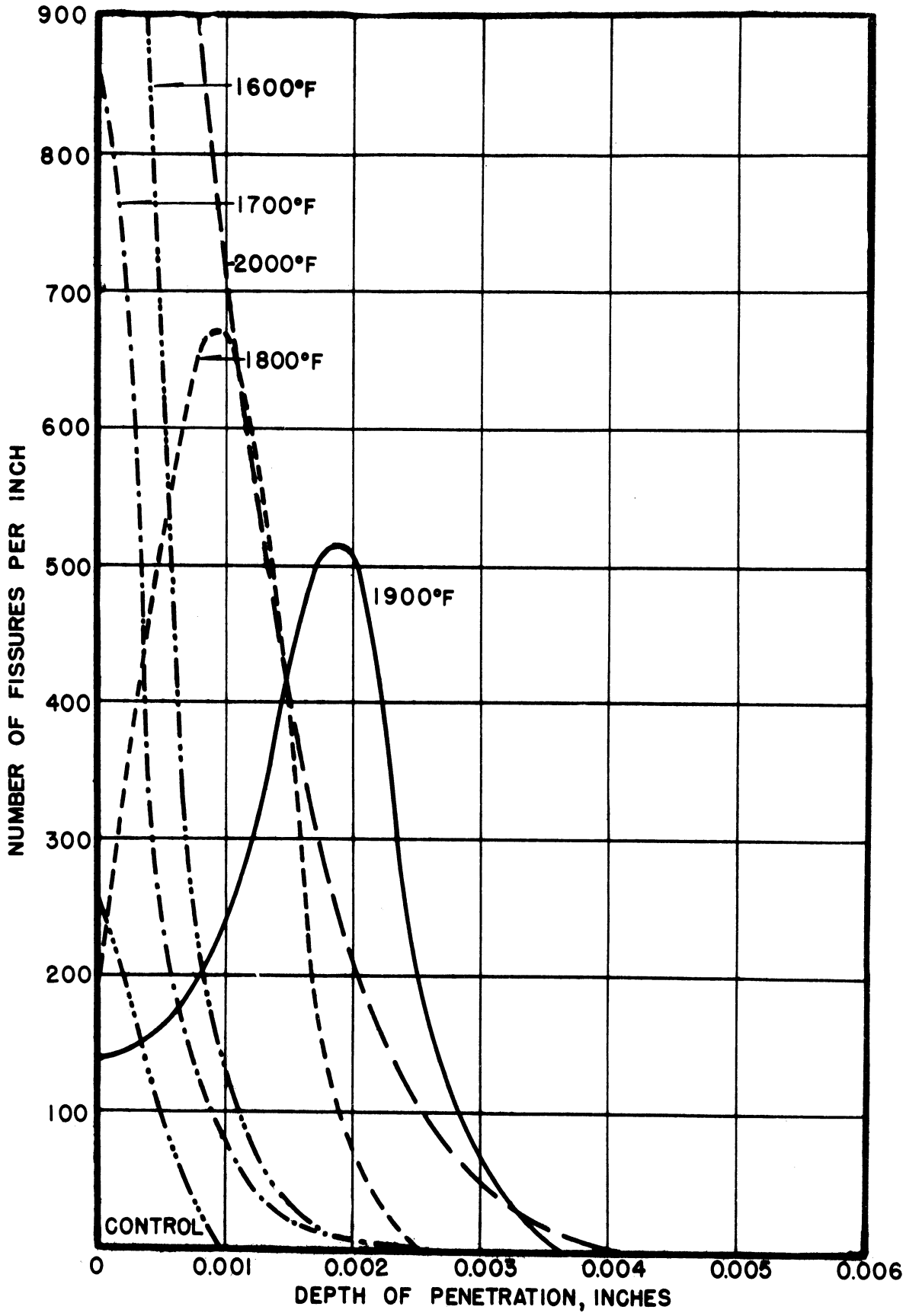

FIG. 56- PENETRATION VS. DEPTH BELOW SURFACE.
TYPE 310 ALLOY, HEAT X11306. RUNS 21 & 27.

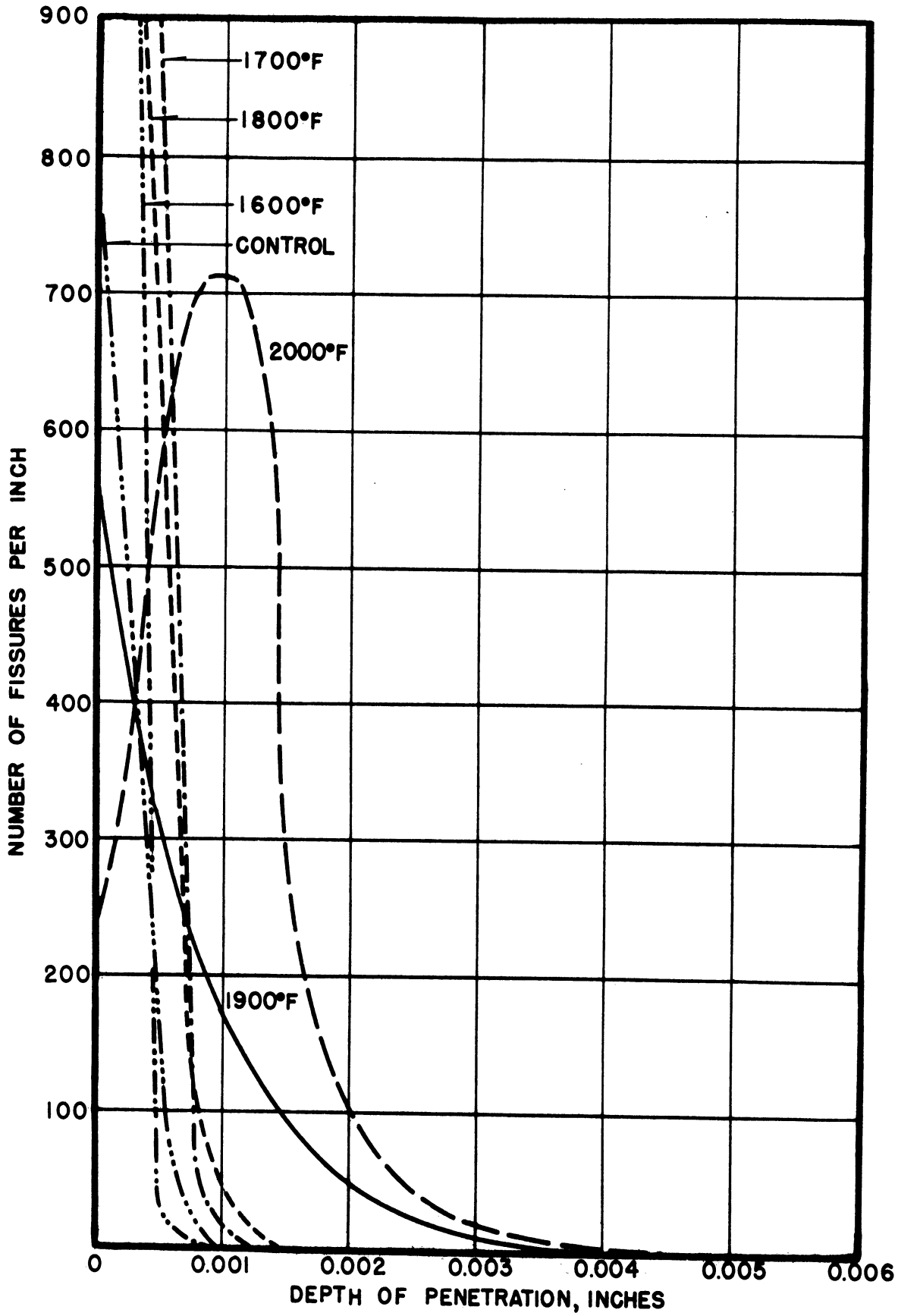

FIG. 57- PENETRATION VS. DEPTH BELOW SURFACE.
TYPE 310 ALLOY, HEAT X11338. RUNS 21 & 27.

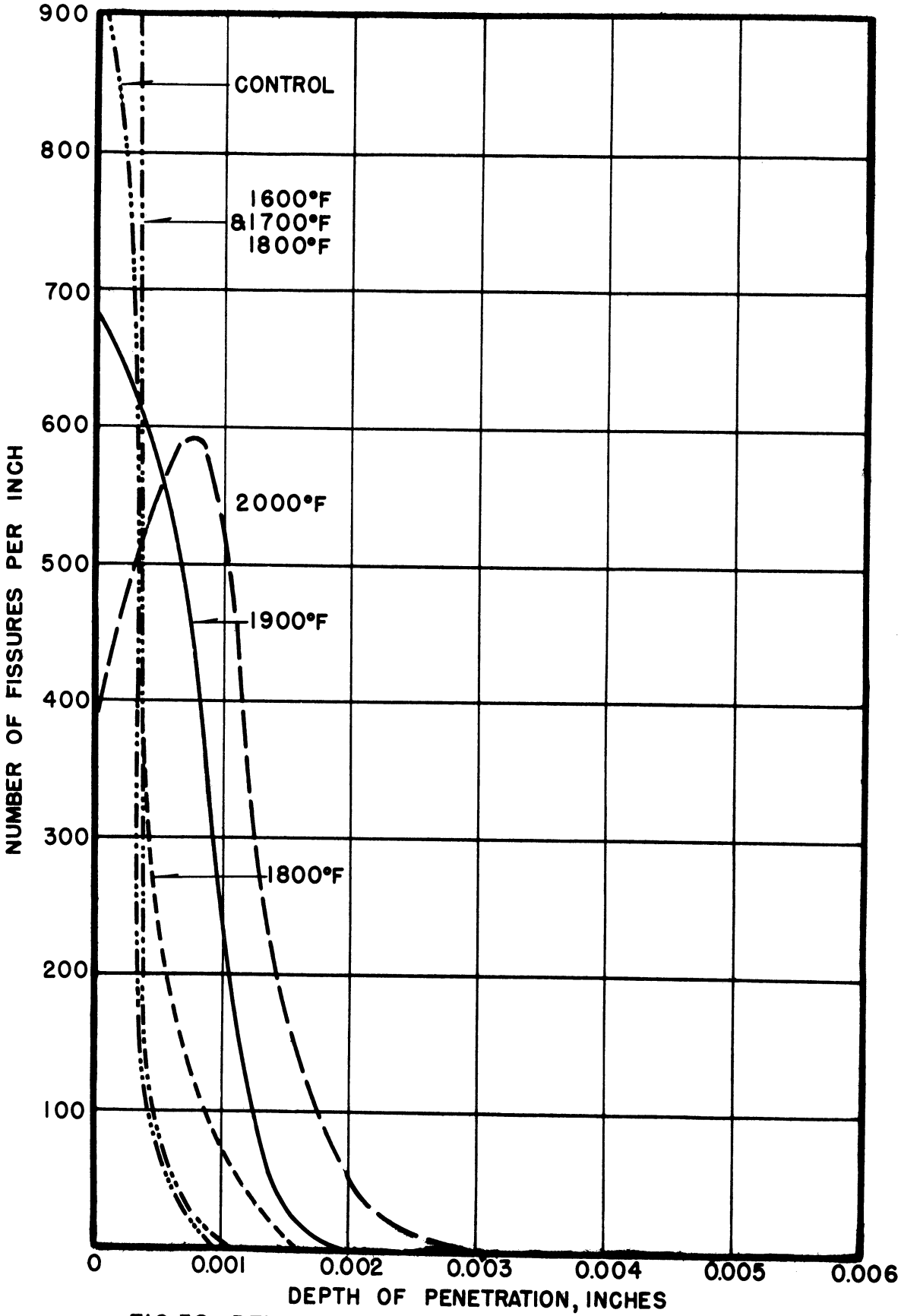

FIG. 58- PENETRATION VS. DEPTH BELOW SURFACE. TYPE 310 ALLOY, HEAT X27258. RUNS 21 & 27.

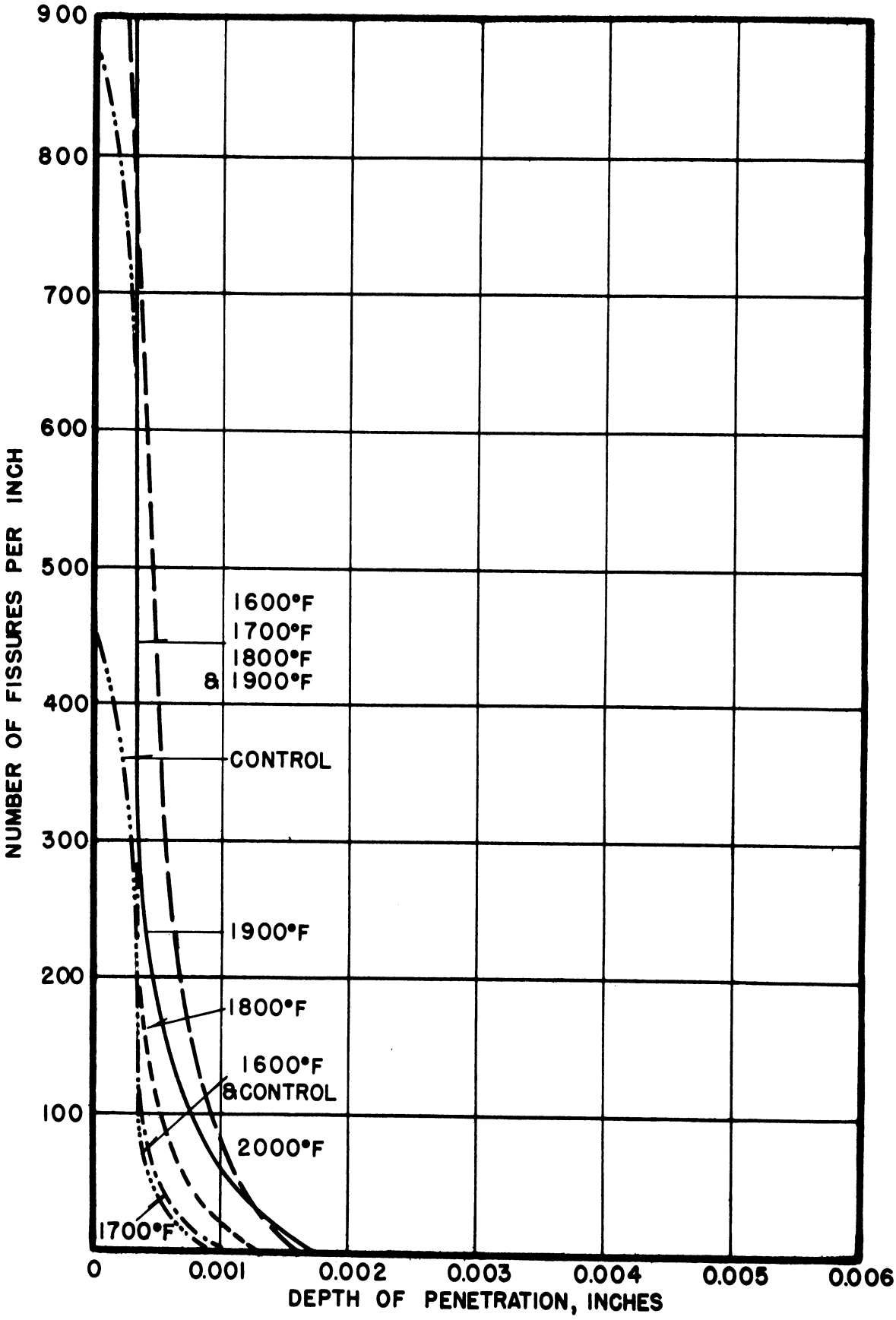

FIG. 59 - PENETRATION VS. DEPTH BELOW SURFACE.
TYPE 310 ALLOY, HEAT X 45558. RUNS 22 & 26.

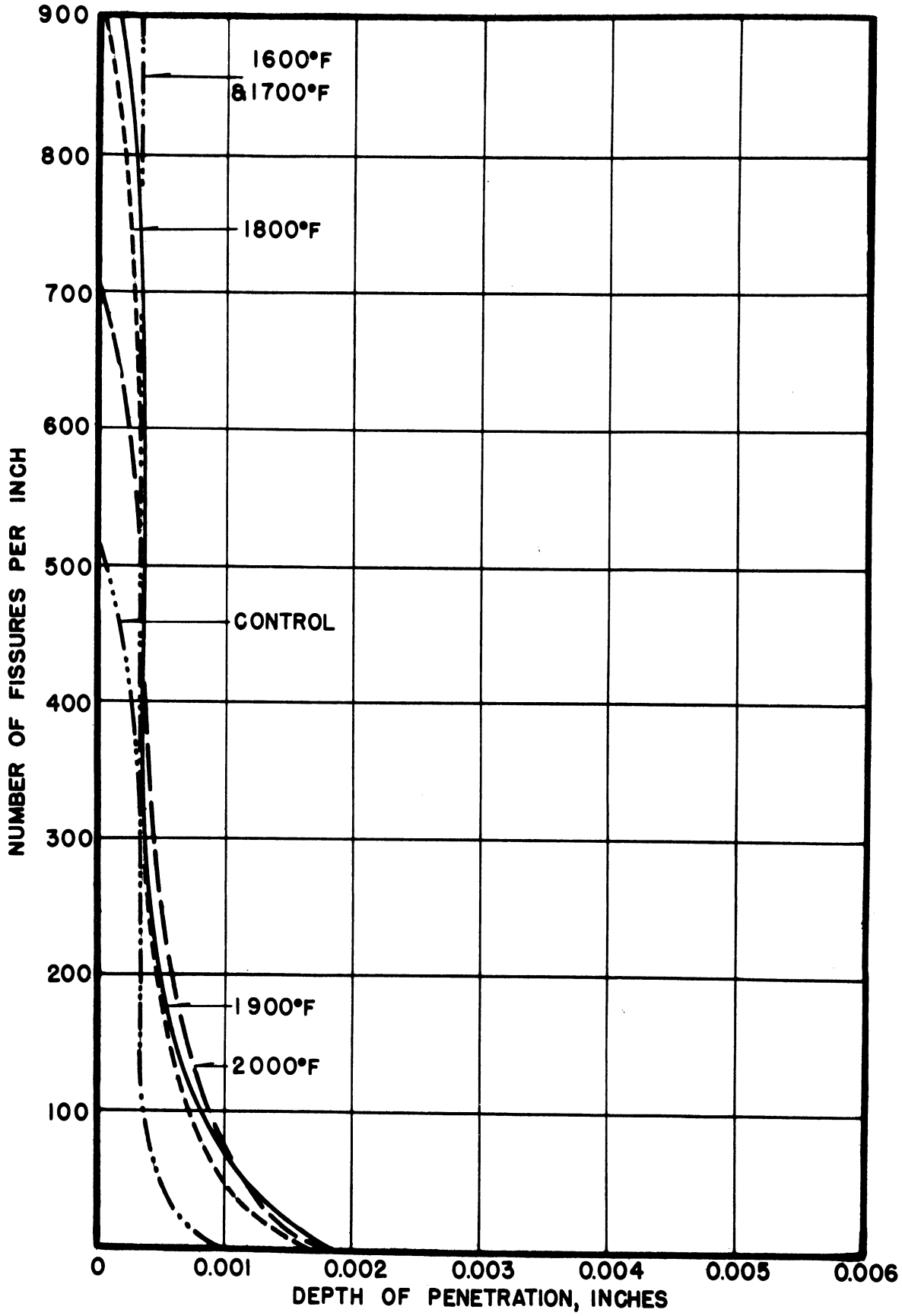

FIG. 60-PENETRATION VS. DEPTH BELOW SURFACE.
TYPE 310 ALLOY, HEAT X46063. RUNS 22 & 26.

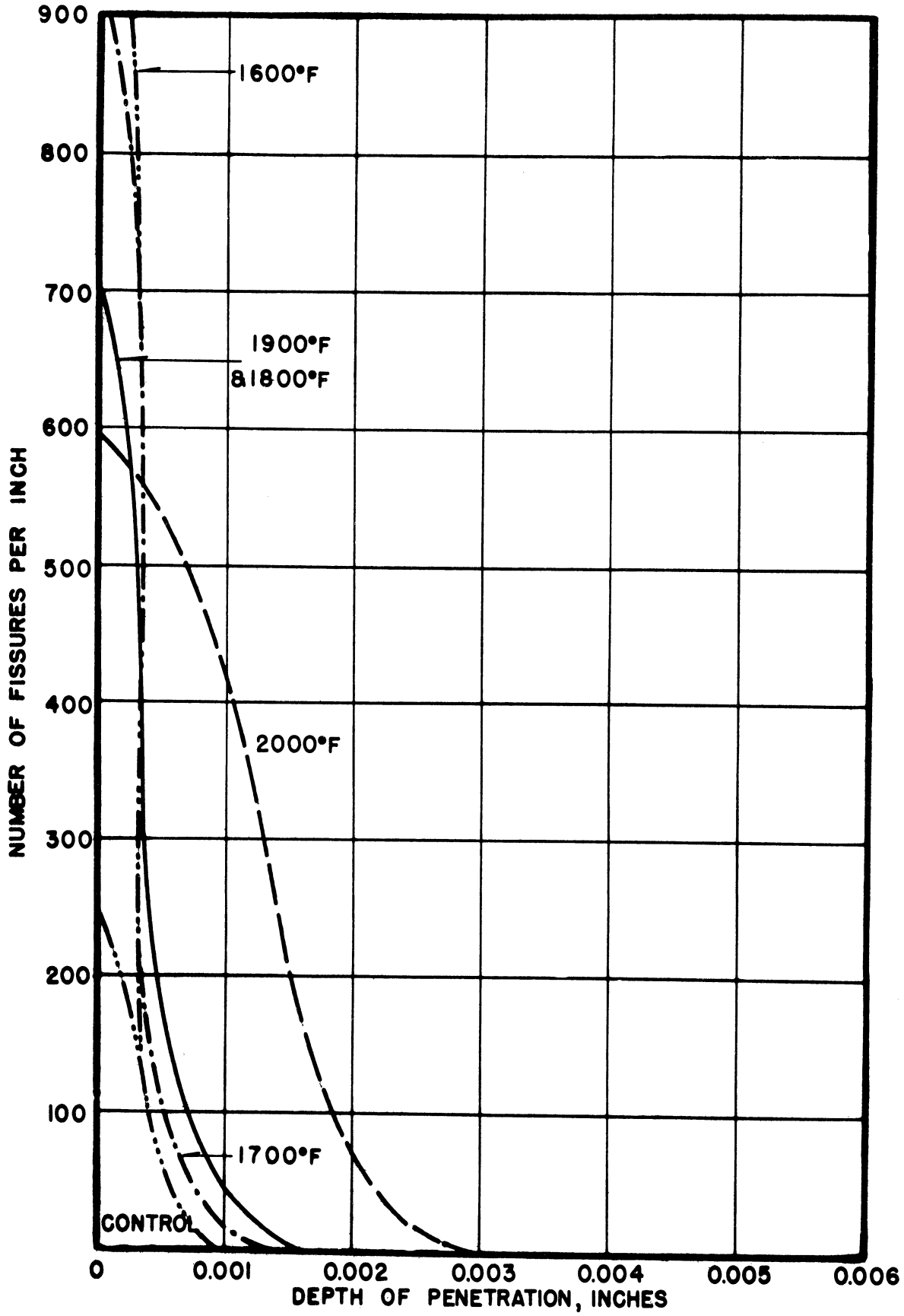

FIG. 61 - PENETRATION VS. DEPTH BELOW SURFACE.
TYPE 310 ALLOY, HEAT X46572. RUNS 22 & 26.

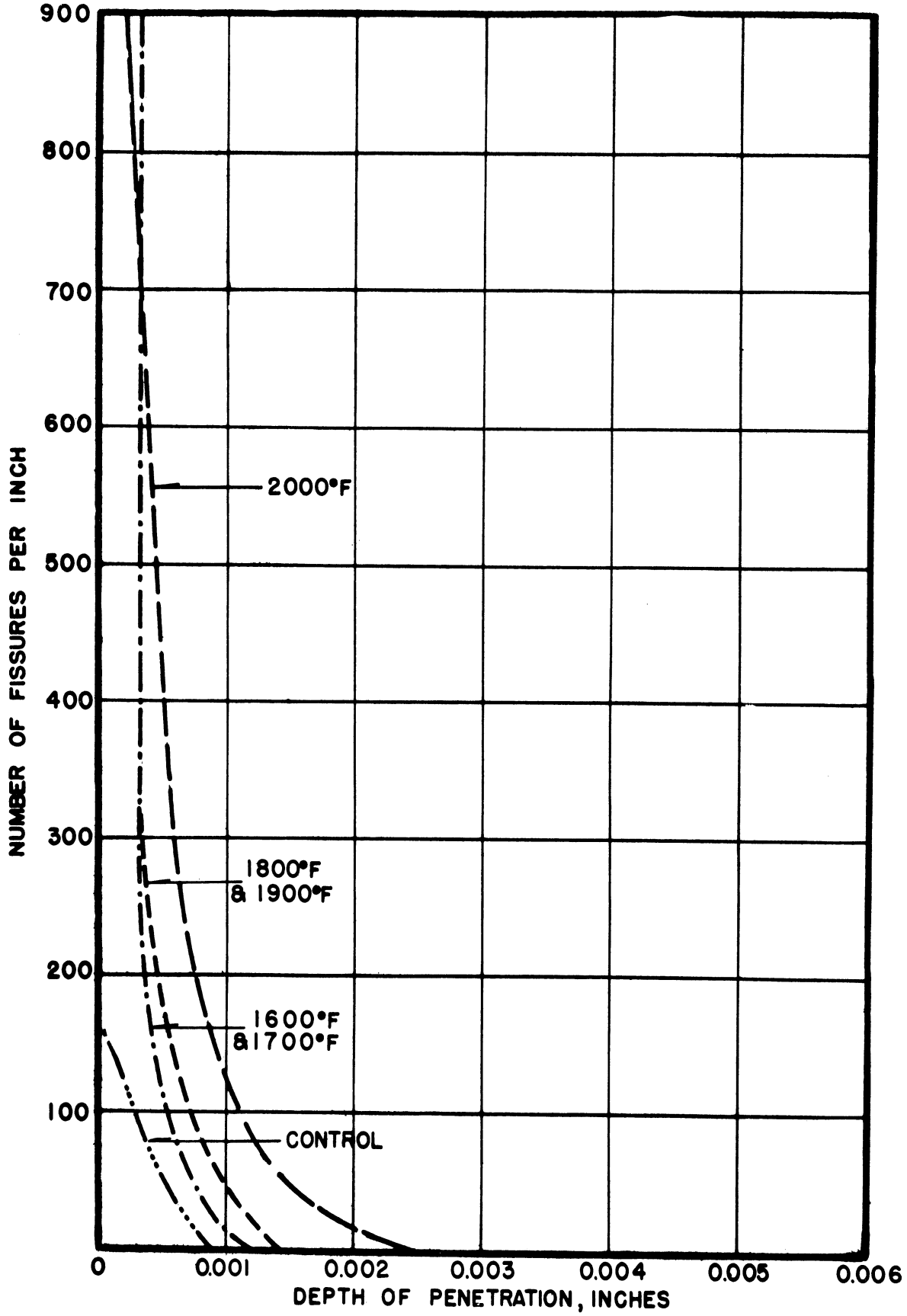

FIG. 62 - PENETRATION VS. DEPTH BELOW SURFACE.
TYPE 310 ALLOY, HEAT X 45558. RUNS 23 & 27.

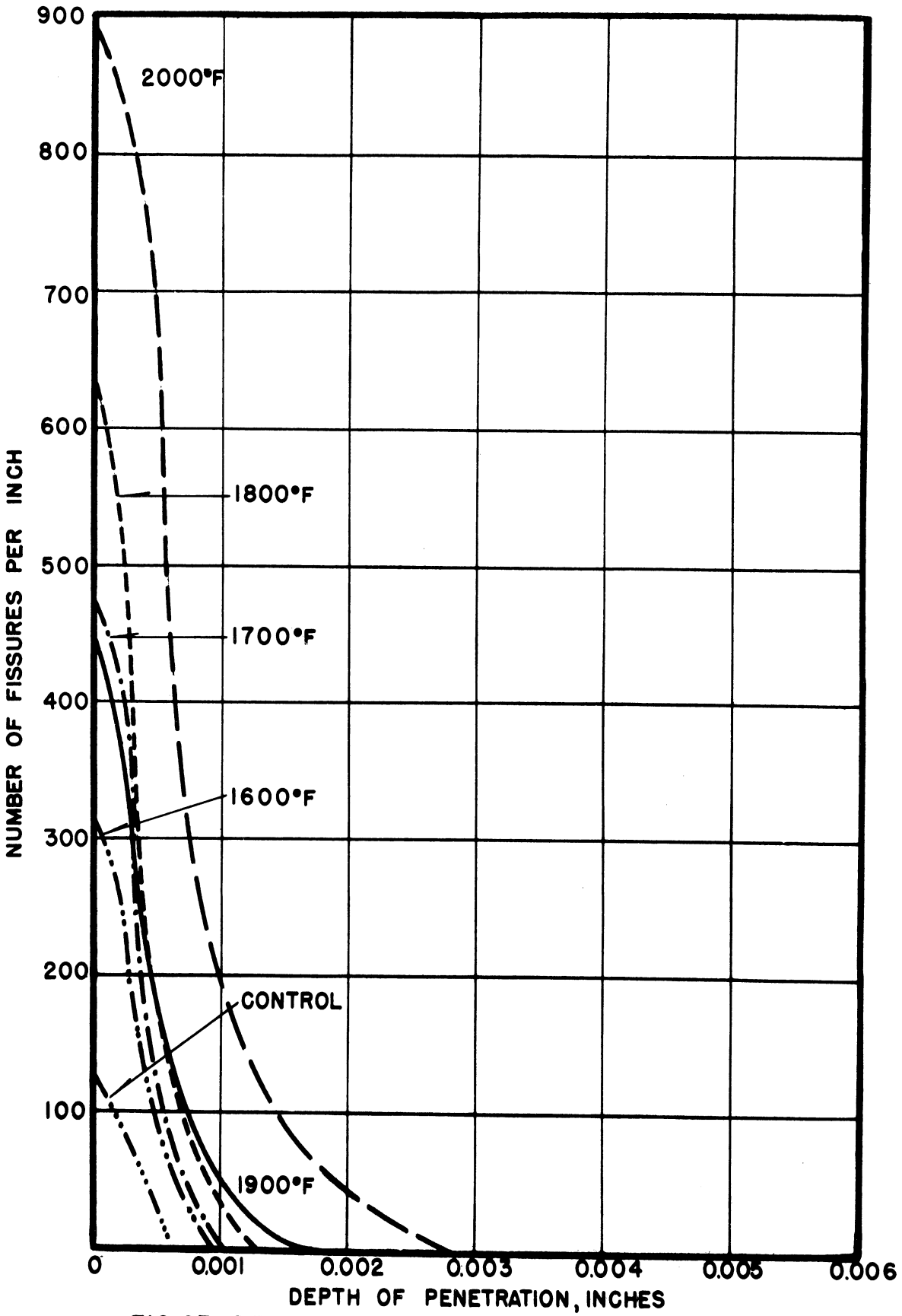

FIG. 63 - PENETRATION VS. DEPTH BELOW SURFACE.
TYPE 310 ALLOY, HEAT X46063. RUNS 23 & 27.

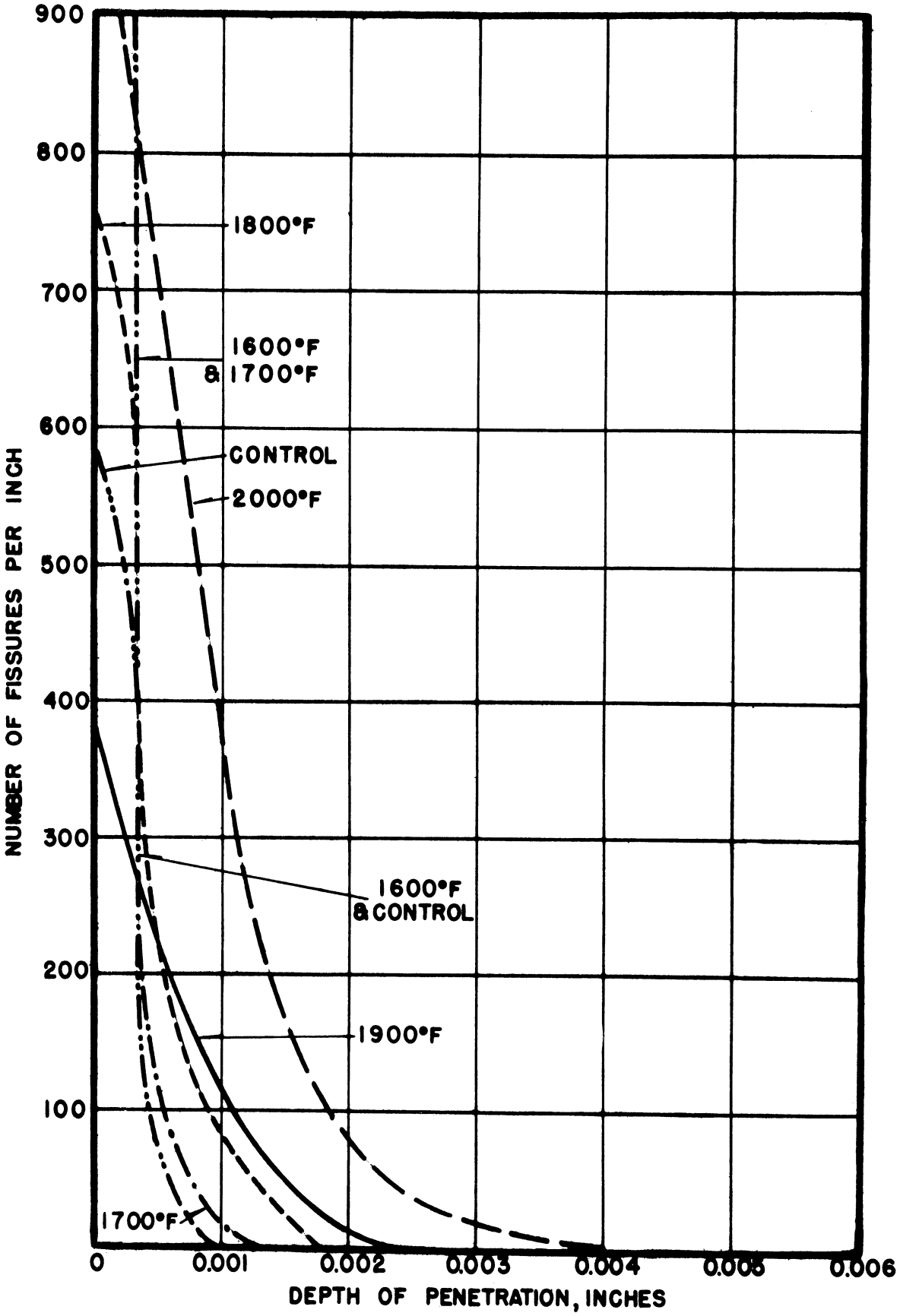

FIG. 64 - PENETRATION VS. DEPTH BELOW SURFACE.
TYPE 310 ALLOY, HEAT X46572. RUNS 23 & 27.

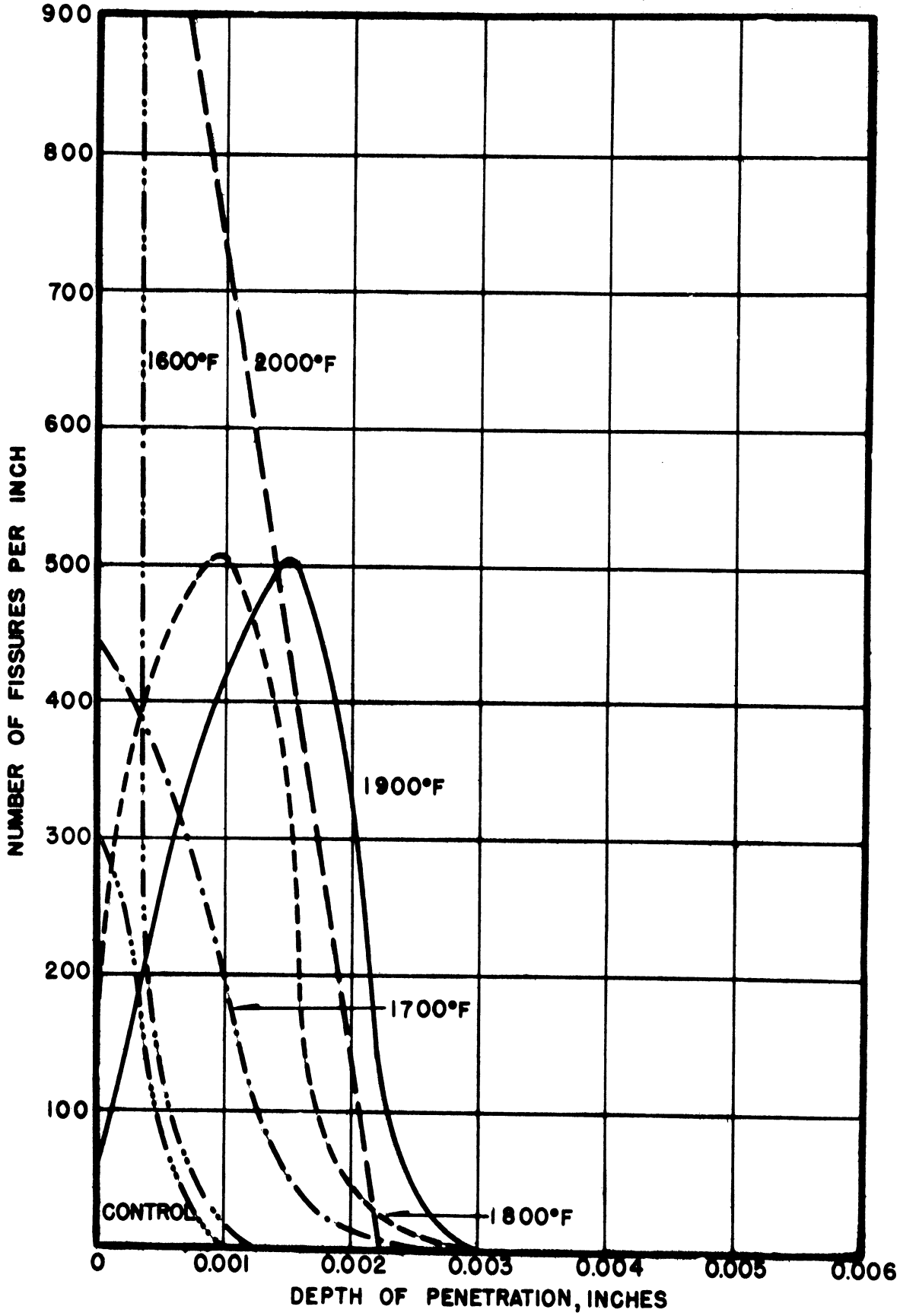

FIG. 65 - PENETRATION VS. DEPTH BELOW SURFACE.
TYPE 310 ALLOY, HEAT X 11306. RUNS 24 & 26.

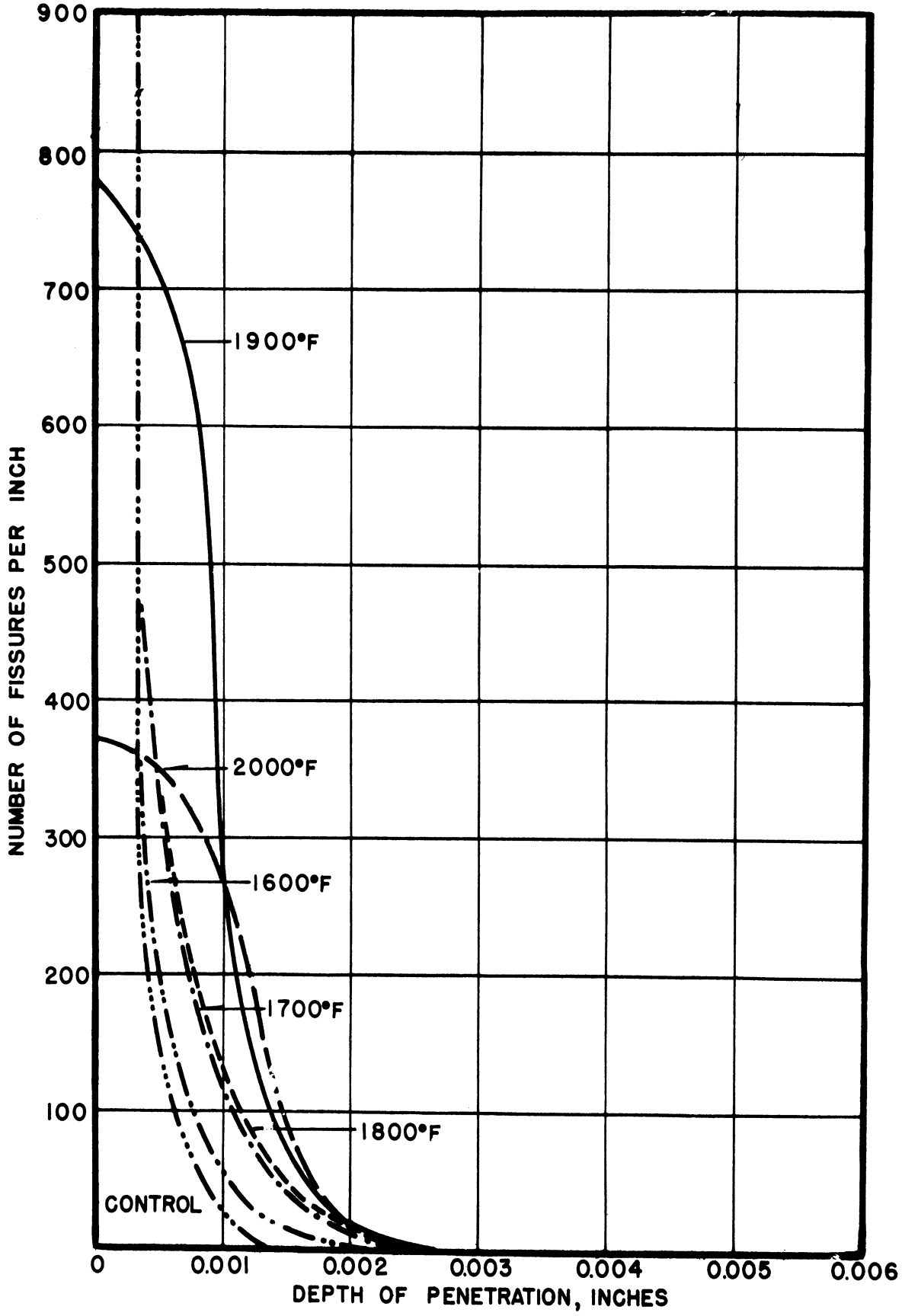

FIG. 66-PENETRATION VS. DEPTH BELOW SURFACE.
TYPE 310 ALLOY, HEAT X11338. RUNS 24 & 25.

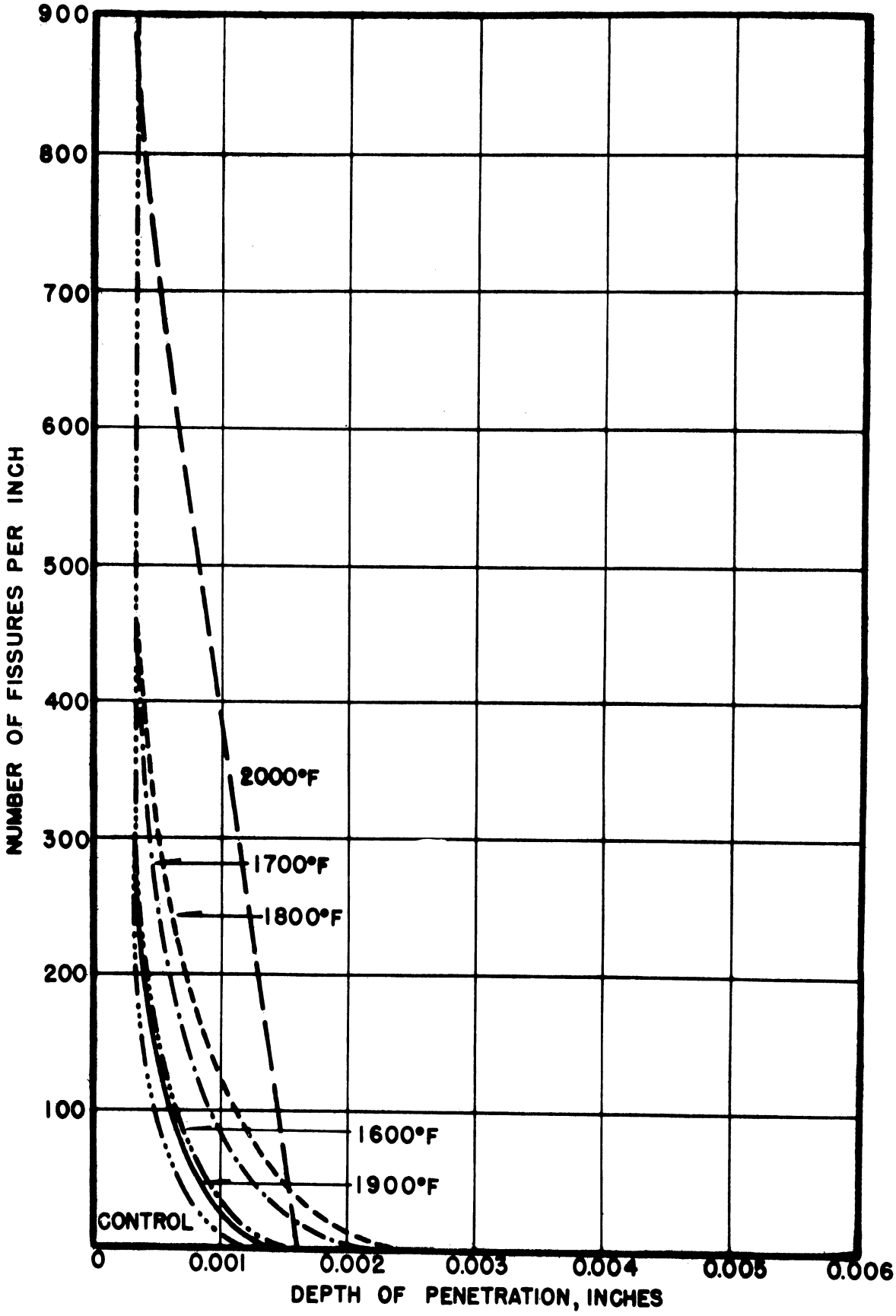

FIG. 67- PENETRATION VS. DEPTH BELOW SURFACE.
TYPE 310 ALLOY, HEAT X 27258. RUNS 24 & 26.

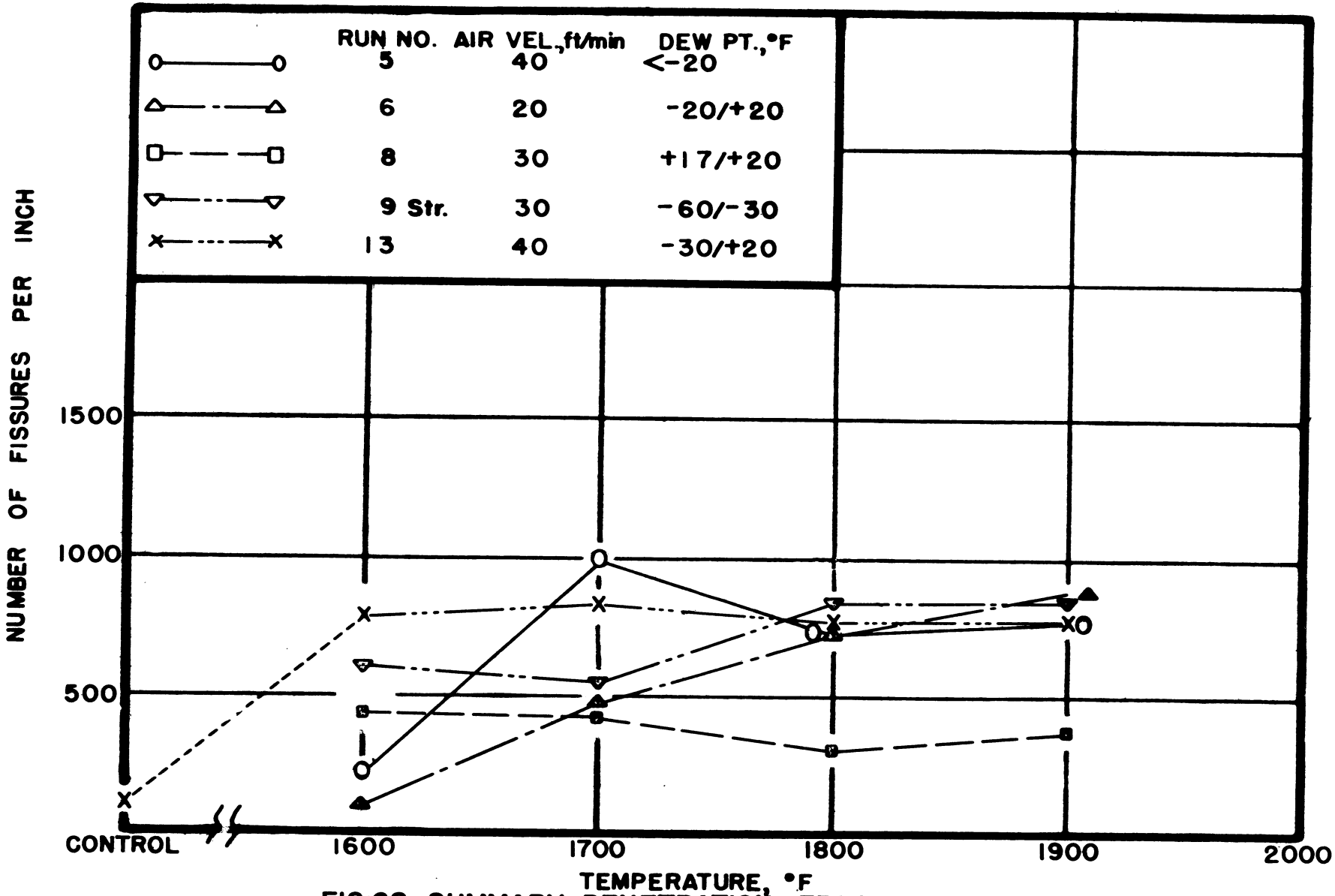

FIG.68-SUMMARY PENETRATION FREQUENCY CURVES. TYPE 309+Nb ALLOY. 100 HOURS DURATION. EFFECT OF AIR VELOCITY AND HUMIDITY.

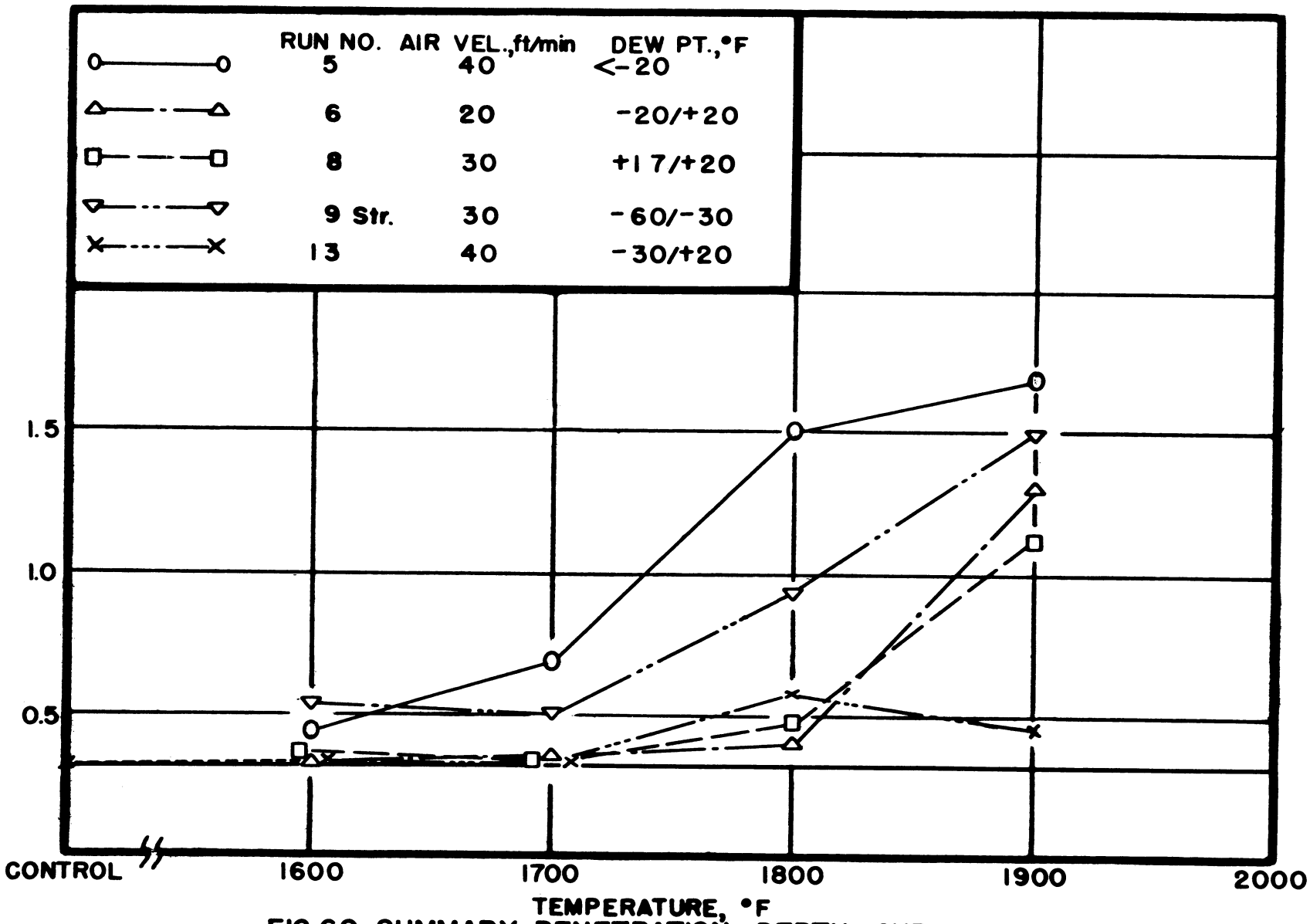

FIG.69-SUMMARY PENETRATION DEPTH CURVES.
TYPE 309+Nb ALLOY. 100 HOURS DURATION.
EFFECT OF AIR VELOCITY AND HUMIDITY.

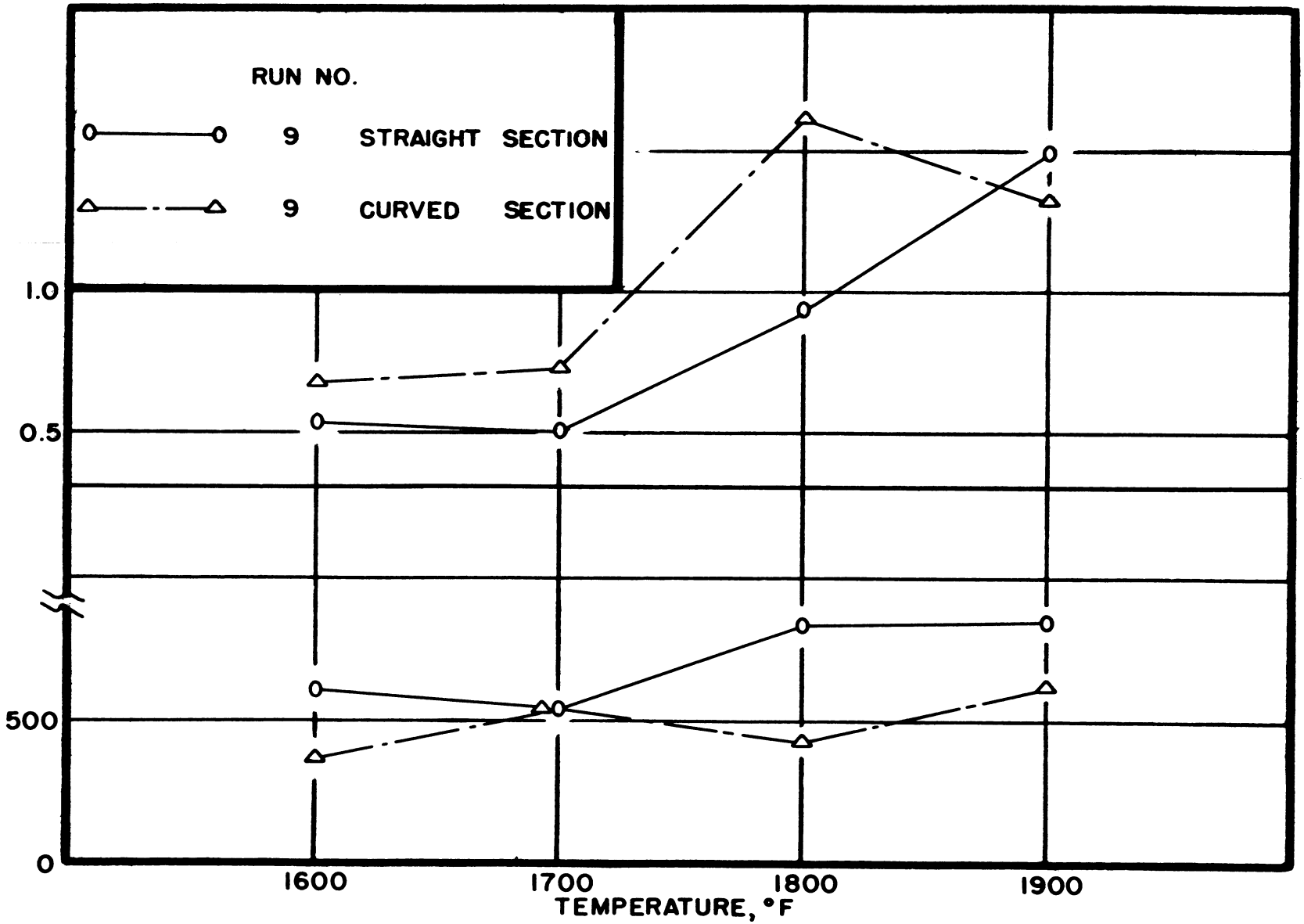

FIG. 70 - SUMMARY PENETRATION FREQUENCY AND DEPTH CURVES. TYPE 309 + Nb ALLOY. EFFECT OF COLD WORK. 100 HOURS DURATION.

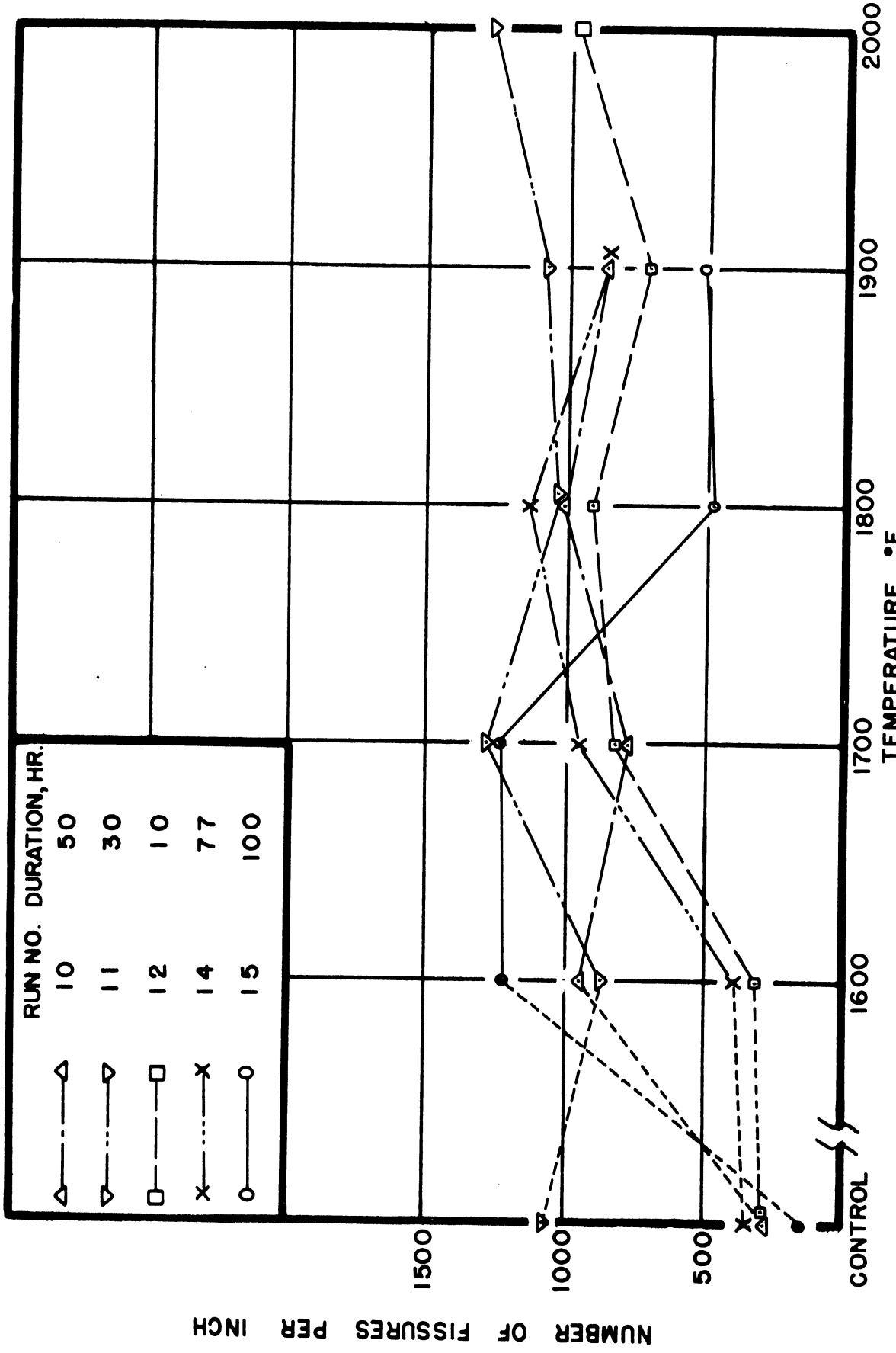

FIG. 71 – SUMMARY PENETRATION FREQUENCY CURVES. TYPE 309+Nb ALLOY. EFFECT OF TIME.

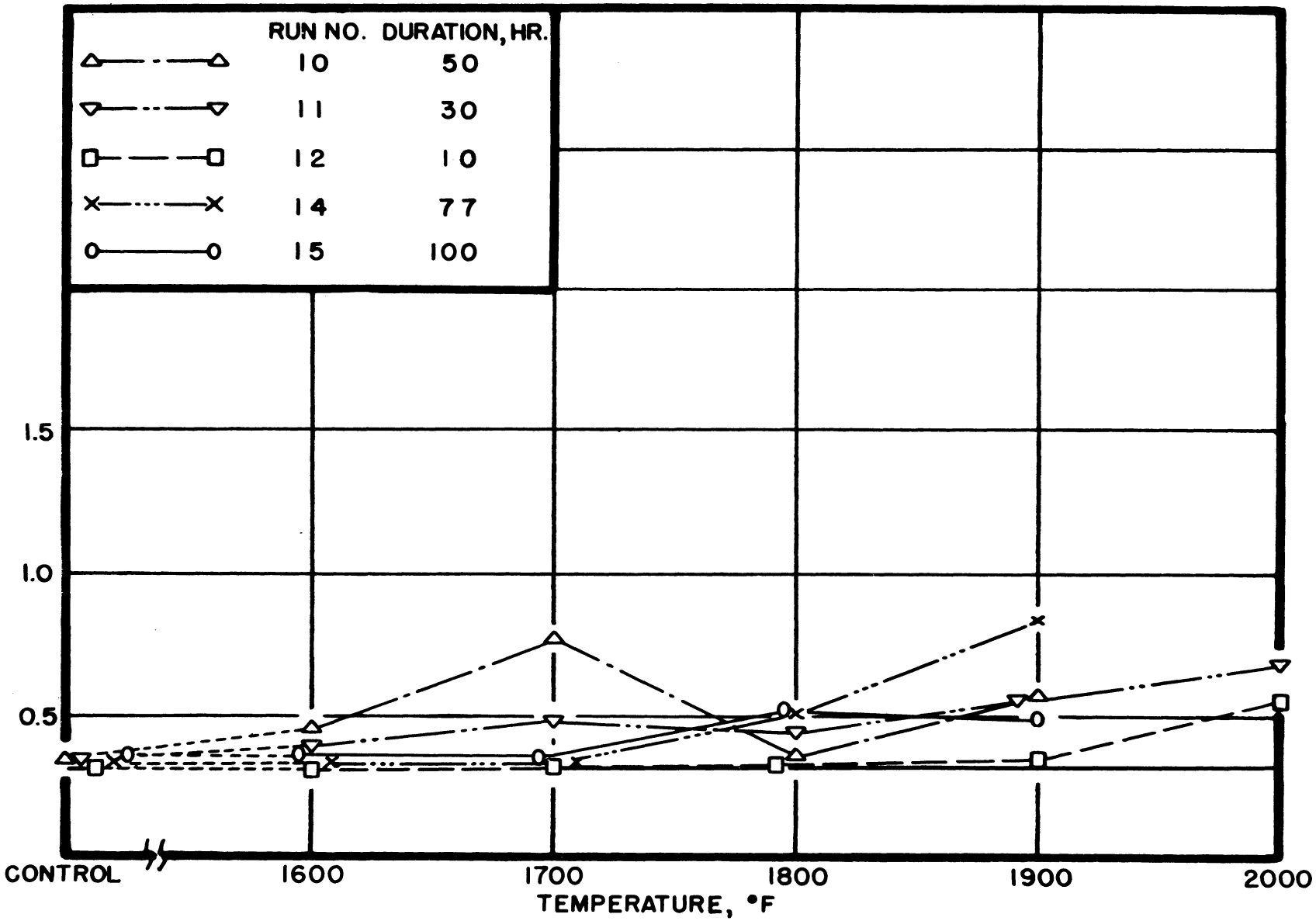

FIG. 72—SUMMARY PENETRATION DEPTH CURVES.
TYPE 309+Nb ALLOY. EFFECT OF TIME.

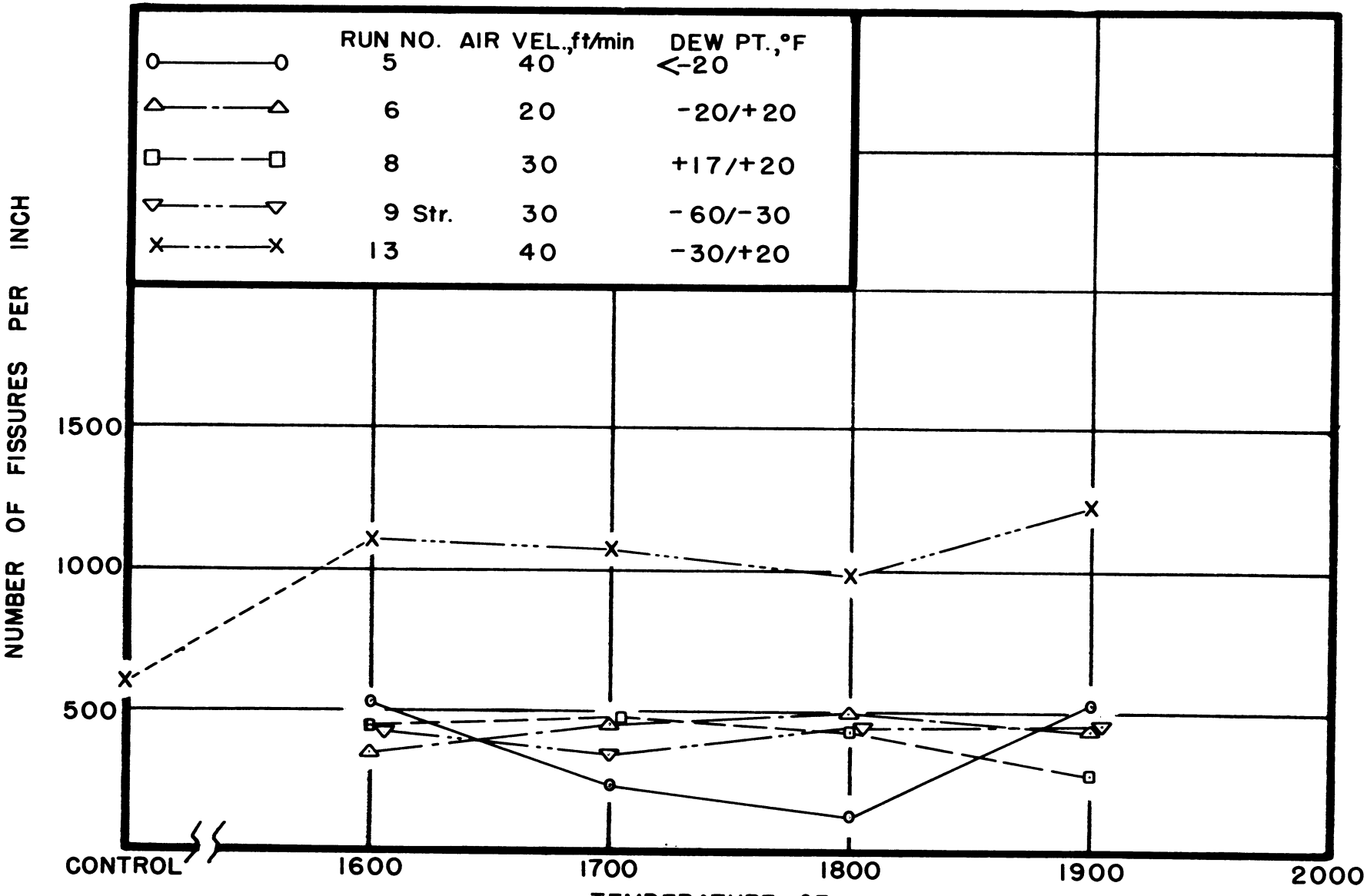

FIG. 73-SUMMARY PENETRATION FREQUENCY CURVES.
TYPE 310 ALLOY, HEAT 64177. 100 HOURS DURATION.
EFFECT OF AIR VELOCITY AND HUMIDITY.

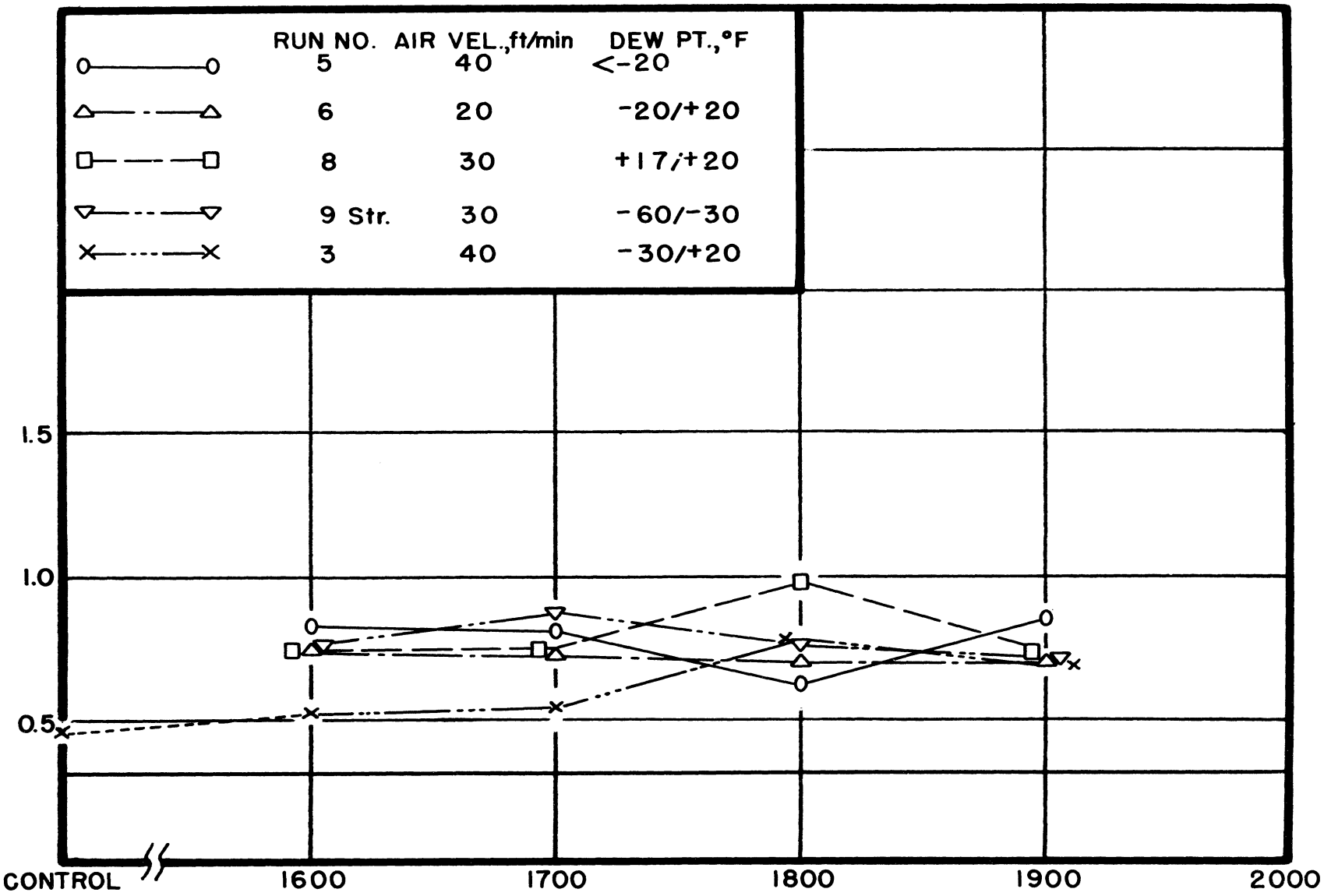

FIG. 74 - SUMMARY PENETRATION DEPTH CURVES.
TYPE 310 ALLOY, HEAT 64177. 100 HOURS DURATION.
EFFECT OF AIR VELOCITY AND HUMIDITY.

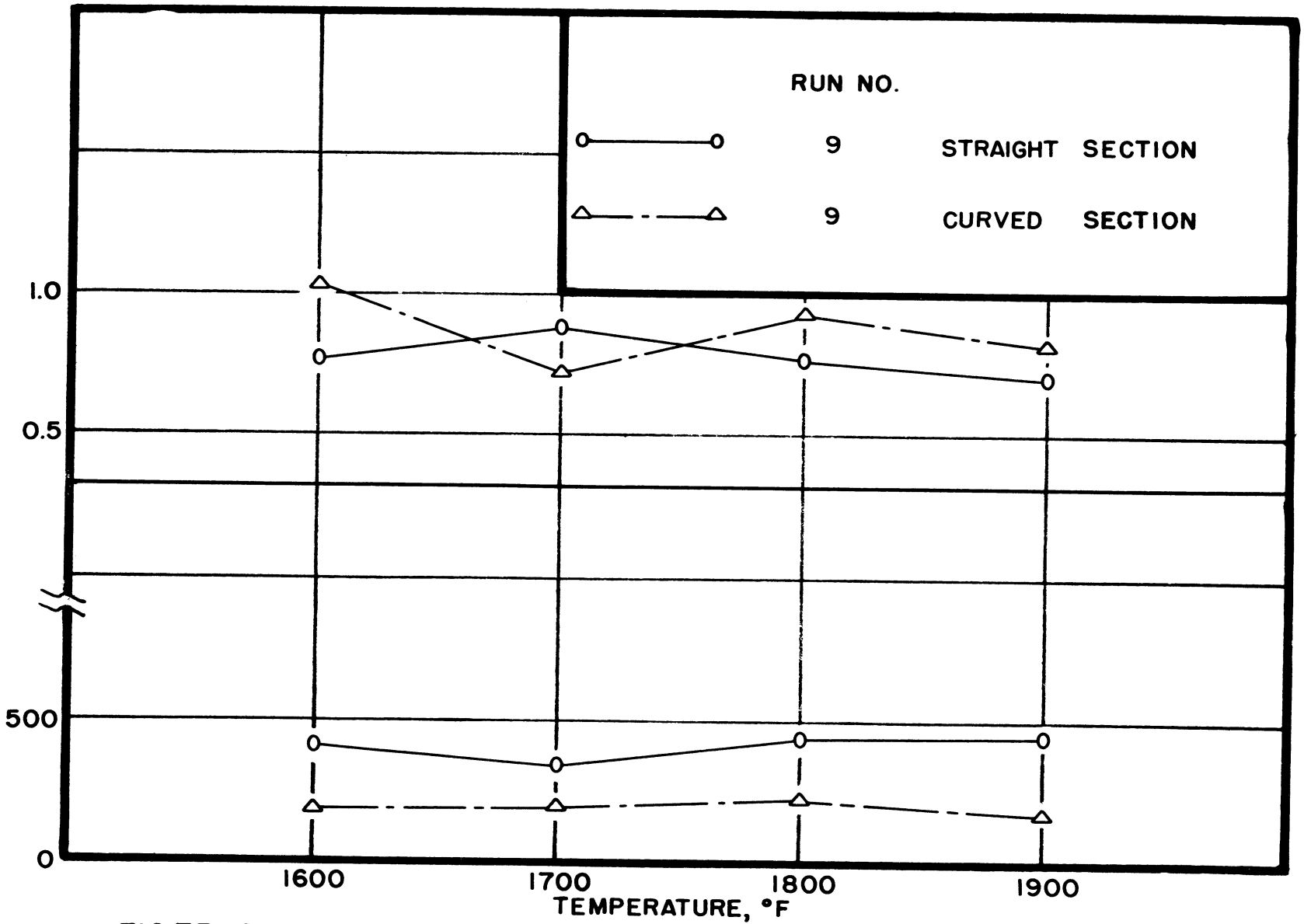

FIG. 75 - SUMMARY PENETRATION FREQUENCY AND DEPTH CURVES. TYPE 310 ALLOY, HEAT 64177. EFFECT OF COLD WORK. 100 HOURS DURATION.

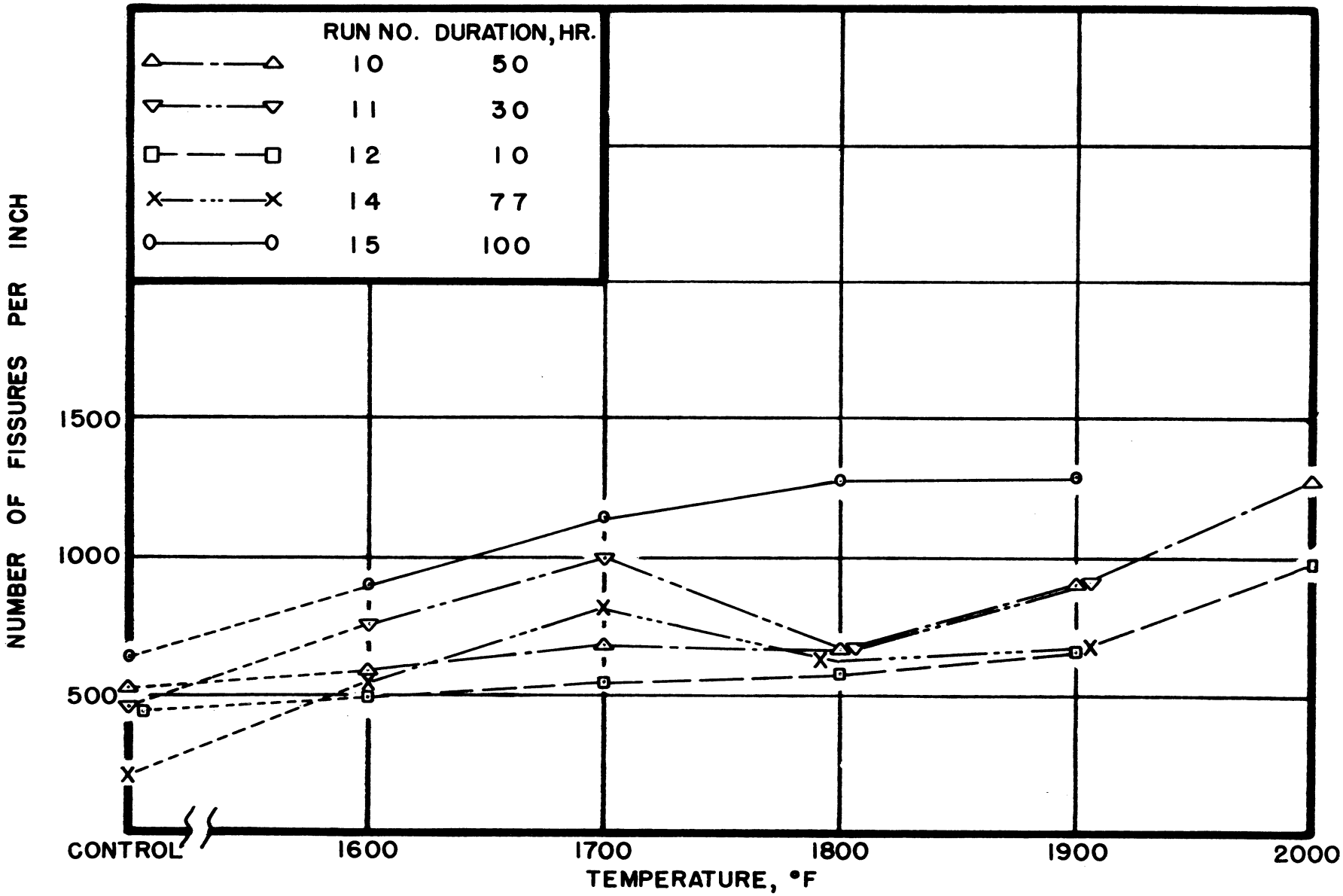

FIG. 76-SUMMARY PENETRATION FREQUENCY CURVES.
TYPE 310 ALLOY, HEAT 64177. EFFECT OF TIME.

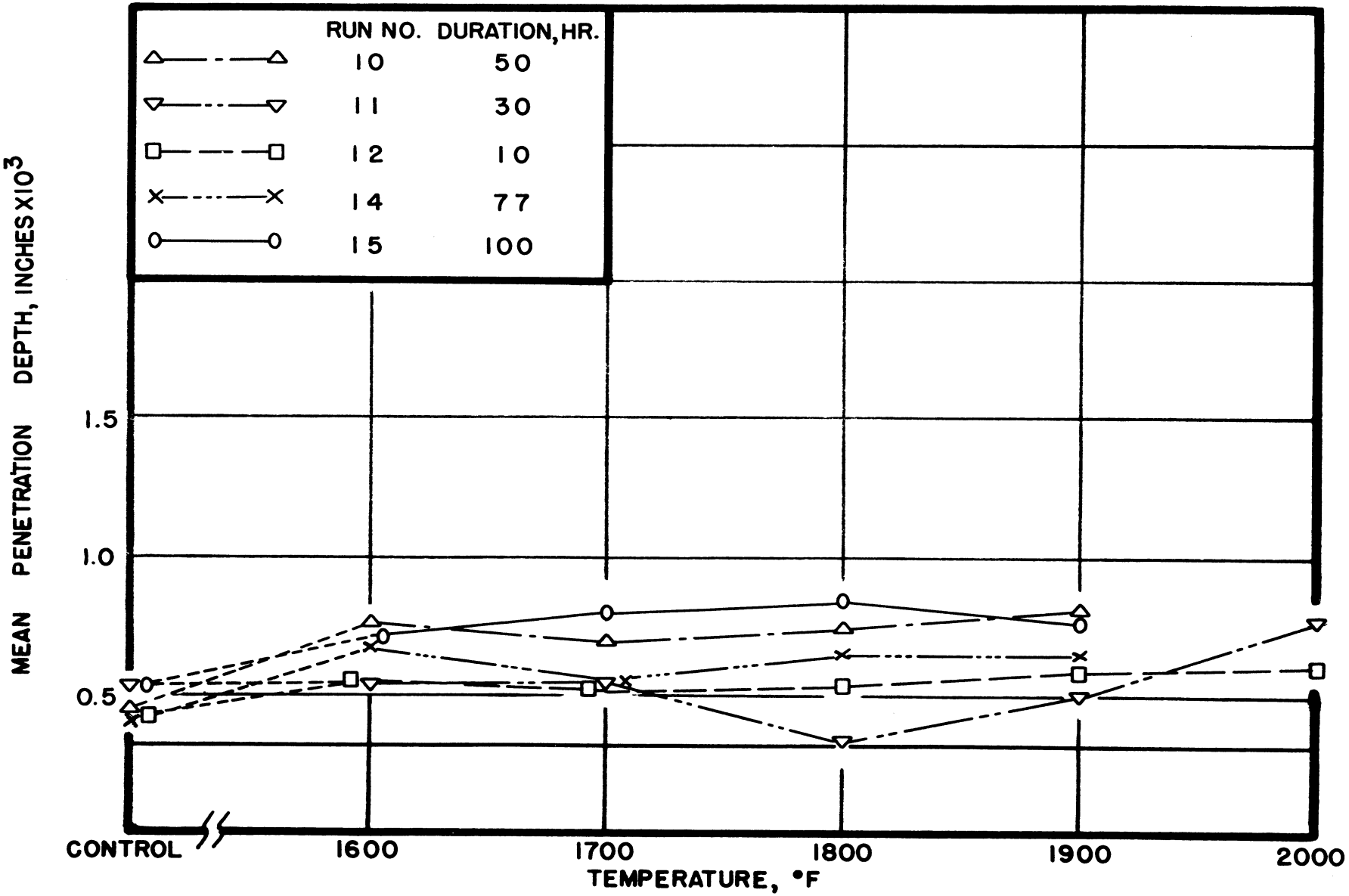

FIG. 77- SUMMARY PENETRATION DEPTH CURVES.
TYPE 310 ALLOY, HEAT 64177. EFFECT OF TIME.

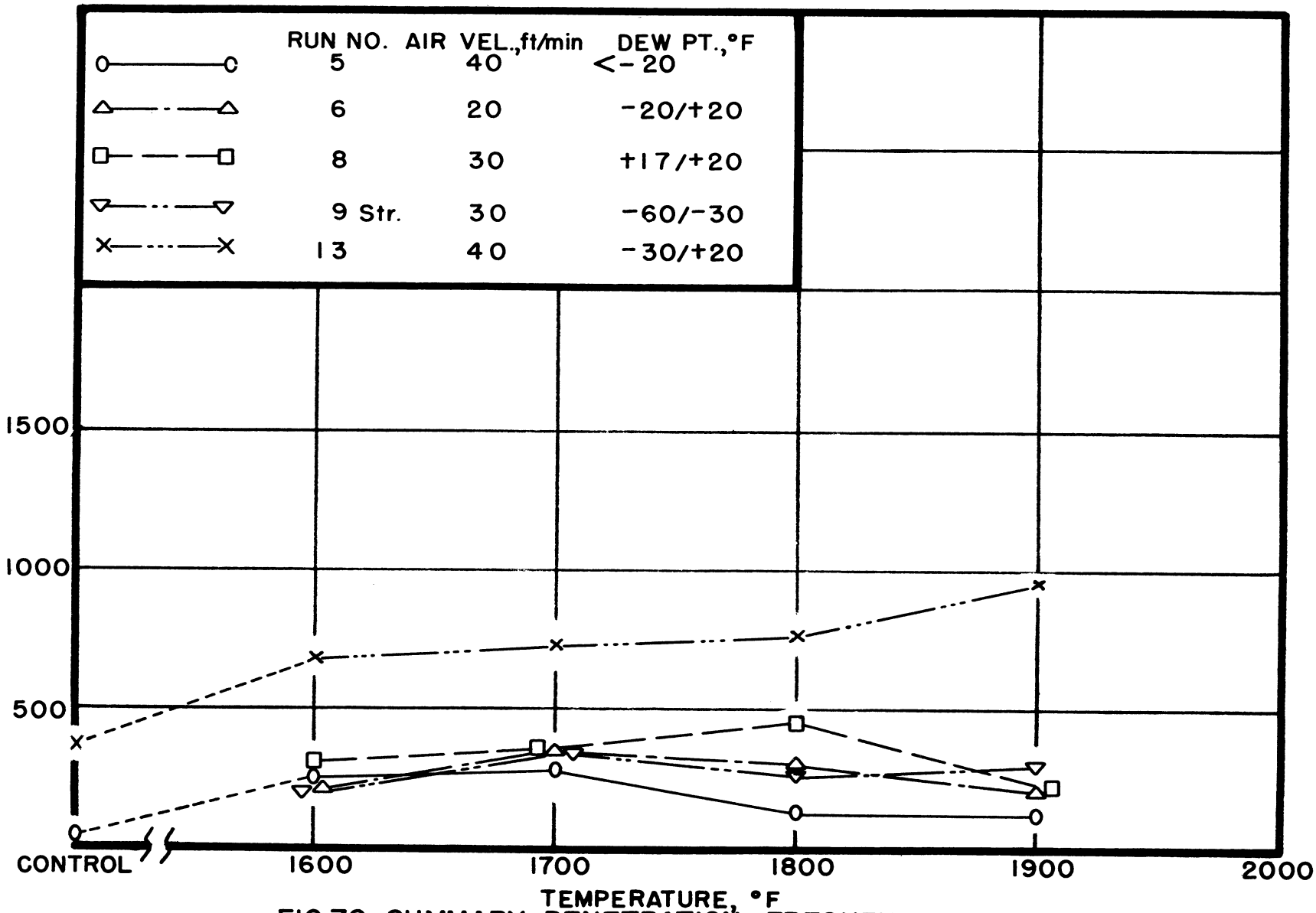

FIG.78-SUMMARY PENETRATION FREQUENCY CURVES.
TYPE 310 ALLOY, HEAT 64270. 100 HOURS DURATION.
EFFECT OF AIR VELOCITY AND HUMIDITY.

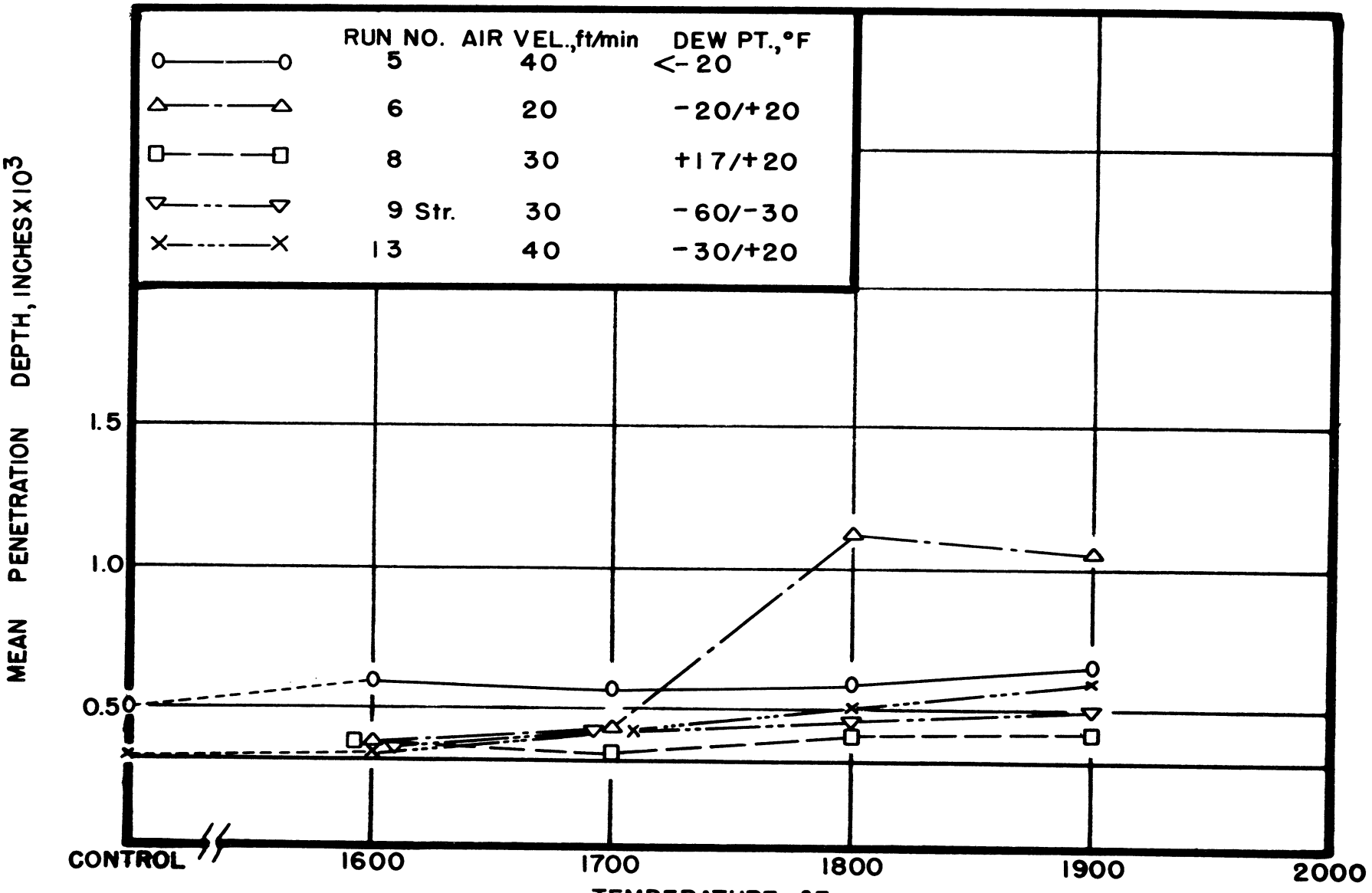

FIG. 79-SUMMARY PENETRATION DEPTH CURVES.
TYPE 310 ALLOY, HEAT 64270. 100 HOURS DURATION.
EFFECT OF AIR VELOCITY AND HUMIDITY.

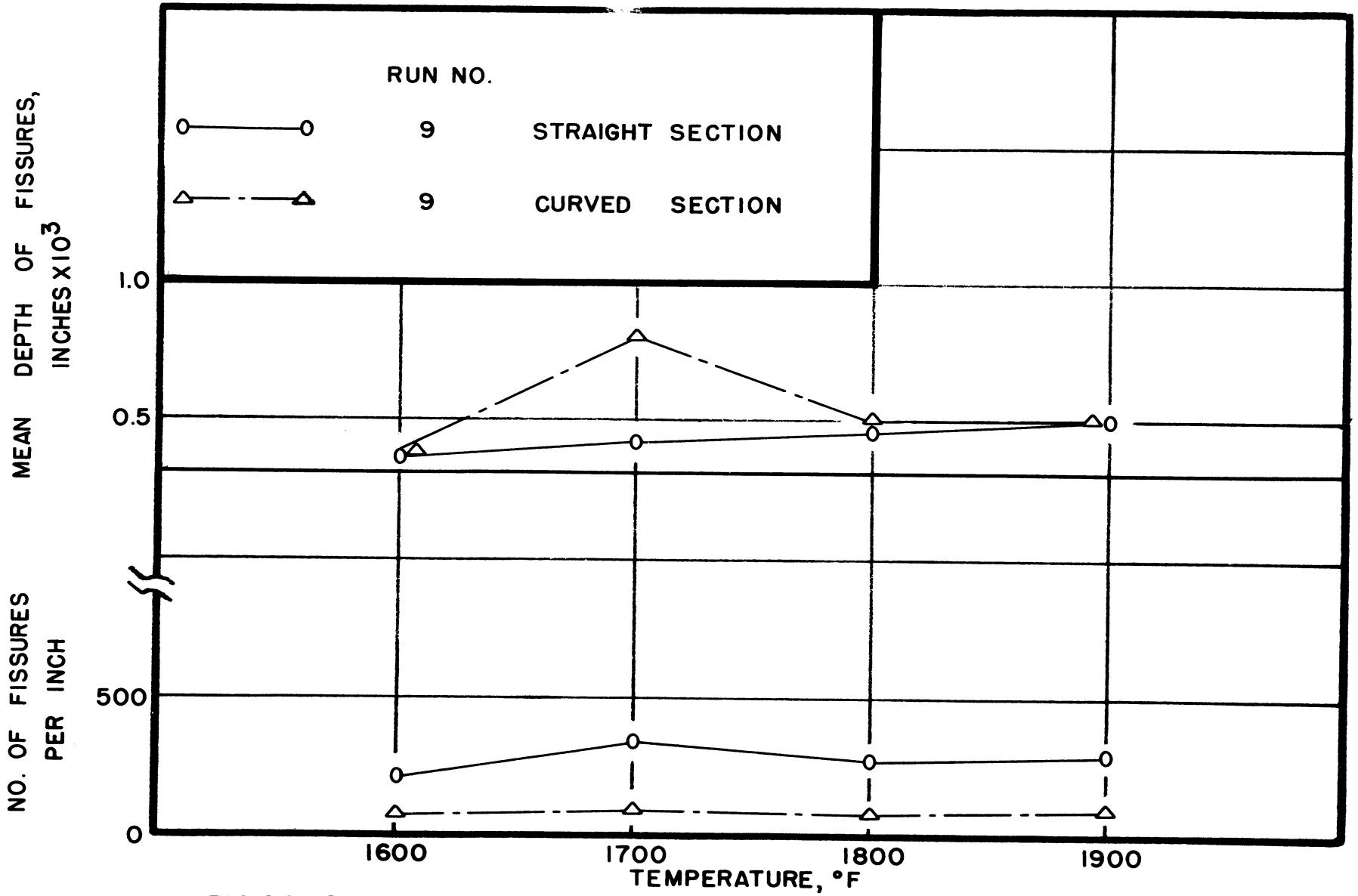

FIG.80-SUMMARY PENETRATION FREQUENCY AND DEPTH CURVES. TYPE 310 ALLOY, HEAT 64270. EFFECT OF COLD WORK. 100 HOURS DURATION.

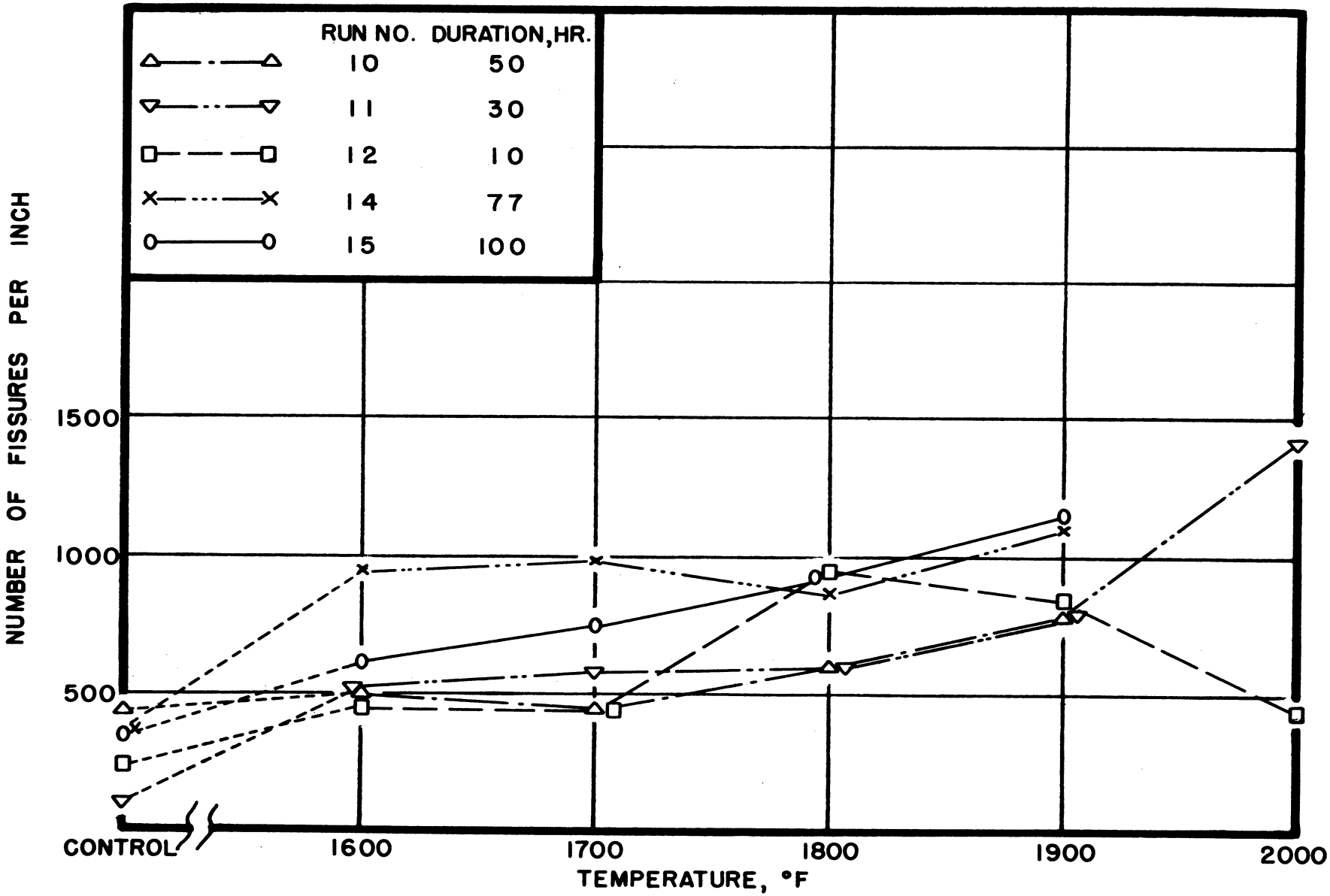

FIG. 81 - SUMMARY PENETRATION FREQUENCY CURVES.
TYPE 310 ALLOY, HEAT 64270. EFFECT OF TIME.

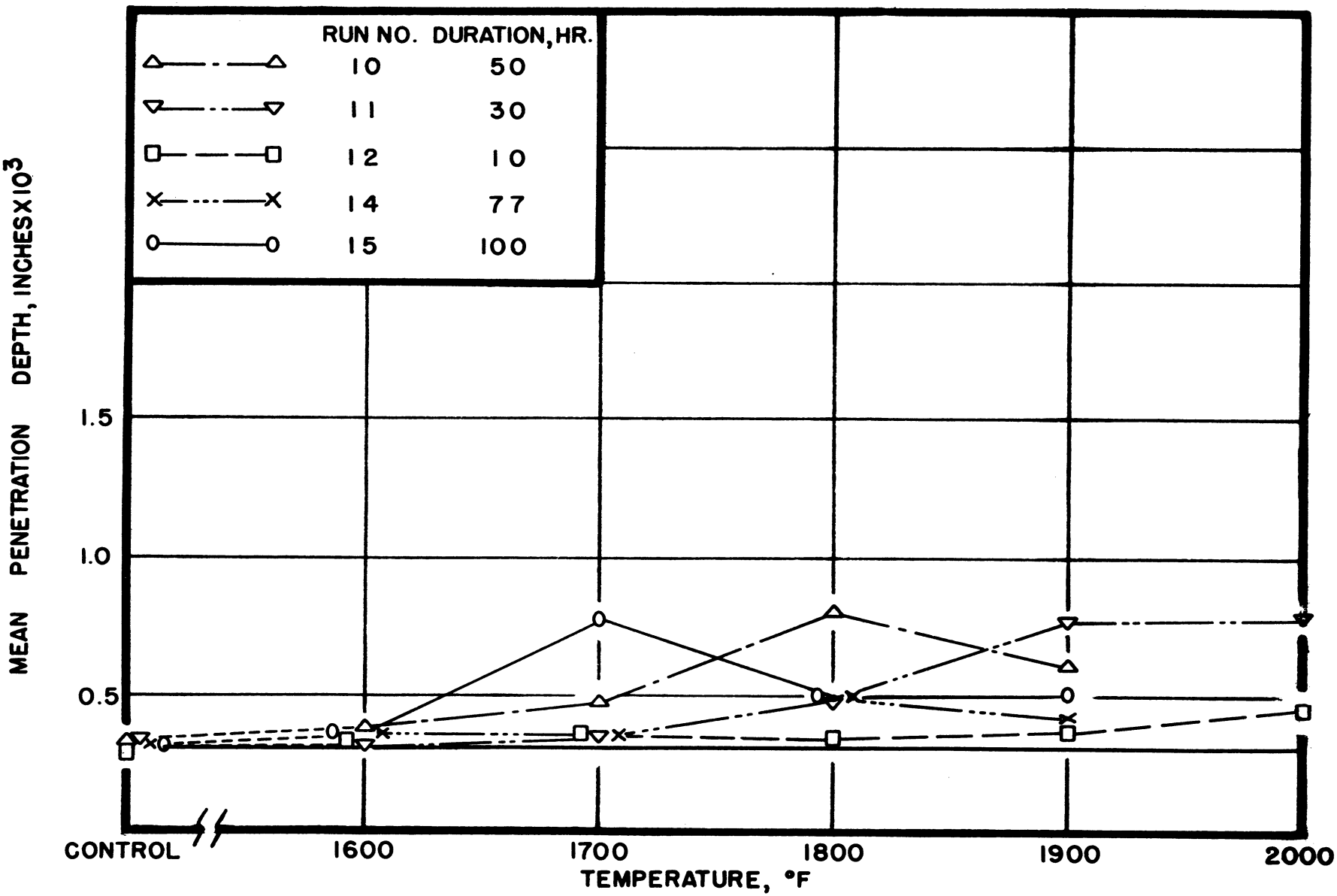

FIG. 82 - SUMMARY PENETRATION DEPTH CURVES.
TYPE 310 ALLOY, HEAT 64270. EFFECT OF TIME.

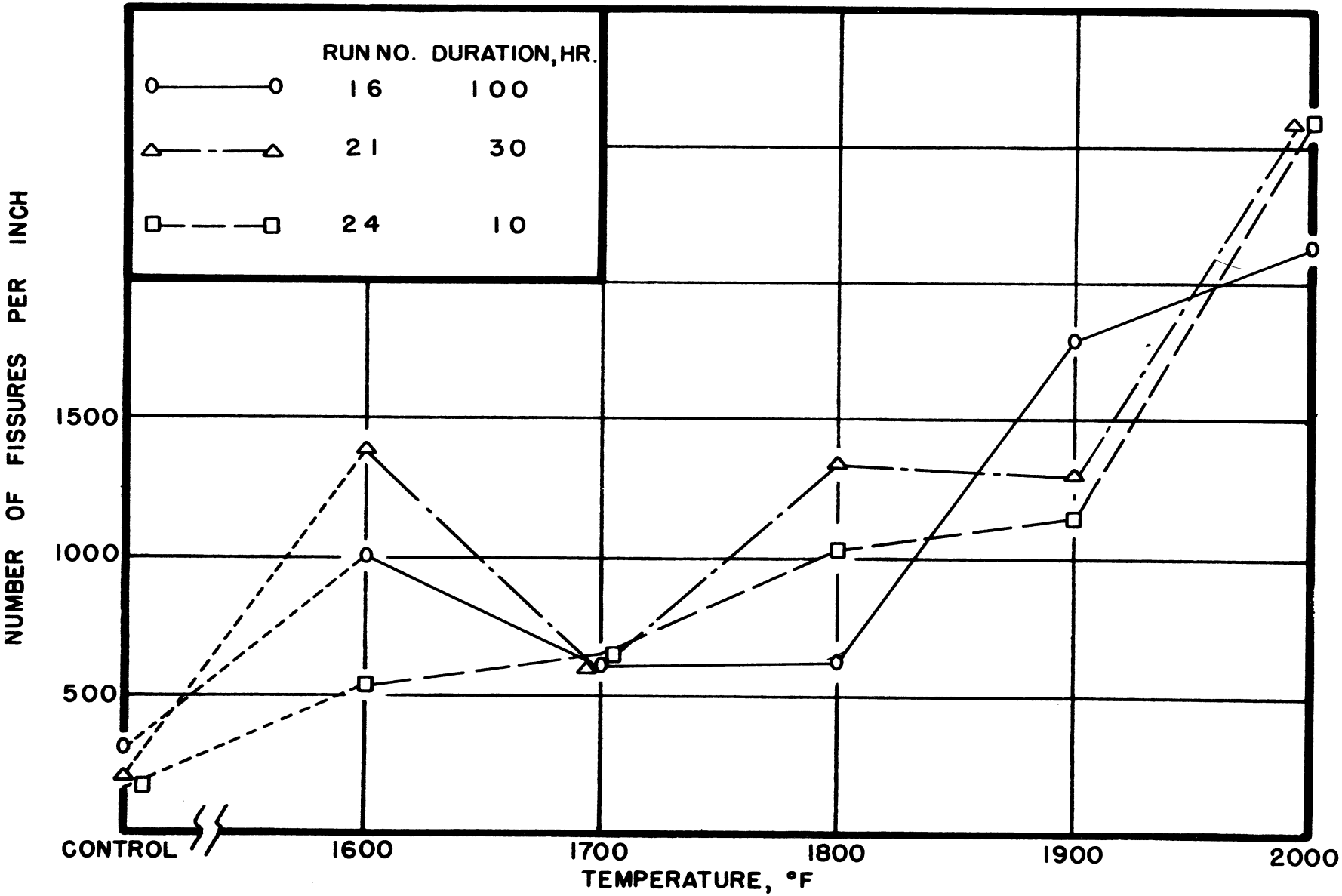

FIG. 83 - SUMMARY PENETRATION FREQUENCY CURVES.
TYPE 310 ALLOY, HEAT X11306. EFFECT OF TIME.

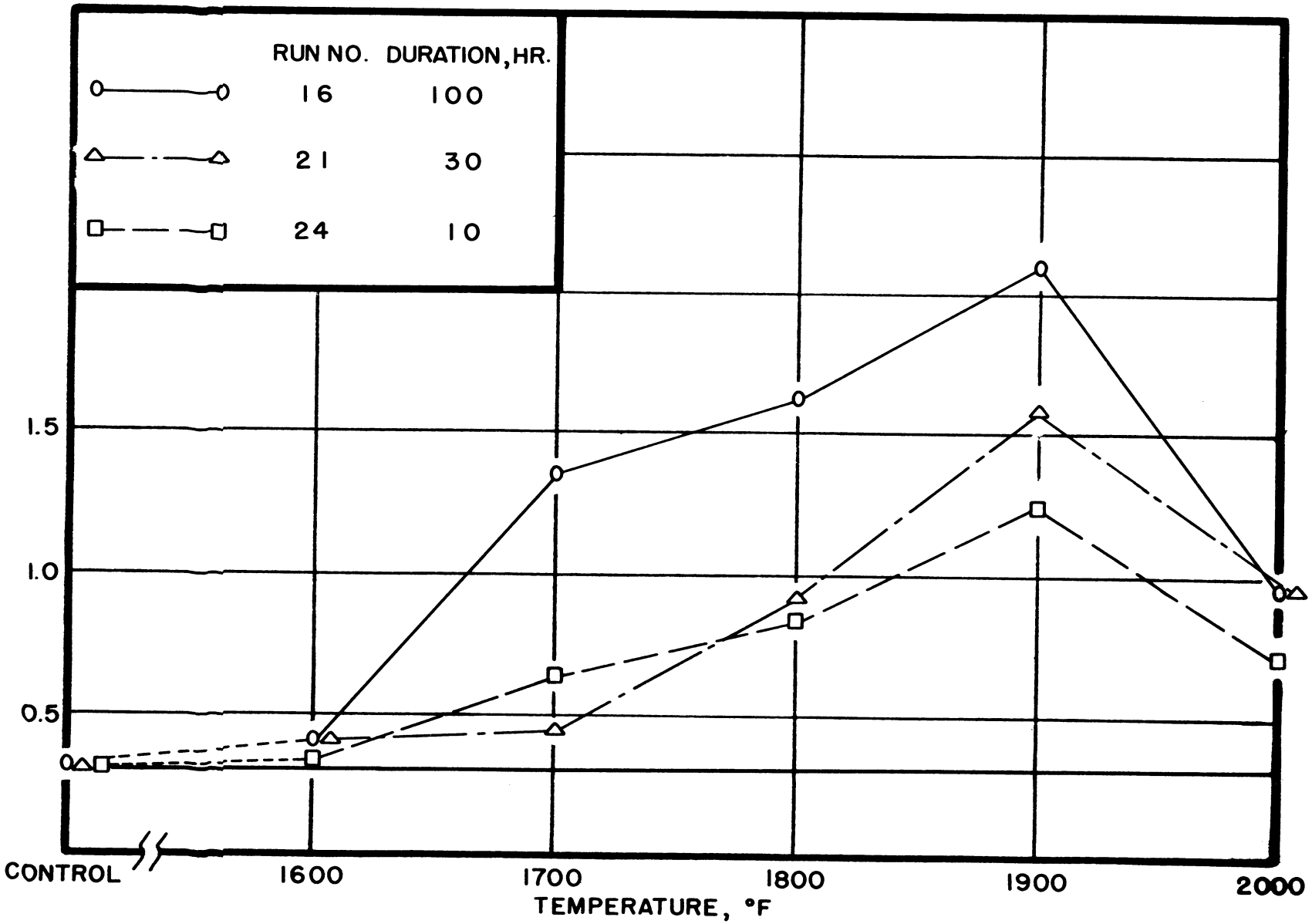

FIG.84-SUMMARY PENETRATION DEPTH CURVES.
TYPE 310 ALLOY, HEAT X11306. EFFECT OF TIME.

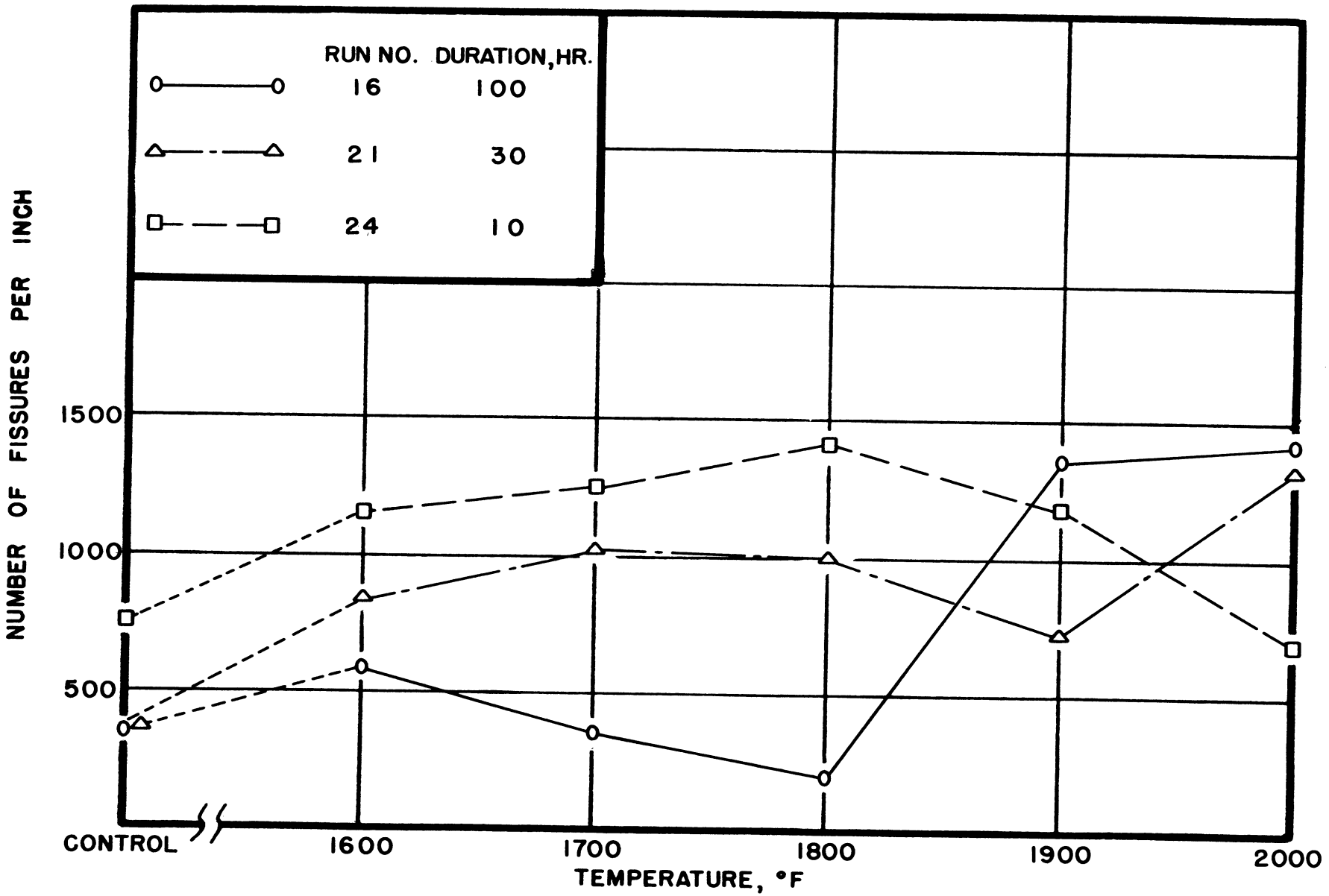

FIG. 85 – SUMMARY PENETRATION FREQUENCY CURVES.
TYPE 310 ALLOY, HEAT X11338. EFFECT OF TIME.

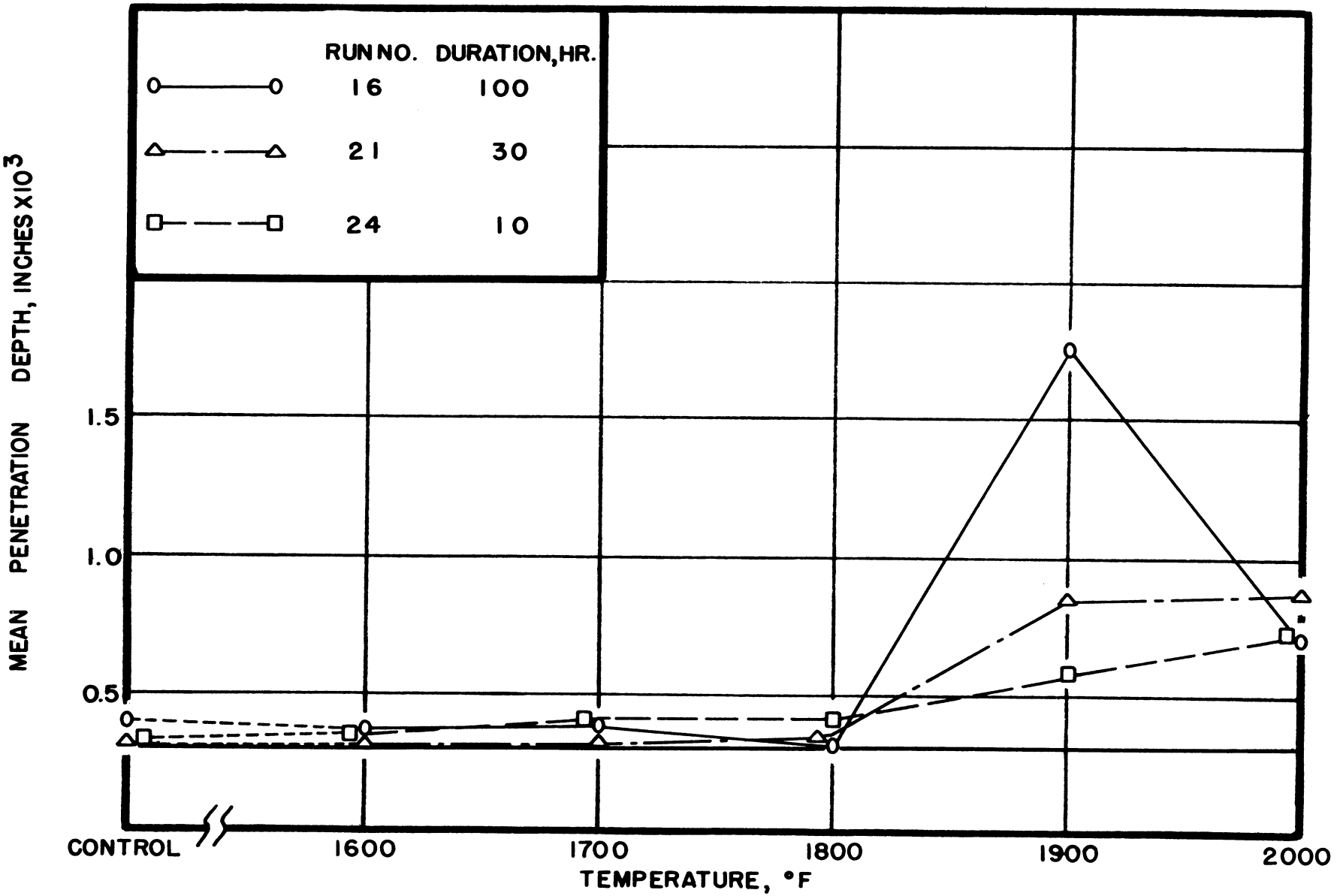

FIG. 86 - SUMMARY PENETRATION DEPTH CURVES.
TYPE 310 ALLOY, HEAT X11338. EFFECT OF TIME.

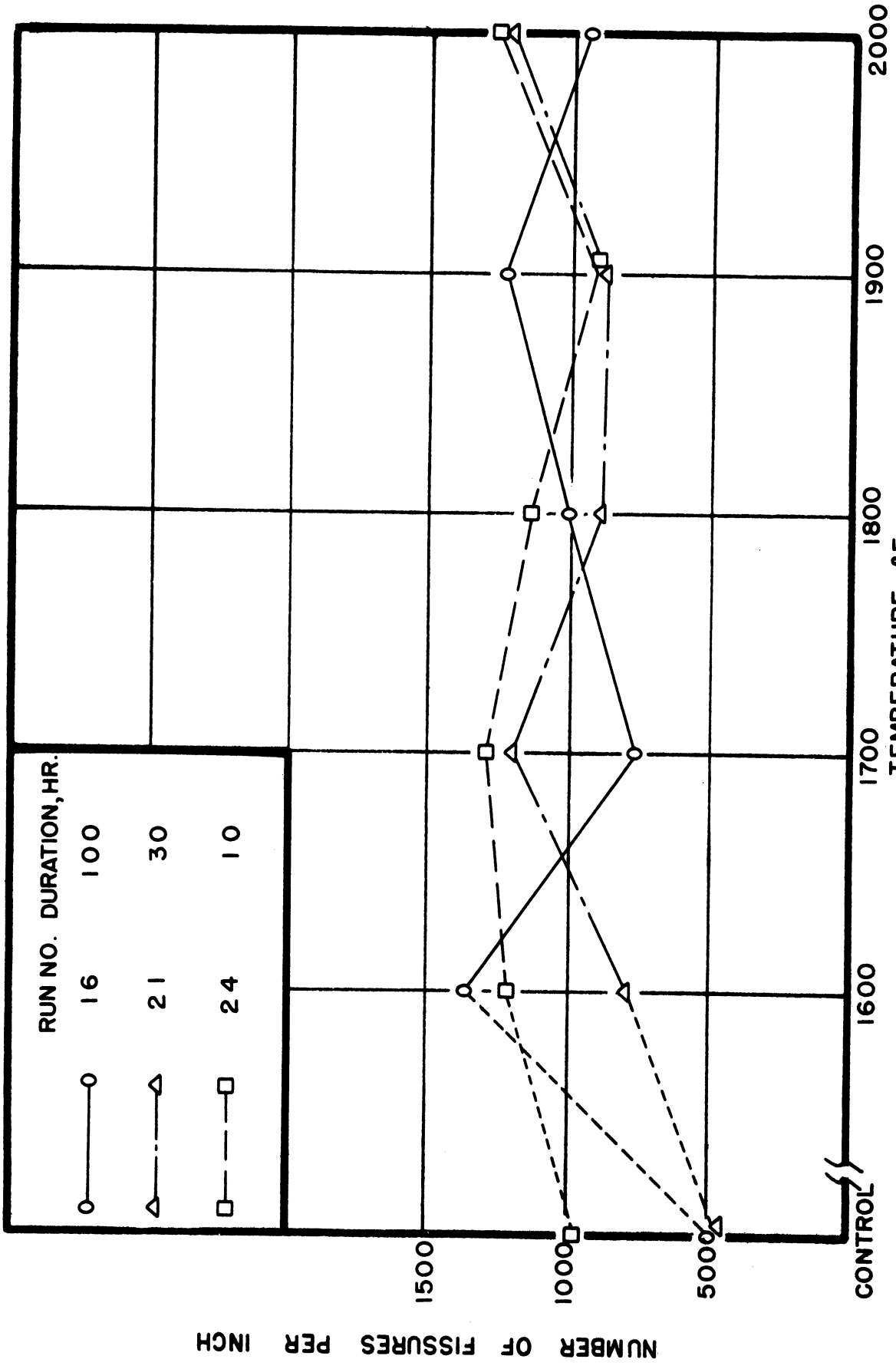

FIG.87-SUMMARY PENETRATION FREQUENCY CURVES.
TYPE 310 ALLOY, HEAT X27258. EFFECT OF TIME.

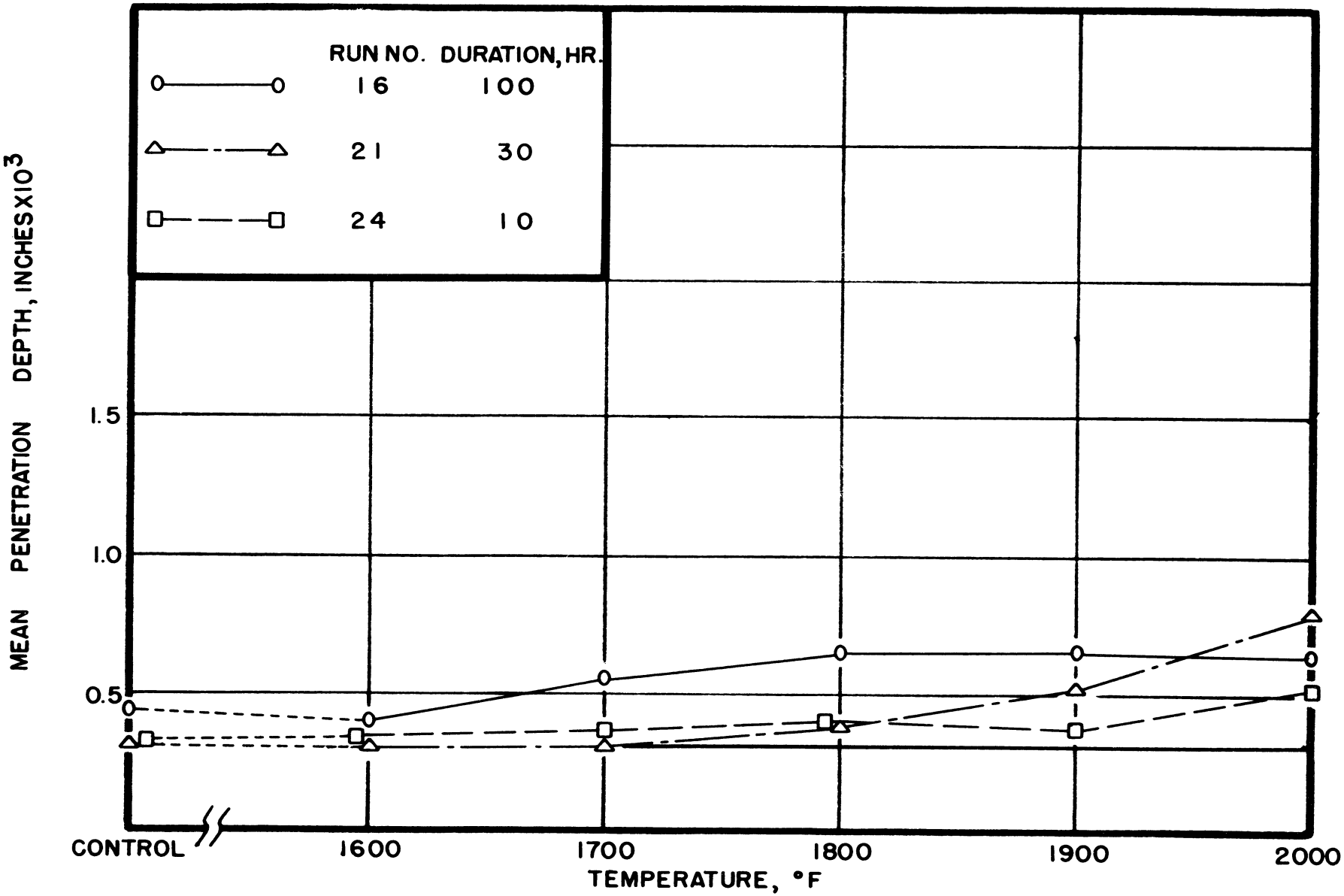

FIG. 88 - SUMMARY PENETRATION DEPTH CURVES.
TYPE 310 ALLOY, HEAT X27258. EFFECT OF TIME.

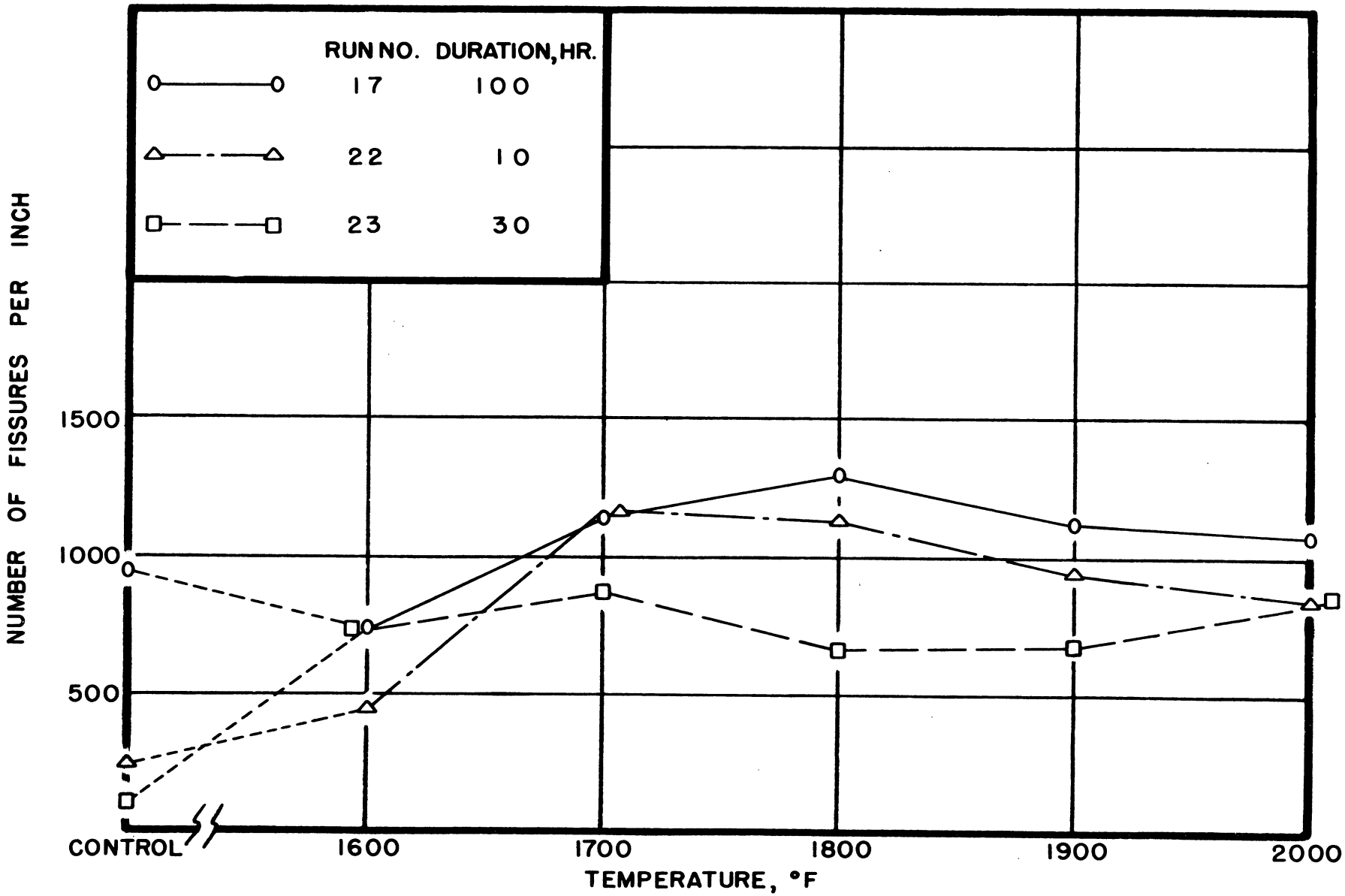

FIG. 89 - SUMMARY PENETRATION FREQUENCY CURVES.
TYPE 310 ALLOY, HEAT X45558. EFFECT OF TIME.

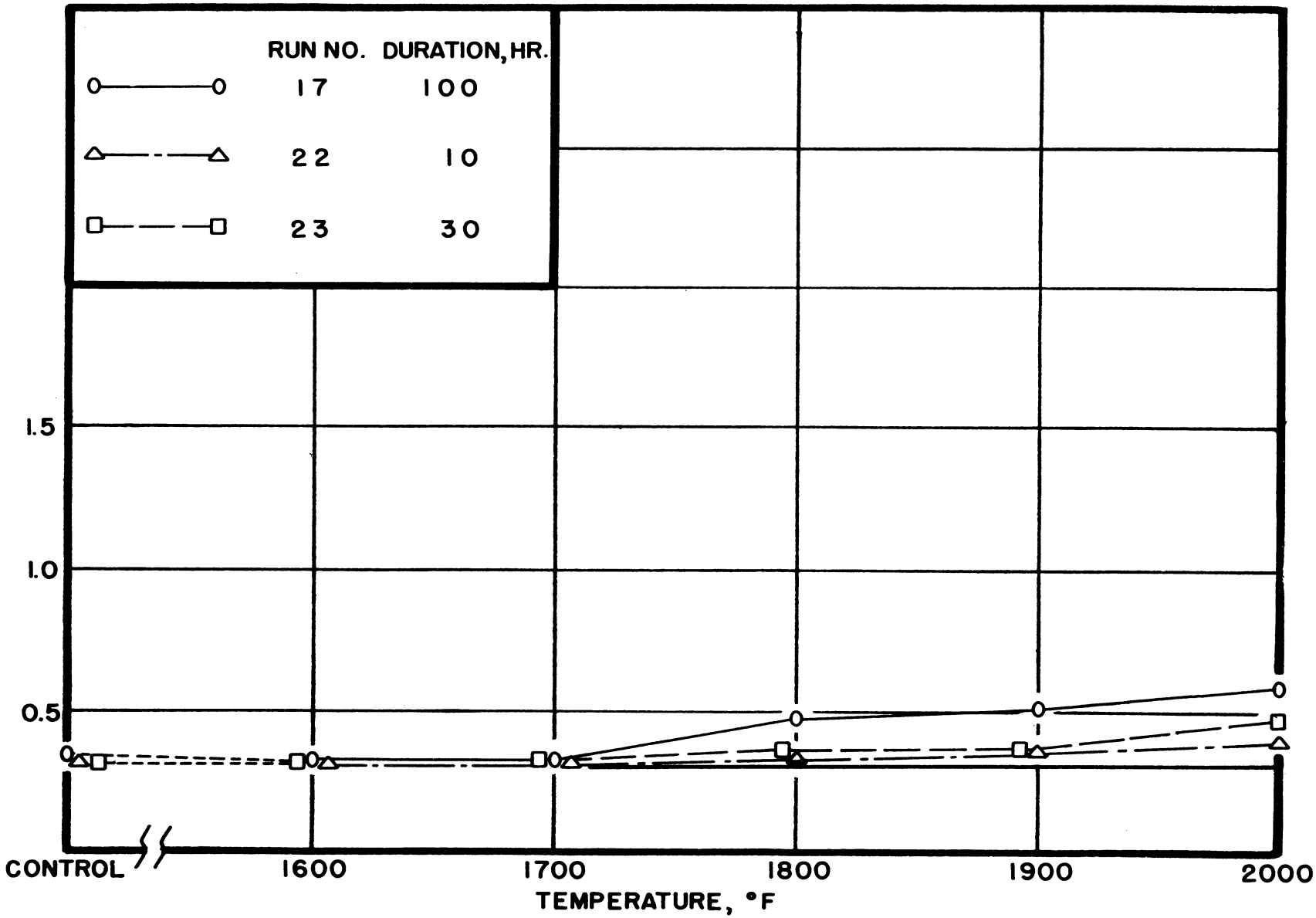

FIG. 90–SUMMARY PENETRATION DEPTH CURVES.
TYPE 310 ALLOY, HEAT X45558. EFFECT OF TIME.

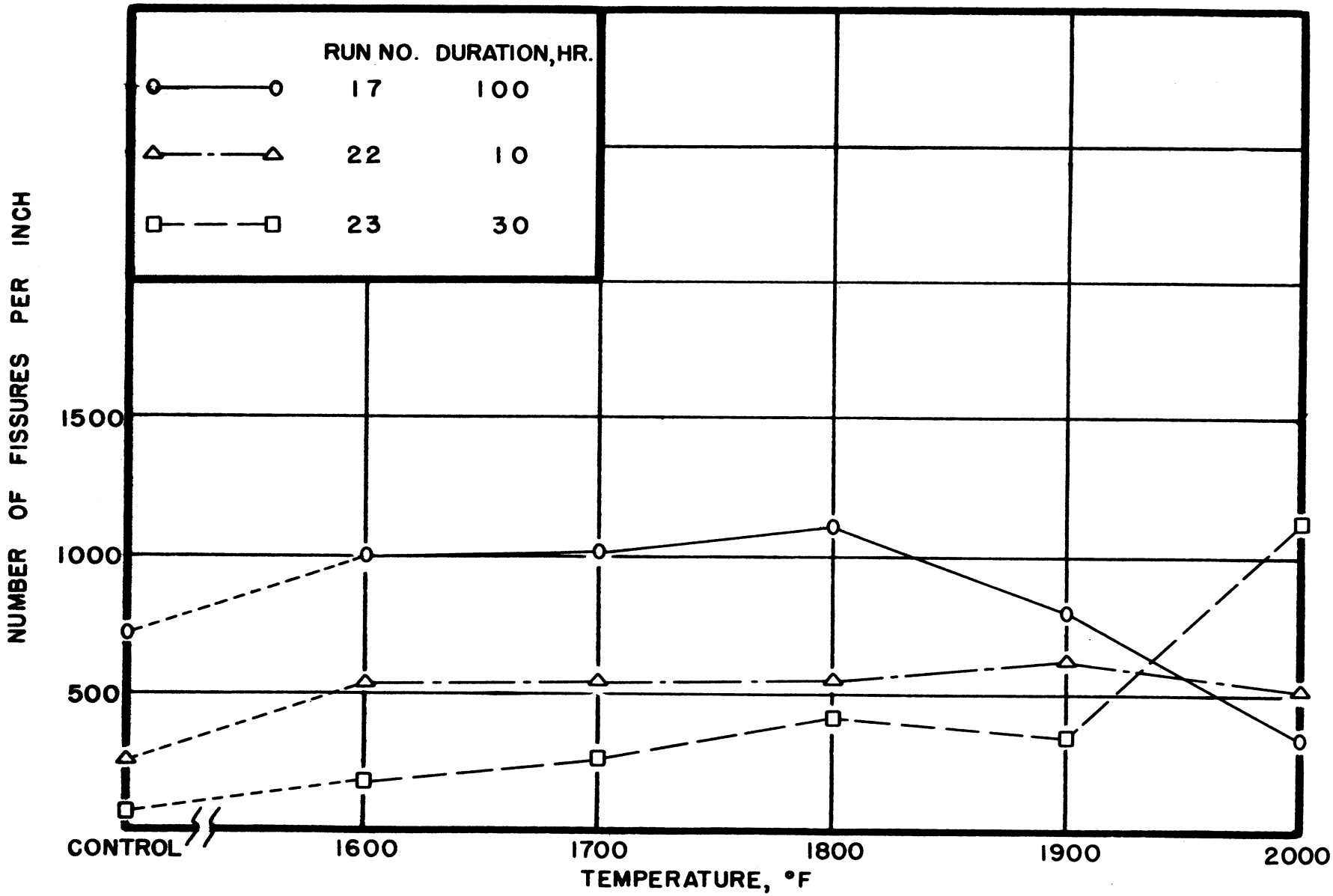

FIG. 91 - SUMMARY PENETRATION FREQUENCY CURVES.
TYPE 310 ALLOY, HEAT X46063. EFFECT OF TIME.

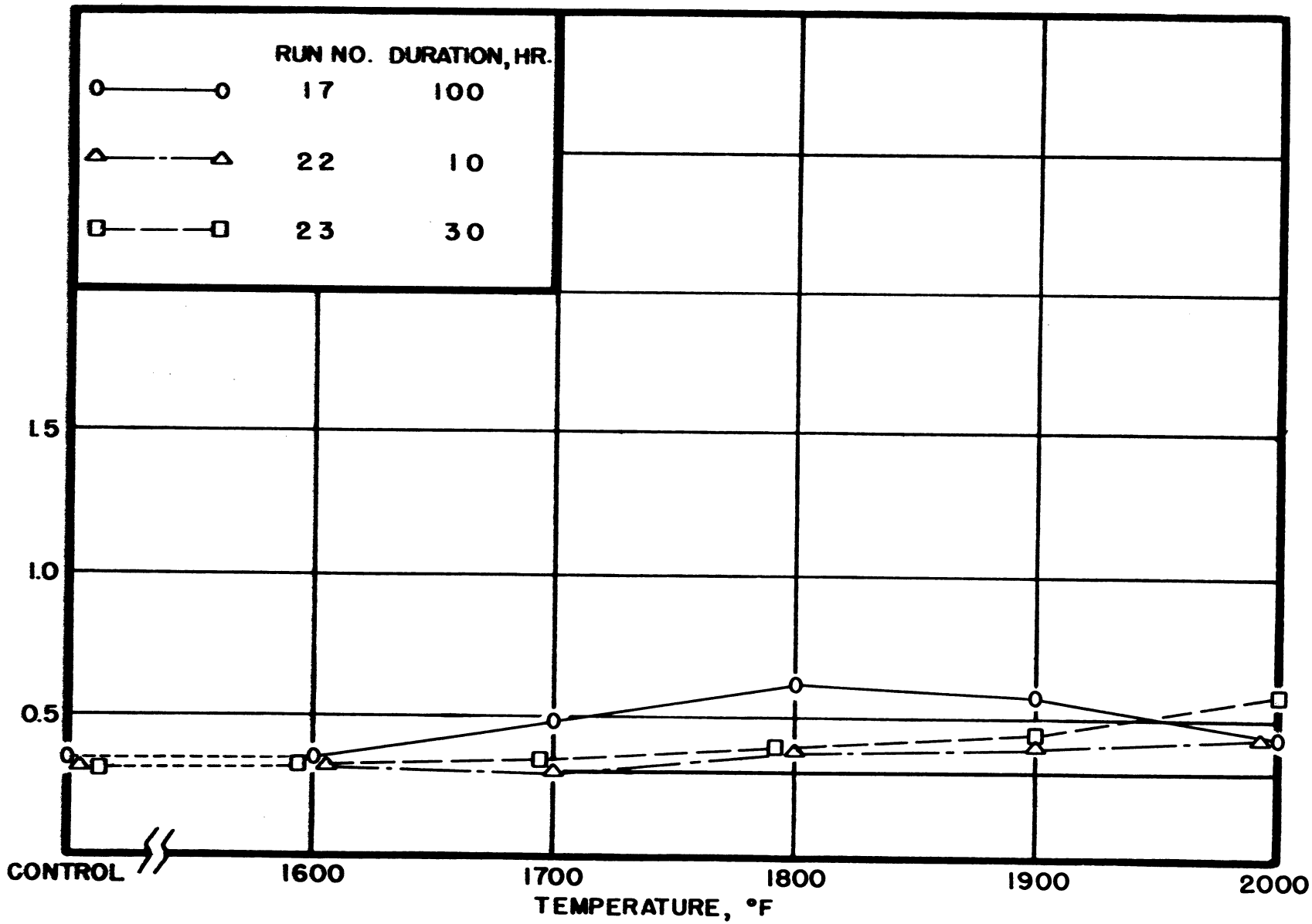

FIG. 92 – SUMMARY PENETRATION DEPTH CURVES.
TYPE 310 ALLOY, HEAT X46063. EFFECT OF TIME.

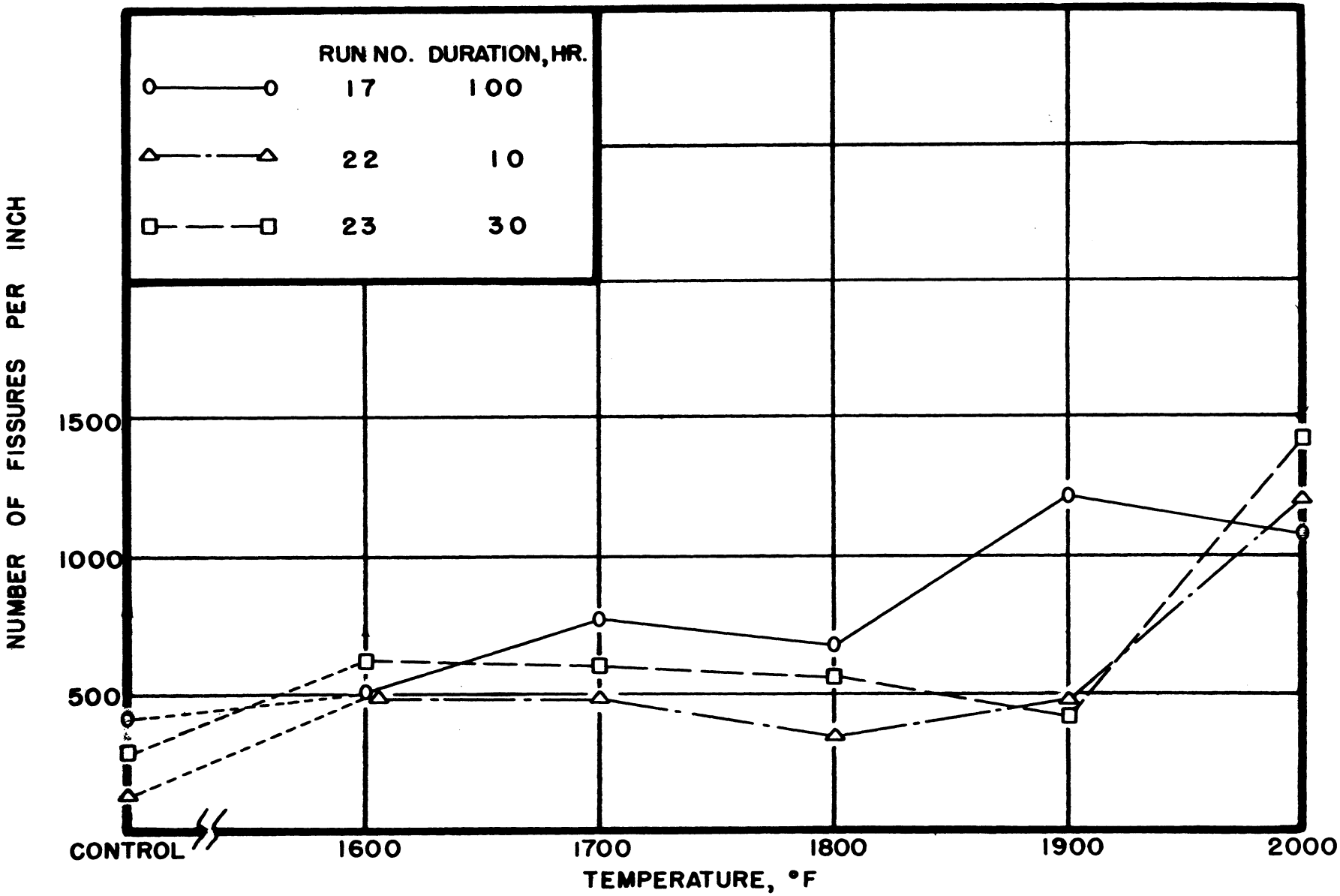

FIG. 93 - SUMMARY PENETRATION FREQUENCY CURVES.
TYPE 310 ALLOY, HEAT X46572. EFFECT OF TIME.

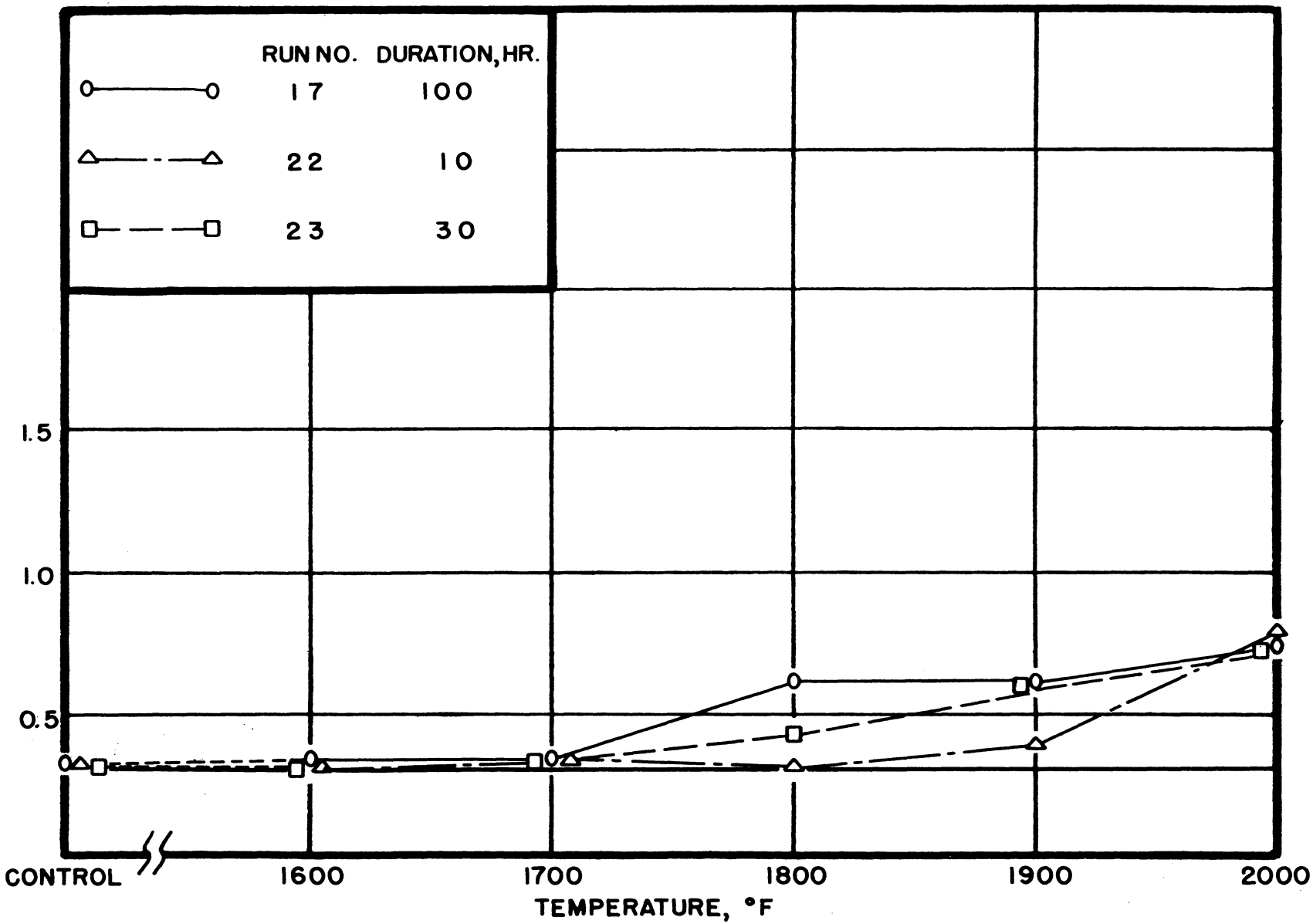

FIG. 94—SUMMARY PENETRATION DEPTH CURVES.
TYPE 310 ALLOY, HEAT X46572. EFFECT OF TIME.

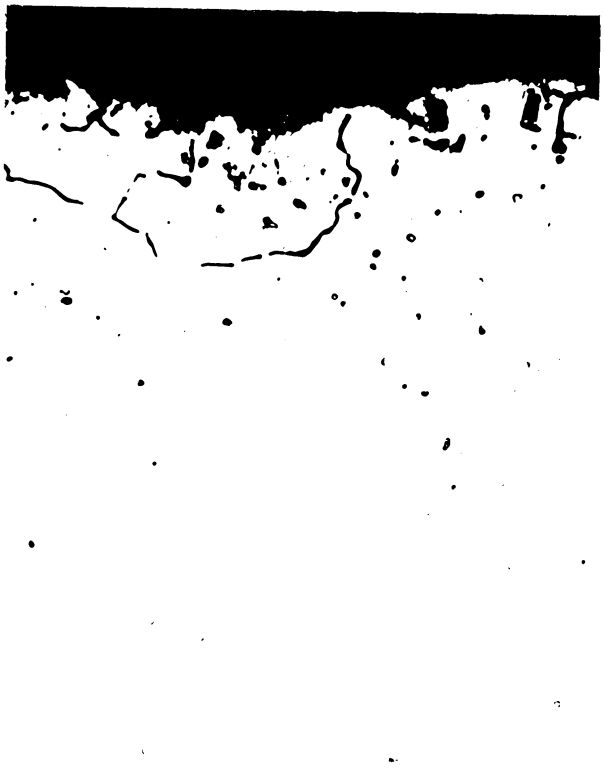

Fig. 95. Type I Penetration. Web from Surface. Type 309 + Nb Alloy. 1900°F and 100 hr. 750x. Cross Section. Unetched.

Fig. 96. Type II Penetration. Web from Pits. Type 310 Alloy, Heat 64270. 1800°F and 100 hr. 750x. Cross Section. Unetched.

Fig. 97. Type III Penetration. Rough Web. Type 310 Alloy, Heat 64177. 1900°F and 100 hr. 750x. Cross Section. Unetched.

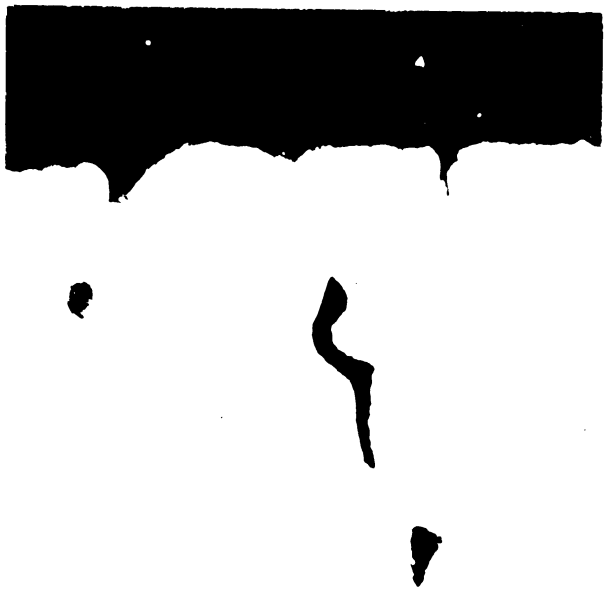

Fig. 98. Type IV Penetration. Smooth Fissures. Type 310 Alloy, Heat X 11338. 1800°F and 100 hr. 750x. Cross Section. Unetched.

Fig. 99. Type V Penetration. Developed Web. Type 310 Alloy, Heat X 11338. 1900°F and 100 hr. 750x. Cross Section. Unetched.

Fig. 100. Type VI Penetration. Coalesced Web. Type 310 Alloy, Heat X 11338. 2000°F and 100 hr. 750x. Cross Section. Unetched.

Fig. 101. Grain Boundaries before Testing. Type 310 Alloy, Heat 64270. As Received. 750x. Cross Section. Etch: Electr. Chromic Acid.

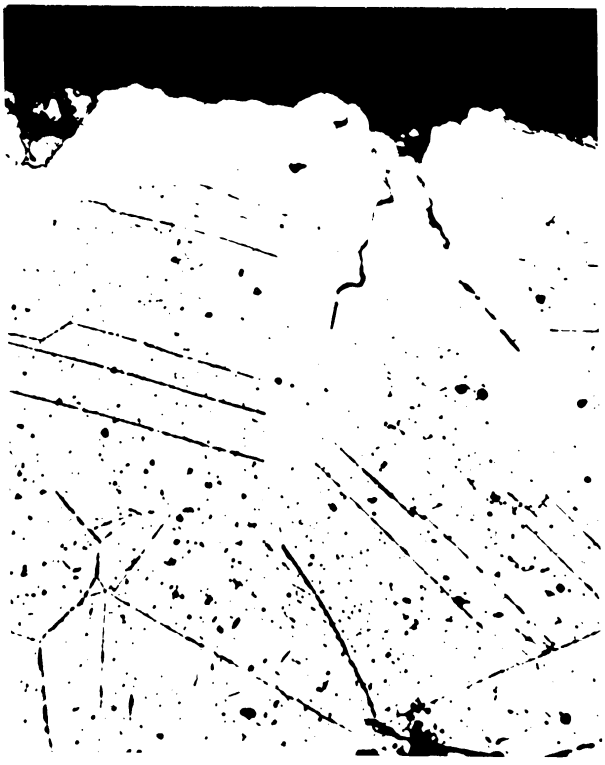

Fig. 102. Penetration and Grain Structure. Type 310 Alloy, Heat 64270. 1700°F and 100 hr. 750x. Cross Section. Etch: Electr. Chromic Acid.

Fig. 103. Penetration and Precipitation. Type 310 Alloy, Heat X 11306. 1600°F and 100 hr. 750x. Cross Section. Unetched.

Fig. 104. Penetration and Precipitation. Type 310 Alloy, Heat X 11306. 1900°F and 100 hr. 750x. Cross Section. Unetched.

Fig. 105. Penetration and Precipitation. Type 310 Alloy, Heat X 11306. 2000°F and 100 hr. 750x. Cross Section. Unetched.

Fig. 106. Penetration and Precipitation. Type 310 Alloy, Heat X 11306. 2000°F and 10 hr. 750x. Cross Section. Unetched.

Fig. 107. Developed Web Penetration. Type 310 Alloy, Heat X 11338. 1900°F and 100 hr. 750x. Cross Section. Etch: Electr. Chromic Acid.

Fig. 108. Developed Web Penetration. Type 310 Alloy, Heat X 11338. 1900°F and 100 hr. 500x. Cross Section. Unetched.

Fig. 109. Oxide-filled Pits. Type 310 Alloy, Heat X 45558. 2000°F and 100 hr. 750x. Cross Section. Unetched.

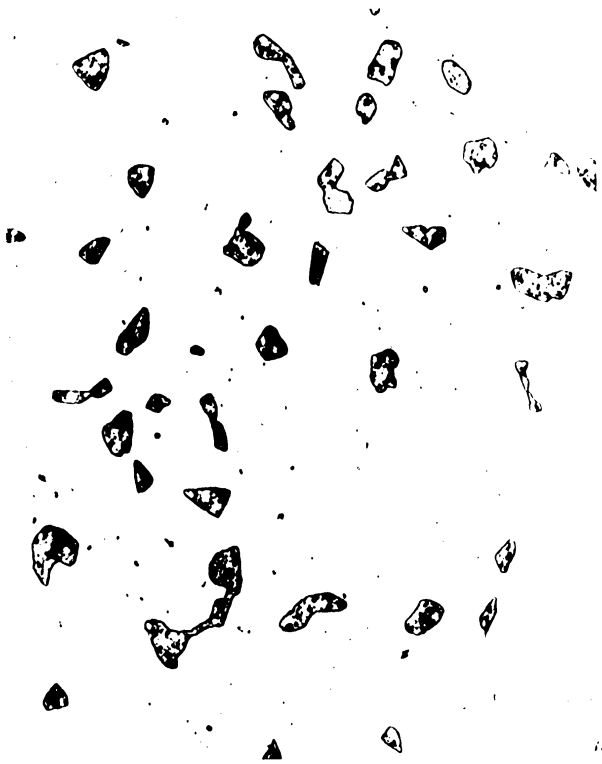

Fig. 110. Delta Ferrite. Type 309+ Nb Alloy. 1700°F and 100 hr. 1000x. Cross Section. Etch: Murakami's Reagent.

Fig. 111. Sigma Phase. Type 310 Alloy, Heat X 27258. 1600°F and 100 hr. 1000x. Cross Section. Etch: Murakami's Reagent.

Fig. 112. Matrix and Boundary Precipitation. Type 310 Alloy, Heat X 11338. 1600°F and 100 hr. 250x. Cross Section. Etch: Electr. Chromic Acid.

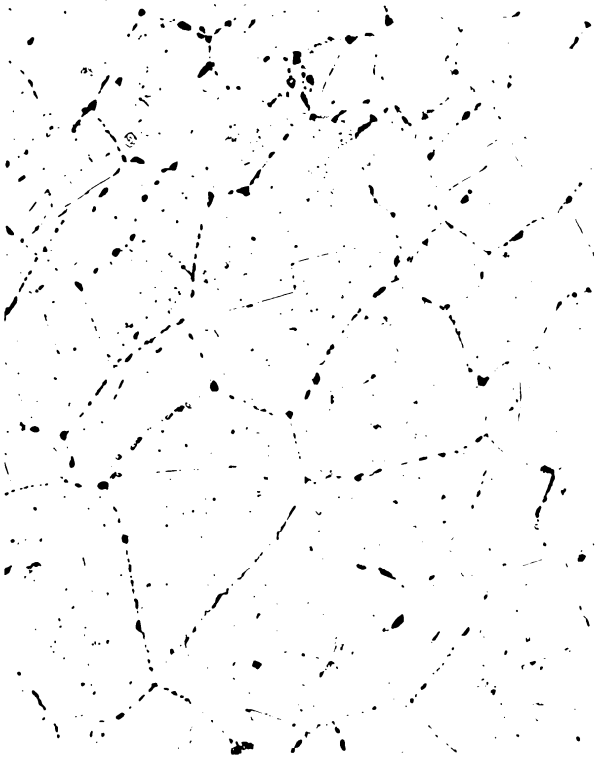

Fig. 113. Matrix and Boundary Precipitation. Type 310 Alloy, Heat X 11338. 1900°F and 100 hr. 250x. Cross Section. Etch: Electr. Chromic Acid.

Fig. 114. Oxygen-Rich Layer. Type 310 Alloy, Heat X 27258. 1900°F and 10 hr. 1000x. Cross Section. Oblique Light. Etch: Electr. Chromic Acid.

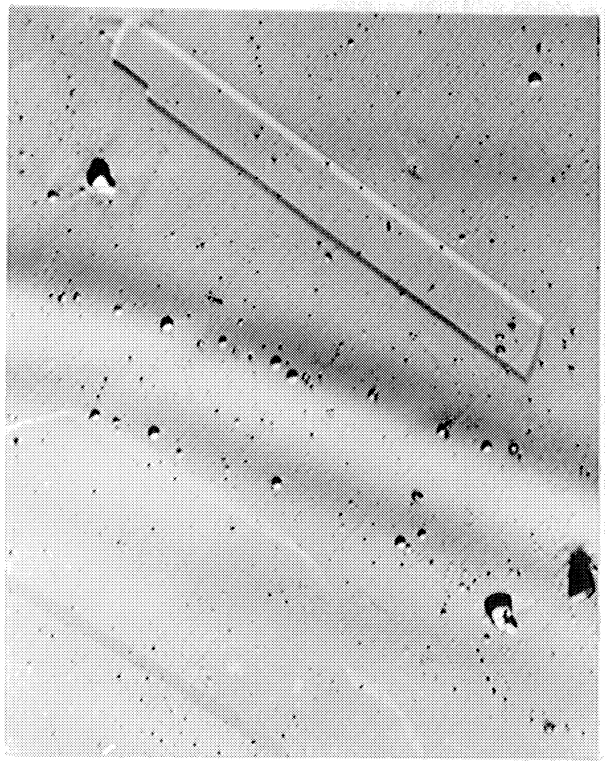

Fig. 115. Concentration Gradients. Type 310 Alloy, Heat X 45558. As Received. 1000x. Cross Section. Oblique Light. Etch: Electr. Chromic Acid.

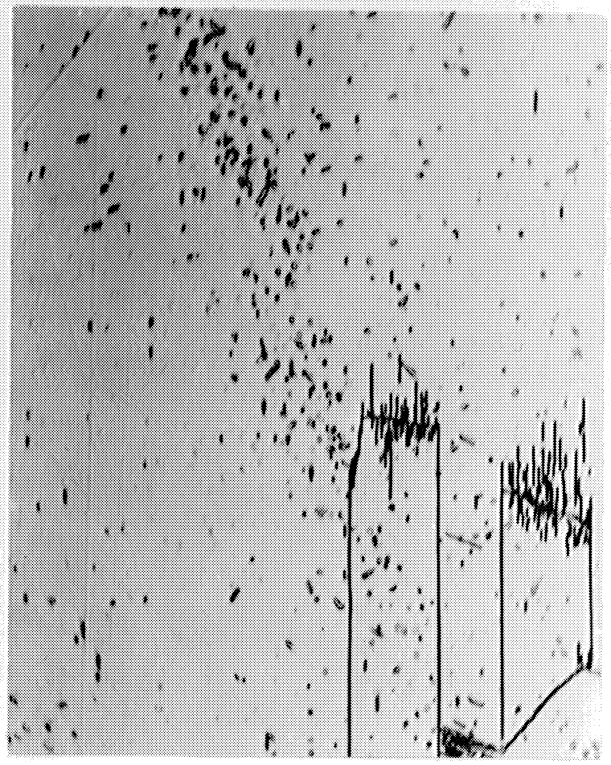

Fig. 116. Carbide Precipitation Bands. Type 310 Alloy, Heat X 45558. 1600°F and 10 hr. 1000x. Cross Section. Etch: Electr. Chromic Acid.

Fig. 117. Carbide Precipitation Bands. Type 310 Alloy, Heat X 45558. 1600°F and 10 hr. 250x. Cross Section. Etch: Electr. Chromic Acid.

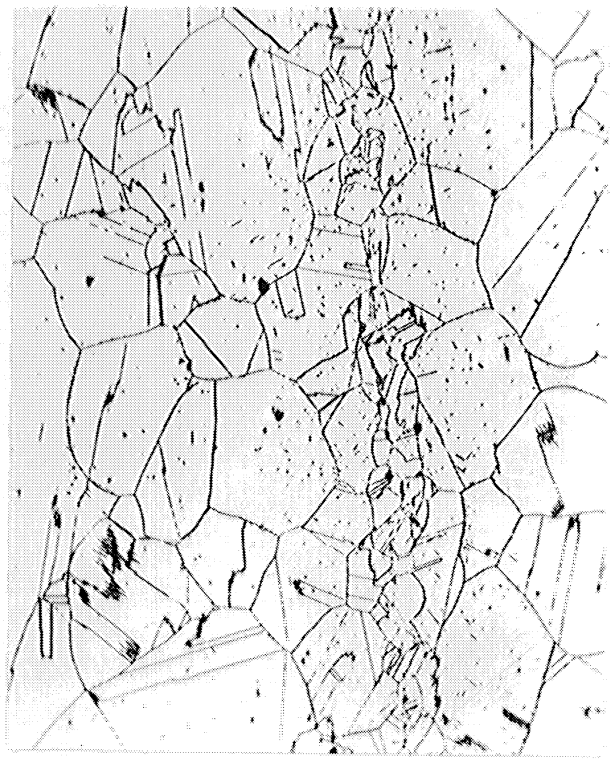

Fig. 118. Carbide Bands and Grain Refinement. Type 310 Alloy, Heat X 45558. 1600°F and 100 hr. 250x. Cross Section. Etch: Electr. Chromic Acid.